

AD-A153 808

EROSION CONTROL OF SCOUR DURING CONSTRUCTION REPORT 8
SUMMARY REPORT(U) ARMY ENGINEER WATERWAYS EXPERIMENT
STATION VICKSBURG MS HYDRAULICS LAB L 2 HALES JAN 85

1/3

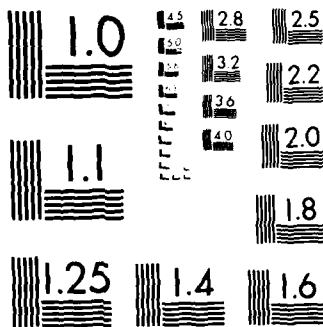
UNCLASSIFIED

MES/TR/HL-80-3-8

F/G 13/2

NL





MICROCOPY RESOLUTION TEST CHART
NATIONAL BUREAU OF STANDARDS 1963-A



US Army Corps of Engineers

AD-A 153 808

TECHNICAL REPORT NUMBER

EROSION CONTROL OF SCOUR DURING CONSTRUCTION

Report 8

SUMMARY REPORT

by

Lyndell Z. Hales

Coastal Engineering Research Center

DEPARTMENT OF THE ARMY
Waterways Experiment Station, Corps of Engineers
PO Box 631
Vicksburg, Mississippi 39180-0631



DTIC
ELECTRIC
MAY 16 1985
S A D

January 1985

Report 8 of a Series

Approved For Public Release - Distribution Unlimited

DTIC FILE COPY

HYDRAULICS



LABORATORY

DEPARTMENT OF THE ARMY
US Army Corps of Engineers
Washington, DC 20314-1000

Hydraulics Laboratory
US Army Engineer Waterways Experiment Station
PO Box 631, Vicksburg, Mississippi 39180-0631

85 4 23 075

Destroy this report when no longer needed. Do not return
it to the originator.

The findings in this report are not to be construed as an official
Department of the Army position unless so designated
by other authorized documents.

The contents of this report are not to be used for
advertising, publication, or promotional purposes.
Citation of trade names does not constitute an
official endorsement or approval of the use of
such commercial products.

Unclassified

SECURITY CLASSIFICATION OF THIS PAGE (When Data Entered)

REPORT DOCUMENTATION PAGE		READ INSTRUCTIONS BEFORE COMPLETING FORM
1. REPORT NUMBER Technical Report HL-80-3	2. GOVT ACCESSION NO. AD A133928	3. RECIPIENT'S CATALOG NUMBER
4. TITLE (and Subtitle) EROSION CONTROL OF SCOUR DURING CONSTRUCTION; Report 8, SUMMARY REPORT		5. TYPE OF REPORT & PERIOD COVERED Report 8 of a series
		6. PERFORMING ORG. REPORT NUMBER
7. AUTHOR(s) Lyndell Z. Hales		8. CONTRACT OR GRANT NUMBER(s)
9. PERFORMING ORGANIZATION NAME AND ADDRESS US Army Engineer Waterways Experiment Station Coastal Engineering Research Center PO Box 631, Vicksburg, Mississippi 39180-0631		10. PROGRAM ELEMENT, PROJECT, TASK AREA & WORK UNIT NUMBERS
11. CONTROLLING OFFICE NAME AND ADDRESS DEPARTMENT OF THE ARMY US Army Corps of Engineers Washington, DC 20314-1000		12. REPORT DATE January 1985
		13. NUMBER OF PAGES 226
14. MONITORING AGENCY NAME & ADDRESS (if different from Controlling Office) US Army Engineer Waterways Experiment Station Hydraulics Laboratory PO Box 631, Vicksburg, Mississippi 39180-0631		15. SECURITY CLASS. (of this report) Unclassified
		15a. DECLASSIFICATION DOWNGRADING SCHEDULE
16. DISTRIBUTION STATEMENT (of this Report) Approved for public release; distribution unlimited.		
17. DISTRIBUTION STATEMENT (of the abstract entered in Block 20, if different from Report)		
18. SUPPLEMENTARY NOTES Available from National Technical Information Service, 5285 Port Royal Road, Springfield, Virginia 22161.		
19. KEY WORDS (Continue on reverse side if necessary and identify by block number) Breakwaters (LC) Water waves (LC) Coastal engineering (LC) Hydraulic structures (LC) Scour (Hydraulic engineering) (LC) Shore protection (LC)		
20. ABSTRACT (Continue on reverse side if necessary and identify by block number) When major stone structures such as jetties, breakwaters, or groins are erected in the coastal zone, they alter the existing tidal, wave-induced, or wind-driven currents that are in a dynamic equilibrium with the existing bathymetry. These altered currents and waves breaking on such structures under construction may change the existing bathymetry by causing bottom material to be suspended and transported from the region. This removal of material from (Continued)		

DD FORM 1 JAN 73 1473

EDITION OF 1 NOV 65 IS OBSOLETE

Unclassified

SECURITY CLASSIFICATION OF THIS PAGE (When Data Entered)

20. ABSTRACT (Continued).

around structures is often not compensated for by an influx of additional material, and the result is a scour hole that usually develops in the near vicinity of the toe of the partially completed structure. In order to ensure structural stability, any such scour area must be filled with nonerodible material (sufficiently stable to withstand the environmental forces to which it will be subjected) to allow construction to proceed to completion. This may result in significant additional quantities of material being required during construction that can potentially lead to substantial cost overruns.

Four fundamentally different materials are presently being used to combat scour from wave-induced erosion around major stone structures. These are:

- a. A layer of crushed or quarry-run stone (graded or ungraded) placed as a foundation blanket on sandy or otherwise semiconsolidated foundations to prevent upward migration of loose materials and settlement of larger stone sizes.
- b. Fabricated gabion units placed underneath stone structures to form a continuous layer in lieu of a crushed stone foundation blanket.
- c. A wide assortment of synthetic filter fabrics placed underneath rock structures to prevent settlement into otherwise unconsolidated foundations.
- d. To a lesser extent, the use of Gobimats, particularly for toe protection of shore-connected structures such as seawalls or slope revetments.

The objectives of this research were to develop techniques and knowledge for estimating resulting wave characteristics and wave-induced current fields in the vicinity of major coastal structures. Both analytical and laboratory experimental studies were conducted during the investigation. The analytical developments regarding wave heights and wave-induced currents were verified by the use of precise experimental studies of shore-connected breakwaters. Additional underlayer stability experimental studies were conducted for estimating the size of stone comprising the foundation bedding material which would remain stable under various wave conditions.

A two-dimensional finite element numerical simulation model (FINITE) was developed by Houston and Chou (1984) that calculates wave heights under combined refraction and diffraction for both long and short waves approaching structures from any arbitrary direction. The wave equation solved governs the propagation of periodic, small amplitude surface gravity waves over a variable depth seabed. A computational scheme is employed that allows the solution of large problems with relatively small time and memory storage requirements, necessary for practical problem solutions.

A generalized wave-induced current numerical model (CURRENT) was developed by Vemulakonda (1984) to estimate the magnitude of longshore currents and nearshore circulations in the vicinity of structures. This model retains the unsteady terms of the equations of motion, as well as advection and lateral mixing terms. Comparisons with known analytic solutions and experimental results provided good agreement. The model was successfully applied to a complex actual prototype field situation with reasonable results.

PREFACE

The study reported herein was authorized as a part of the Civil Works Research and Development Program by the Office, Chief of Engineers (OCE), US Army. This particular work unit, Erosion Control of Scour During Construction, is part of the Improvement of Operations and Maintenance Techniques (IOMT) Program. Mr. James L. Gottesman, OCE, and Mr. Charles W. Hummer, Water Resource Support Center, were the Technical Monitors for the IOMT Program during preparation and publication of this report. Messrs. Milt Millard and William Godwin were the OCE Technical Monitors during the publication of previous reports of this series.

This research work unit was conducted during the period 1 October 1977 through 30 September 1984 by personnel of the Hydraulics Laboratory and the Coastal Engineering Research Center of the US Army Engineer Waterways Experiment Station (WES). General supervision from the Hydraulics Laboratory was provided by Messrs. H. B. Simmons, Chief of the Hydraulics Laboratory; F. A. Herrmann, Jr., Assistant Chief of the Hydraulics Laboratory; R. A. Sager, Chief of the Estuaries Division; Dr. R. W. Whalin, former Chief of the Wave Dynamics Division; Mr. D. D. Davidson, Chief of the Wave Research Branch; and Dr. J. R. Houston, Research Engineer and Principal Investigator for the Erosion Control of Scour During Construction work unit. The Wave Dynamics Division was transferred to the Coastal Engineering Research Center (CERC) of WES on 1 July 1983 under the direction of Dr. Whalin, Chief of the Coastal Engineering Research Center.

The numerical simulation modeling techniques developed under this research work unit for estimating wave heights and wave-induced currents near structural measures were performed by Drs. Houston and R. S. Vemulakonda, Research Hydraulic Engineer, and by contract with Dr. P. L. Liu, Cornell University. Laboratory tests performed during the experimental phase of this program were conducted by Messrs. C. Lewis, Civil Engineering Technician, and G. Pierce, Student Aid, under the supervision of Dr. L. Z. Hales, Research Hydraulic Engineer. Messrs. R. D. Carver, Research Hydraulic Engineer, and D. G. Markle, Research Hydraulic Engineer, assisted with physical model design and test program planning. Mr. K. A. Turner, Computer Specialist, Ms. M. L. Hampton, Computer Technician, and Mr. R. E. Ankeny, Computer Technician, performed the data collection and numerical processing. Drs. Houston and Hales

CONTENTS

	<u>Page</u>
PREFACE	1
CONVERSION FACTORS, US CUSTOMARY TO METRIC (SI) UNITS OF MEASUREMENT	5
PART I: INTRODUCTION	6
Statement of the Problem	6
Purpose of the Study	9
PART II: PRESENT DESIGN AND CONSTRUCTION PRACTICE	13
Great Lakes Region	13
North Atlantic Region	18
South Atlantic Region	21
Gulf of Mexico	26
South Pacific Region	31
North Pacific Region	36
Alaska	40
Hawaii	42
PART III: STABILITY OF UNDERLAYER MATERIAL	45
General Considerations	45
Design Wave Selection	46
Structure Cross Section	48
Experimental Parameters	49
Experimental Facilities	49
Test Program	53
Data Analysis	56
PART IV: COMBINED REFRACTION AND DIFFRACTION	73
Literature Review	73
Shore-Connected Breakwater Normal to Shoreline	83
Shore-Connected Breakwater at 60-deg Angle to Shoreline	113
PART V: NUMERICAL MODEL OF COMBINED REFRACTION AND DIFFRACTION	145
Numerical Model Background	145
Wave Equation	146
Finite Element Solution	147
Verification	151
Comparison with Three-Dimensional Numerical Model	157
Comparison with Laboratory Experiments	162
Finite Element Wave Model Summary	163
PART VI: NUMERICAL MODEL OF WAVE-INDUCED CURRENTS	166
Background of Model Development	166
Equations of Motion	167
Numerical Model	171
Tests for Idealized Conditions	174
Difficulties in Applications to Field Situations	178
Prototype Field Application	179
Wave-Induced Current Model Summary	184

	<u>Page</u>
PART VII: PREDICTED SCOUR MAGNITUDE	185
Scour by Unidirectional Currents	186
Scour by Wave Action	190
Scour by Combined Current and Wave Action	194
PART VIII: RESEARCH PROGRAM SUMMARY	199
The Problem of Scour and Erosion During Construction	199
Present Design and Construction Practice	199
Stability of Underlayer Material	201
Combined Refraction and Diffraction	204
Numerical Model of Combined Refraction and Diffraction	206
Numerical Model of Wave-Induced Currents	207
Predicted Scour Magnitude	207
PART IX: CONCLUSIONS	211
REFERENCES	214
APPENDIX A: NOTATION	A1

CONVERSION FACTORS, US CUSTOMARY TO METRIC (SI)
UNITS OF MEASUREMENT

US customary units of measurement used in this report can be converted to metric (SI) units as follows:

<u>Multiply</u>	<u>By</u>	<u>To Obtain</u>
acres	0.4047	hectares
cubic feet	0.02831685	cubic metres
cubic yards	0.7645549	cubic metres
feet	0.3048	metres
feet per second	0.3048	metres per second
feet-feet per second	0.0929	metres-metres per second
feet per second per second	0.3048	metres per second per second
foot-pounds per foot per foot	148.8164434	kilogram-centimetres per metre per metre
inches	25.4	millimetres
knots (international)	0.5144444	metres per second
miles (US statute)	1.609344	kilometres
mils	0.0254	millimetres
pounds (force) per square inch	6894.757	pascals
pounds (mass)	0.4535924	kilograms
pounds (mass) per cubic foot	16.01846	kilograms per cubic metre
pounds (mass) per foot	1.488189	kilograms per metre
pounds (mass) per square foot	4.882428	kilograms per square metre
pounds (mass) per second	0.4535924	kilograms per second
pounds-second-second per foot per foot per foot per foot	52.5540137	kilograms-second-second per metre per metre per metre per metre
square feet	0.09290304	square metres
square yards	0.8361274	square metres
tons (2,000 lb, mass)	907.1847	kilograms
yards	0.9144	metres

EROSION CONTROL OF SCOUR DURING CONSTRUCTION

SUMMARY REPORT

PART I: INTRODUCTION

Statement of the Problem

1. When major stone structures such as jetties, breakwaters, or groins are erected in the coastal zone, they alter the existing tidal, wave-induced, or wind-driven currents that are in a dynamic equilibrium with the existing bathymetry. These altered currents and waves breaking on such structures under construction may change the existing bathymetry by causing bottom material to be suspended and transported from the region. This removal of material from around structures (Figure 1) is often not compensated for by an

PROBLEM

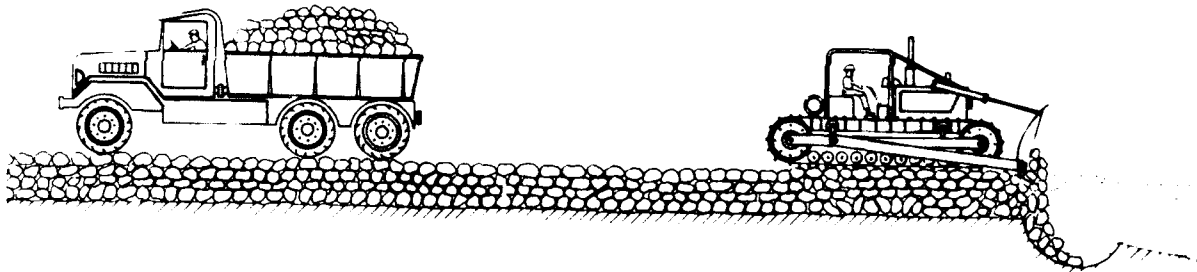


Figure 1. When major stone structures are erected through the surf zone, waves breaking on the structures will toss material into suspension which is transported from the region by existing currents, resulting in a scour hole that may endanger the structures stability and require additional material quantities to fill

influx of additional material, and the result is a scour hole that usually develops in the near vicinity of the toe of the partially completed structure. In order to ensure structural stability, any such scour area must be filled with nonerodible material (sufficiently stable to withstand the environmental forces to which it will be subjected) to allow construction to proceed to completion. This may result in significant additional quantities of material

being required during construction that can potentially lead to substantial cost overruns. Such cost overruns attributable to scour problems have been documented by Hales (1980a). To minimize potential cost increases due to scour during construction, it is necessary to quantify the probability and ultimate extent of potential scour during the scheduled construction period. This interaction of waves and currents with structures and sediments (bottom materials) (Figure 2) is an extremely complex problem and quantification of the probability of potential scour will always be site-specific.

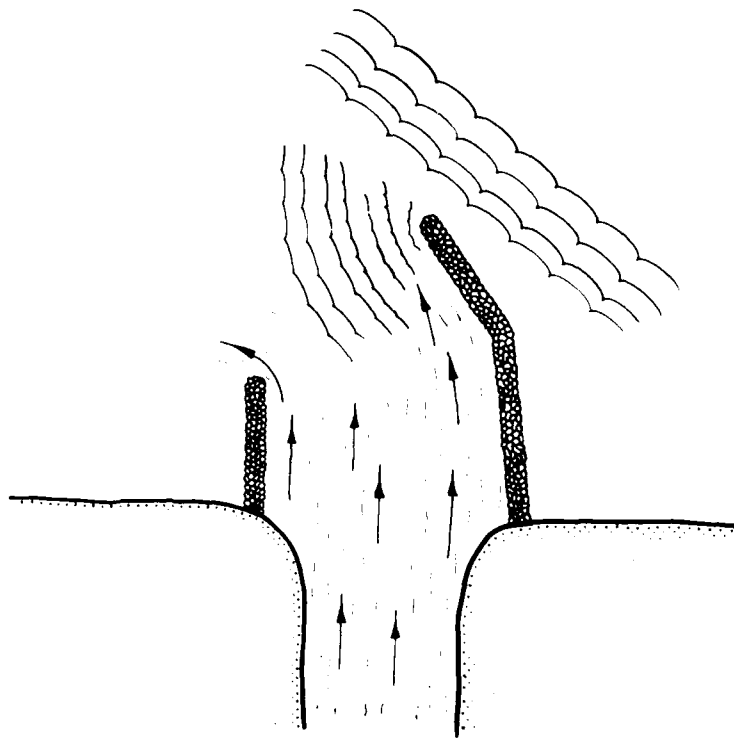


Figure 2. The interaction of surface gravity waves with tidal or wave-induced currents, and their resulting effects on sediment and bottom material movement in the near-vicinity of major coastal structures, is a highly complex phenomenon requiring site-specific analyses

2. Effective, comprehensive, and low cost procedures do not exist for eliminating scour during construction in the nearshore environment. Determination of potential alternative procedures is seriously hampered by the inability to predict the extent of potential scour. Just as there are a wide variety of climatic regions around the nation, there is an assortment of design and construction techniques presently being used to overcome the problem of scour and erosion during nearshore construction (both new construction and maintenance construction). These differing techniques have evolved through years of experience in working under varying wave and soil conditions and reflect the accumulated knowledge of many individuals gained over many construction seasons. The extremes in wave climate are represented by the high energy environment of the north Pacific coastal waters (particularly northern California, Oregon, and Washington, excluding Puget Sound) and the relatively low energy levels of the Great Lakes because of the limited fetches. The relatively

mild wave climate of the Gulf of Mexico is partially offset by the adverse foundation characteristics of the Mississippi River deltaic formations on the Louisiana coast.

3. Over the years, those responsible for the integrity of major engineering works of improvement have developed construction techniques to minimize quantity and cost overruns. Because of varying wave and current conditions from one locality to another, those techniques that are optimum for one location may not be applicable to another region. While in most cases these procedures are regional in nature, it is generally accepted that most major stone structures require a foundation blanket as a bearing surface to support the mass of the structure above and to serve as scour protection during the actual construction. The thickness and design features of this blanket of underlayer material vary with location but have historically been on the order of 2 to 5 ft* thick and have extended on either side of the structure from 5 to 25 ft beyond the toe. This foundation blanket of underlayer bedding material also has been placed along the axis of the structures ahead of the core construction for varying distances to prevent scouring that could potentially undermine the working section. Currently, this is the most widely used construction practice to reduce scour problems that occur during construction in the nearshore zone.

4. Four fundamentally different materials are presently being used to combat scour from wave-induced erosion around major stone structures. These are:

- a. A layer of crushed or quarry-run stone (graded or ungraded) placed as a foundation blanket on sandy or otherwise semi-consolidated foundations to prevent upward migration of loose materials and settlement of larger stone sizes.
- b. Fabricated gabion units placed underneath stone structures to form a continuous layer in lieu of a crushed stone foundation blanket.
- c. A wide assortment of synthetic filter fabrics that are placed underneath rock structures to prevent settlement into otherwise unconsolidated foundations.
- d. To a lesser extent, the use of Gobimats, particularly for toe protection of shore-connected structures such as seawalls or slope revetments.

* A table of factors for converting US customary units of measurement to metric (SI) units is presented on page 5.

Figure 3. Gabion unit prior to filling with stone (after Terra Aqua Conservation, Bekaert Steel Wire Corp., 1977)

partments are formed of equal capacity by wire netting diaphragms or partitions. These partition walls add strength to the container and help retain its shape during the filling operation. They also provide assurance that the fill will remain evenly distributed, even after extensive settlement.

38. Gabion units are normally filled with hand-size stones, usually dumped into them mechanically. The filled gabion then becomes a large, flexible, and permeable building block from which a broad range of structures can be built. This is done by setting and wiring individual units together in courses and filling them in place, or by filling and then placing individual units. The wire mesh used in gabions is heavily galvanized. It may be safely used in fresh water and in areas where the pH (acidity indicator) is not greater than 11. For highly corrosive conditions, a PVC (polyvinyl chloride) coating should be used over the galvanizing. Such treatment is an economical solution to deterioration of the wire near the ocean, in some industrial areas, and in some polluted streams.

39. The foundation blanket specified for Masonboro Inlet consisted of two parts: the foundation layer of Stone I (ranging in size from 2 to 12 in.) between stations 1300 and 1400, and consisted of 12-in.-deep gabion baskets lined with synthetic filter fabric and filled with foundation blanket Stone II (ranging in size from 2 to 8 in.) between sta. 1400 and 1450. The foundation

Knowledge of the magnitude of the amount of scour to be expected from the design storm was imprecise. Guidance along this line was obtained from studying the effects of known storms at specific locations. It was ultimately determined that an expected scour of 6-ft depth in front of concrete seawalls would not be unrealistic from the design storm. Therefore seawall toe protection of a graded layer topped by cover stone was developed, as it had previously been observed that wooden bulkheads had been completely destroyed by stone being tossed like missiles under severe wave attack.

South Atlantic Region

36. Masonboro Inlet, a natural inlet through the coastal barrier beaches of North Carolina, is located in the southern portion of the state, approximately 8 miles northeast of Wilmington, North Carolina. Evidently, the inlet has been open almost continuously since around 1733, although it has migrated extensively to its present location. Improvements for the inlet, authorized in 1949, included two jetties, an ocean entrance channel between the jetties, and interior navigation channels to the Atlantic Intracoastal Waterway. Due to funding limitations, it was proposed to construct the north jetty initially since it was on the apparent updrift side of the inlet. The plan of improvement consisted of a north jetty with a low interior weir, a deposition basin adjacent to the north jetty, and the reestablishment of the navigation channel. Construction of this plan was completed in June 1966. Within 3 years, the navigation channel had migrated through the deposition basin and was endangering the stability of the north jetty. WES (Seabergh 1976) was requested to conduct a physical model study of the inlet to investigate, among other things, the optimum length and alignment of the south jetty. It was determined that the south jetty should be located on a sandy shoal region where the mean water depth is typically about 5 or 6 ft. Because of this, the project design included foundation scour control blankets, and construction was under way during the spring and summer of 1979. Gabions were specified as the elements to comprise the foundation scour control blankets.

37. Gabions are relative newcomers to American construction but have been installed in their present form in Europe since the late 1800's when the metal gabion was developed. Gabions are compartmented rectangular containers made of galvanized steel hexagonal wire mesh and filled with stone (Figure 3).

width up to 5 miles. The width of the barrier beach is generally less than 1/2 mile and in some locations is less than 100 ft. The islands are interrupted by inlets at several locations, and navigation improvements such as dredging and stabilization structures are maintained as well as shore protection features such as groins. The characteristics of the incoming surface gravity waves in this area are, generally, such that the direction of net longshore sediment transport is to the west along Long Island and then south along the New Jersey, Delaware, Maryland, and Virginia coasts. The inlets along the south shore of Long Island that are exposed to the full forces of the north Atlantic storms have previously been stabilized by major jetties. A significant amount of maintenance dredging is required to keep the inlets navigable as littoral drift on the order of 200,000 cu yd net annually is transferred past the east jetties and into the channels. While rehabilitation work to the existing structures is performed as required, major new stoneworks are not anticipated in the foreseeable future. The rehabilitation work which has been performed to the existing structures in this region was such that additional foundation stabilization measures were not necessary.

34. Barnegat Inlet, New Jersey, approximately 55 miles south of Sandy Hook, is an example of a rehabilitation work of sufficient magnitude to require specific foundation design measures. The project consists of a channel protected by two converging stone jetties. In order to allow for successful maintenance dredging of the inlet channel, raising of the north jetty was begun in August 1972 and completed 1 year later at a cost of approximately 1.4 million dollars. The purpose of a foundation mat was not only to distribute the load over a wider base but also to prevent shear failure and erosion of the underlying soil at the toe of the rock mound. When load is placed on a soil exceeding its bearing strength, the soil will fail by shearing along a curved plane, cutting the bottom at some distance beyond the toe of the superimposed load. Therefore a base of material stronger than the soil but smaller than the core stone should be laid that extends beyond the toe and the plane of failure. A mat layer of material varying in size from 3 to 50 lb and approximately 2 ft thick was required to protect the structure from settlement and scour failure.

35. The Delaware Coast Hurricane and Flood Protection Study was a major analysis of proposed interrelated structures such as levees, dikes, seawalls, bulkheads, and groins to protect this region of coastline from a design storm.

south jetty (as wave energy penetrated the jettied entrance). Waves overtopping the north jetty eroded approximately 260 ft of beach sand from the area. In an attempt to halt the erosion process, a rock revetment structure was constructed. The purpose of this revetment was to prevent flanking of the south jetty structure. The US Army Engineer Waterways Experiment Station (WES) was requested to conduct a physical model study to investigate, among other things, the mechanism by which scour and erosion are taking place inside the south jetty. Based on results of the three-dimensional model investigation by Curren and Chatham (1979), it was determined that of the improvement plans tested involving the north jetty, a 900-ft extension was optimum with respect to wave protection, prevention of erosion on Plum Island, and construction costs. Hence, the secondary construction effects produced by wave energy passing between the jetties can be alleviated by an extension and a curvature of the north jetty.

31. It is customary in this region to put a filter blanket layer of gravel or small rock under new stonework, but this is usually not necessary in the rehabilitation of existing structures. In order to prevent scour around the toe during construction, the filter layer is placed ahead of the core and cover stone approximately 50 ft from the entire width of the structure base. Gabion units have been used as riverbank stabilization measures but have not been utilized beneath breakwaters or jetties in the New England region.

32. Scour may not in all cases be considered a detriment. For example, the functional design of jettied navigation entrances to harbors considers the application of tidal currents to keep the channel open by removing sediment and littoral drift and thus minimize dredging. In general, navigation channels in the New England area do not migrate a sufficient amount to cause undermining of the structures. This is reflected by the fact that the New England Division does not have to spend an unusually large amount of time or money rehabilitating the jetties. Because the scour control methods appear to be working and because of the physiography of the glaciated coastal region, scour is not a pressing high-priority problem in the New England area. Future anticipated work on the exposed shores of the Cape Cod islands is expected to encounter greater problems with scour.

Central North Atlantic region

33. The south shore of Long Island is characterized by a series of barrier beaches, which are separated from the mainland by tidal bays that vary in

North Atlantic Region

27. Hard, enduring rock symbolizes the area of the Atlantic coast north of New York City, and most of the beaches reflect the nature of their development. The New England coastline has had a complex history of glacial scour and this has resulted in the most irregular shoreline in the nation. Sand is not nearly as plentiful on most parts of this region as elsewhere because the hard rocks of the area do not produce much sand by weathering, and the rivers generally discharge into drowned valleys. South of New York City the coastline is deeply embayed, with the coastal plain being bordered by long sandy barrier island beaches. These barrier beaches are, in general, separated from the mainland by partially filled lagoons. The coasts of this region are exposed to the full force of the Atlantic hurricane, as well as the local "northeasters" which consistently plague the region north of Cape Cod and are occasionally felt all the way south to Cape Hatteras.

New England region

28. In the New England area, it is standard practice to recommend to coastal work contractors that sand placement and other structures be built only at certain times of the year. It is probably impossible to work at all during the period December-February because of inclement weather throughout the region and additional ice problems. However, in the summer months, the beaches are crowded with bathers, and the use of heavy equipment can be problematical. Hence, it is virtually necessary to perform construction in the spring and fall.

29. The ordinary wave climate varies considerably along the New England coast. Lower Cape Cod to the shores of Connecticut along the Long Island Sound usually has waves about 2 to 3 ft in height. The northeastern shore of Cape Cod through the Boston area has essentially an unlimited fetch distance, and therefore the waves in this region are frequently in the range of 5 to 7 ft. In addition, the spring tide levels are higher than the average tide range, and the wave climate is superimposed on top of already high water levels. Hence, the potential for wave damage and erosion varies from relatively moderate along the Connecticut coast to potentially high north of the cape.

30. Between 19 and 27 February 1969, three very large storms entered the Merrimack Embayment and caused extensive damage to the shore side of the

24. Early pilot projects of construction in Lake Erie in the early 1960's used core stone as a foundation layer, but it was found that settlement of the structures occurred as the material penetrated into the lake bottom. The material that is ultimately designated as the bedding layer depends on both the consolidation of the bottom material and the currents that are expected to exist in the local region.

25. Essentially three placement methods are used for positioning material at the structure site in Lake Erie. They are:

- a. Self-unloaders, which are modified ore-carrying ships whose compartments are filled at the quarry with minus 8-in. material to be placed at the site. Conveyor belts carry the material from inside the ship and dump over the side of the vessel.
- b. Bottom-dump scows or large barges fabricated in such a manner that the bottom sections can be opened to allow the transported material to free-fall to the underwater parts of the structure.
- c. Crane and bucket operations for placing large cover stone and forming final grade lines.

The methods of transporting the material to the site really depend largely on the type of material being moved and the location of the quarry. Bedding and core material usually comes by boat or barge. The larger cover stone may be transported by barge or may be moved near the site by rail and trucked the remaining distance to the construction area.

Lake Ontario

26. Secondary construction effects experienced in other lakes regarding the propagation of wave crests along vertical sheet-steel breakwaters and scouring of the shore section to collapse of the structures have also been observed in Lake Ontario. In addition to this phenomenon, at Great Sodus Bay, New York, another separate and distinct problem existed in which surface wind stress and other meteorological conditions caused a setup of elevation of the water surface in the bay. The resulting seiches, acting as short-period low-amplitude tides, caused flow to occur into and out of Great Sodus Bay. The outflow currents, or ebb flows, would tend to meander and cause the location of the navigation channel between the 450-ft-wide jetties to shift temporally. Eventual meandering brought the channel in close proximity of the south jetty, and scouring and erosion at the toe resulted. During the mid-1960's, it was necessary to rehabilitate this structure with sloped rubble-mound construction in order to provide stability to both the jetty and the navigation channel.

generated in Saginaw Bay proper, and caused significant damage to occur to the diked structure. It was not known if the visible erosion at the top of the structure (as a result of wave uprush and runup) is matched by corresponding erosion at the toe of the structure as a result of downrush. No toe structural damage was apparent. In May 1979, a similar event occurred that caused even greater erosion and scour. As a remedial measure, the cover layer was extended to a higher elevation. Efforts are under way to ascertain and quantify the physical processes responsible for damaging the retaining dike.

Lake Erie

22. The situations regarding secondary construction effects encountered in the other lakes are equally applicable in Lake Erie. Additionally, a primary construction scour problem arose during construction of the Buffalo Disposal Dike No. 4, when it was found that the fine underlayer material would not remain at the design slopes. Dike No. 4 was built in the east end of the lake and the bottom is composed of loose silts and soft silty clays. In order to keep the core stone from settling into the unconsolidated foundation, the soft sediments were intended to be bridged with a 6-ft-thick layer of sand composed of minus 3/8 in. to No. 200 sieve size material. When storm conditions arose, large waves would cause mass transport of water to pile up against adjacent existing breakwaters, and from continuity, the return flow to the main lake would create currents sufficient to scour this sand underlayer from the design 1V-on-5H slope. Bottom lake return currents had not been accounted for in the original design, and the solution to this problem was the placement of additional volumes of sand until the stable slope was formed between 1V-on-10H and 1V-on-20H. This was indeed a boundary condition problem caused by setup of waves that developed return flow currents resulting in scour of the foundation. Approximately 20 percent of additional material was necessary to stabilize the foundation layer.

23. When the Cleveland Disposal Dike No. 14 was being constructed, a slightly different problem arose that may more properly be attributed to construction techniques rather than to scour and erosion as normally considered. The self-unloading container ships that were transporting the core material to the work site would place large sections of the dike core above the waterline for reshaping later. Material less than about 100 lb simply could not be retained in the wave climate occurring at the time without additional protection by cover stone.

progressed toward the existing first half, it was discovered that a tremendous scour hole had developed off the end of the first half of the jetty. Since tidal currents are of no significance in the Great Lakes, the scouring action must be attributable to wind- and wave-generated currents that were deflected by the massive rubble-mound structure. The only practical method for combating this situation was "rapid placement" of construction materials; i.e., fill the scour hole as rapidly as possible with whatever amount of material was required to bring the structure up to design grade.

18. As in Lake Superior, it is envisioned that the foreseeable work load in Lake Michigan will be rehabilitation and maintenance of existing facilities where breakwater and harbor facilities are involved. Public Law 91-611 (Rivers and Harbors Act of 1970) authorized the Corps to construct, operate, and maintain structures to confine polluted dredged materials to improve the quality of water in the Great Lakes. About a dozen diked disposal sites will probably be developed for Lake Michigan. When sited in open water, these diked facilities should be of sound design and should be built with construction techniques that will minimize scour or erosion.

Lake Huron

19. Engineering works of improvement in Lake Huron are exposed to the same potentials for scour during construction and secondary construction effects as those structures in Lakes Michigan and Superior. Additionally, a scour-erosion problem developed in late 1978 at the open-water diked disposal site in Saginaw Bay that may possibly be attributed to a lack of historical wave data on which to base the structure design.

20. Because of the polluted sediments of the Saginaw River near Saginaw, Michigan, and since it is necessary to dredge a portion of this river and a navigation channel for some 3 miles into Saginaw Bay, it was necessary to construct a diked disposal site to confine these polluted dredgings. The facility was constructed without incident, with cover stone extending part way up the face of the structure to an elevation determined to be the maximum extent of the runup for the design wave. The remainder of the structure was exposed, small crushed rock that constituted the major volume of the fill.

21. The diked disposal site is situated near the south end of Saginaw Bay; and in September 1978, a northeasterly storm developed over Lake Huron, generated waves propagating toward Saginaw Bay that penetrated the bar section at the mouth of the bay, re-formed waves that combined with those waves being

15. Big Bay Harbor, Michigan, constitutes a vivid example of "secondary construction effects," although there is evidence of the same phenomenon occurring at several other locations on Lake Superior (i.e., Grand Traverse Bay Harbor, the upper entrance to the Keeweenaw Waterway, Black River Harbor, etc.). The problem arises when the wave approach is such that the wave crest propagates along the section of vertical sheet-steel pile on the upcoast side of the harbor, increases in amplitude because of refraction effects and the Mach-stem phenomenon, and terminates as a geyser of water plunging over the crest of the breakwater at the shore end. Depending on the intensity of the storm, the water plume may reach 10 to 12 ft in height, and the resulting dynamic forces are sufficient to severely damage or destroy the structure. It has become necessary to rehabilitate and maintain these types of structures with huge amounts of stone riprap.

16. The procedures for combating the problems of scour and damage to the structures on Lake Superior include repairing the vertical sheet-steel pile with sloping rubble-mound structures that absorb or dissipate a large part of the wave energy as the crest travels along the breakwater. This also assists in the problem of ice damage, as the ice breaks up and overlaps, pushing against the vertical walls. If breakwaters were constructed of rubble-mound stone instead of vertical sheet-steel piles, the initial construction cost would probably increase; however, the maintenance cost of repairing rubble-mound structures should be significantly less if adequate size stone were used in the initial construction.

Lake Michigan

17. Problems previously mentioned regarding Lake Superior also exist in Lake Michigan. Additionally, "primary" scour problems have arisen at Leland Harbor, Michigan (and other locations), during construction of rubble-mound breakwaters. Since Lake Michigan completely freezes over in the winter, it is necessary to cease construction operations until spring on those projects that cannot be completed before ice begins to form on the lake. The existing project at Leland Harbor provides for a harbor of refuge consisting of a breakwater about 1,200 ft long running parallel to the shore for some distance and then angling toward the shore at its northern end. During a fall construction season, half of the breakwater was completed. During the next construction season, the second half of the breakwater was built, starting at the opposite end of the structure and joining the two halves in the middle. As work

PART II: PRESENT DESIGN AND CONSTRUCTION PRACTICE

12. The present techniques used by the Corps of Engineers in the design and construction of major coastal structures were evaluated with respect to the possibility of developing the more promising aspects and incorporating these procedures in guideline recommendations. Due to the large number and wide variety of nearshore construction projects, both completed and planned, it is convenient to consider a regional or geographic analysis of the various structures and construction techniques.

Great Lakes Region

13. The design of breakwaters or jetties on the Great Lakes requires provisions for stability against wave forces comparable to the maximum probable pressure that might be developed by an ice sheet. Since the maximum wave forces and ice thrust cannot occur at the same time, no special allowance for overturning stability to resist ice thrust need be made. However, adequate precautions must be observed to ensure that the structure is secure against sliding on its base. This is usually accomplished by heavy stone placement if the structure is of the cellular sheet-steel pile variety.

Lake Superior

14. In the late 1800's, harbors for the protection of fishing fleets were constructed at many locations along the coast of Lake Superior. At that time, timber was plentiful and relatively inexpensive; and it was not uncommon to find this and other readily available material being used in the fabrication of wave protection measures. Timber cribs were often formed and filled with whatever stone sizes could be obtained locally. Over the years, these structures gradually deteriorated, and maintenance or replacement procedures had to be developed. With a dramatically rising cost of both labor and timber, it was no longer practical to use the earlier techniques. For those locations where the wave climate was sufficiently quiet to permit their installation, sheet-steel pile breakwaters became the accepted method of offering harbor protection. The sheet-steel pile construction is usually built in conjunction with cellular modules that provide stability against sliding, as the sheet steel which forms the outer casing is driven several feet into the foundation and the entire unit is filled with sand and/or rock.

Wave-induced current field
numerical simulation model

10. There is a growing need for generalized numerical models for long-shore currents and nearshore circulation that solve the complete equations of motion, are flexible in the formulations chosen for various terms, and can be applied to actual prototype field situations at reasonable cost. One such model (CURRENT) (Vemulakonda 1984) was developed during the conduct of this investigation, because the removal of material from the near vicinity of major structures is dependent in large part on wave-induced currents. The model was first tested by comparing its results with known analytical solutions and experimental data, for which there was good agreement. The model was next applied to an actual prototype field situation near Oregon Inlet, North Carolina. Here the results appeared to be reasonable and the computational costs were modest.

Predicted scour magnitude

11. Scour and erosion that occur around most open-ocean structures are the results of a combination of current and wave action, to a greater or lesser degree. The forcing functions causing scour and erosion in all cases are the stresses induced by the currents and the incident wave climate. The determination of these forcing functions (unidirectional current magnitudes, wave characteristics of height and period, and wave-induced currents) must be ascertained in the regions where scour can be anticipated before estimates of the ultimate scour magnitudes can be made. Unidirectional current magnitudes (river or tidal) may be determined by appropriate current gaging methods. A detailed determination of the wave field near structures may be obtained by the finite element numerical simulation model (FINITE) that calculates wave heights under combined refraction and diffraction. Wave-induced currents caused by the incident wave climate may be determined by the numerical simulation model (CURRENT) that solves the complete equations of motion. When the incident wave field and the current magnitudes (unidirectional and wave-induced) have been determined, these quantities may be utilized as subsequently discussed in conjunction with results of critical laboratory experiments and precise prototype observations for predicting the ultimate extent of scour and erosion to be expected near coastal structures.

blanket) placed in advance of construction which will ensure its stability during construction. Prior to this time, such guidance did not exist; and consequently, expensive trial-and-error actions were used whenever a structure was constructed. In some instances, construction cost may be much greater than necessary since the material is larger than that required, or it may be placed farther in advance of construction than is necessary. In other cases, the material may be smaller than that required or the spatial extent of its placement ahead of construction inadequate, and scour problems may develop and increase cost. Proper design guidance minimizes costs and ensures stability of the material placed in advance of construction (and thus stability of the sand bottom).

Three-dimensional experimental studies

8. The purpose of the three-dimensional experimental tests was to obtain quantitative and detailed laboratory measures of combined refraction and diffraction in the lee of a jetty or shore-connected breakwater. These measurements included both the wave-height distribution downwave of the structure and the associated wave-induced current field and circulation patterns. These data were also used to verify numerical models that simulate the phenomena. Two different breakwater geometries were utilized in the study. The first consisted of a shore-connected, vertical, thin, impermeable breakwater normal to the shoreline. The second configuration was placed at a 60-deg angle to the shoreline to simulate a larger range of prototype jetties and breakwaters in existence at the present time.

Wave field numerical simulation model

9. Because waves and wave-induced currents play a major role in producing scour and erosion near structures, it is important to be able to predict the wave field in the vicinity of structures. Structures of interest may be complex and the surrounding bathymetry may be very complex. Both long- and short-period waves may attack the structure from many different angles. The purpose of this phase of the research program was to develop a numerical simulation model (FINITE) (Houston and Chou 1984) that can determine wave fields near arbitrary structures in a region of arbitrary and variable bathymetry. The model is capable of simulating both long- and short-period waves approaching structures from any arbitrary direction. In addition, the model is efficient, allowing application to real coastal engineering problems.

Table 1
Estimated Scour Effects at Typical Locations

Project	Estimated Cost due to Scour	Estimated Percent Increase due to Scour	Price Level	Estimated Cost due to Scour in 1984 Dollars*
Murrells Inlet South Jetty	\$ 300,000**	3.0**	1979	\$ 445,631
Baptiste Collette Jetties	449,249†	41.0†	1979	667,331
Tiger Pass Jetties	295,838†	28.0†	1979	439,448
Ventura Marina Breakwater	62,159	4.0	1972	160,728
Dana Point Harbor Breakwaters	515,818	6.5	1970	1,435,609
Ponce de Leon Jetties	1,676,140	73.0	1971	4,469,706
Buffalo Disposal Dike No. 4	699,776	5.0	1977	1,247,820
Colorado River Jetties, Texas	1,477,433††	25.1††	1977	2,634,516
Destin East Pass Jetties	92,623	13.0	1970	257,785
Tillamook South Jetty	1,844,090‡	21.1‡	1972	4,768,375
Total				\$16,526,949

* Based on Consumer Price Index referenced to 1967; The World Almanac and Book of Facts 1984, 1970--0.860; 1971--0.824; 1972--0.799; 1973--0.752; 1974--0.677; 1975--0.620; 1976--0.587; 1977--0.551; 1978--0.512; 1979--0.459; 1980--0.405; 1981--0.368; 1982--0.339; 1983--0.325; 1984--0.309 (based on an assumed inflation rate of 5 percent for 1984).

** Construction still in progress at time of 1979 estimate.

† Includes both scour and foundation settlement effects.

†† Construction actually began in late 1979; scour effects estimated during 1977 planning stage.

‡ Phase I and Phase II.

For those situations where the extension of an existing structure is required across a large scour hole, the technique of "accelerated core placement" has been applied. If the scour hole can effectively be traversed, normal construction procedures are resumed. Nonstructural techniques for estimating additional material to be required as a result of potential scour may be lumped all-inclusively into "experience factors," such as the estimated equivalent uniform scour computations of the US Army Engineer District, Galveston, or the void ratio adjustment determination of the US Army Engineer District, Los Angeles.

5. An indication of the magnitude of the scour and erosion problem can be obtained by analyzing records of both ongoing construction and previously completed projects. Not only will operation time be lost while scour holes are filled with material quantities usually unaccounted for in original estimates, but also the prime stonework contractor may require downtime compensation for those days when stone placement is not possible due to excessive scour and erosion. Documented cost directly attributable to scour and erosion at typical representative locations is presented in Table 1.

Purpose of the Study

6. The objectives of this research were to develop techniques and knowledge for estimating resulting wave characteristics and wave-induced current fields in the vicinity of major coastal structures. This information is required in order to predict the probable magnitude of scour that may result as a function of the wave climate. Both analytical and laboratory experimental studies were conducted during the investigations. The analytical developments regarding wave heights and wave-induced currents were verified by the use of the precise experimental studies of shore-connected breakwaters. Additional underlayer stability experimental studies were conducted for estimating the size of stone comprising the foundation bedding material that would remain stable under various wave conditions.

Two-dimensional experimental studies

7. The purpose of the two-dimensional flume tests conducted as a part of the overall research investigation was to develop equations or design curves that for given expected wave conditions would provide design guidance on characteristics of the underlayer material (stone size and length of underlayer

blanket was composed of tough, durable stone reasonably free from dirt or other foreign particles. The blanket stone consisted of either shell (marine) limestone having a unit weight not less than 118 lb/cu ft saturated dry (specific gravity 1.9) or granite stone having a unit weight not less than 160 lb/cu ft saturated surface dry (specific gravity 2.56). The stone was graded from 2 to 12 in., with a weight gradation of less than 5 lb up to a maximum weight of 100 lb.

40. The contractor at Masonboro Inlet was instructed to conduct his operations in a manner to minimize scour by placement of the foundation blanket at least 200 ft ahead of the underlayer and cover stone. Toe protection measures to eliminate scour and undermining of the structure consisted of stone weighing from 3,000 to 5,600 lb (sta 0+00 to 25+00) with at least 60 percent of the stone weighing 4,600 lb or more. Between sta 8+00 and 13+00, the stone consisted of elements with weights from 5 to 8 tons with at least 75 percent of the stones weighing 6.5 tons or more. Between sta 13+00 and 34+50, the stone consisted of elements weighing from 14 to 22 tons with at least 75 percent of the stones weighing 18 tons or more.

41. Improvements to Oregon Inlet, North Carolina, are in the planning stage and consist of dual stone or dolos jetties extending approximately 6,000 ft from shore. These structures will be constructed on sandy shoal regions, and present plans envision the use of gabions as foundation bedding material. WES was requested to perform both a three-dimensional model investigation (Hollyfield, McCoy, and Seabergh 1983) to aid in determining the optimum length and alignment of the jetties, and a two-dimensional and three-dimensional model investigation (Carver and Davidson 1983) of the stability of the proposed jetties against wave attack.

42. Based on the hydrography and physiography of the region, and on historical data from near localities, conclusions were reached by the US Army Engineer District, Wilmington, regarding the stability tests of the head sections of the jetties. It is believed that after construction of the jetties, the flow fields and current patterns over the bar region will be altered to such an extent that the shoal region will readjust itself to more nearly conform to the offshore topography upcoast and downcoast. This will result in the removal of material for a depth of about 11 ft in the vicinity of the structure head section, and the conclusion was reached that the readjustment will develop on a slope of about 1V on 5H. Hence, the stability tests were

conducted as if the hydrography in the near region of the structure head were readjusted for a depth of around 11 ft, with a resulting 1V-on-5H slope away from the structure to deeper water. An analysis of past wave conditions in the area suggested that a 17.6-ft wave height would be appropriate for a 1-in-50-year stability analysis. Additionally, because of the relatively frequent large storm and hurricane probability for the region, 8-ft storm surges are not uncommon. Therefore the design wave height of 17.6 ft may arrive at either a low water elevation or any other elevation up to the maximum storm surge height. Stability tests of the jetty head were conducted for both breaking and nonbreaking waves using a design wave height of 17.6 ft.

43. Physical model tests were performed at WES by Perry, Seabergh, and Lane (1978) to aid in determining the optimum solution to navigation problems at Murrells Inlet, South Carolina. The final plan included a system of jetties to be constructed across the existing ebb current outflow channel and onto a shoal region. The north jetty was completed in early 1979 and included a foundation blanket of filter material for bearing strength and erosion control. Scour was minimal to nonexistent during construction of this north jetty.

44. Construction of the south jetty was initiated upon completion of the north jetty in February 1979. Since the south jetty was planned to be constructed across the existing ebb channel and onto the offshore shoal region, it was necessary to excavate some areas in order to reach the design grade for the structure foundation. The operational procedure for keeping a trench open long enough to physically place two or three grades of stone (developed from the best available design guidance) is difficult at best; hence, it was anticipated (desired) that as construction of the south jetty proceeded from the south shoreline across the ebb channel, beneficial scour would result. A 2-ft-thick foundation blanket was designed to support the core stone, and the initial placement was uneventful. It was expected that as closure of the channel proceeded, the reduced cross-sectional area for flow would experience an increased current velocity sufficient to initiate sediment movement and assist in the necessary excavation of the shoal. Since the shoal was visible at low tide but was not exposed at high water, it was necessary to excavate about 2 ft of material to reach the design grade for the south jetty. It was estimated that as construction proceeded across the ebb channel, shoal erosion of 8 to 10 ft might occur on the shoal slope until the ebb discharge

could redistribute and become concentrated in the new relocated navigation channel.

45. Scouring action that resulted from partial closure of the ebb channel was more severe and intense than anticipated, and the channel bottom scoured to approximately 5 ft below the design grade for the structure. More importantly, the ebb current was so intense that the foundation bedding material, which was being placed in the channel, would not remain long enough for the stabilizing core stone to be placed. Emergency operation procedures were initiated when it became apparent that ordinary construction techniques would not be sufficient to permit further placement of structure material. It was necessary to divert the dredging operation to provide fill material by pumping sand along and in front of the new jetty section. This action was successful to the extent that the contractor was able to proceed with construction as the pumping and filling operations were able to stay ahead of the stone placement.

46. The problem of crossing and closing a channel containing a strong tidal current is indeed a unique construction operation, and one for which the usual scour control techniques may not be entirely successful. This situation is somewhat similar to the Netherlands problems of closure of large estuaries on the North Sea. However, those dike construction projects are enormous in magnitude; and that nation is mobilized sufficiently to combat the problems whereas smaller contractors working on smaller individual projects may be required to devise new techniques on a site-to-site basis as the need arises, based on the recommendations of van Heemskerck (1963).

47. The most recent jetties structures constructed along the Florida east coast were the north and south jetties at Ponce de Leon Inlet, approximately 100 miles south of Jacksonville, completed in 1972. Construction was initiated without design of a foundation blanket. Scour on the order of 10 ft occurred as construction proceeded seaward, and material overruns as much as 300 percent were experienced along some sections of the jetties. A foundation blanket design was subsequently added to the contract and alleviated most of the scour problems.

48. Actually, scour was not an uncommon occurrence when the first jetty construction projects were undertaken in this region. Contractors were accustomed to the necessity of having to place additional material to account for the development of a scour hole. Originally, cypress mats were fabricated and secured on the bottom with large stones. The graded rock filter foundation

blanket was introduced later. When a tidal hydraulic head of 2 to 3 ft exists across an inlet connecting a fairly large estuary to the ocean, velocities of about 6 to 9 fps are not uncommon, and observations indicate that scour holes may develop which approach 12 to 15 ft in depth. Early contractors were believed to have unbalanced their contract bids on jetty projects; i.e., they appeared to bid a relatively low unit price on the core and cover stone, but the bid price of the foundation bedding layer would be unusually large in the anticipation that large quantity overruns would be necessary to fill scour holes. However, the philosophy of the time was that the additional material required to fill scour holes actually contributed to a much stronger and more stable structure.

49. A "rule of thumb" to estimate the expected scour over a long period of time near reflecting structures (USAEWES 1984) is that the maximum depth of a scour trough below the natural bed is about equal to the height of the maximum unbroken wave that can be supported by the original depth of water at the toe of the structure. This is occasionally interpreted as the maximum scour depth to be expected should be of the same order of magnitude as the significant wave height that occurs during storms at the local area.

Gulf of Mexico

Eastern gulf coast region

50. Several project studies are being evaluated for this area between Key West, Florida, and the Mississippi coast that may require jetties or other major stone structures. In general, the low wave energy and the undeveloped nature of portions of this region have historically not required such works. Construction and continued maintenance of jetties and weir-jetty systems have been required along the coast of northwest Florida from Apalachicola Bay to Perdido Bay, Alabama. Rehabilitation is required as periodic inspections reveal that the continual wave attack, even though the waves are relatively mild, causes the cover and core stone to shift and settle; and this combined with foundation movement produces damage factors sufficient to require maintenance procedures to be employed. Most of this work is conducted with barge-mounted draglines.

51. During rehabilitation work where required, and on all new stone construction projects, the procedure and technique developed by the US Army

District, Mobile, is first to place approximately one-half of the foundation blanket material thickness, and subsequently to place a second layer comprising the second half of the blanket. The purpose of this procedure is to initially stabilize the sand bottom by reducing the amount of time that the end section of the foundation layer is exposed to wave attack; e.g., scour is always expected at the tip end of the foundation blanket and the intent is to minimize the time required to lay a specified length of blanket, usually 50 ft. Associated with this practice is the philosophy that successful contractors simply do not try to work in adverse wave conditions. The foundation blanket material usually consists of quarry-run stone which varies in size from 5 to 200 lb.

52. Similar weir-jetty systems have been constructed at Perdido Pass, Alabama, and at Destin East Pass, Florida. These are both converging, arrow-head type jetty configurations, but the weir section is in the east jetty at Perdido Pass and is located in the west jetty at East Pass. The wave climate of the region is such that there is believed to be a reversal with season in the direction of littoral transport, and the direction and magnitude of the net annual drift are subject to considerable debate. The consensus of opinion in the engineering community is that the direction of net transport, on an annual basis, is probably west at Perdido Pass and is probably east at East Pass. Hence, the purpose of the weir location is to intercept a significant portion of the net transport and prevent it from penetrating the navigation channel, and the converging jetty alignment is designed to permit flow of littoral material around the end of the jetties (that which does not pass over the weir). That sand which passes over the weir section is intended to be collected in a deposition basin so the dredge can operate in a relatively calm area.

53. No unusual scour problems occurred during construction of the jetty system at Perdido Pass. However, problems of a significant nature existed at Destin East Pass; and they may be attributed in part to scour and erosion effects and in part to improper construction techniques on the part of the contractor. The weir design specifications required the erection of concrete sheet piles driven 8 ft into the foundation and stabilized by massive timber wales that were bolted together. Construction problems began to occur when it appeared that some of the connecting bolts were not threaded enough to provide a rigid member. Waves breaking onto the sheet piling caused separation of

some of the piles sufficient to allow currents and littoral material to pass, and scour holes up to 14 ft deep developed at the weir. Ebb currents on the order of 6 to 10 fps were not uncommon. Excessive torque developed in the wales, bolts sheared, and 100 ft of the weir section collapsed into the scour hole. The damaged section of the weir jetty was repaired by construction of a rubble-mound section instead of the originally designed concrete sheet piling.

Louisiana coastal region

54. Coastal problems of the State of Louisiana are so distinctly different from those of other regions that they merit special investigations and unique solution processes. This is the region that has produced the greatest change in planform in recent times, and these changes are directly the result of the Mississippi River. This is one of the world's largest river systems and transports a tremendous sediment load. When this huge river reaches the Gulf of Mexico, the sediments carried as suspended and bed load are deposited. Much of this deposition takes place in the form of a bar at the mouth of the river, but many of the fine materials in suspension are swept away by the gulf currents and carried many miles before settling out. The delta area thus being formed extends into the Gulf of Mexico beyond the general coastline. Marshy and swampy areas cover much of this coastal region and the materials are generally highly unconsolidated.

55. Maintenance of sufficient navigation depths on the Mississippi River from Baton Rouge to the gulf is an undertaking of major importance. The Port of New Orleans, which is about 95 miles above the Head of Passes on the Mississippi River, is the second largest port in the United States in waterborne commerce. Authorized channel dimensions from New Orleans to the gulf are: New Orleans to Head of Passes, 40 ft by 1,000 ft; Southwest Pass, 40 ft by 800 ft; Southwest Pass bar channel, 40 ft by 600 ft; South Pass, 30 ft by 450 ft; and South Pass bar channel, 30 ft by 600 ft. A seaway canal, the Mississippi River Gulf Outlet (MRGO), from New Orleans to the gulf along a shorter route has also been constructed with authorized dimensions of 36 ft by 500 ft. All these passes require extensive and significant structural measures for their stability and functional effectiveness, including headland dikes, spur dikes, bulkheads, revetments, and jetties. Additional outlets south of Venice, Louisiana, will be provided by enlargement of the existing channels of Baptiste Collette Bayou, Grand, and Tiger Passes.

56. The structure-foundation problems of the US Army Engineer District,

New Orleans (LMN), are in many cases associated with current and wave conditions occurring at the time of construction. In other situations, unidirectional river currents combined with ship waves, and occurring over long periods of time, gradually undermine many stabilizing structures and extensive rehabilitation is necessary. LMN is actively engaged in experimental programs of significant magnitude to evaluate different scour control and foundation settlement reduction techniques. Among these are foreshore revetment materials that have not previously been used and combinations of filter fabrics and placement of filter fabrics at different locations within rock structures. To ascertain the effectiveness of these prototype experimental studies, LMN will conduct annual surveys on all foreshore rock work presently under construction or which will be constructed in the future where there are test sections of different foundation techniques. Profiles and cross sections of this and all offshore jetties also will be obtained.

57. Grand Isle is located on the gulf, and is one of the many low, irregular islands separated by bays, lagoons, and bayous that form such a large part of the shoreline of Louisiana. It is a base of operation for large offshore petroleum and sulphur industries and is a commercial fishing and sport fishing center. Because of Grand Isle's location and topography, improvements on the island are subject to damage from erosion along its gulf shore and from the combined effect of winds and surges generated by hurricanes. In recent years, severe scour has occurred on the west end of the island. The first effort to solve this problem was construction of vertical sheet-steel pile bulkheads to stabilize the location of the shoreline. These reflecting walls agitated the situation and the scour and erosion became much more severe. Finally, a rock jetty structure was built on the west end of the island that has minimized the excessive erosion.

58. Baptiste Collette Bayou is located east of Venice, Louisiana, and extends from the Mississippi River to Breton Sound. The navigation channel had been previously constructed, and the work submitted for bids in late 1978 consisted of furnishing and placing approximately 41,000 cu yd of shell and approximately 83,000 tons of stone at specified marine locations in Baptiste Collette Bayou, including the designated test areas where the addition of approximately 15,000 sq yd of synthetic filter fabric was to be placed for test purposes. Soil borings of the area indicated that the foundation is almost entirely gray, soft to very soft, oxidized, fat, inorganic clay of high

plasticity. Six different tests are being conducted in four different test sections, two sections in each of the east and west jetties. The purpose of this experimental prototype testing is to determine which combination of filter fabric, location of filter fabric, and stone sizes successfully and significantly reduces the amount of settlement into the relatively unconsolidated foundation.

59. The largest overrun of quantities was experienced for the main armor protection of graded Stone B at Baptiste Collette Bayou, Grand, and Tiger Passes which was 2 ft thick on the typical cross sections. The specifications allowed for a 12-in. tolerance in placing stone beyond the cross section. This alone could account for a 50 percent increase in the Stone B quantities. Detailed records of settlement during construction are not available; however, field inspection indicated that the jetty exceeded the minimum elevation in several reaches, but also experienced significant subsidence up to 7 ft in some reaches. It is the opinion of LMN that portions of the overrun may be attributed to rock tolerance specifications. The large armor rocks could have caused settlement although no data are available from settlement plates during construction. Settlement plates have now been installed in the center line of both jetties approximately every 500 ft for the purpose of accurately determining the effectiveness of each variation in test section of the Baptiste Collette Bayou experimental prototype jetty investigation.

Western gulf coast region

60. The physiography of the Texas coastline is such that a wide continental shelf exists along the northern sections of the State, decreasing in width in a southerly direction. The effect of this variation in shelf topography is to allow the deepwater wave energy to propagate closer to the coastline in a relatively undiminished state. At the same time, the sediments comprising the foundation material in the northern parts of the State are much finer and more unconsolidated than the sandier deposits that exist farther south. These situations are compensating to the extent that while the scouring may be less in the northern regions of the State, the displacement due to settlement will probably be greater.

61. The US Army Engineer District, Galveston, has found from many years of experience that the additional materials needed to provide final grade to massive rock structures are the result of a combination of "displacement and scour." On the average, the determination of this combination from historical

records has provided the approximation factor to estimate quantities of structure material along the Texas coast without the necessity of decomposing the material overruns from past work into "displacement effects" and "scour effects." The application of this "displacement and scour" adjustment factor is then applied to the template estimates.

62. The procedure developed for this region is to compute the quantities of material to be advertised for bids as that which would exist above a hypothetical groundline uniformly 3 ft below the actual groundline, and extending from the surf zone to the end of the structure in a seaward direction. Because this additional 3 ft of height will require the structure side slopes to generate a wider base, all quantities will theoretically be affected. Hence, the core stone and armor stone estimates are increased accordingly. It has been learned that when working conditions are good, the rate of construction progress will be rapid enough so that the amount of scour or displacement in front of the structure will not exceed 3 ft. However, when conditions are inclement or contractor construction procedure contributes to less than satisfactory rates of progress, there may be sufficient time for larger scour holes to develop.

63. Foundation blanket stone is always designed for placement under stone structures for bearing and scour control. The blanket is composed of quarry-run stone, reasonably well graded and varying in size from 1/2 in. to 200 lb. The thickness of the blanket is designed to be 3 ft under the trunk section of the jetties or breakwaters, increasing in thickness to 5 ft under the head section.

South Pacific Region

64. Along the Pacific coast of the United States, there are problems quite unlike those that dominate the Atlantic and gulf regions. The shoreline is largely cliffed coasts with rocky promontories, and cliff erosion which was practically unknown in other localities becomes a significant source of beach material. The coastline of the State of California can effectively be considered as an entity, although the physiographic and climatological characteristics begin to change north of Cape Mendocino, approximately 100 miles south of the California-Oregon border. In this northern extremity, the dry summers come to an end and the annual rainfall increases to around 10 times that which falls in San Diego.

Southern California

65. The coast of southern California south of Point Conception is shielded to a considerable degree by the group of eight offshore islands that are separated from the mainland by deep water. The sheltering afforded by these islands protects the mainland coast from a portion of the deepwater wave energy propagating toward shore; thus the wave climate on the beach is significantly less than that for those regions north of the Point. White sandy ocean beaches and steep coastal cliffs rising from the sea make this a land of great contrasts. Because ocean waters are warm enough for water-contact sports throughout the year, ocean-oriented sports are a way of life for a large part of the population. Eight small-craft harbors have been constructed in the region, although some reaches of the coastline between all-weather harbors exceed 35 miles, which is the spacing considered desirable by the State for small-craft harbors of refuge. Erosion along this region is a continuing problem. Only about 27 miles of the 233 miles of shoreline is considered stable by the US Army Engineer Division, South Pacific (1977), with the remaining shoreline being eroded at varying rates. Critical erosion is taking place along 160 miles of the shore and threatens highways, homes, businesses, and recreational beaches.

66. The US Army Engineer District, Los Angeles (SPL) encompasses essentially all of the south coastal basin, where major stone structures consist of jetties, shore-connected and offshore breakwaters, and groins for beach stabilization. The problems associated with surf zone and open-ocean construction have been known to include scour and erosion effects ever since the necessity arose for this type of endeavor. In past years, foundation bedding material was not used, and the core stone would slump and settle into the sandy foundation. Since each individual project was unique in this respect, the technique of on-the-job problem solving was considered a requirement for doing business. The successful contractors developed a significant amount of expertise, and it has been determined that the equipment operators make a considerable difference regarding the degree of difficulty encountered in construction operations. Over the years, the use of foundation bedding material evolved, so that it is now standard procedure to incorporate this feature into the design requirements. Historically, filter fabric has not been used, although it is now being considered in the design of pending structures. It is recommended that when filter fabric is used, a layer of quarry-run stone be

laid on top of the fabric to minimize the probability of large stones tearing the membrane.

67. Since it is known that scour during construction will increase the volume of stone required relative to that determined by template projections, SPL compensates for this increase by using a correction factor based on an analysis of past stone construction contracts. It has been observed that the final payment quantities are, in general, a function of the void ratio of the structure and of specific gravity or unit weight of the rock. Quantities of material are usually computed based on a void ratio of 35 percent and a unit weight of 165 lb/cu ft. This consistently results in final quantities approximately 10 percent greater than estimated. It has been determined that estimates based on a void ratio of 26 percent and a unit weight of 170 lb/cu ft will predict final quantities approximately equal to that actually placed. While this procedure does not solve the problem of scour during construction, it is apparently a very good operational solution for avoiding unanticipated cost overruns due to scour during construction.

68. Rip currents resulting from wave energy typically develop along the toe of groins or breakwaters, and frequently a 2- to 4-ft-deep scour area develops overnight and can be observed in the mornings before construction resumes. To minimize this problem, an operational procedure has evolved that consists of placing an additional 20 to 40 ft of foundation bedding material in front of the core stone and cover stone at the end of the day. The specific distance is usually determined by the size and reach of crane available for the construction job. Larger cranes working from the structure crest can place a 30-ft section of foundation bedding material ahead of the core. This procedure tends to reduce the amount of scour that would otherwise occur. SPL believes that the additional material required to fill scour holes adds to stability of the structure by providing a better foundation.

69. In southern California, it is usually necessary to work on coastal construction projects after the major tourist season. When advancing from shore, it is also expedient to work with the tide, at least through the surf zone. If the foundation blanket material is placed at low tide, the cover stone can be placed before significant movement occurs. The philosophy of SPL is that the bedding material is the foundation of the whole structure; therefore it is desirable to have plenty of bedding stone, probably 2 ft thick and extending beyond the toe of the structure on each side for approximately

5 ft. Side slopes of the structure are dependent on the precise design and type of cover material. The contractor should be encouraged to use an adequate amount of stone to make sure that the template projections are satisfied.

Central and northern California

70. While the number of coastal structures in this region is less than those in southern California, because of the more severe wave attack, the problems arising from scour and erosion during and after construction may be more significant than those to the south. The large wave heights and long periods are capable of disturbing bottom particles at greater depths than that experienced elsewhere; and strong tidal currents, particularly at Humboldt Bay, can displace the material and undermine the toes of structures. In order to properly design for the scour effects, it is necessary to know both the wave and current energy fields on both sides of breakwaters and jetties.

71. Humboldt Harbor is located on a land-locked bay at Eureka, California, about 225 miles north of San Francisco. Improvements to the harbor were first authorized in 1881; and the project consists of nearly 2 miles of jetties, assorted channels, and turning basins. The jetties are exposed to storm waves originating from the south-southwest to north. Deepwater wave hindcast statistics for this region indicate that a significant wave height of 34 ft and a period of 13 sec will occur occasionally. Because of the effects of refraction by the underwater topography, this significant wave height may be amplified to around 40 ft at the structure.

72. The north and south jetties at Humboldt Bay have been damaged and repaired several times since their initial construction. Large monolith concrete features were added to the north and south jetties in 1961 and 1963, respectively. Limited amounts of armor protection were provided to the south jetty with the placement of 256 unlinked 100-ton concrete cubes. The north monolith was undermined by scour, broke into several large irregular blocks, and gradually deteriorated due to the forces of the wave action. The south monolith also became badly damaged and the 100-ton cubes were displaced. The water depths at the head of the jetties are such that 40-ft-high waves can break directly on the structure. The head section of the jetties deteriorated severely in the mid-1960's, and WES (Davidson 1971) was requested to perform a physical hydraulic model study to determine, among other things, the optimum shape of the armor units that will be stable for the selected design wave conditions. The final section used for the repairs, based on this model study,

consisted of 42-ton dolosse forward and 43-ton dolosse toward the trunks of the heads.

73. Concern has arisen over the years regarding the stability of the south jetty. Deep scour pockets occasionally develop along the inside as a result of wave energy penetration through the entrance and a strong ebb current regime. Scour holes up to 50 ft deep have been detected, and past endeavors during rehabilitation efforts have resulted in extension of the toe and the base slope has become flattened. As a result of these actions, the scour appears to have lessened and channel migration is now at an acceptable magnitude. The series of severe storms which devastated the entire coast of the State of California during the early months of 1983 caused the most recent movement of armor stone and dolosse, and these current problems are in the process of being repaired.

74. The Half Moon Bay structures consist of two breakwaters that form a protected harbor for commercial fishing vessels and recreational craft. As a remedial measure to eliminate excessive surge, construction of a 1,050-ft extension to the west breakwater was completed in 1967. Fifteen- to twenty-foot waves that occurred at the entrance caused a Mach-stem effect which was felt all the way to the bottom of the bay along the breakwater. The 4-ft-high waves that existed adjacent to the breakwater were sufficient to cause scour of the toe of the structure, and the side slopes have steepened as armor has settled into the holes. Core stones have settled and large cavities up to 13 ft deep have developed along the center line of the structure with the shell remaining essentially intact by arching.

75. Rehabilitation of the toe scouring problems at Half Moon Bay was accomplished in 1978 by the placement of foundation bedding material where necessary and 6- to 20-ton cover stone where appropriate. The bedding material size varied from a No. 4 sieve to 6-in. size particles. The irregular holes in the breakwater crest were from 3 to 13 ft deep, with widths from 2 to 4 ft and lengths from 2 to 6 ft. The holes were repaired with concrete, cast in place in synthetic filter cloth membrane bags. In holes shallower than 6 ft, one unit was cast; in holes deeper than 6 ft, two units of approximately equal volume were cast, one on top of the other. In order to adequately anticipate scour and erosion problems that may occur at Half Moon Bay in the future, knowledge of the wave and current conditions inside the channel and harbor after crossing the bar is desirable.

76. The philosophy of the US Army Engineer District, San Francisco, regarding the control of scour and erosion during coastal construction may be summarized in the following two statements: (a) on foundations of thick, loose, sandy material, always use foundation blanket material (graded) extending for a distance of 5 ft beyond the toe of the structure; (b) on foundations of thin, loose, sandy material, excavate any loose material down to a firm foundation before the placement of any stone.

North Pacific Region

77. The coastlines of the States of Oregon and Washington probably come closer to being in their natural state than any other section of coastline in the continental United States. No large cities and only a few small towns overlook the shore as the major cities have been situated farther inland on the rivers such as the Columbia or on the shores of Puget Sound. The reason for this, according to Stambler (1972), is the trend toward colder temperatures, damp overcast skies for a large portion of the time, and fierce storms in winter. This region is, therefore, less attractive for both large resort towns and seaports than the gentler regions to the south.

78. The character of the coastal region completely changes beyond Cape Flattery, at the entrance to the Strait of Juan de Fuca. This strait is the southernmost of the deep glacial troughs that continue northward toward Alaska. While the strait separating northern Washington State from Vancouver Island is quite uniform, the eastern reaches known as Puget Sound consist of a series of intricate embayments and numerous passages between the San Juan Islands; and this produces a coast more irregular than encountered elsewhere. This glaciated area has an abundance of natural shelters for all boats, unlike the absence of many natural harbors on the Pacific Ocean coasts.

Northwest coastal area

79. Probably the most severe case of scour during construction ever experienced occurred while building the south jetty at Tillamook Bay entrance channel. The south jetty was designed to extend from the shore across a flood channel and onto a large shoal region. It had been anticipated that 3 to 5 ft of scour could result from the wave climate known to exist in the area and because of the effect of the strong tidal current. As jetty construction progressed across the flood channel, scour and erosion began to undermine the end

propagate along the major axis of the structure. A two-dimensional section of structure was placed in the wave basin with a length sufficient to ensure that wave energy would not penetrate through the structure and be reflected from the rear of the basin. It was desired that the wave energy which penetrated the core of the structure be effectively dissipated internally within the structure. Kenulegan's (1973) expressions for wave dissipation inside porous structures indicated that any section of structure in excess of 10 ft would dissipate over 99 percent of the wave energy approaching the structure (i.e., essentially no fluid motion would be detected within the structure at a distance of 10 ft from the incident face). The test structure was placed on a nearshore beach slope of 1V on 25H, which was considered typically representative of many coastal zones. This also provided a shoaling region whereby the waves of various periods could be forced to break directly at the toe of the structure, as this had been determined to be the situation of most severe condition.

Wave flume

110. This experimental study was conducted in a two-dimensional wave flume 120 ft long by 6 ft wide by 6 ft deep (Figures 4 and 5). The concrete flume was modified by the installation of a beach with a slope of 1V on 25H to simulate representative prototype conditions and to facilitate the breaking wave phenomenon under investigation. The test structure was placed on the concrete slope at the end of the flume.

Wave generator

111. A dual channel irregular wave generation system had previously been installed in the wave flume and was used to generate the monochromatic waves utilized in this study. The wave generator consisted of: (a) a rotational actuator assembly with a 6-in. stroke and a dynamic force of 2,500-lb tension or 7,000-lb compression; (b) a translational actuator assembly with a 6-in. stroke and a dynamic force of 2,500-lb tension or 7,000-lb compression; (c) a hydraulic power supply system providing 10 gpm at 3,000 psi; (d) a wave-board system provided both translation and rotation capabilities, either independently or simultaneously; and (e) an electronic console system providing variable controllers and accelerometer conditioners. The wave generator equipment can be programmed with both analog and digitally generated random data; therefore the equipment will reproduce waves that vary from cycle to cycle in both amplitude and period. The wave-board motion does not vary in

-1.5H should have a minimum of two thicknesses of quarystone; these should weigh about 1/20 the overlying secondary armor unit (W/300). The second underlayer for that part below -1.5H, and the core and bedding layer material, can be as light as W/6,000, or quarry-run stone.

Experimental Parameters

107. It is apparent that the composition of the material comprising the core of a rubble-mound breakwater or jetty can vary over a large range of values without affecting the structural integrity of the system. Considering the range of test breaking wave heights up to 1.8 ft, the maximum prototype breaking wave height that could be tested under a representative linear scale ratio of 16-to-1 is 28.8 ft. Prototype core material corresponding to this wave height could vary over a range of values from 15 to 1,500 lb. The structure was not intended to transmit wave energy; hence the test structure specifications were not overly restrictive in adhering to scaled prototype rock size gradation as the bulk of the material was placed for structure volume filler substance. Because of the orientation of the test structure for these specific purposes, it was necessary, however, to ensure that a sufficient section of structure was being modeled to preclude any transmitted wave energy along the major axis to the rear of the section (in this case, through the structure).

108. The minimum weight stone existing in the prototype structure (15 lb) can be effectively represented as a cube of side length 5.4 in. Based on LeMéhauté (1965) and Keulegan (1973) scaling relations, a 50 percent increase in the test linear scale will preclude significant scale effects. This indicates that a test core material with a representative dimension of 8.0 in. prototype (0.5 in. model) and a 16-to-1 linear scale ratio will satisfactorily comprise the core of the model structure. A composite material mix with a 50 percent finer by weight of 0.5 in. was formulated ($d_{50} = 0.5$ in. model = 8.0 in. prototype = 50 lb prototype).

Experimental Facilities

109. The physical tests were operated under the assumption that waves would approach directly perpendicular to the offshore contours and would thus

Structure Cross Section

104. A rubble structure is normally comprised of a bedding layer and a core of quarry-run stone covered by one or more layers of larger stone, and an exterior layer(s) of large quarrystone or concrete armor units. The thickness of the cover layer and the number of armor units required can be determined from USAEWES (1984) as:

$$r = nk_{\Delta} \left(\frac{w}{w_r} \right)^{1/3} \quad (2)$$

where

r = average cover layer thickness, ft

n = number of quarrystone or concrete armor units in thickness comprising the cover layer, dimensionless

k_{Δ} = layer coefficient obtained from Table 1, dimensionless

W = weight of individual armor units, lb

w_r = unit weight of armor unit, lb/ft³

Primary cover layer

105. The stability of armor units is related to the design wave height, H , and other parameters according to the stability formula, Equation 1, which is based on the results of extensive small-scale model testing and some preliminary verification by large-scale model testing. Equation 1 is intended for conditions where the crest of the structure is high enough to prevent major overtopping.

Underlayers and bedding layer

106. The first underlayer (directly beneath the primary armor units) should have a minimum thickness of two quarrystones ($n = 2$), and these should weigh about 1/10 the weight of the overlying armor units ($W/10$). This applies where: (a) cover layer and first underlayer are both quarrystones, or (b) first underlayer is quarrystone and the cover layer is concrete armor units with a stability coefficient $K_D \leq 12$. When the cover layer is of armor units with $K_D \leq 20$, the first underlayer quarrystone should weigh about $W/5$, or 1/5 the weight of the overlying armor units. The second underlayer for this part of the structure should have a minimum equivalent thickness of two quarrystones; these should weigh about 1/20 the weight of overlying quarrystones ($W/200$). The first underlayer for that part below

coast of the United States, the weather pattern is more uniform, and severe storms are likely to occur each year. The use of H_s as a design wave height under these conditions could result in extensive annual damage and frequent maintenance because of the higher frequency and duration of waves greater than H_s in the spectrum. Here, a higher design wave of about H_{10} may be advisable. (H_{10} is the average of the highest 10 percent of the waves, whereas H_s is the average of the highest 33 percent of the waves at a given location.)

103. The selected design wave is used to determine the weight, W , of the cover layer of armor units as:

$$W = \frac{\omega_r H^3}{K_D (S_r - 1)^3 \cot \theta} \quad (1)$$

where

- W = weight of an individual armor unit in the primary cover layer, lb
- ω_r = unit weight of rock, lb/ft³
- H = design wave height at the structure, ft
- K_D = stability coefficient that varies primarily with the shape of the armor units, roughness of the armor unit surface, sharpness of edges, and degree of interlocking obtained in placement, dimensionless
- S_r = specific gravity of armor unit relative to the water at the structure ($S_r = \omega_r / \omega_w$), dimensionless
- ω_w = unit weight of water, lb/ft³ (fresh water = 62.4 lb/ft³, seawater = 64.0 lb/ft³)
- θ = angle of structure slope measured from horizontal, deg

The experimental facilities utilized in this study could produce a range of breaking wave heights up to a maximum of 1.8 ft. By considering a prototype-to-model linear scale ratio of 16 to 1, the maximum prototype wave height that could be tested was 28.8 ft. For rough, angular, quarystone armor units of two layers thickness placed randomly, a suggested K_D value for no-damage criteria and minor overtopping is 3.5. The core and bedding layer for a rubble-mound section with breaking wave conditions and moderate overtopping may consist of material that varies from $W/200$ to $W/4,000$. These data indicate that the dimension of the model core material should be $d_{50} = 0.50$ in. A material mix for this purpose was formulated to this specification.

the bottom, the rubble will settle into the sand until it reaches the depth below which the sand will not be disturbed. Large amounts of material may be required to allow for this loss during construction.

Design Wave Selection

100. The choice of the design wave height depends on whether the structure is subjected to the attack of nonbreaking, breaking, or broken waves, and on the geometrical and porosity characteristics of the structure. The type of wave action experienced by a structure may vary with position along the structure and with water level and time at a given structure section. For these reasons, wave conditions should be determined at various points along a structure and for various water levels. Critical wave conditions that result in maximum forces on structures such as groins, breakwaters, or jetties may be found at a location other than the seaward end of the structure.

101. If breaking in shallow water does not limit wave height, a non-breaking wave condition exists. For nonbreaking waves, the design height is selected from a statistical height distribution. The selected design height depends on whether the structure is defined as rigid, semirigid, or flexible. For flexible structures, such as rubble-mound structures, the design height is usually taken as the yearly significant wave height, H_S^* (USAEWES 1984), where H_S is the average of the highest one-third of waves in a storm. Waves higher than H_S impinging on flexible structures for short durations of time seldom create serious damage although some stone may be displaced (rehabilitation is relatively easy to perform).

102. Damage to rubble-mound structures is usually progressive, and an extended period of destructive wave action is required before a structure ceases to provide protection. It is therefore necessary in selecting a design wave to consider both frequency of occurrence of damaging waves and economics of construction and maintenance. While hurricanes occasionally (although infrequently) occur along the Atlantic and gulf coasts of the United States, it may be uneconomical to build a structure that could withstand hurricane conditions; hence H_S is a reasonable design wave height. On the North Pacific

* For convenience, symbols are listed and defined in the Notation (Appendix A).

PART III: STABILITY OF UNDERLAYER MATERIAL

97. Because of the extensive utilization of an underlayer blanket of foundation bedding material ostensibly for the purpose of scour and erosion control during nearshore construction, an experimental study was performed to investigate the functional relation existing between the size of the underlayer material and the pertinent physical parameters influencing its stability.

98. The purpose of this study was to develop equations or design curves that for given expected wave conditions would provide design guidance on characteristics of the underlayer material (stone size and length of blanket) placed in advance of construction that ensure its stability during construction. Presently, there is no guidance, and consequently, expensive trial-and-error actions must be used whenever a structure is constructed. In some instances, construction cost may be much greater than necessary since the material is larger than that required or placed farther in advance of construction than is necessary. In other cases, the material may be smaller than that required or the spatial extent of its placement ahead of construction inadequate, and scour problems may develop and increase costs. Proper design guidance minimizes costs and ensures stability of the material placed in advance of construction (and thus stability of the sand bottom).

General Considerations

99. A rubble structure is composed of several layers of random-shaped and random-placed stones, protected with a cover layer of selected armor units of either quarriestones or specially shaped concrete units. Armor units in the cover layer may be placed in an orderly manner to obtain good wedging or interlocking action between individual units, or they may be placed at random. Wave action against such a rubble structure will often scour the natural bottom and the foundation of the structure, even at depths usually considered unaffected by such action. A foundation bedding of underlayer material should be used to protect the structure from undermining except: (a) where depths are many times greater than the maximum wave height, or (b) where the bottom is a hard, durable material such as bedrock. When large quarriestones are placed directly on a sand foundation at depths where waves and currents act on

to provide adequately for the structure safety but at the same time to avoid excessive and costly overbuilding.

and construction operations. Scour is a serious problem at shore protection project sites in Hawaii (as well as American Samoa, Guam, and the Northern Mariana Islands). While the effects of flood and ebb currents discharging through estuary inlets are virtually nonexistent in the Islands, exceedingly severe wave climates frequently occur; and the accompanying structural damage combined with undermining and erosion of the toe by wave-induced currents can produce complete failure of the structure. The construction procedure practiced by the US Army Engineer Division, Pacific Ocean (POD), is to essentially bury the toe of the structure. This is accomplished by excavating a trench in those situations where the material is not being moved by the naturally existing forces, usually 2 to 6 ft deep, and building the base of the structure in this excavation. In some cases, this can be difficult and costly as the newly excavated material may try to return to the cavity; in other situations, the current-induced scour tends to assist the operation by removing portions of the loose material. POD philosophy regarding scour and erosion during construction of major breakwaters or jetties can be summarized as follows: generally, an attempt is made to place the toe on solid reef rock or basalt. Where the shoreline is sandy and no solid substrate is near the surface, excavation is performed as deep as practicable (about 6 ft in sand) to place the toe of the structure below the anticipated scour depth. In addition, the toe stone is extended seaward to reduce the impact of toe scour on the stability of the structure.

95. A good example of burying the toe of a structure is the Kekaha shore protection project on the Island of Kauai, under construction in 1980. This project consisted of 5,900 ft of rubble placed on a sandy foundation with a history of serious erosion. The revetment crest elevation is +12 ft mllw, and was constructed to a 1V-on-1.5H slope with two layers of 2- to 4-ton armor over a bedding underlayer of spalls which range up to 500-lb stone. The toe was excavated to -6 ft mllw with a 12-ft-wide bench of armor stone and underlayer extending seaward.

96. Often only localized pockets of sand exist in the vicinity of coral reefs, or perhaps a thin veneer of sand covers the reef. Under these conditions, the sandy material is removed all the way to the reef or otherwise solid foundation. It is desirable that guidance be specified regarding the depth of penetration necessary for structures on thick sand or regarding the degree and extent of toe protection on thin layers of sandy material in order

change would cause a decay in the magnitude of the current, at which time construction would resume and work would continue as far as possible before an increased tidal current again made construction advancement impossible. By scheduling the hours of contractor operation in this manner, it was possible to extend the training dike across an area of strong tidal currents with only minimal loss of material due to scour or erosion during the actual construction operation.

92. Other unique construction elements have been utilized as temporary solutions until the permanent situation could be finalized in Alaska. For example, operations are frequently conducted on frozen soil or under icy conditions where a quagmire would otherwise prevent any progress from being accomplished. Under other circumstances at Fairbanks, it was required to divert the river into a new channel. Problems arose with preventing the flow from continuing down the old channel even after the cutoff plug had been removed. In this situation, large chunks of ice were placed into the old existing channel and covered with mud and soil and successfully served as channel blockage temporarily until the permanent levee could be installed. These solutions are unique to the State of Alaska, where the problems are dissimilar from those of the other states; hence, these techniques probably cannot be extrapolated elsewhere, nor can solutions to problems in the other states necessarily be expected to be viable in Alaska.

Hawaii

93. The beaches of the Hawaiian Islands are composed primarily of remains of organisms that lived in the sea, and are often called coral sand beaches, although coral is only one constituent and basaltic material is part of the composite. This beach sand has a lighter unit weight and the grain size is more rapidly reduced by abrasion than the quartz and feldspar sands that are commonly found on most other beaches of the world. Most of the Hawaiian Islands are subject to serious erosion and the most famous, Waikiki Beach, is at present largely artificial.

94. The problem of scour and erosion of sandy or otherwise unconsolidated material has been a continuing (although not extremely serious) problem at most Hawaiian Island sites where breakwaters and jetties have been constructed or are being planned, from the standpoint of both design procedures

disaster associated with working in such adverse conditions, construction safeguards are clearly spelled out in contract specifications. Among the routine restrictions are limitations on the hours of the day when placement of stone or other material will be permitted due to the probability of strong tidal currents. Also, limitations are sometimes imposed because of wave characteristics. It is common practice to specify a 3-ft-thick foundation blanket composed of quarry-run stone both to serve as a bearing surface for the mass of the structure and to combat the scour potential of the anticipated strong tidal and wave-induced currents. Because of the prior planning and other precautions that are absolutely essential under these environmental conditions, damage to major structures while under construction has been minimal.

90. A typical example of the design and magnitude of a representative small-boat harbor on the southeastern portion of Alaska is Ketchikan Harbor, and a typical example on the other extreme end of southwest Alaska, in the Aleutian Islands, is King Cove Harbor. The project at Thomas Basin, Ketchikan Harbor, adopted in 1930, provided for a small-boat basin approximately 13 acres in area dredged to a depth of 10 ft mllw. The basin was protected on the south by a concrete-capped rock breakwater 950 ft long and 23 ft above mllw. Subsequent to 1933, the completion date, shoaling induced by the flow of the Ketchikan Creek into the basin has required maintenance dredging. In 1954, the project was modified to include a second basin at Bar Point with three breakwaters, 700, 450, and 1,100 ft in length. Construction, except for the 450-ft west breakwater which is deferred indefinitely, was completed in 1958. Sand and gravel were used not only for the foundation blanket material but also as the central core element for a large portion of the structure.

91. King Cove Harbor, a small-boat harbor, was constructed in 1973-74 in the Aleutian Islands of southwest Alaska. The harbor included an 11-acre anchorage basin and a 100-ft-wide entrance channel about 450 ft long, a 200-ft rock groin to protect the entrance, and the development of a 1,500-ft-long training dike to deflect tidal flows away from the area. Tides of about 12 ft occur regularly, and serious problems were anticipated in constructing the training dike in the strong current field generated by this tidal flow. Construction was carried out under frosty and light ice conditions. A 3-ft-thick foundation blanket of quarry-run stone was placed under the structure. Advancement would continue until the tidal current became so strong that material began to move from the area; work would then cease until the tidal flow

the toe. The walls were rebuilt and stabilized with rock riprap and are being maintained by the pulp companies at a cost of about one-half million dollars per year. With the cliff erosion under control, serious scour of the west side of the spit began to occur.

87. To stabilize the spit, NPS developed shore revetment plans to be constructed and operated in conjunction with beach nourishment techniques. Some previous revetment works had been built in the past, and the necessity existed for excavating portions of the old structure. Parts of these former works were constructed with little or no toe or filter bed material and had eroded and scoured underneath the structure; thus insight was provided into the necessity of designing adequate toe and filter bed erosion protection features. The construction specifications required that the old structure be excavated adequately to receive the foundation blanket material for the new work, that the blanket be composed of Class C stone with a thickness of 3 ft, and that the blanket extend beyond the toe of the new revetment structure for a distance of 20 ft. Following completion of the revetment, 170,000 tons of cobble beach nourishment was placed, with the material ranging in size from 1 to 12 in., and with 50 percent of the material larger than 3 in.

Alaska

88. Alaska, the largest state, has more miles of coastline than all the other states combined. Not considering the small bays, there are about 7,000 miles of shore situated in three climatic zones (temperate, subarctic, and arctic). There are approximately 35 navigation projects under the jurisdiction of the US Army Engineer District, Alaska, 20 of which have required some type of major structure in the coastal zone or in semiprotected inlet waters. Most of these basins are small-boat harbors which are used for individual transport, for subsistence and commercial fishing, and for lighter moorage.

89. Unique problems that do not exist elsewhere are associated with construction in the Alaskan coastal waters, and their solutions are also unique. However, these problems are well recognized and well respected by those responsible for operations in this region. These problems include large waves, strong tidal currents, very large tide ranges, extreme cold, many types of ice problems, and high sedimentation rates. Because of the potential for

This important body of water, clearly the result of glacial erosion, is the connecting channel between the Pacific Ocean and the interisland passages extending southeastward into Puget Sound and northeastward to the inland waters of British Columbia. The strait has very steep sides, and the water depths descend rapidly. The 100-fathom contour penetrates up the strait for almost 40 miles. The coastline along the strait is generally steep with narrow beaches of coarse sand and large boulders. West of Port Angeles there are large sweeping sandy beaches, but to the east the shoreline is more gravelly except for the mud flats of Dungeness. Waves generated in the North Pacific Ocean enter the strait as swell. In addition, shorter period waves may be generated in the strait due to the relatively long fetch and predominant west-northwest winds.

85. Puget Sound proper is connected to the strait by a series of waterways, channels, and inlets. The shoreline of Puget Sound is very dissimilar in character to that of other coastal areas of the continental United States. Of the total of over 2,000 miles, the greater portion is faced with bluffs ranging from 50 to 500 ft composed of glacial till. A generally narrow beachline is found at the base of these bluffs; and Puget Sound has, surprisingly, a considerable number of beaches. Puget Sound beaches consist either of gray coarse sand or a mixture of sand with small gravel. The climate of the area is typically maritime. Winds may exceed 60 knots during winter storms; but because of the limited fetches, waves rarely exceed 6 ft in height, even in the larger open areas of the sound.

86. The sandy spit at Port Angeles, Washington, which extends out into the Strait of Juan de Fuca, provides great protection to the town and harbor from wind-generated waves and the swell propagating from the North Pacific Ocean. The Ediz Hook spit, approximately 3.5 miles in length, built eastward by material from erosion of the bluffs immediately to the west. This spit is owned by the US Government and the City of Port Angeles; parts of the Government portion are leased on a long-term basis to the city, and portions are, in turn, subleased to large pulp mill operations. The pulp mills use tremendous quantities of fresh water and have constructed reservoirs in the mountains near Port Angeles for supply purposes. The pulp mills have also constructed a pipeline to transport the fresh water to the mills. The pipeline was placed at the base of the cliffs which fed the spit. To protect the pipeline, the pulp mills originally erected sheet-steel pile walls that failed by erosion at

the structure would eventually be undermined unless the scour could be controlled. As a result of a physical hydraulic model study by WES (1955), it was decided that the outer 6,000 ft of the south jetty should be allowed to deteriorate to about elevation 0.0 ft mllw to alleviate the very serious erosion problem at Point Chehalis.

82. The inner 4,000 ft of the south jetty was rehabilitated in 1966 to elevation +20 ft mllw and a blanket of quarry rock was placed along the channel side slope of the jetty to prevent undermining. Disposition of the blanket material was a special concern during construction because strong tidal currents, heavy wave action, and placement to depths of -60 ft mllw prevented assurance that adequate slope protection was being attained. However, the jetty is still at project height and apparently the slope protection has successfully prevented undermining to date. The outer 6,000 ft of jetty continues to subside and is presently well below mllw. The outer end of the submerged jetty is retreating landward as scour to a depth of -50 ft mllw progressively undermines the end.

83. In 1975, the US Army Engineer District, Seattle (NPS) rehabilitated all but 300 ft of the outer 6,300 ft of north jetty to elevation +20 ft mllw. The jetty had deteriorated to at or below the high-water line. Either a scour hole as a result of waves overtopping the low jetty or an accumulation of sand existed along the inside toe. As construction proceeded, the contractor was required to either fill the scour hole with bedding rock or partially excavate the sands and backfill with excess bedding material. The bedding rock then provided a base for placement of the large capstones and/or was of sufficient excess quantity to fill scour holes that might subsequently develop. In estimating the quantities to be required in the rehabilitation of the north jetty, a fairly substantial contingency factor had been applied in anticipation of the necessity to fill scour holes. The philosophy of NPS regarding stability of the structure may be considered as: (a) either excavate the anticipated scour region if it does not occur naturally during construction and fill with sufficient stone; or (b) provide excess stone on the toe of the structure to adequately fill the scour hole should it develop at some time following construction.

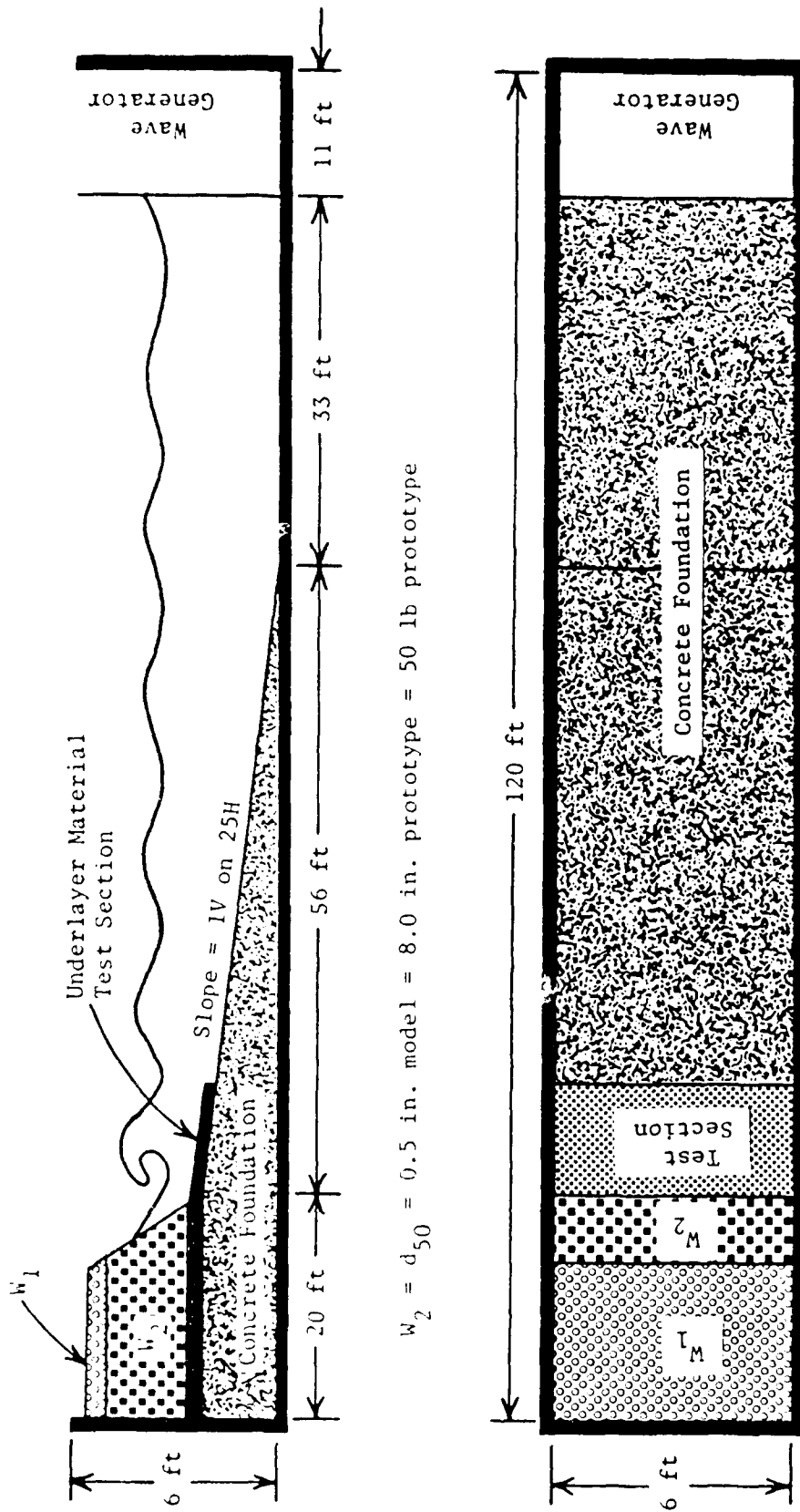
Strait of Juan de Fuca and Puget Sound

84. The Strait of Juan de Fuca separates the southern shore of Vancouver Island, Canada, from the northern coast of the State of Washington.

of the structure; and the channel proceeded to migrate at the same rate as the new jetty construction. The result was that a 40-ft-deep scour hole (unaccounted for in cost estimates) had to be filled. During the first year of construction, substantial overruns of stone quantities were experienced, reflected by the fact that approximately 5,000 ft of structure had been expected to be built and less than 3,000 ft was actually constructed.

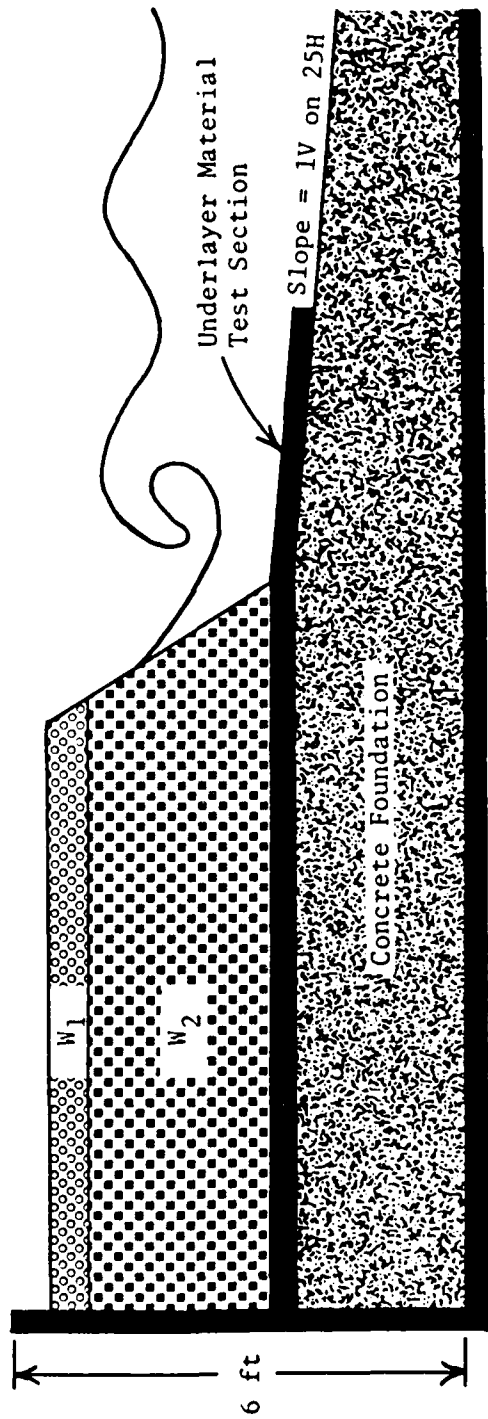
80. During the second construction year of the Tillamook Bay south jetty, the technique of "accelerated core placement" was developed by the US Army Engineer District, Portland. To minimize scour of the ocean bottom ahead of the jetty, rapid placement of the core stone was essential. During construction, the contractor was required to work all daylight hours, 7 days per week, except as prevented by weather or sea conditions, and was required to place the core stone at a minimum rate of 650 tons per hour. Sufficient equipment and personnel were available for this rate of placement. Core stone placement was accomplished only when predicted tides for the 10-day period following were not expected to exceed a 9-ft differential between lower low water and higher high water. It was the intent to place stone during a period when scouring velocities ahead of the core construction were lowest and most favorable for the work. Prior to the start of each season's core construction, core stone was stockpiled in amounts sufficient to ensure uninterrupted placement at the above specified rate. During a construction season, the contractor was instructed to place no more core stone than could be armored that season. This accelerated placement technique reduced the depth of the scour hole by about 50 percent, from a 40-ft-deep hole during the first construction year to around 20 ft for the subsequent construction periods.

81. Grays Harbor, Washington, is located about 45 miles north of the mouth of the Columbia River. The natural entrance to the harbor was about 2.5 miles wide and is now protected by two converging rubble-mound jetties that are 6,500 ft apart at their outer ends. The top elevation of both jetties as originally constructed was +8.0 ft mllw. The outer bar and entrance channel are actually self-maintaining for the authorized dimensions and thus require no maintenance dredging. Controlling depths on the outer bar are about -35 ft mllw and maximum depths in the channel are about -70 ft mllw. Following the rehabilitation of the south and north jetties in the late 1930's and early 1940's to +20 ft mllw, the entrance channel migrated south to a location adjacent to the south jetty. Scour along this jetty caused fear that



$w_2 = d_{50} = 0.5$ in. model = 8.0 in. prototype = 50 lb prototype

Figure 4. Two-dimensional wave flume



$W_2 = d_{50} = 0.5$ in. model = 8.0 in. prototype = 50 lb prototype

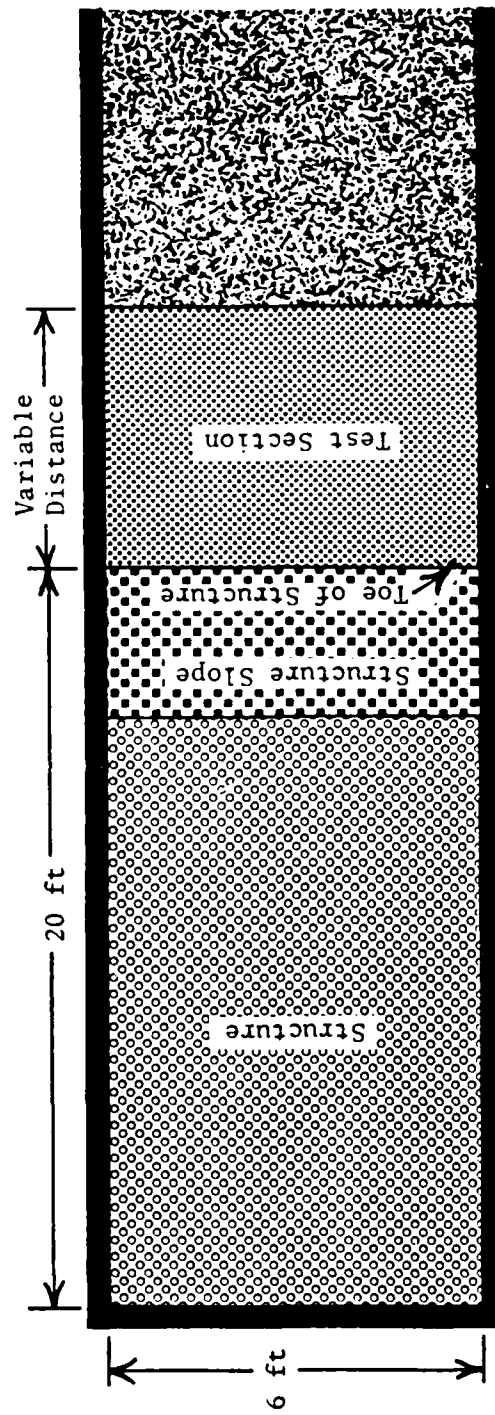


Figure 5. Details of model structure and test section in two-dimensional wave flume

amplitude from the programmed value more than +5 percent over a range of amplitude from 10 to 80 percent of maximum motion. Wave period does not vary by more than +1 percent.

112. Automated Data Acquisition and Control Systems (ADACS) have been designed and built at the US Army Engineer Waterways Experiment Station (WES) for the purpose of collecting wave data and controlling operations of hydraulic wave models. The computer hardware configuration for each system consists of a minicomputer with 32K 16-bit words of memory, a magnetic tape controller with two 9-track tape drives, one moving head disc controller with one removable platter and one nonremovable platter, an interval timer (1 μ sec), an analog-to-digital 12-bit converter featuring 64 analog (± 10 volts) inputs and a 45 kHz multiplexer, a teletype unit, 96 sense/control lines, and one matrix electrostatic printer/plotter.

Test Program

113. A limited range of wave conditions was used initially in order to develop a test program for investigating the effects of various wave parameters and underlayer material characteristics on resulting scour near major rubble-mound structures. The range of parameter variations to be used in the experimental investigation was established in this preliminary evaluation. Based on Froude scaling laws (gravity being the restoring function for recurring surface water waves), test materials were obtained and a structure representing a typical prototype was constructed. Various combinations of parameters were considered, and it was determined that the most severe wave condition (that situation producing the most movement of underlayer material) existed when the waves were permitted to break and plunge directly at the toe of the structure.

114. Based on the results of these preliminary underlayer experimental tests, it was determined that the stability of the underlayer material section is functionally related to the size of the material comprising the stabilization layer and to certain parameters of the incoming wave climate. These wave characteristics may consist of the wave period T , plunging breaker wave height H_b , still-water depth d , wave celerity C , and wavelength λ . It was also determined that the most severe scour condition resulted from a breaking wave which plunged directly at the toe of the major stone structure.

Certain of these wave parameters may not be completely independent, i.e., the breaking wave height at the toe of the structure may depend on the water depth and wave period.

$$\text{Stability} = (W_{UL}, H_b, T, C, g, d, L, \lambda, w_r, w_w) \quad (3)$$

where

- W_{UL} = weight of representative stone in the underlayer section, lb
- H_b = maximum breaker wave height when wave plunges at structure toe, ft
- T = wave period, sec
- C = wave celerity, ft/sec
- g = gravitational constant, 32.174 ft/sec²
- d = still-water depth, ft
- L = width of underlayer structure section, ft
- λ = wavelength, ft
- w_r = unit weight of underlayer material, lb/ft³
- w_w = unit weight of water, lb/ft³

The functional relation of Equation 3 was determined by these physical model experiments.

Underlayer material

115. The size of quarry-run stone and the routine requirements of rubble-mound stone construction provide an indication of the size of stone material that can be reasonably feasible to obtain for utilization as underlayer material. Based on a Froudian scaling, and a 16-to-1 linear scale ratio between prototype dimensions and test size, seven material sizes were selected for investigation (Table 2). To investigate the effect of underlayer material extent on the scour phenomena, three different lengths of underlayer section were tested (3 ft, 5 ft, and 7 ft model, or 48 ft, 80 ft, and 112 ft prototype, respectively). The remaining pertinent variables of Equation 3 are related to water depth and wave climate.

Wave characteristics

116. Because breaking waves are being evaluated (with plunging occurring directly at the toe of the major stone structure), the breaking wave height, H_b , should be directly related to the water depth, d . Hence more than one water depth should be tested to isolate any scale effects. Also, a range of wave periods is necessary to determine the inherent relation between

Table 2
Underlayer Test Section Materials

Material	Model Dimension		Prototype Weight		Prototype Weight lb	Prototype Size in.
	Retained Screen Size in.	Passing Screen Size in.	Retained lb	Passing lb		
1	3/8	1/2	20	50	35	7
2	1/2	5/8	50	95	72	9
3	5/8	3/4	95	165	130	11
4	3/4	7/8	165	260	212	13
5	7/8	1	260	390	325	15
6	1	1-1/4	390	765	577	18
7	1-1/4	1-1/2	765	1,320	1,042	22

wave period, T , and breaking wave height. Test wave periods of 2, 3, 4, and 5 sec were selected to be generated in water depths of 0.50 and 1.00 ft. The wave generation system was capable of producing breaking waves under these conditions on the 1V-on-25H slope that was selected for the tests. The breaking wave heights were determined along the center line of the flume by the ADACS system (Table 3). The wave generator was operated as a sinusoidally

Table 3
Test Wave Characteristics

Water Depth, d ft	Wave Period, T sec	Maximum Breaker Wave Height, H_b ft
0.50	2	0.65
0.50	3	0.70
0.50	4	0.80
0.50	5	0.68
1.00	2	1.09
1.00	3	1.11
1.00	4	1.45
1.00	5	1.12

moving wave maker, and the shallow-water waves broke down into a primary and one or more secondary waves. The primary and secondary waves traveled at different speeds (depending on their individual wave heights), and the resulting water surface exhibited secondary waves, depending on the distance from the wave generator. The fact that the breaking wave heights for the 5-sec waves of Table 3 were determined by the ADACS system to be less than the breaking wave heights for the 4-sec waves is attributed to this secondary wave phenomenon.

Flume slope

117. A 1V-on-25H slope was molded in a 6-ft-wide flume using fixed-bed concrete materials. This slope fit into the geometry of the existing 6-ft-wide wave flume satisfactorily and would provide the required characteristics necessary to induce breaking of all waves desired to be tested in this program. This bottom slope of 1V-on-25H is typical of many prototype conditions.

Experimental test conditions

118. Two water depths (0.50 and 1.00 ft) and four wave periods (2, 3, 4, and 5 sec) were tested. These eight combinations of wave periods and water depths were evaluated using three different widths of underlayer section (3, 5, and 7 ft). Each of these three different widths of underlayer sections was constructed of seven separate gradations of material, ranging from that which passed a 1/2-in. screen to that which passed a 1-1/2-in. screen (prototype size range of 7 to 22 in., with the average weight of each material being 35, 72, 130, 212, 325, 577, and 1,042 lb, prototype). These combinations of material sizes, underlayer structure width, water depth, and wave periods resulted in 168 separate tests.

Data Analysis

119. The stability of the major rubble-mound structures has been investigated quite thoroughly from both an analytical and experimental standpoint. Even though the importance of the underlayer foundation blanket for scour prevention during construction has been recognized, the stability of this underlayer material has been given only empirical rule-of-thumb design considerations. Because of the many similarities that exist between a rubble-mound structure and the underlayer material on which it is placed, it is desirable to perform an analysis of the stability during construction of the underlayer

material along analogous lines to those which have been developed for rubble-mound structures.

Stability of rubble-mound structures

120. The classic analysis of the stability of the armor units which protect a rubble-mound structure from excessive damage due to wave attack was presented by Iribarren Cavanilles (1938), and has come to be known as the Iribarren formula:

$$W_R = \frac{K_B H_B^3 S_{cr}}{(\cos \theta - \sin \theta)^3 (S_{cr} - 1)^3} \quad (4)$$

where

W_R = weight of individual cap rock, kg

K_B = 15 and 19 for breakwaters constructed of natural rock fill and artificial blocks, respectively, kg/m³

H_B = height of wave which breaks on the structure, m

S_{cr} = specific weight of cap rock, metric tons/m³

θ = angle, measured from horizontal, of the sea-side slope, deg

This expression, in the form of Equation 4, is not dimensionally homogeneous; and the coefficient, K_B , is not dimensionless. These limitations restrict the equation from being universally applicable in its present form.

121. In 1951, a comprehensive investigation of rubble-mound breakwaters was begun at the WES for the Office, Chief of Engineers (OCE). These studies have been discussed by Hudson (1957, 1958, 1961, 1974, 1975), and Hudson and Jackson (1953). In 1951, it was assumed that the Iribarren formula could be used to correlate test data and that it could be made sufficiently accurate for use in designing full-scale rubble-mound breakwaters, if sufficient test data were available to evaluate the experimental coefficient, K_B . Early tests in this investigation showed that the friction coefficient in Iribarren's formula, as measured by the tangent of the angle of repose, varied appreciably with the shape of armor units and with the method used to place these units in the cover layer. These results led to the realization that the experimental coefficient, K_B , could not be determined accurately from small-scale breakwater stability tests unless accurate comparative values of the friction coefficient could be obtained for the different shapes of armor units. This realization was made more acute by the fact that Iribarren's

force diagram, from which his basic stability equation was derived, is predicated on the assumption that the friction between armor units, specifically that component of the friction force parallel to the breakwater slope, is the primary force that resists the forces of wave action and determines the stability of the armor units. Based on the results of the tests to determine friction coefficients, correlation of test data by the use of Iribarren's formula was abandoned; and a new stability equation, similar to the Iribarren formula but capable of more general application, was derived by Hudson (1957).

122. A dimensionless parameter, designated the stability number, N_s , was developed by Hudson (1957) as:

$$N_s = \frac{w_r^{1/3} H}{(S_r - 1) W^{1/3}} \quad (5)$$

where

w_r = unit weight of the rock

H = design wave height

W = weight of an individual armor stone

When damage was allowed to occur to the breakwater (by use of wave heights greater than the design wave height), the geometry of the structure, the motion of the water particles, and the resulting forces on the breakwater differed from those resulting from tests in which the no-damage criterion was used. Thus a damage parameter, D , defined as the percentage of armor units displaced from the cover layer by wave action, was included by Hudson (1957).

123. For breakwater sections investigated in the first phase of the testing program, in which the armor units were rocks simulating rounded and smooth quarrestones placed randomly, it was found that:

$$N_s = \frac{w_r^{1/3} H}{(S_r - 1)^{1/3}} = (\theta, H/\lambda, d/\lambda, D) \quad (6)$$

In the second phase of the testing program, the armor units used were patterned after the tetrapod, and the rubble mound was protected by two or more layers of armor units placed over one or two quarrestone underlayers. For these tests, it was determined that:

$$N_s = \frac{\omega_r^{1/3} H}{(S_r - 1)W^{1/3}} = f(\theta, H/\lambda, d/\lambda, r) \quad (7)$$

Here r is the thickness of the cover layer.

124. Data obtained from stability tests of quarystone and tetrapod-shaped armor units for the no-damage criteria are shown in Figure 6 in the form of log-log plots, with the stability number, N_s , as the ordinate, $\cot \theta$ as the abscissa, and the shape of the armor unit as the parameter. Analysis by Hudson (1957) of the test data indicated that for the conditions tested, the effects of the variables H/λ and d/λ on the stability of armor units are of second order in importance when compared with the effects of breakwater slope, θ , and the shape of the armor units, D or r (no period effect could be ascertained from these data).

125. A formula for determining the weight of armor units necessary to ensure stability of rubble-mound breakwaters of the types tested, and in relatively deep water, can be obtained from the equation of the approximate best-fit lines of Figure 6. The lines AB and MN were drawn through the data points with a best-fit slope of 1/3. The equation of this straight line on log-log paper is of the form $y = ax^b$, where a is the y-intercept at $x = 1$, and b is the slope of the line. The equation of lines AB and MN therefore is:

$$N_s = \frac{\omega_r^{1/3} H}{(S_r - 1)W^{1/3}} = a (\cot \theta)^{1/3} \quad (8)$$

for which, if $a^3 = K_D$:

$$W = \frac{\omega_r H^3}{K_D (S_r - 1)^3 \cot \theta} \quad (1 \text{ bis})$$

Equation 1 has been applied with apparent success to many model-prototype studies under varying conditions of wave climate and local topography, i.e., Davidson (1971, 1978), Carver (1976, 1980), and Carver and Davidson (1977).

126. In recent years, other investigators have become concerned that there may indeed be a period dependency effect on the stability of armor units of rubble-mound structures. Whillock and Price (1976) reported that during an

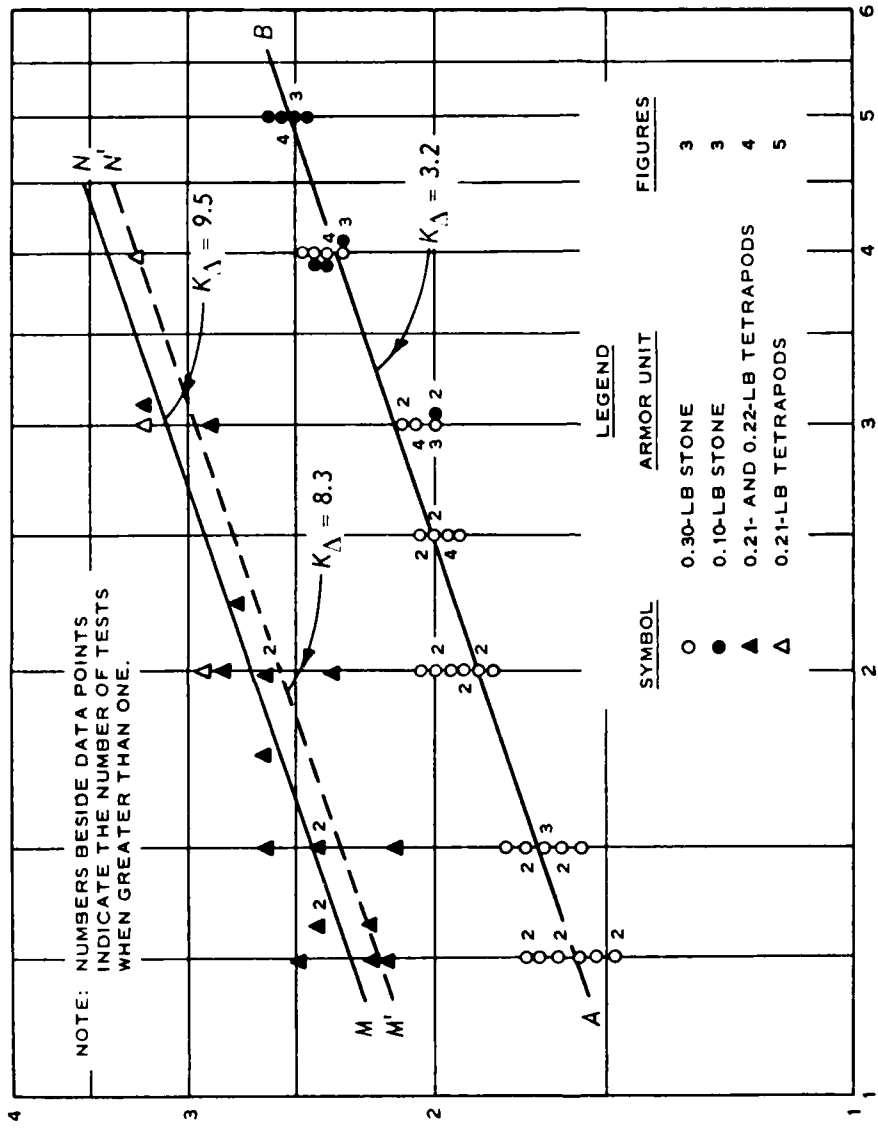


Figure 6. Stability of quarrystone and tetrapod armor units, N_s , as a function of Δ and θ for no-damage and no-overtopping criteria (after Hudson 1957)

investigation for the design of dolosse for the High Island Breakwater in Hong Kong, various slopes of breakwater were subjected to waves of different periods. Having selected a wave period, the wave height was increased until failure occurred. A definite influence of wave period, T , was observed by these researchers. As the wave period increased, the wave tended to surge onto the protective layer rather than break. This set up high velocities over the surface layer. It was suspected from observations of many tests that although dolosse were very stable to plunging breakers acting normal to the slope, their weakness lies in their inability to resist the drag caused by this surface flow.

127. Bruun and Gunbak (1976) and Bruun (1979) found a "phase difference" to be the dominant factor in the relation between waves and structure geometry. They defined this period effect "phase difference" as the ratio of the runup time to the wave period, T . Sollitt and DeBok (1976) found that for a given value of wave steepness and depth, the short-period waves always produced less absolute runup. For a given wave period, T , shallower water produced more runup relative to the depth, and this was reflected in more damage to the structure armor stone.

128. Hannoura and McCorquodale (1979) conducted experimental studies of waves breaking on rubble-mound structures and of the instantaneous pressure distribution due to the wave impact. They believed they observed an effect of period as a result of these studies. Gravesen, Jensen, and Sorensen (unpublished manuscript) have conducted numerous stability tests at the Danish Hydraulic Institute. They report that the stability coefficient, K_D , in Hudson's Equation 1, is proportional to the characteristic wave steepness, H/λ , with the wavelength, λ , being a function of both water depth, d , and wave period, T .

Stability of underlayer material

129. Test conditions. The experimental study performed in this investigation was conducted in a 6-ft-wide, 6-ft-deep, and 120-ft-long wave flume. A portion of the flume length was occupied by the wave generator and model (16-to-1 scale) of the rubble-mound structure (breakwater, jetty, groin, etc.). The model structure was assumed to be oriented in a manner such that the incoming surface gravity waves were propagating directly onto the long axis of the structure, as construction proceeded seaward from the coastline. Because of the finite length of wave flume remaining (89 ft), it was necessary

to generate the test waves in a burst of finite duration, to then cease wave generation, and to allow the water surface to become still before generating another burst of waves. This method prevented reflected wave energy from returning to the wave generator and being rereflected with the newly generated waves back toward the structure (thus distorting the initial wave calibration).

130. The duration of an actual burst of generated waves varied, depending on the period of the wave and the water depth. The duration consisted of the time necessary for a generated wave to travel from the wave generator to the model structure and return to the wave generator. This time increment was about 30 to 45 sec; however, the amount of time necessary to allow the water surface to become still before the next burst of waves was generated was approximately 5 min. Only 6 to 12 waves could be generated in a burst (depending on the travel time of 2-, 3-, 4-, and 5-sec waves in 0.50 and 1.00 ft of water depth). Hence a significant portion of the model operation time was spent in quieting the water surface. A longer flume would have permitted more waves to be generated in a burst, thus reducing the amount of time required to perform this experimental physical model investigation. A minimum number of at least 500 individual waves were generated at each of the sections of underlayer material tested. If significant movement of material occurred prior to this number of waves being generated, then testing of a particular material and wave combination may have been terminated, as it could be concluded that this particular combination of parameters produced an unstable condition. Occasionally, the number of waves in a test would be continued to gain additional information for supplemental purposes.

131. Preliminary tests used for the development of this experimental test program had indicated that the greatest amount of underlayer material movement would be produced by breaking waves which plunge directly onto the toe of the rubble-mound structure. For a given wave period, T , higher waves would break seaward of this location and the reduced wave energy would not cause as much material movement. Lower waves at this period would break on the structure, and the effects would be less noticeable on the underlayer material. Hence, in the testing operation, it was necessary to set the desired wave period and then adjust the stroke of the wave generator to produce a wave that would break at the desired location (the position of most severe wave effects).

132. The majority of the failures occurred as material moved from the

seaward edge of the underlayer section toward the base of the rubble-mound structure. The temporal movement was functionally related to the wave characteristics (wave height, H_b , and/or wave period, T), and to the size of the material being tested. For some tests that utilized an underlayer section which was relatively long when compared with the water depth, d , or wave height, H_b , the instability would be reflected as a failure section at some location other than the toe of the underlayer section. This implies that if all sections could be extended far enough seaward, the instability would appear as a scour hole development through the underlayer section, and the stability then becomes also a function of the layer thickness. (All tests in this study were conducted with a layer test section thickness of 2 ft prototype.) It is impractical to extend an underlayer section for an infinite distance seaward; hence the optimization of material size, W_{UL} , and layer extent, L , with wave characteristics is necessary for efficient construction methods. The 168 tests performed in this study are presented in Table 4.

133. Data display. A review of the pertinent variables involved indicates that the stability of an underlayer section (for fixed underlayer thickness) may be expressed as some functional relation between nine basic parameters:

$$f(\omega_w, \omega_r, W_{UL}, H_b, T, g, d, L, \lambda) = 0 \quad (9)$$

All symbols have been defined previously, and $S_r = \omega_r / \omega_w$. A layer of 2-ft-thick prototype underlayer material was utilized throughout these tests; hence the dependency on thickness was not evaluated in this study. Since it was desired to display these data in a manner similar to that of Hudson (1957) for the armor slope stability of rubble-mound structures, the stability number, N_s , can again be expressed as Equation 5 and becomes functionally related to two other fully independent dimensionless terms:

$$N_s = \frac{\omega_r^{1/3} H_b}{(S_r - 1) W_{UL}^{1/3}} = f\left[\frac{L}{d}, \frac{d}{g}^{1/2}, \frac{1}{T}\right] = f\left(\frac{L}{d}, \frac{d}{\lambda}\right) \quad (10)$$

Since shallow-water waves were used, $\lambda = T(gd)^{1/2}$, and the angle of the breakwater seaward slope with the horizontal, θ , becomes meaningless for the underlayer material section of this analysis.

Table 4
 Test Conditions, Underlayer Material and Wave Characteristics

Still-Water Depth d, ft	Wave Period T, sec	Maximum Breaker Wave Height H _b , ft	Wave- length λ, ft	Underlayer Material Extent L, ft	$\frac{L}{\lambda}$	Average Model Stone Weight W _{UL} , lb	$\frac{w_r^{1/3} H_b}{(S_r - 1) W_{UL}^{1/3}}$	Stable, S
								or Unstable, U
0.5	2	0.65	8.02	3	0.37	0.0085	11.05	S
0.5	2	0.65	8.02	3	0.37	0.0175	8.68	S
0.5	2	0.65	8.02	3	0.37	0.0315	7.14	S
0.5	2	0.65	8.02	3	0.37	0.0520	6.05	S
0.5	2	0.65	8.02	3	0.37	0.0795	5.25	S
0.5	2	0.65	8.02	3	0.37	0.1405	4.34	S
0.5	2	0.65	8.02	3	0.37	0.2540	3.56	S
0.5	2	0.65	8.02	5	0.62	0.0085	11.05	S
0.5	2	0.65	8.02	5	0.62	0.0175	8.68	S
0.5	2	0.65	8.02	5	0.62	0.0315	7.14	S
0.5	2	0.65	8.02	5	0.62	0.0520	6.05	S
0.5	2	0.65	8.02	5	0.62	0.0795	5.25	S
0.5	2	0.65	8.02	5	0.62	0.1405	4.34	S
0.5	2	0.65	8.02	5	0.62	0.2540	3.56	S
0.5	2	0.65	8.02	7	0.87	0.0085	11.05	S
0.5	2	0.65	8.02	7	0.87	0.0175	8.68	S
0.5	2	0.65	8.02	7	0.87	0.0315	7.14	S
0.5	2	0.65	8.02	7	0.87	0.0520	6.05	S
0.5	2	0.65	8.02	7	0.87	0.0795	5.25	S
0.5	2	0.65	8.02	7	0.87	0.1405	4.34	S
0.5	2	0.65	8.02	7	0.87	0.2540	3.56	S
0.5	3	0.70	12.04	3	0.25	0.0085	11.91	S
0.5	3	0.70	12.04	3	0.25	0.0175	9.34	S
0.5	3	0.70	12.04	3	0.25	0.0315	7.69	S
0.5	3	0.70	12.04	3	0.25	0.0520	6.51	S
0.5	3	0.70	12.04	3	0.25	0.0795	5.65	S
0.5	3	0.70	12.04	3	0.25	0.1405	4.67	S
0.5	3	0.70	12.04	3	0.25	0.2540	3.84	S
0.5	3	0.70	12.04	5	0.42	0.0085	11.91	S
0.5	3	0.70	12.04	5	0.42	0.0175	9.34	S
0.5	3	0.70	12.04	5	0.42	0.0315	7.69	S
0.5	3	0.70	12.04	5	0.42	0.0520	6.51	S
0.5	3	0.70	12.04	5	0.42	0.0795	5.65	S
0.5	3	0.70	12.04	5	0.42	0.1405	4.67	S
0.5	3	0.70	12.04	5	0.42	0.2540	3.84	S
0.5	3	0.70	12.04	7	0.58	0.0085	11.91	S
0.5	3	0.70	12.04	7	0.58	0.0175	9.34	S
0.5	3	0.70	12.04	7	0.58	0.0315	7.69	S
0.5	3	0.70	12.04	7	0.58	0.0520	6.51	S
0.5	3	0.70	12.04	7	0.58	0.0795	5.65	S
0.5	3	0.70	12.04	7	0.58	0.1405	4.67	S
0.5	3	0.70	12.04	7	0.58	0.2540	3.84	S
0.5	4	0.80	16.05	3	0.19	0.0085	13.61	U
0.5	4	0.80	16.05	3	0.19	0.0175	10.68	U
0.5	4	0.80	16.05	3	0.19	0.0315	8.78	U
0.5	4	0.80	16.05	3	0.19	0.0520	7.44	S
0.5	4	0.80	16.05	3	0.19	0.0795	6.46	S
0.5	4	0.80	16.05	3	0.19	0.1405	5.34	S
0.5	4	0.80	16.05	3	0.19	0.2540	4.39	S
0.5	4	0.80	16.05	5	0.31	0.0085	13.61	U
0.5	4	0.80	16.05	5	0.31	0.0175	10.68	U
0.5	4	0.80	16.05	5	0.31	0.0315	8.78	S
0.5	4	0.80	16.05	5	0.31	0.0520	7.44	S
0.5	4	0.80	16.05	5	0.31	0.0795	6.46	S
0.5	4	0.80	16.05	5	0.31	0.1405	5.34	S
0.5	4	0.80	16.05	5	0.31	0.2540	4.39	S
0.5	4	0.80	16.05	7	0.44	0.0085	13.61	S
0.5	4	0.80	16.05	7	0.44	0.0175	10.68	S
0.5	4	0.80	16.05	7	0.44	0.0315	8.78	S
0.5	4	0.80	16.05	7	0.44	0.0520	7.44	S
0.5	4	0.80	16.05	7	0.44	0.0795	6.46	S
0.5	4	0.80	16.05	7	0.44	0.1405	5.34	S
0.5	4	0.80	16.05	7	0.44	0.2540	4.39	S

(Continued)

(Sheet 1 of 3)

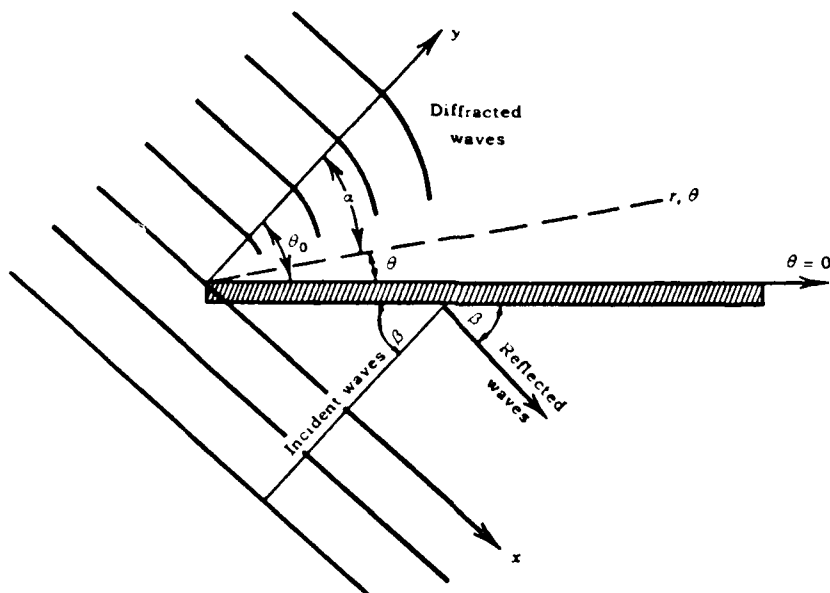


Figure 12. Definitive sketch, wave diffraction around a breakwater

where

η = water-surface elevation, ft

a = wave amplitude, ft

C = wave celerity, ft/sec

i = square root of -1

$F(r, \theta)$ is a function which satisfies the wave equation in cylindrical coordinates:

$$\frac{\partial^2 F}{\partial r^2} + \frac{1}{r} \frac{\partial F}{\partial r} + \frac{1}{r^2} \frac{\partial^2 F}{\partial \theta^2} + k^2 F = 0 \quad (20)$$

In the presence of a jetty or breakwater, the boundary condition is imposed that the normal component of the fluid velocity is zero along the breakwater, leading to the solution:

$$F(r, \theta) = \frac{1}{\sqrt{2}} e^{i \left[\frac{\pi}{4} - k_r \cos(\theta_0 - \theta) \right]} \int_{-\infty}^u e^{1 - \frac{i\pi u^2}{2}} du + \frac{1}{\sqrt{2}} e^{i \left[\frac{\pi}{4} - k_r \cos(\theta_0 - \theta) \right]} \int_{-\infty}^{u_2} e^{-\frac{i\pi u^2}{2}} du \quad (21)$$

n = ratio of group velocity c_g , to phase velocity c , dimensionless
 ω = angular frequency, $2\pi/T$, 1/sec

Define:

$$\delta = \left(\frac{a_{xx} + a_{yy}}{k^2 a} \right) \quad (18)$$

The commonly used existing procedures (Dunham 1951, Liu and Mei 1976, USAEWES 1984) for construction or computation of refraction diagrams utilize phase speeds that are obtained by neglecting δ .

Water wave diffraction

145. Diffraction of water waves is the phenomenon by which wave energy propagates into the sheltered lee of a structure even in the absence of bathymetric refraction. In these situations, wave crests bend (even in constant depth water) and gradients of wave height exist along the wave crest. This phenomenon is most visible when a train of regular waves is interrupted by an obstruction such as a jetty or shore-connected breakwater. The theory of water wave diffraction can be explained by Huygens' principle. Each point of an advancing wave front (wave crest) may be considered as the center of a secondary circular wave that advances in all directions. The resultant shape of the crest is the envelope of all these secondary waves. In a straight-crested wave train, the envelope of the secondary waves is a straight line also. When the wave passes an obstruction, the energy intensity at a certain point is a vector combination of all the circular waves emitted by every point of the passing wave train.

146. Sommerfeld (1896) presented a solution for the diffraction of light waves past the edge of a semi-infinite screen. Penny and Price (1944) showed that this is also the solution of the water wave diffraction problem at the end of a semi-infinite obstacle such as a jetty or shore-connected breakwater. This exact solution of the surface elevations behind the breakwater is applicable only to water of constant depth and waves of small amplitude. Putman and Arthur (1948) summarized the solution of Penny and Price (1944) for the definitive sketch of Figure 12. In cylindrical coordinates, the water-surface elevation is:

$$\eta = \frac{aikC}{g} e^{ikCt} \cosh kd F(r, \theta) \quad (19)$$

be considered a finite amplitude intermediate and shallow-water theory.

144. The refraction of surface gravity waves propagating in an ideal fluid was investigated by Battjes (1968) with small amplitudes so that linear theory was applicable and harmonic in time. It was known a priori that the velocity of propagation of a wave crest (to third order and greater) is a function of the wave height. In zones of convergence or divergence of wave energy, gradients in wave height will exist along sections of the wave crest. The regions of greater wave height will propagate faster than the regions of lesser wave height and this will, in turn, create bending of the wave crest (in addition to that bending caused by the bottom topography, called refraction). This supplemental bending is not usually accounted for by refraction analysis. Battjes (1968) developed an expression for this local correction to the wave speed because of wave-height variations along the crest from an exact derivation of the wave number, k . It was determined that the magnitude of the exact wave number equals k plus corrections which depend on the second derivative of the wave amplitude. This correction of the wave number implies, in turn, a correction to the phase speed c , which was found to be:

$$c = (g/k \tanh kd)^{1/2} \left(1 + \frac{a_{xx} + a_{yy}}{k^2 a} \right)^{-1/2} \quad (16)$$

where

g = gravitational constant, 32.174 ft/sec²

k = wave number, $2\pi/L$, 1/ft

d = local water depth, ft

a = local wave amplitude, ft

The second derivative of the wave amplitude in the horizontal plane is given by a_{xx} or a_{yy} . The rate of power transmission P , or energy flux, was determined to be:

$$P\Delta b = (1/2 \rho g a^2 n \frac{\omega}{k} \Delta b) \left(1 + \frac{a_{xx} + a_{yy}}{k^2 a} \right)^{1/2} \quad (17)$$

where

Δb = wave ray spacing, ft

ρ = fluid density, lb-sec²/ft⁴

by requiring the appropriate energy conservation. This was also the basic idea for the work of Koh and LeMéhauté (1966) in which the transformation of progressive waves was investigated as they travel from deep water to shore. The Stokes' theory at a fifth order of approximation was applied along with the method of conservation of energy flux. The first, third, and fifth orders of approximation were compared with each other and with experiments. The differences between the predictions of wave-height changes based on the three orders of approximation were found to be small, on the order of 5 percent. For practical purposes, the third-order theory was found to give reliable results. The third and fifth order Stokes' theories are based on a series expansion in terms of H/L where terms of the order of $(H/L)^3$ and $(H/L)^5$, respectively, are retained and higher order terms are neglected. It should be noted that this theory is based on an expansion in terms of the wave steepness, H/L , and consequently can be expected to better approximate limit steepness waves in deep water. However, it cannot be expected to do a very good job of approximating waves in shallow water since water depth is not a parameter in the series expansion. It also is assumed that the wave is simply harmonic in time. This theory could be considered as a finite amplitude deep-water wave theory.

143. In cases of limiting shallow water, the wave conditions are nearly independent of wavelength, and the important parameters are water depth and the ratio of wave height to water depth. Mathematical arguments show that Stokes' waves are most nearly valid in water deeper than about $d/L > 1/8$ to $1/10$ (Keulegan 1950). In shallower water, the theory for a wave type known as cnoidal appears to be more satisfactory, and Masch (1964) investigated the problem of wave shoaling using cnoidal wave theory with the formulas developed by Keulegan and Patterson (1940). Masch (1964) assumed hydrostatic pressure distribution and neglected the convective inertia term in his expression for the energy flux. The third and fifth order cnoidal theories are based on a series expansion in terms of H/d , where terms of the order of $(H/d)^3$ and $(H/d)^5$, respectively, are retained and higher order terms neglected. It should be noted that this theory is based on an expansion of the relative wave height (H/d) and can be expected to better approximate the wave form in shallow water. However, it cannot be expected to do a very good job of approximating the wave form for limiting steepness waves in deep water. In that case, water depth is unimportant and wavelength is crucial. This theory could

Water wave refraction

140. In intermediate and shallow water, the phase speed of a surface gravity wave depends on water depth. Since wave celerity decreases as depth decreases, phase velocity varies along the crest of a wave propagating at an angle to underwater contours because that part of the wave in deeper water moves faster than that part in shallower water. This variation causes the wave crest to bend toward alignment with the contours. This bending effect due to changes in bottom topography, called refraction, depends on the relation of water depth to wavelength, d/L , and is analogous to refraction of other types of waves such as light. A basic assumption in wave refraction theory is the conservation of energy between wave orthogonals (i.e., no diffraction of energy along wave crests). The change in wave direction of different parts of the wave results in convergence or divergence of wave energy and materially affects the forces exerted by waves on structures and of the capacity of waves to transport sand either alongshore or onshore/offshore.

141. Procedures for the computation of refraction of surface gravity waves on water of nonuniform depth involve the assumption that a wave with a curved crest pattern and variable amplitude along the crest behaves locally as a straight-crested wave of constant amplitude. Rayleigh (1877) appears to have been the first to use the approximations of geometrical optics in this analysis, and theoretical results have been developed with respect to energy flux and phase speed. As expressed by Keller (1958), the geometrical optics theory defines a propagation velocity at each point on the water surface, with this velocity being exactly that which waves of given period would have in water of uniform depth at all points. By employing Fermat's principle of optics, wave rays are defined and surface waves are assumed to propagate along these rays. The variation of the amplitude along the rays is determined by the use of the principle of conservation of energy. This principle (in its optical form) states that the flux of energy is the same at all cross sections between two adjacent wave rays. The energy flux is proportional to the square of the amplitude of the waves and to the distance between the rays, and hence the wave-height variation along the ray is available.

142. In problems of linear wave propagation over mild slopes, the principle of geometrical optics has been applied by Carrier (1966) as the first approximation in a systematic perturbation scheme while the bottom is considered to be locally horizontal. The depth variation was dealt with afterward

PART IV: COMBINED REFRACTION AND DIFFRACTION

138. The present state of nearshore current and wave theories has reached the point where detailed experimental investigations are required for the verification of analytical developments and numerical simulation models. To provide a firm foundation for further advancements, a simple beach profile consisting of straight, uniform contours parallel with the shoreline was physically molded for experimental testing. Two series of experiments were conducted in this three-dimensional facility. The first series consisted of detailed measurements of wave heights and wave-induced currents downwave of a shore-connected breakwater normal to the shoreline. The second series of experiments consisted of detailed measurements of wave heights downwave of a shore-connected breakwater oriented at a 60-deg angle to the shoreline. The purpose of these experiments was to obtain quantitative and detailed laboratory measurements of combined refraction and diffraction in the lee of a jetty or shore-connected breakwater.

Literature Review

139. The approximate solution of water wave refraction caused by a variable bathymetry is well known and can be derived by assuming that bottom reflections are negligible, or by the more rigorous Wentzel-Kramers-Brillouin (WKB) approximation. The exact solution for the diffraction of surface waves by vertical barriers of simple cross section in water of constant depth also is well known (being analogous to classical problems of physics). However, an analytical theory for the practical case of combined refraction and diffraction has not been completely developed. The present engineering practice for determining wave heights under this condition is a stepwise procedure (Dunham 1951; Liu and Mei 1976; USAEWES 1984). The procedure involves the following steps: (a) calculate refraction effects up to the barrier (jetty or shore-connected breakwater); (b) calculate for a "few" wavelengths the effects of diffraction, assuming a constant water depth; and (c) beyond this region calculate the refraction effects only. This procedure is obviously imprecise, and Mobarek (1962) indicates that the method is suitable only for intermediate water depths. In addition, Whalin (1972) states that this procedure is only valid for small refraction effects.

The test material used to develop these conservative expressions was sorted, passing one gradation screen and being retained by the next size screen. Furthermore, the size of the material used in a test was defined as the midpoint between these two screen sizes.

from which the weight, W_{UL} , of a representative stone in the underlayer material section is:

$$W_{UL} = \frac{w_r H_b^3}{23,150(S_r - 1)^3 \left(\frac{L}{\lambda}\right)^2} \quad (13)$$

137. Because of experimental scatter in a few of the data points of Figure 11, the average best-fit line (Equation 12) lies above some of the test results. This implies that on the average Equation 12 describes the stability of an underlayer material section; however, some tests were found to exceed the values of stone weight indicated by this expression and by Equation 13. In order to ensure that all the experimental data fall within the stability region described by a stability number, a conservative stability number should be established which will include all the experimental data used to generate the representative stone weight size, W_{UL} , in the underlayer section. Such a conservative line should remain parallel on the log-log plot of Figure 11 with the average best-fit line, but be displaced until it passes through the data point of known stability that lies adjacent to a companion test which proved to be unstable. That is, for a relative underlayer section length, $L/\lambda = 0.31$, the experimental test which produced a stability number, $N_s = 7.95$, was stable. The most nearly adjacent test in this family of experiments at the same value of $L/\lambda = 0.31$ was unstable and produced a stability number of $N_s = 9.68$. (These are the data which are displaced lower in Figure 11 from the average best-fit line.) Hence the conservative curve should pass through point $L/\lambda = 0.31$, $N_s = 7.95$, as this was a value of known stability from the experimental test results. The expression of this conservative line, in terms of stability number, N_s , is:

$$N_s = \frac{w_r^{1/3} H_b}{(S_r - 1) W_{UL}^{1/3}} = 17.5 \left(\frac{L}{\lambda}\right)^{2/3} \quad (14)$$

For this conservative expression, the weight, W_{UL} , of a representative stone comprising such an underlayer material section can be developed as:

$$W_{UL} = \frac{w_r H_b^3}{5,360(S_r - 1)^3 \left(\frac{L}{\lambda}\right)^2} \quad (15)$$

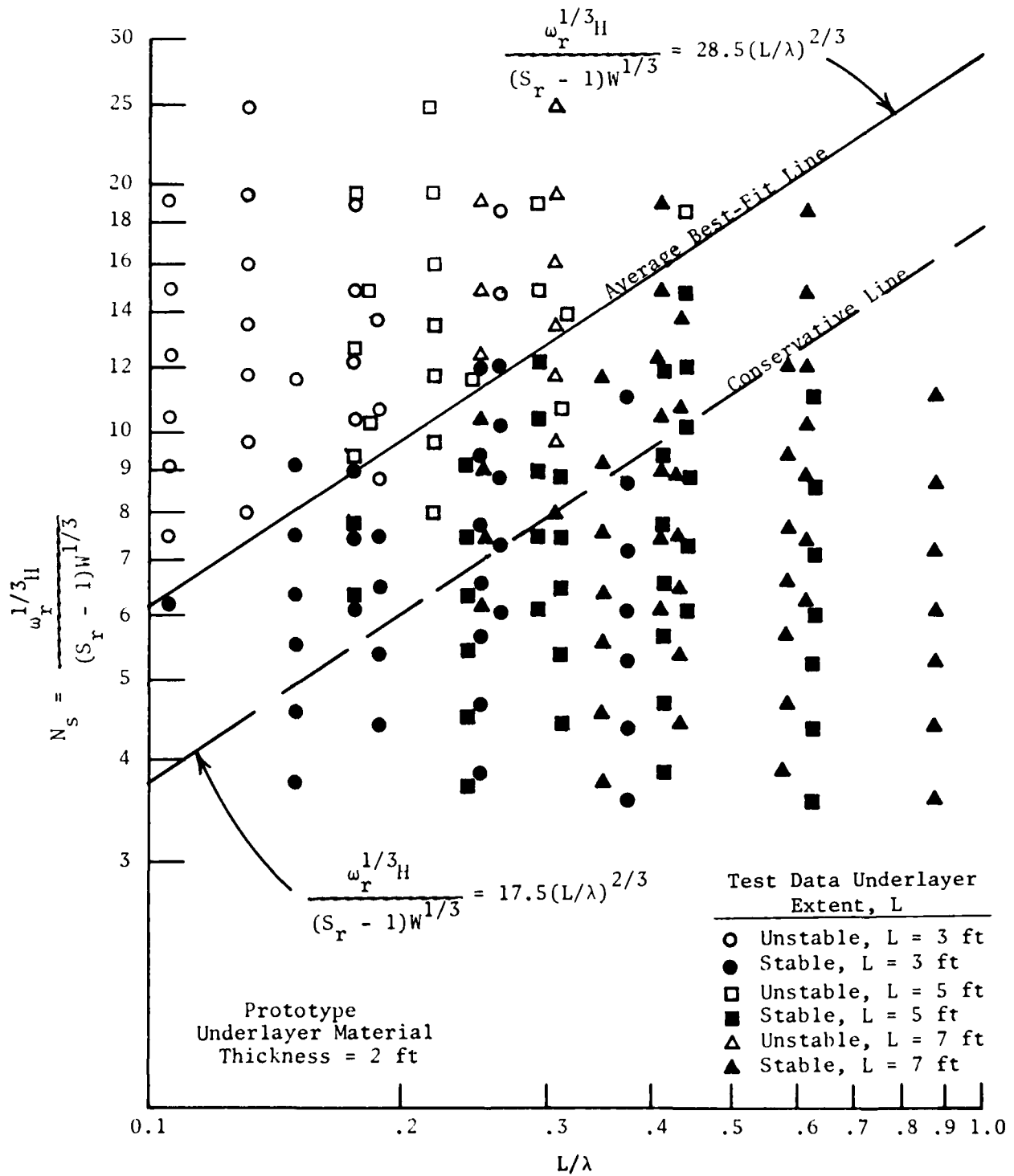


Figure 11. Stability number, N_s , versus the relative underlayer section length, L/λ , showing the average best-fit line to all the experimental data, and the conservative line enveloping all unstable conditions tested

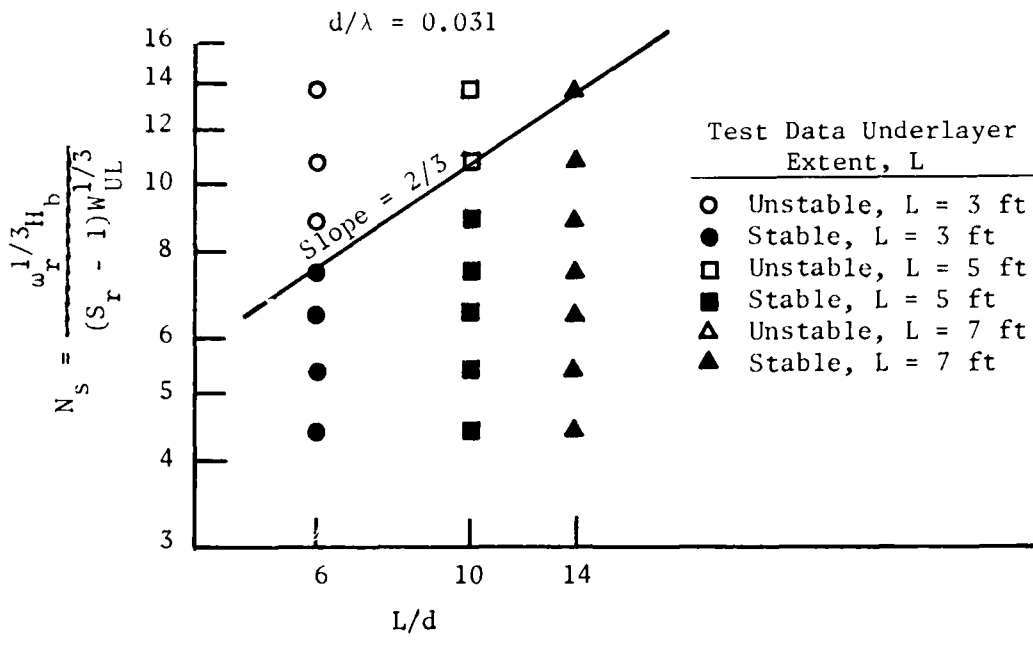


Figure 9. Stability number, N_s , versus the structure parameter, L/d , for relative water depth, $d/\lambda = 0.031$

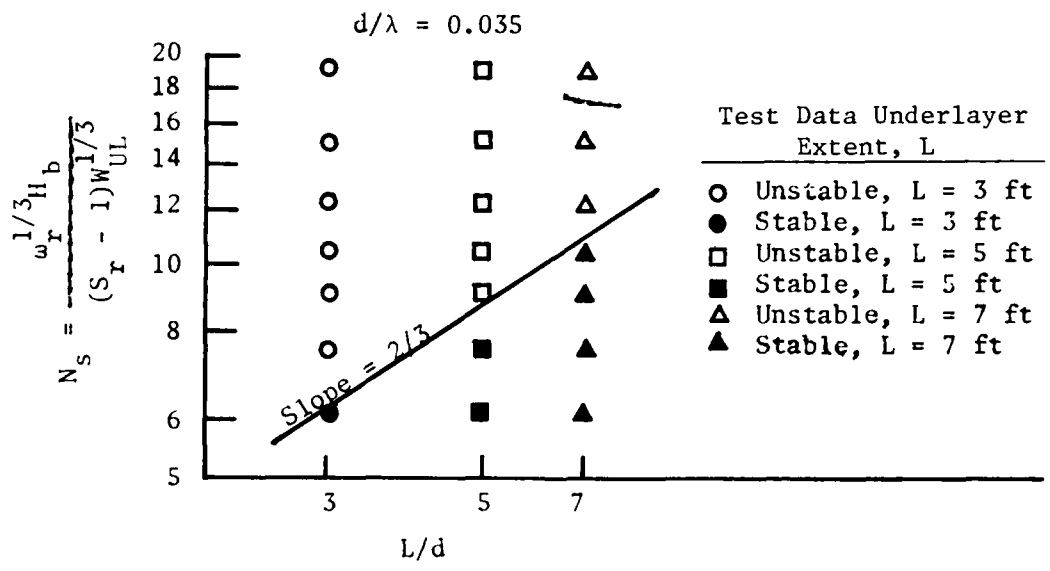


Figure 10. Stability number, N_s , versus the structure parameter, L/d , for relative water depth, $d/\lambda = 0.035$

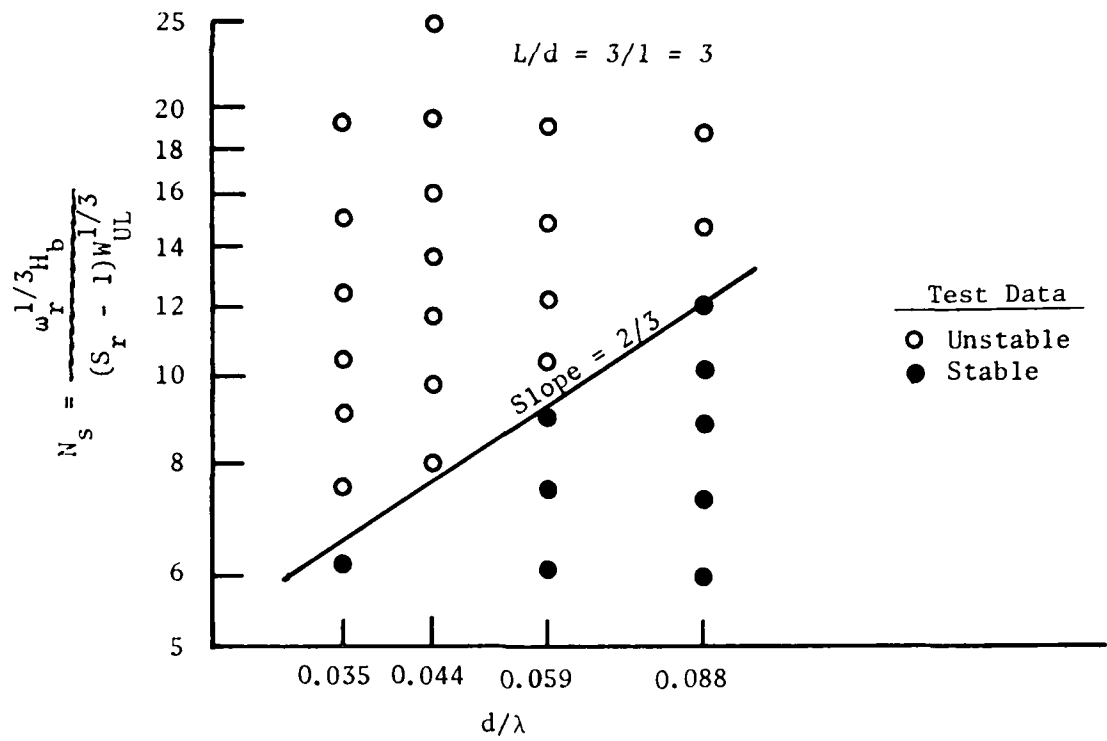


Figure 7. Stability number, N_s , versus the relative water depth, d/λ , for a 3-ft extent of test underlayer section ($L/d = 3$)

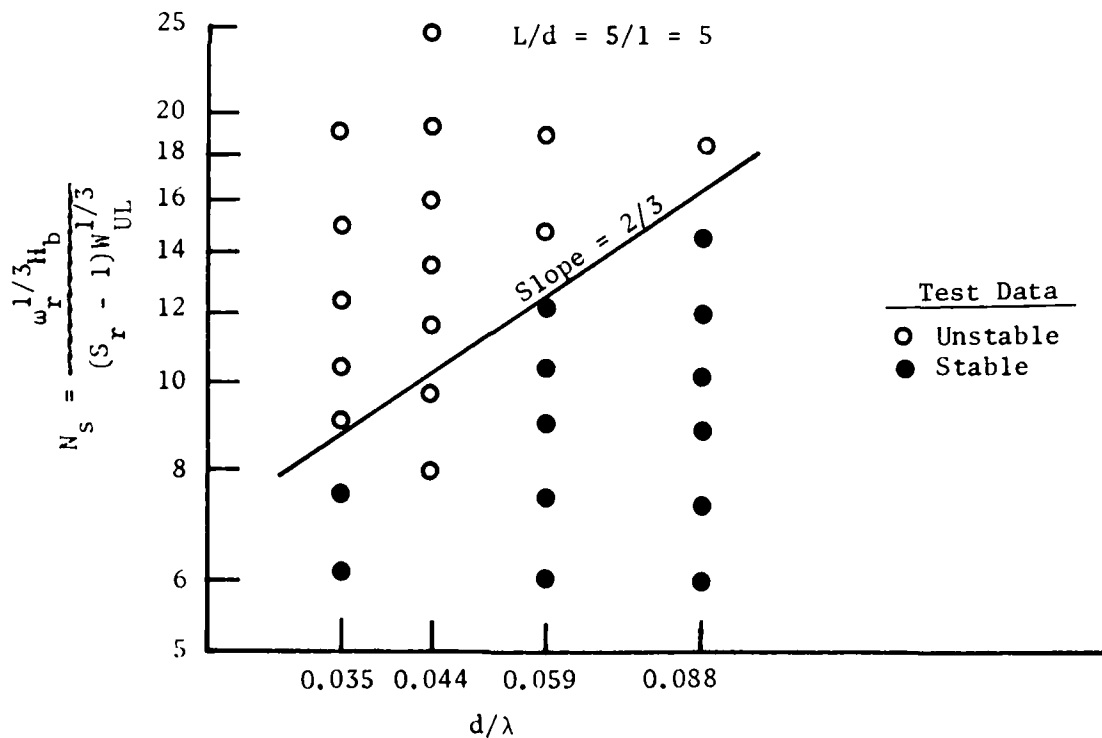


Figure 8. Stability number, N_s , versus the relative water depth, d/λ , for a 5-ft extent of test underlayer section ($L/d = 5$)

134. For constant values of the parameter L/d , typical representative values of the data of Table 4 are displayed in Figures 7 and 8 as N_s versus d/λ , where L is the extent of the underlayer section, and λ is the wavelength. While the data are fairly limited for each individual value of L/d , it does appear reasonable to separate the regions of stability from the unstable regions by a straight line on these log-log plots. While the precise slope of such a straight line cannot be determined, it appears that the same line slope could equally well be fit to each of these figures and to the other data of Hales and Houston (1983).

135. Typical representative values of the data of Table 4 are again displayed in Figures 9 and 10 as N_s versus L/d , for constant values of the parameter d/λ . Here again, the data are fairly limited for each individual value of d/λ ; however, the regions of stability may be separated from the unstable regions adequately with a straight line on these log-log plots. Again, the slope of such a straight line cannot be precisely ascertained; however, it appears that the same slope can be equally as well fit to data sets displayed in Figures 7 and 8 and Figures 9 and 10 (as well as the other data displayed in Hales and Houston 1983).

136. If indeed the same slope line can be fit to the data of constant values of L/d as can be fit to the data of constant values of d/λ , then the regions of stability can be separated from the unstable regions on a display that plots the stability number, N_s , of Equation 10 versus the relative underlayer section length, L/λ :

$$N_s = \frac{\omega_r^{1/3} H_b}{(S_r - 1) \omega_{UL}^{1/3}} = f\left(\frac{L}{\lambda}\right) \quad (11)$$

The precise functional representation can be determined from Figure 11. The average best-fit line slope on this log-log plot which separates the regions of stability from the unstable regions is determined to have a value of $2/3$. While some scatter was found to exist in the experimental data, this value of $2/3$ can be satisfactorily fit to the data of Figures 7-10. The average best-fit line generated a stability number:

$$N_s = \frac{\omega_r^{1/3} H_b}{(S_r - 1) \omega_{UL}^{1/3}} = 28.5 \left(\frac{L}{\lambda}\right)^{2/3} \quad (12)$$

Table 4 (Concluded)

Still-Water Depth d, ft	Wave Period T, sec	Maximum Breaker Wave Height H _b , ft	Wave- length λ, ft	Underlayer Material Extent L, ft	L λ	Average Model Stone Weight W _{UL} , lb	$\frac{w_r^{1/3} H_b}{(S_r - 1) W_{UL}^{1/3}}$	Stable, S or Unstable, U
1.0	4	1.45	22.70	3	0.13	0.0085	24.66	U
1.0	4	1.45	22.70	3	0.13	0.0175	19.35	U
1.0	4	1.45	22.70	3	0.13	0.0315	15.92	U
1.0	4	1.45	22.70	3	0.13	0.0520	13.49	U
1.0	4	1.45	22.70	3	0.13	0.0795	11.70	U
1.0	4	1.45	22.70	3	0.13	0.1405	9.68	U
1.0	4	1.45	22.70	3	0.13	0.2540	7.95	U
1.0	4	1.45	22.70	5	0.22	0.0085	24.66	U
1.0	4	1.45	22.70	5	0.22	0.0175	19.35	U
1.0	4	1.45	22.70	5	0.22	0.0315	15.92	U
1.0	4	1.45	22.70	5	0.22	0.0520	13.49	U
1.0	4	1.45	22.70	5	0.22	0.0795	11.70	U
1.0	4	1.45	22.70	5	0.22	0.1405	9.68	U
1.0	4	1.45	22.70	5	0.22	0.2540	7.95	U
1.0	4	1.45	22.70	7	0.31	0.0085	24.66	U
1.0	4	1.45	22.70	7	0.31	0.0175	19.35	U
1.0	4	1.45	22.70	7	0.31	0.0315	15.92	U
1.0	4	1.45	22.70	7	0.31	0.0520	13.49	U
1.0	4	1.45	22.70	7	0.31	0.0795	11.70	U
1.0	4	1.45	22.70	7	0.31	0.1405	9.68	U
1.0	4	1.45	22.70	7	0.31	0.2540	7.95	S
1.0	5	1.12	28.37	3	0.11	0.0085	19.05	U
1.0	5	1.12	28.37	3	0.11	0.0175	14.95	U
1.0	5	1.12	28.37	3	0.11	0.0315	12.30	U
1.0	5	1.12	28.37	3	0.11	0.0520	10.42	U
1.0	5	1.12	28.37	3	0.11	0.0795	9.04	U
1.0	5	1.12	28.37	3	0.11	0.1405	7.47	U
1.0	5	1.12	28.37	3	0.11	0.2540	6.14	S
1.0	5	1.12	28.37	5	0.18	0.0085	19.05	U
1.0	5	1.12	28.37	5	0.18	0.0175	14.95	U
1.0	5	1.12	28.37	5	0.18	0.0315	12.30	U
1.0	5	1.12	28.37	5	0.18	0.0520	10.42	U
1.0	5	1.12	28.37	5	0.18	0.0795	9.04	U
1.0	5	1.12	28.37	5	0.18	0.1405	7.47	S
1.0	5	1.12	28.37	5	0.18	0.2540	6.14	S
1.0	5	1.12	28.37	7	0.25	0.0085	19.05	U
1.0	5	1.12	28.37	7	0.25	0.0175	14.95	U
1.0	5	1.12	28.37	7	0.25	0.0315	12.30	U
1.0	5	1.12	28.37	7	0.25	0.0520	10.42	S
1.0	5	1.12	28.37	7	0.25	0.0795	9.04	S
1.0	5	1.12	28.37	7	0.25	0.1405	7.47	S
1.0	5	1.12	28.37	7	0.25	0.2540	6.14	S

Table 4 (Continued)

Still-Water Depth d, ft	Wave Period T, sec	Maximum Breaker Wave Height H_b , ft	Wave- length λ , ft	Underlayer Material Extent		Average Model Stone Weight W_{UL} , lb	$\frac{w_r^{1/3} H_b}{(S_r - 1) W_{UL}^{1/3}}$	Stable, S or Unstable, U
				L, ft	$\frac{L}{\lambda}$			
0.5	5	0.68	20.06	3	0.15	0.0085	11.57	U
0.5	5	0.68	20.06	3	0.15	0.0175	9.08	S
0.5	5	0.68	20.06	3	0.15	0.0315	7.47	S
0.5	5	0.68	20.06	3	0.15	0.0520	6.33	S
0.5	5	0.68	20.06	3	0.15	0.0795	5.49	S
0.5	5	0.68	20.06	3	0.15	0.1405	4.54	S
0.5	5	0.68	20.06	3	0.15	0.2540	3.73	S
0.5	5	0.68	20.06	5	0.25	0.0085	11.57	U
0.5	5	0.68	20.06	5	0.25	0.0175	9.08	S
0.5	5	0.68	20.06	5	0.25	0.0315	7.47	S
0.5	5	0.68	20.06	5	0.25	0.0520	6.33	S
0.5	5	0.68	20.06	5	0.25	0.0795	5.49	S
0.5	5	0.68	20.06	5	0.25	0.1405	4.54	S
0.5	5	0.68	20.06	5	0.25	0.2540	3.73	S
0.5	5	0.68	20.06	7	0.35	0.0085	11.57	S
0.5	5	0.68	20.06	7	0.35	0.0175	9.08	S
0.5	5	0.68	20.06	7	0.35	0.0315	7.47	S
0.5	5	0.68	20.06	7	0.35	0.0520	6.33	S
0.5	5	0.68	20.06	7	0.35	0.0795	5.49	S
0.5	5	0.68	20.06	7	0.35	0.1405	4.54	S
0.5	5	0.68	20.06	7	0.35	0.2540	3.73	S
1.0	2	1.09	11.35	3	0.26	0.0085	18.54	U
1.0	2	1.09	11.35	3	0.26	0.0175	14.55	U
1.0	2	1.09	11.35	3	0.26	0.0315	11.97	S
1.0	2	1.09	11.35	3	0.26	0.0520	10.14	S
1.0	2	1.09	11.35	3	0.26	0.0795	8.80	S
1.0	2	1.09	11.35	3	0.26	0.1405	7.27	S
1.0	2	1.09	11.35	3	0.26	0.2540	5.98	S
1.0	2	1.09	11.35	5	0.44	0.0085	18.54	U
1.0	2	1.09	11.35	5	0.44	0.0175	14.55	S
1.0	2	1.09	11.35	5	0.44	0.0315	11.97	S
1.0	2	1.09	11.35	5	0.44	0.0520	10.14	S
1.0	2	1.09	11.35	5	0.44	0.0795	8.80	S
1.0	2	1.09	11.35	5	0.44	0.1405	7.27	S
1.0	2	1.09	11.35	5	0.44	0.2540	5.98	S
1.0	2	1.09	11.35	7	0.62	0.0085	18.54	S
1.0	2	1.09	11.35	7	0.62	0.0175	14.55	S
1.0	2	1.09	11.35	7	0.62	0.0315	11.97	S
1.0	2	1.09	11.35	7	0.62	0.0520	10.14	S
1.0	2	1.09	11.35	7	0.62	0.0795	8.80	S
1.0	2	1.09	11.35	7	0.62	0.1405	7.27	S
1.0	2	1.09	11.35	7	0.62	0.2540	5.98	S
1.0	3	1.11	17.02	3	0.18	0.0085	18.88	U
1.0	3	1.11	17.02	3	0.18	0.0175	14.81	U
1.0	3	1.11	17.02	3	0.18	0.0315	12.19	U
1.0	3	1.11	17.02	3	0.18	0.0520	10.33	U
1.0	3	1.11	17.02	3	0.18	0.0795	8.96	S
1.0	3	1.11	17.02	3	0.18	0.1405	7.41	S
1.0	3	1.11	17.02	3	0.18	0.2540	6.08	S
1.0	3	1.11	17.02	5	0.29	0.0085	18.88	U
1.0	3	1.11	17.02	5	0.29	0.0175	14.81	U
1.0	3	1.11	17.02	5	0.29	0.0315	12.19	S
1.0	3	1.11	17.02	5	0.29	0.0520	10.33	S
1.0	3	1.11	17.02	5	0.29	0.0795	8.96	S
1.0	3	1.11	17.02	5	0.29	0.1405	7.41	S
1.0	3	1.11	17.02	5	0.29	0.2540	6.08	S
1.0	3	1.11	17.02	7	0.41	0.0085	18.88	S
1.0	3	1.11	17.02	7	0.41	0.0175	14.81	S
1.0	3	1.11	17.02	7	0.41	0.0315	12.19	S
1.0	3	1.11	17.02	7	0.41	0.0520	10.33	S
1.0	3	1.11	17.02	7	0.41	0.0795	8.96	S
1.0	3	1.11	17.02	7	0.41	0.1405	7.41	S
1.0	3	1.11	17.02	7	0.41	0.2540	6.08	S

(Continued)

(Sheet 2 of 3)

$$u_1 = 4 \sqrt{\frac{kr}{\pi}} \sin \left[\frac{1}{2} (\theta_0 - \theta) \right] \quad (22)$$

$$u_2 = -4 \sqrt{\frac{kr}{\pi}} \sin \left[\frac{1}{2} (\theta_0 + \theta) \right] \quad (23)$$

Bretschneider (1966) has presented computational procedures for evaluating the diffraction coefficients at arbitrary points behind jetties or breakwaters.

147. Wiegel (1962) developed a graphical procedure for determining diffraction coefficients of waves passing the tip of single breakwaters. The family of diagrams shows, for uniform water depth, lines of equal wave-height reduction displayed in terms of the diffraction coefficients. The diffraction diagrams (typical example, Figure 13) are constructed in polar coordinate form centered at the structure tip. The arcs behind the breakwater are spaced one radius-wavelength unit apart so that, in application, a specific diagram must be scaled up or down to the particular wavelength corresponding to the scale of the hydrographic area under investigation. The set of diffraction diagrams

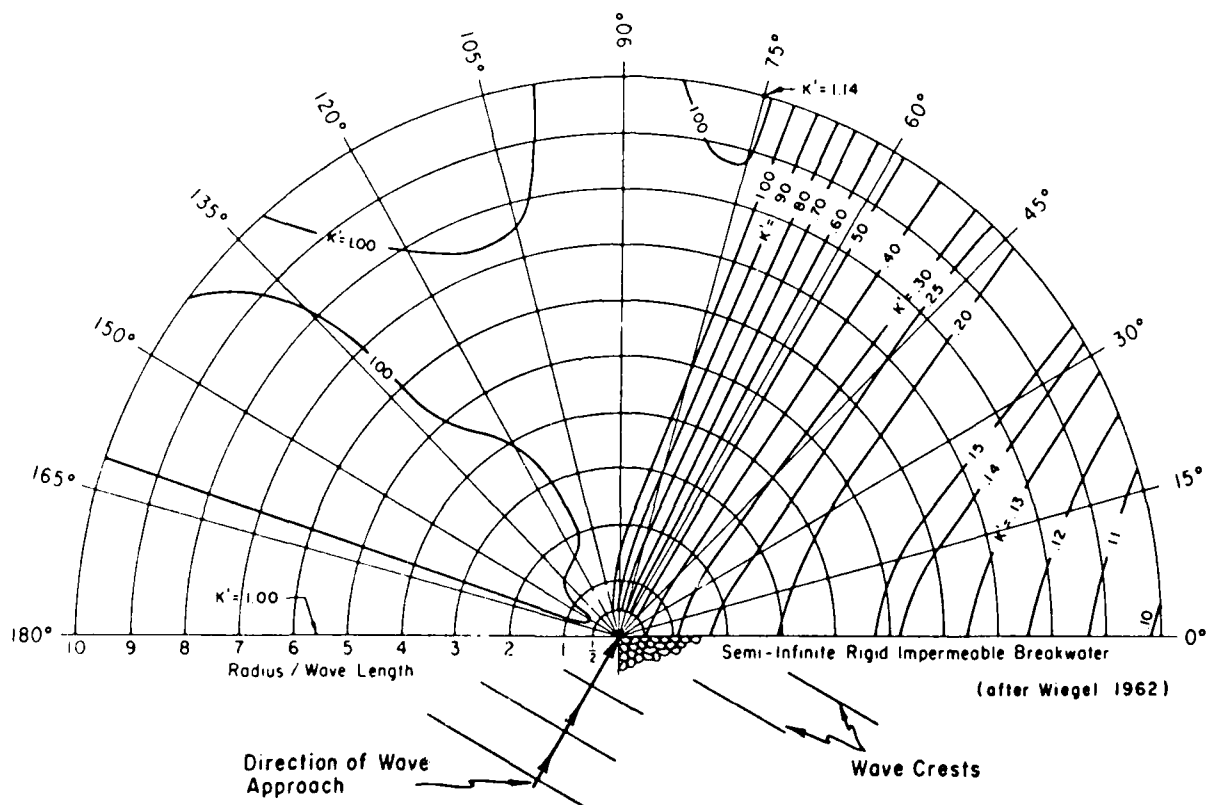


Figure 13. Typical example, wave diffraction past a semi-infinite breakwater, angle of incidence = 60 deg

of waves passing the tip of a single breakwater was presented by USAEWES (1984).

Combined water wave
refraction and diffraction

148. The bathymetry shoreward of a jetty or breakwater usually is not flat or even uniform; hence, refraction generally occurs in addition to the diffraction effects. While a general unified analytical approach to the simultaneous solution of these two distinctly different phenomena has not been entirely developed, considerable insight has been gained through the theoretical work of Liu and Mei (1975, 1976), Lick (1978), Liu and Lozano (1979), and through the earlier experimental work of Mobarek (1962). The procedure usually followed by coastal engineers concerned with wave-height variation behind jetties or breakwaters is to construct refraction diagrams shoreward to the structure, then construct diffraction diagrams for three or four wavelengths shoreward of the jetty, and finally refract the last wave crest on toward the shoreline. This procedure is schematized in Figure 14 where the overall refraction diffraction coefficient, K_{r-d} , in the region behind the structure is:

$$K_{r-d} = K_r K_d \sqrt{b_1 b_2} \quad (24)$$

where

K_r = refraction coefficient at the structure, dimensionless

K_d = diffraction coefficient on last wave crest behind the structure from which additional refraction computations are performed, dimensionless

b_1 = orthogonal spacing at the last diffracted wave crest, ft

b_2 = orthogonal spacing near the shore, ft

149. Mobarek (1962) experimentally investigated the effect of bottom slope on wave diffraction through a gap in a breakwater normal to the incident wave direction. Also investigated was the effect of an abrupt increase or decrease in the water depth behind the breakwater. The theoretical analysis for the comparison of experimental results followed the treatment of Penny and Price (1944) restricted to the case of normal incident, for which the Sommerfeld (1896) solution is simplified, and restricted by the presence of a horizontal bottom. Two fundamentally different basin configurations were used in the study. The first consisted of a longitudinally sloping bottom with the

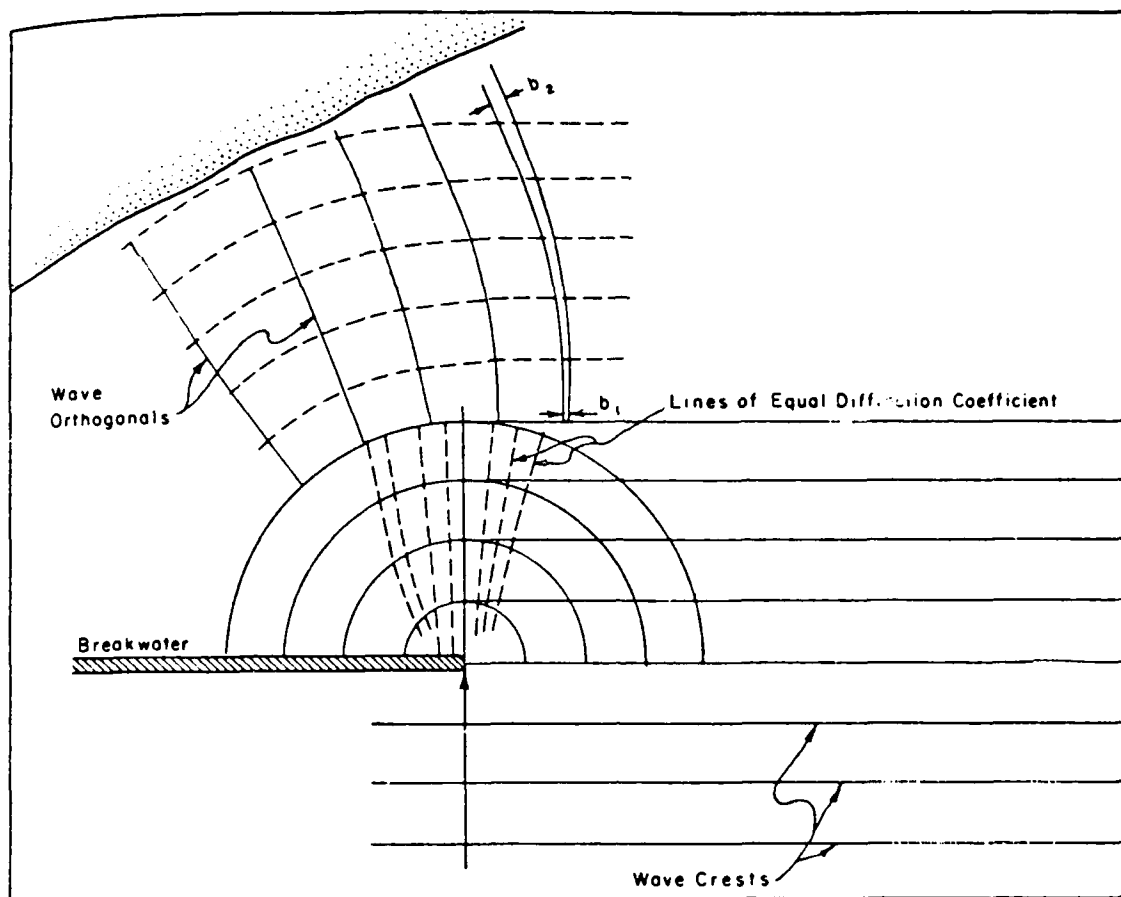


Figure 14. Graphical procedure for determining overall refraction and diffraction effects past a breakwater (after USAEWES 1984)

slope commencing at the breakwater and extending to the shoreline. The second was constructed with a flat bottom extending beyond the breakwater gap but sloping laterally to the shoreline. Taking into consideration the serious limitations of the experimental equipment (very small model, 72 sq ft), the investigation led to the conclusion that the procedure usually followed for estimating wave heights behind jetties or shore-connected breakwaters (Figure 14) was sufficiently good for medium period waves; but in the case of long waves, the effect of the shoaling bottom on waves should be taken into consideration. Experiments on a larger scale were highly recommended.

150. For a long shore-connected breakwater on a slowly varying bottom, an asymptotic theory has been developed by Liu and Mei (1976) which accounts for the combined effects of refraction and Fresnel diffraction of water waves. However, for short jetties or groins, the reflection and diffraction effects may be either too localized or too complicated by virtue of the dominant

influence of the surf zone to be handled by this theory. The approximation is a combination of Kirchhoff's theory and geometrical optics. This permits the diffraction field near the beach to be calculated analytically and this can, in turn, be used for breaker line estimates.

151. A uniformly valid asymptotic solution for water waves has been developed by Liu and Lozano (1979) that accounts for the combined effects of refraction due to slowly varying water depth and diffraction by a long shore-connected breakwater. This solution is more general than the approximate solution developed by Liu and Mei (1976) because this theory is valid near the edge and the tip of the breakwater. The wave behavior in the near field is of particular interest for studying the scour and erosion that may occur near the tip of a breakwater. In this analysis, recent developments in the field of formal geometrical optics have been included to extend the effect of diffraction.

152. Berkhoff (1972), Schonfeld (1972), and Smith and Sprinks (1975) independently derived a two-dimensional equation that governs short-wave propagation over moderately varying depths. Rewriting Berkhoff's expression, Jonsson and Brink-Kjaer (1973) introduced the mild-slope wave equation:

$$\nabla \cdot (cc_g \nabla \eta) + \frac{c_g}{c} \omega^2 \eta = 0 \quad (25)$$

where

∇ = horizontal gradient operator, dimensionless

c = phase velocity, ft/sec

c_g = group velocity, ft/sec

ω = angular frequency, $2\pi/T$, 1/sec

η = complex wave amplitude, ft

Equation 25 can be rewritten in the form:

$$\nabla \cdot (cc_g \nabla \phi) + \frac{c_g}{c} \omega^2 \phi = 0 \quad (26)$$

where ϕ is a velocity potential defined by $\bar{u} = \nabla \phi$ and \bar{u} is a two-dimensional vector. Equation 26 reduces to the diffraction Helmholtz equation in deep or constant-depth water. In shallow water, the equation reduces to the linear long-wave equation.

153. Houston (1980) solved Equation 26 by the use of a hybrid finite

element numerical model originally developed by Chen and Mei (1974) to solve the diffraction Helmholtz equation in a constant-depth region. The appropriate modifications, including variable depth and frequency dispersion, were incorporated by Houston (1980) and the solution of Equation 26 was applied to the geometry of the experimental study of Hales (1980b) (i.e., a uniform slope with a shore-connected breakwater parallel with the shoreline). A problem in simulating those hydraulic experimental tests numerically was that the waves broke in the hydraulic facility near the shoreline and thus dissipated their energy. No mechanism existed to dissipate energy in the numerical model. However, dissipation was simulated by allowing waves to continue to propagate out of the problem area. The breakwater and uniform slope were numerically modeled only to the point where breaking occurred. The depth was then increased to the depth of a semi-infinite ocean region surrounding the region of computation, and the waves were allowed to radiate away from the area of interest.

Shore-Connected Breakwater Normal to Shoreline

Experimental facility

154. This three-dimensional experimental investigation was conducted in a physical experimental facility that was molded in cement mortar and consisted of a 50- by 60-ft area with a water depth of 1 ft in the open-ocean region (Figure 15). The beach slope was 1V on 20H, with a vertical, impermeable breakwater extending perpendicularly from the shoreline for a distance of 15 ft to a point where the water depth was 0.75 ft. The uniform slope continued on to a water depth of 1 ft, beyond which the basin was horizontal to the facility walls. The wave generator was mobile, and two positions were tested (incident waves of 20 and 30 deg). Wave guides extended from the ends of the generator along wave orthogonals toward the shoreline. Orthogonals were determined by standard refraction techniques for waves propagating onto a uniform slope in the absence of the breakwater. The area of interest was downwave of the breakwater. Four sections perpendicular to the breakwater were instrumented with wave-height sensors for determination of the wave field. These sections were located 6, 8, 10, and 12 ft from the mean waterline (shoreline end of the breakwater), and are labeled "distance along the breakwater."

155. Experimental waves were generated by a 30-ft-long wave generator

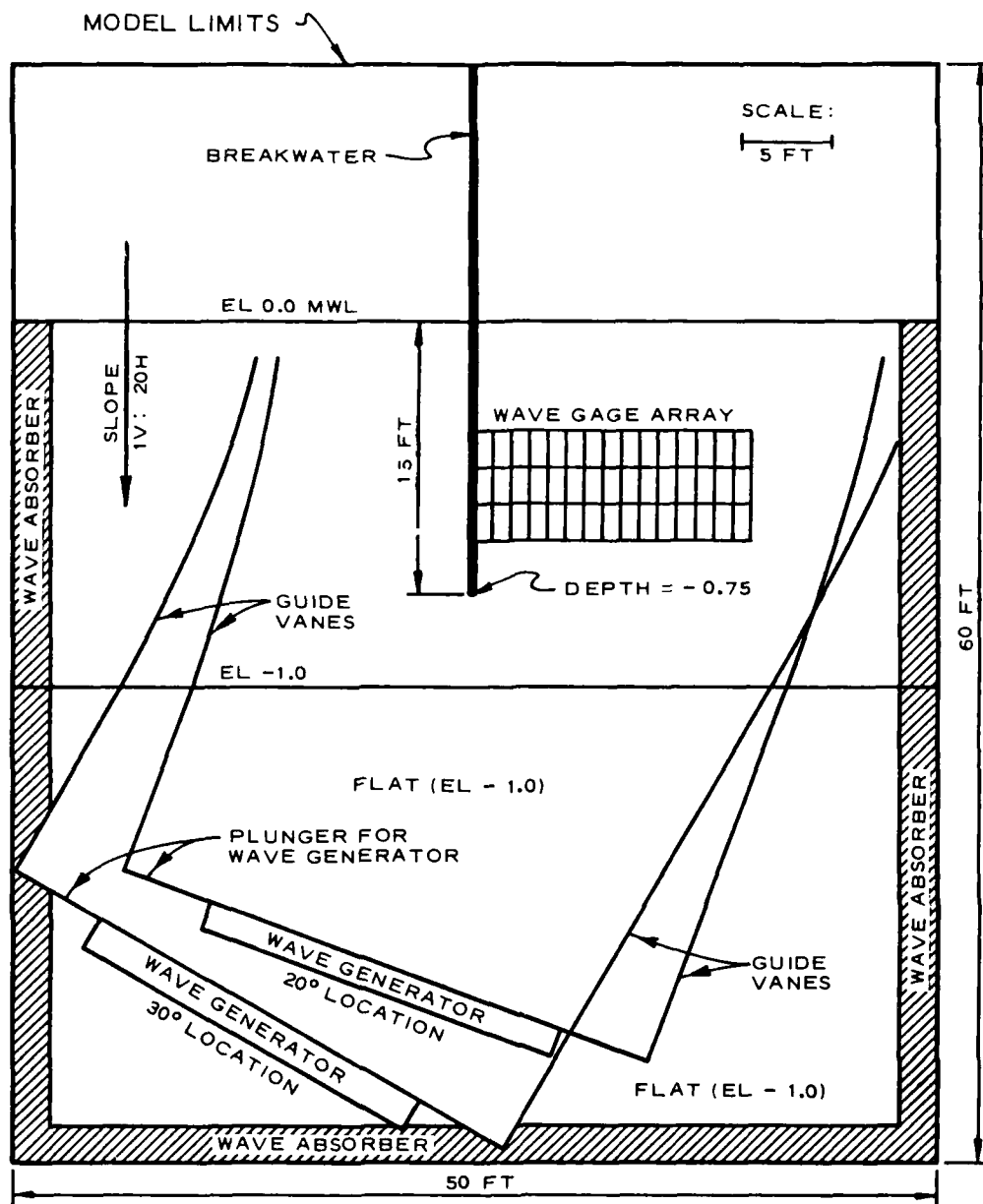


Figure 15. Experimental facility

with a trapezoidal-shaped, vertical-motion plunger. The vertical movement of the plunger caused a periodic displacement of water surface. The length of stroke and the frequency of the vertical motion were variable over the range necessary to generate waves with the required characteristics. In addition, the wave generator was mounted on retractable casters which enabled it to be positioned to generate waves from the required directions. A 2-ft (horizontal solid layer of fiber wave absorber was placed around the inside perimeter of

the facility to damp wave energy that might otherwise be reflected from the facility walls.

Wave-height sensors

156. The data acquired from wave facilities by ADACS (Figure 16) are

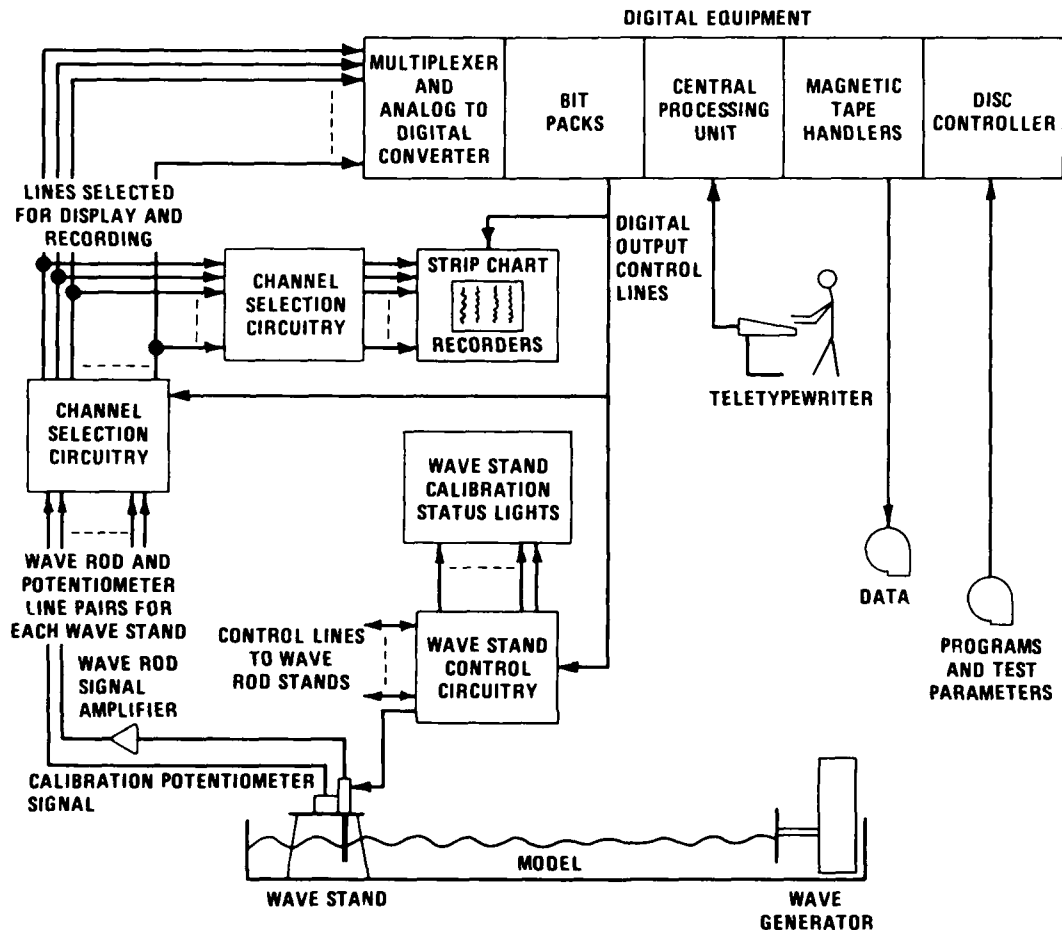


Figure 16. Schematic of components of Automated Data Acquisition and Control System (ADACS)

the water-surface variations about a reference water level. This information is collected at selected geographic locations within the facility for specified wave conditions at the wave generator. Wave sensors are used to obtain this information at selected locations in the facility. Each of the water-surface-piercing, parallel rod wave sensors is connected to a Wheatstone bridge and a transducer measures the conductance of the water between the two parallel rods which are mounted vertically (Figure 17). The conductance is directly proportional to the depth of submergence of the two rods in the water.

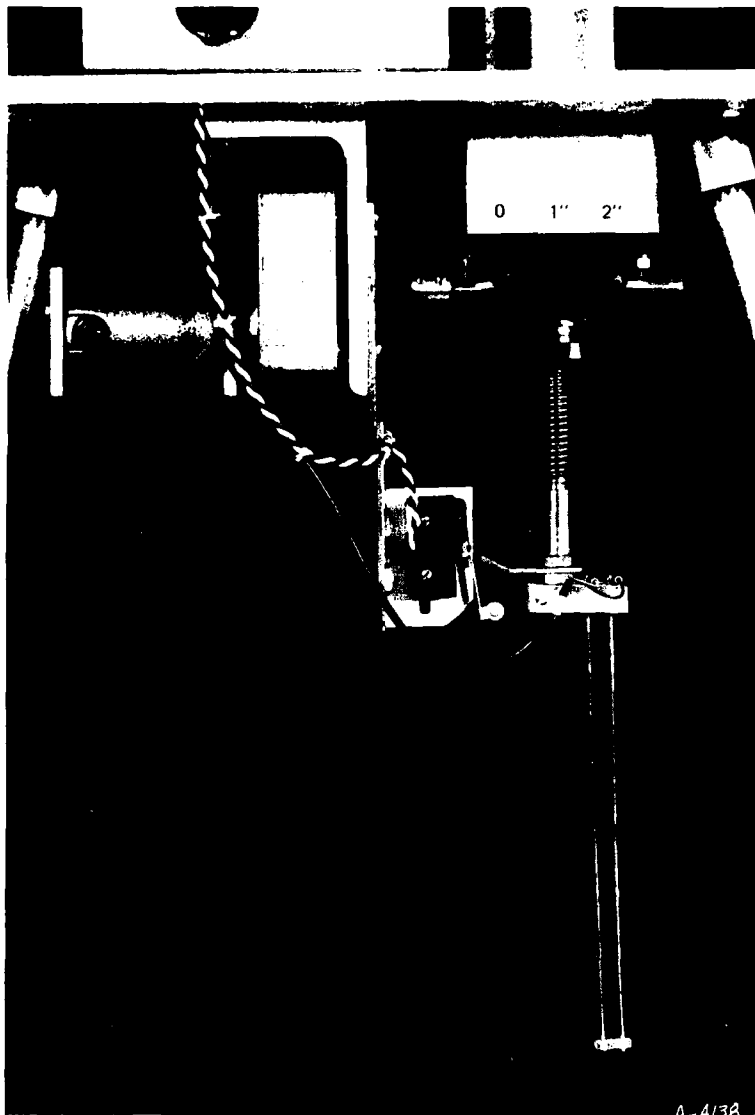


Figure 17. Parallel rod conductance-type wave sensor

brating the wave sensors (maximum of 25 rods simultaneously) prior to collecting data is provided by ADACS. To calibrate each set of parallel rods, the voltage from the signal conditioning equipment is monitored and recorded as the parallel rods are moved vertically a known distance into or out of the water. A precision, linear-position potentiometer is located on the wave sensor stand and is coupled directly to the parallel rods by a gear train driven by an electric motor. By moving vertically the coupled wave sensor and potentiometer with the electric motor and by monitoring the output voltage from the potentiometer, the wave sensor can be moved vertically a precise distance.

The output of each wave sensor is routed through shielded cables to its signal conditioning equipment where it is processed for recording. The ADACS can detect changes in water-surface elevations to an accuracy of 0.001 ft. To obtain this accuracy, ultrastable power supplies and good signal-to-noise ratios are necessary. The carrier source for the wave sensor bridge maintains a variation of less than 0.025 percent.

Calibration

157. In order to convert the water-elevation data in millivolts to water-surface elevations in feet, each wave sensor must be calibrated. The capability of automatically cali-

The electric motor for each wave sensor is controlled by a control/sense line and a relay contact. The minicomputer controls the vertical movement of each wave sensor by actuating the control/sense line. The central processing unit acts as a voltage comparator by monitoring the potentiometer voltage and comparing it with a reference voltage which is determined from desired displacement and potentiometer calibration. When the voltage comparison is satisfied, the control/sense line is reactivated, the electric motor stops, and voltage samples from the rods and potentiometers are acquired. By systematically moving each wave sensor through 11 quasi-equally spaced locations over the range of rod length used, voltage versus known displacements are obtained from which a calibration curve for each sensor can be calculated and recorded on magnetic tape or disc. After collecting the calibration data, the minicomputer analyzes these data by least-squares fitting a set of curves (linear, quadratic, or spline) to the data, determining the best order of fit, and comparing the maximum deviation of the best fit with a previously acceptable value for this maximum deviation.

Data acquisition and analysis

158. During the acquisition mode, wave data for a specified wave condition at the wave generator are collected from a maximum of 50 wave sensors, recorded on analog strip charts, digitized, and recorded on magnetic tape or disc for further analysis. The sampling scheme is flexible and can be tailored for different applications with maximum throughput rates theoretically limited by the multiplexer rate and allocatable buffer size. The sampling scheme used in this investigation was 60 discrete voltage samples equally spaced over each wave period for a predetermined number of 90 wave periods for each of the sensor locations. From input parameters, the minicomputer calculated the lag at the beginning of data acquisition by 10 wave periods after starting the generator, provided timing pulses for synchronizing and controlling the recorders, and determined completion of the test. The determination of the height of each wave of the monochromatic wave train was performed (at each sensor location), the average of these 90 individual heights was calculated, and the standard deviation of these individual observations about the mean was computed. The value displayed as the wave height at each sensor location is this mean value plus or minus one standard deviation. The data were obtained by operating 32 wave-height sensors simultaneously for each test condition and then repeating the same test with the sensors repositioned to allow

better definition of wave-height gradients away from the breakwater. A typical arrangement of the 32 sensors near the breakwater is shown in Figure 18. Only the wave sensor probe penetrates the water surface, thereby minimizing local disturbances.

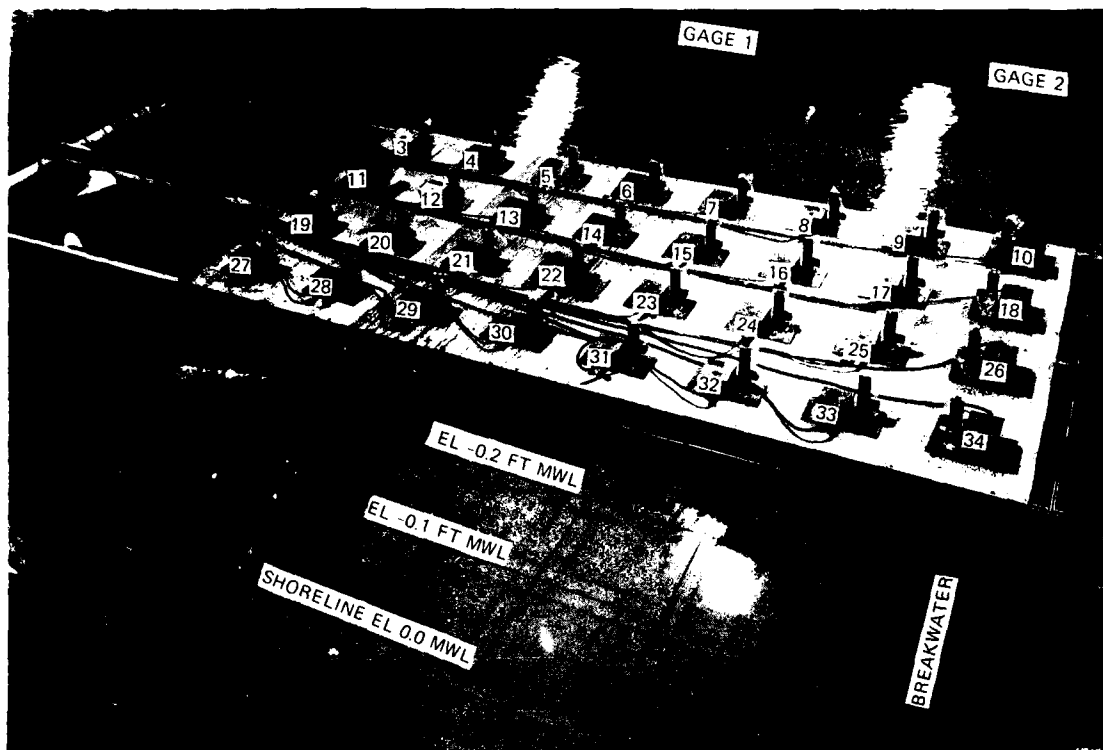


Figure 18. Wave-height sensor arrangement, grid spacing = 2 ft

Average wave-induced current determination

159. To define the circulation patterns downwave of the breakwater, average values of wave-induced velocity were determined at those grid locations shown in Figure 19. The average values were determined at each individual station after the wave generator had been operating for 2 min so that the circulation cell immediately adjacent to the breakwater could become well established prior to measurements. After the measurement at either surface, middepth, or bottom had been obtained at each station, wave generator operation was terminated so that those fluid motions unique to the physical facility (downcoast circulation cell induced by the boundary of the finite experimental area) would not have time to progress into the area of major interest (the immediate vicinity of the structure). It was known a priori that the

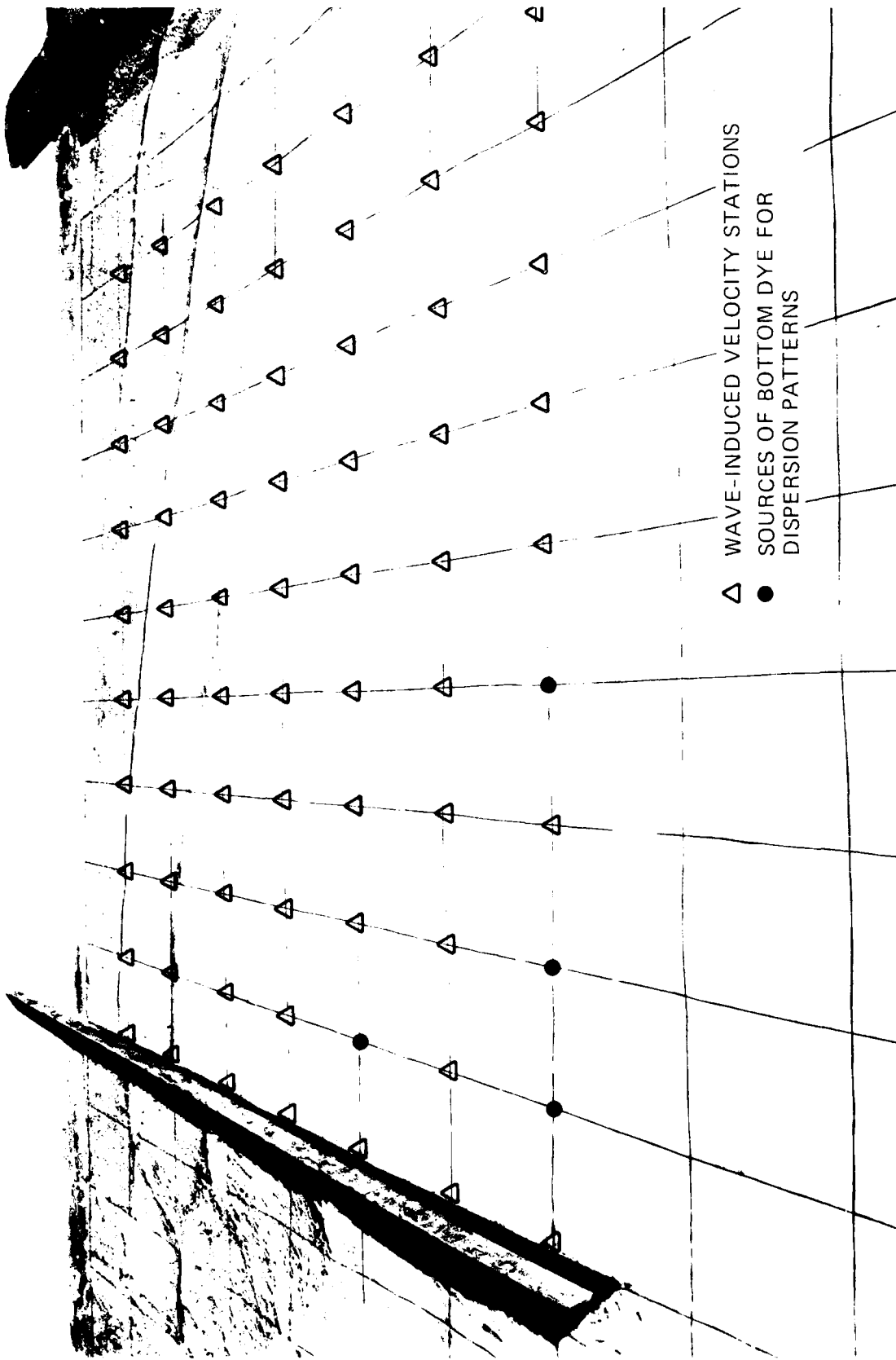


Figure 19. Stations for determining average wave-induced velocities

existence of the downcoast boundary condition would preclude exact duplication of an infinite coastline; however, for the purpose of verifying various theories, numerical models can be formulated to represent a finite area that includes all boundaries appropriately defined.

160. Surface current magnitudes were determined by timing a particle floating on the surface and initially positioned over the grid points. The time and direction required for each particle to traverse a distance of 1 ft were noted and recorded. Surface velocities were especially sensitive to wave orbital motions. Middepth velocities were determined by observing the movement of dye placed at one-half the still-water depth. While a measure of dispersion would tend to occur after a finite time interval, the center of the dye region could be easily ascertained; and this was the element considered in the average velocity determinations. Bottom current velocities and directions were determined by observing dye movement which had been placed essentially on the bottom of the model. Except for those regions in the breaker zone, the dye patterns on the bottom were more easily observable than those at middepth because downward dispersions were precluded. Hence, the dye region moved in a more concentrated form.

Wave field downcoast of breakwater

161. The experimental facility used in this study was constructed so that transition-to-shallow-water waves would exist near the breakwater (representative of prototype waves which are capable of causing scour and erosion). This requirement indicated that transition-depth waves should be generated, since physical facility size and depth constraints precluded the generation of deepwater waves with required characteristics. In addition, the requirement existed that the generated wave heights should be large enough so that small changes in the heights could be detectable, and at the same time the heights should be small enough so that comparisons with linear theories could be performed. Preliminary tests indicated that for the area of major interest and for the range of wave periods considered pertinent, the specific test conditions shown in Table 5 could be experimentally investigated with height changes remaining essentially linear, thus permitting comparisons with theoretical developments. Typical representative wave patterns covering the range of conditions tested are displayed in Figures 20-22 for waves from an incident direction of 20 deg.

162. Thirty-four wave-height sensors were used to determine the wave

Table 5
Test Conditions

Test Condition	Incident Wave Approach Direction				
	30 deg		20 deg		
Wave period, sec	0.75	1.00	0.75	1.00	1.50
Wavelength near generator, ft	2.82	4.52	2.82	4.52	7.69
d/L	0.355	0.221	0.355	0.221	0.130
Wave height near generator, ft (generator stroke = 0.50 in.)	0.111		0.122		
Wave height near generator, ft (generator stroke = 0.75 in.)	0.164	0.101	0.180	0.112	
Wave height near generator, ft (generator stroke = 1.00 in.)	0.221	0.139	0.245	0.154	0.077
Wave height near generator, ft (generator stroke = 1.50 in.)					0.111

heights along the four sections perpendicular to, and downwave of, the vertical breakwater (eight gages along each section and two reference gages in the ocean region near the wave generator). The average of the heights recorded at the two ocean gages was selected to be the input wave height from the wave generator. The heights recorded at the remaining 32 gages were normalized to this input wave height. All 32 gages were recorded simultaneously with each individual reading at all data stations consisting of the average of 90 waves. Ten repeatability tests were conducted under identical test conditions to define the variability of the measurements. The statistical measure of the variability was the square root of the variance, or the standard deviation. The variance is defined as the sum of the squares of the deviates of each individual observation from their average, divided by one less than the total number of deviates. For typical representative conditions, the average of the ratios is displayed in Figures 23-32, with error bars showing plus or minus one standard deviation. One standard deviation is usually 2 to 3 percent of the average value of the observation. The data were originally obtained with the gages positioned at 2-ft intervals starting at the breakwater and extending to a location 14 ft from the breakwater. To provide better definition of the

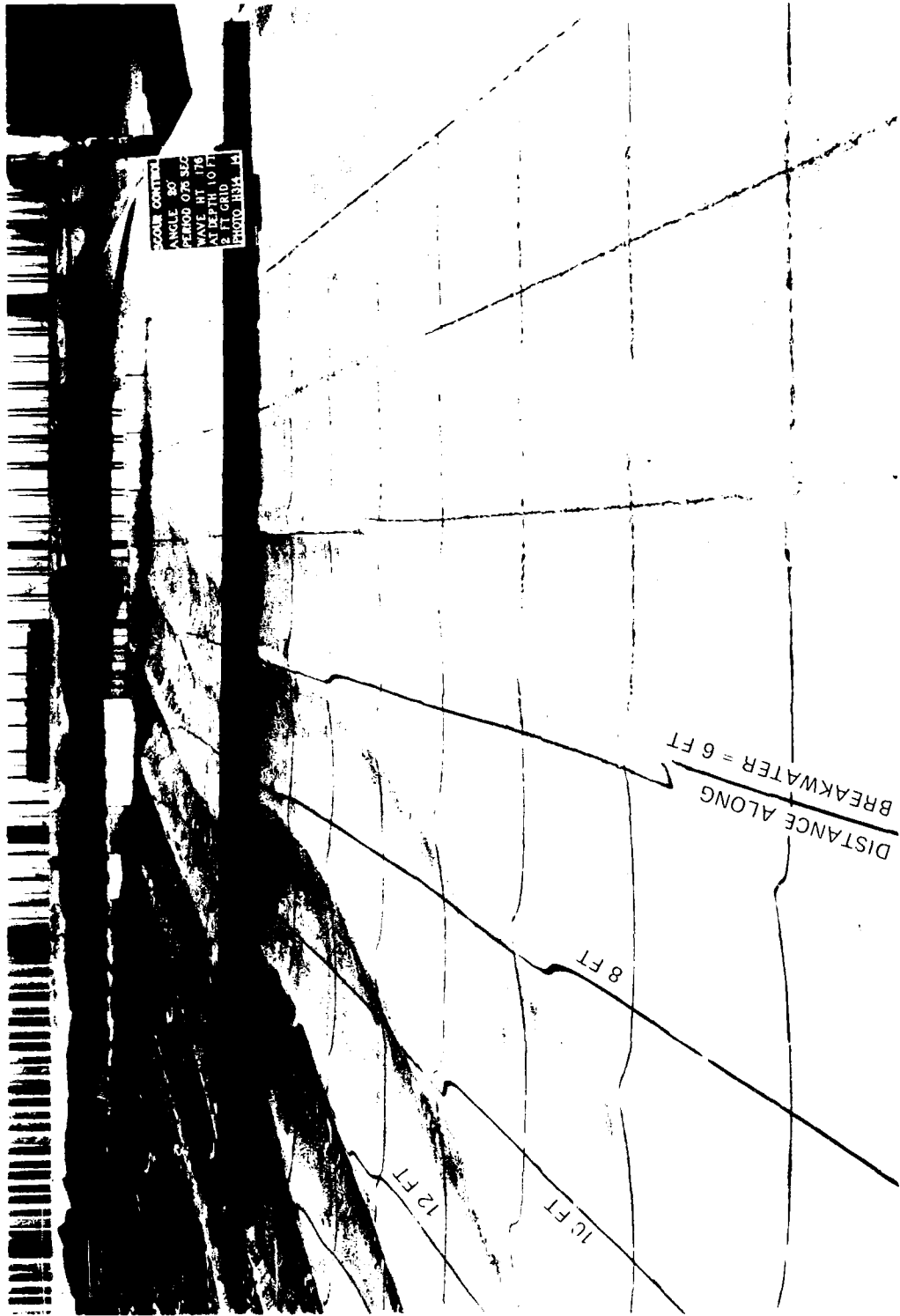
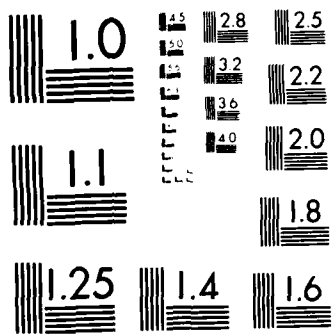


Figure 20. Typical wave pattern for 0.75-sec wave of height 0.176 ft near the wave generator approaching from an incident direction of 20 deg (downwave region)



MICROCOPY RESOLUTION TEST CHART
NATIONAL BUREAU OF STANDARDS 1963-A

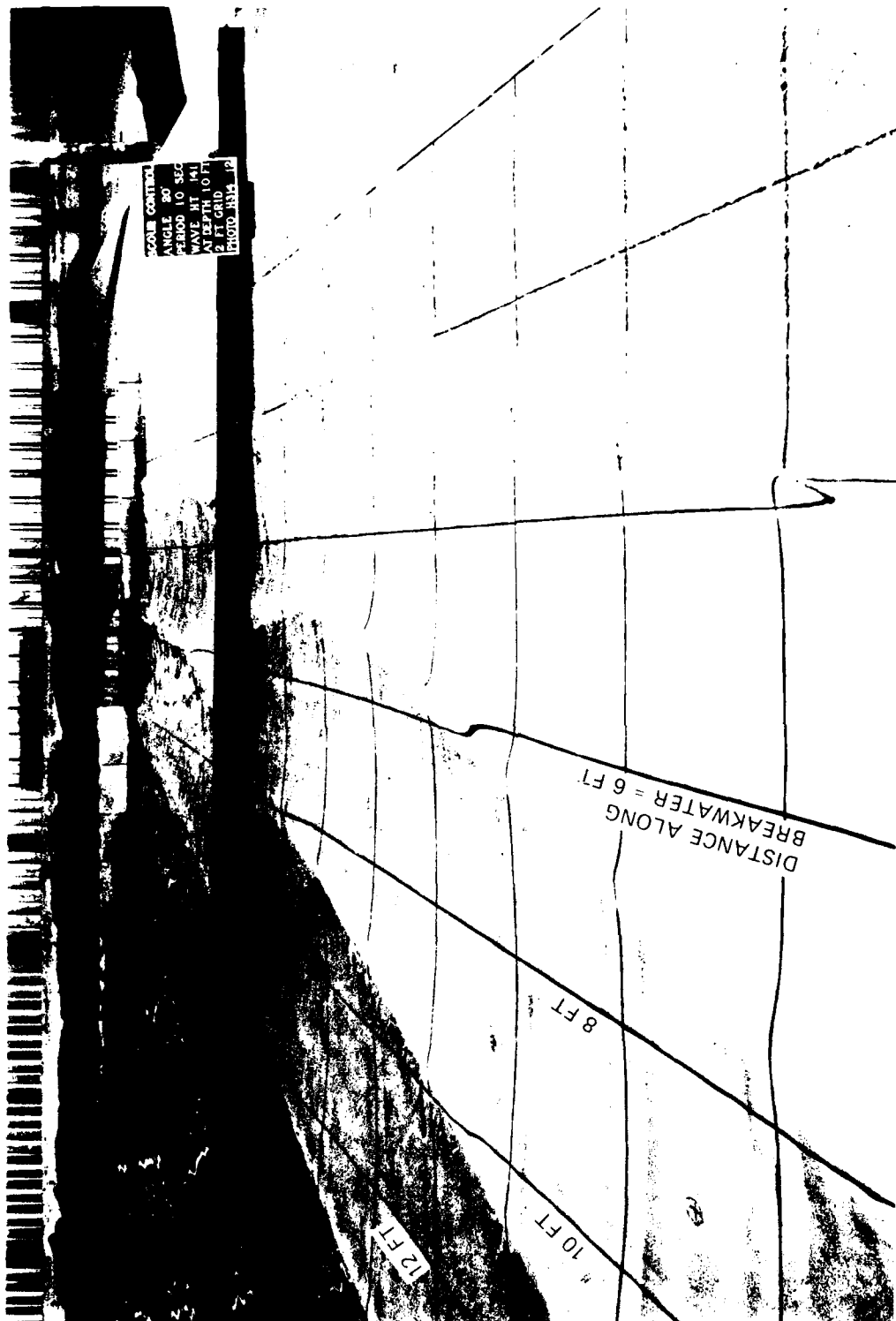


Figure 21. Typical wave pattern for 1.0-sec wave of height 0.141 ft near the wave generator approaching from an incident direction of 20 deg (downwave region)

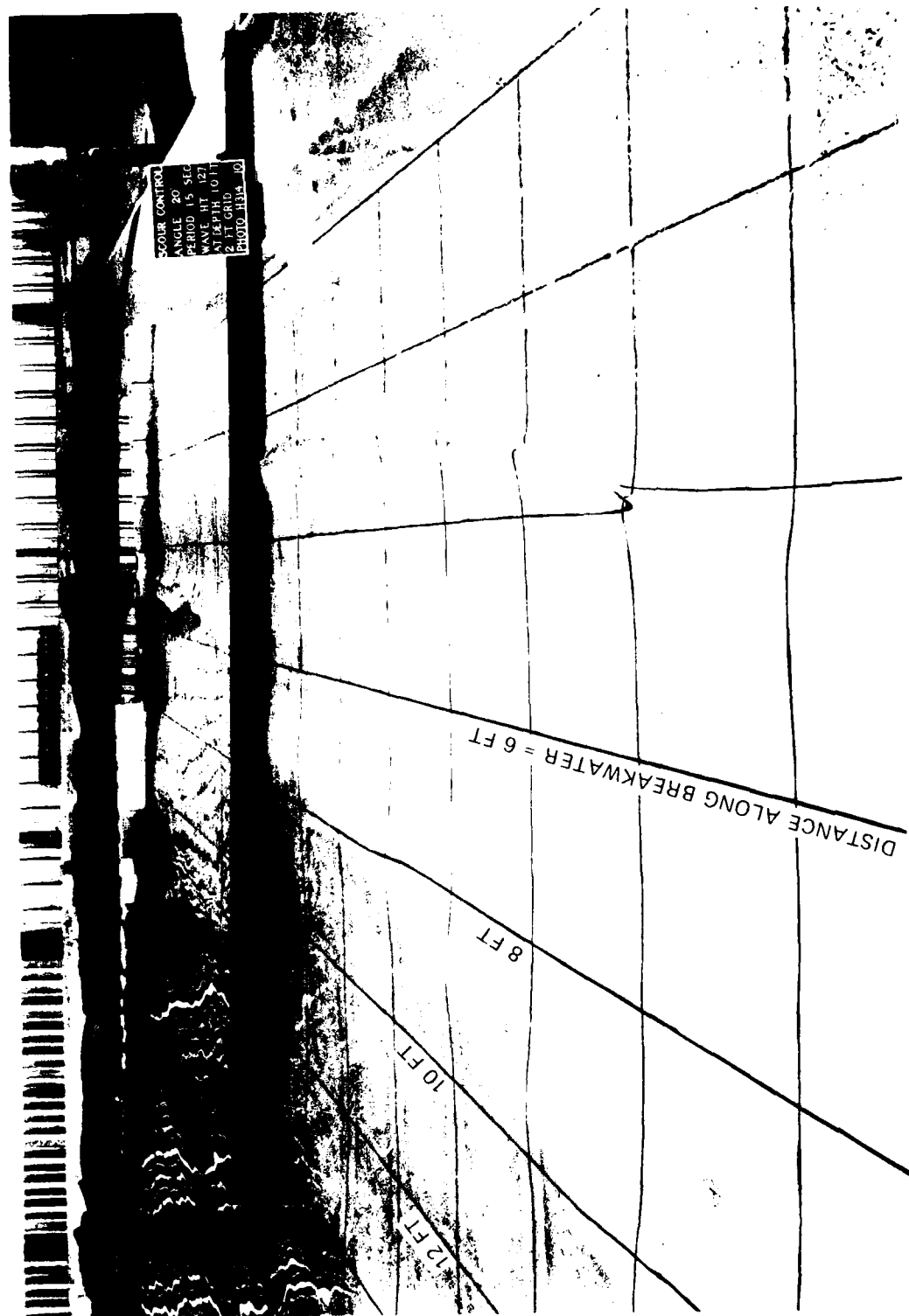


Figure 22. Typical wave pattern for 1.5-sec wave of height 0.127 ft near the wave generator approaching from an incident direction of 20 deg (downwave region)

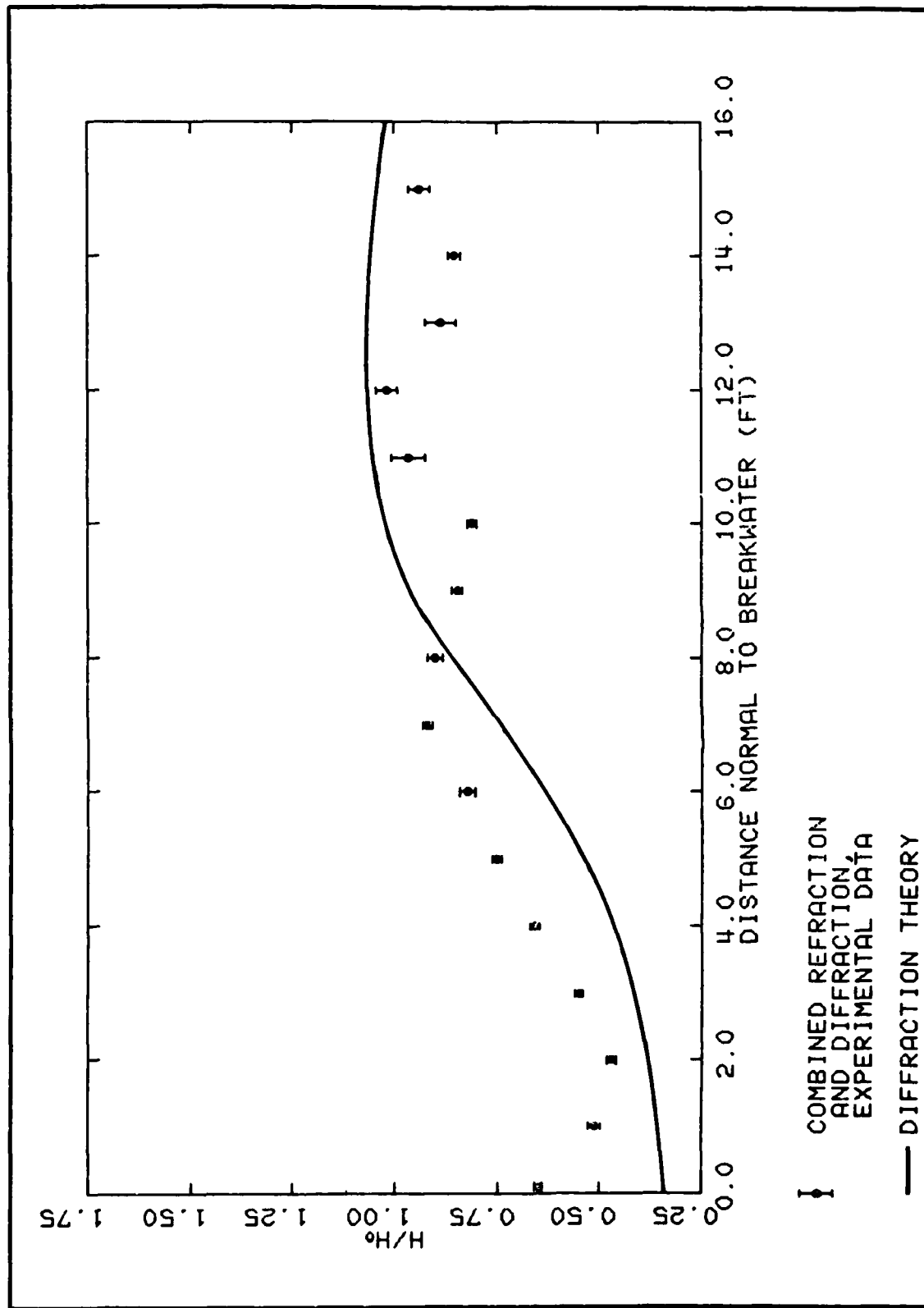


Figure 23. Typical representative wave-height amplification; angle of incidence 30 deg, period 0.75 sec, H_0 0.221 ft, distance along breakwater 6.00 ft

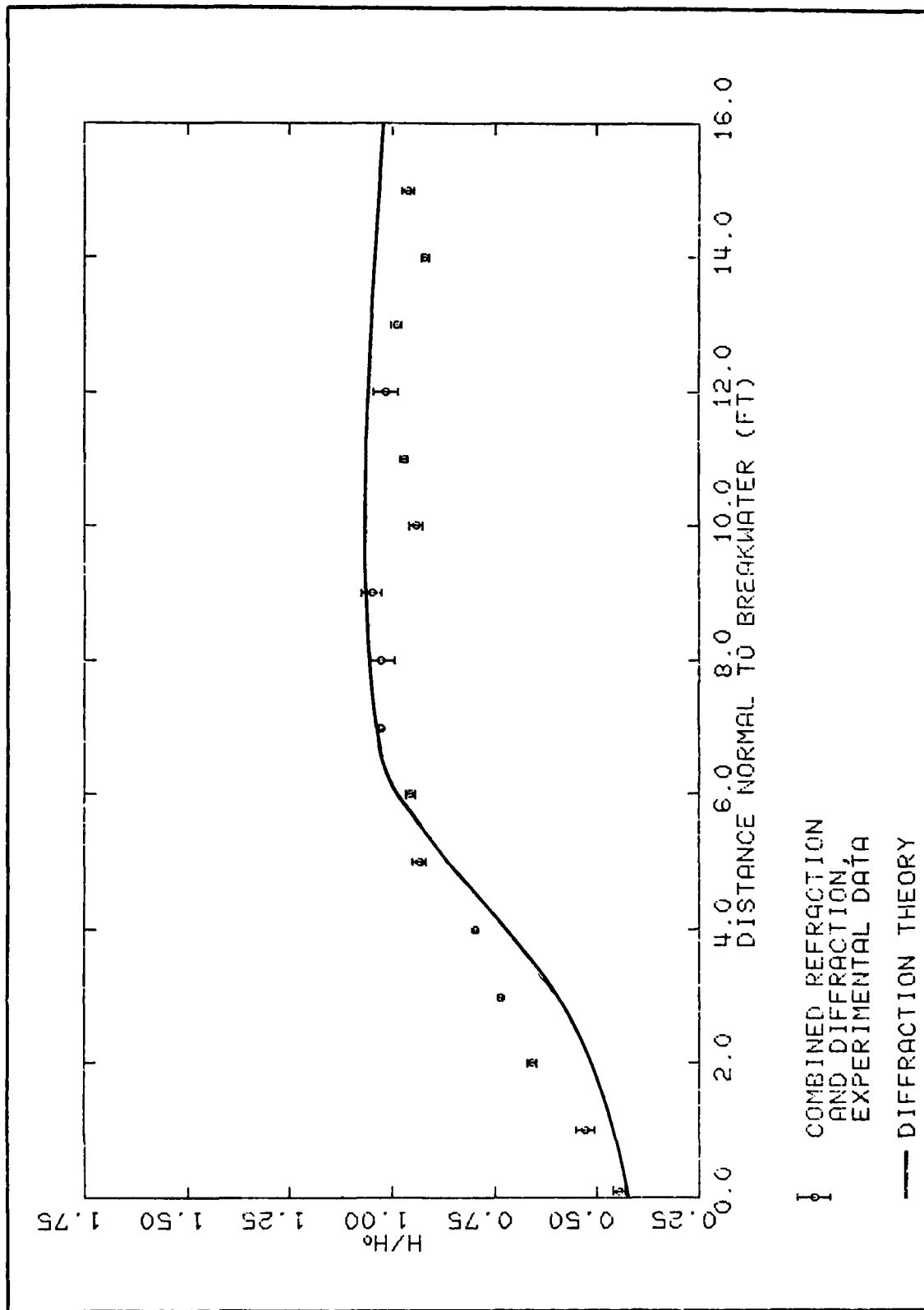


Figure 24. Typical representative wave-height amplification; angle of incidence 30 deg, period 0.75 sec, H_0 0.221 ft, distance along breakwater 10.00 ft

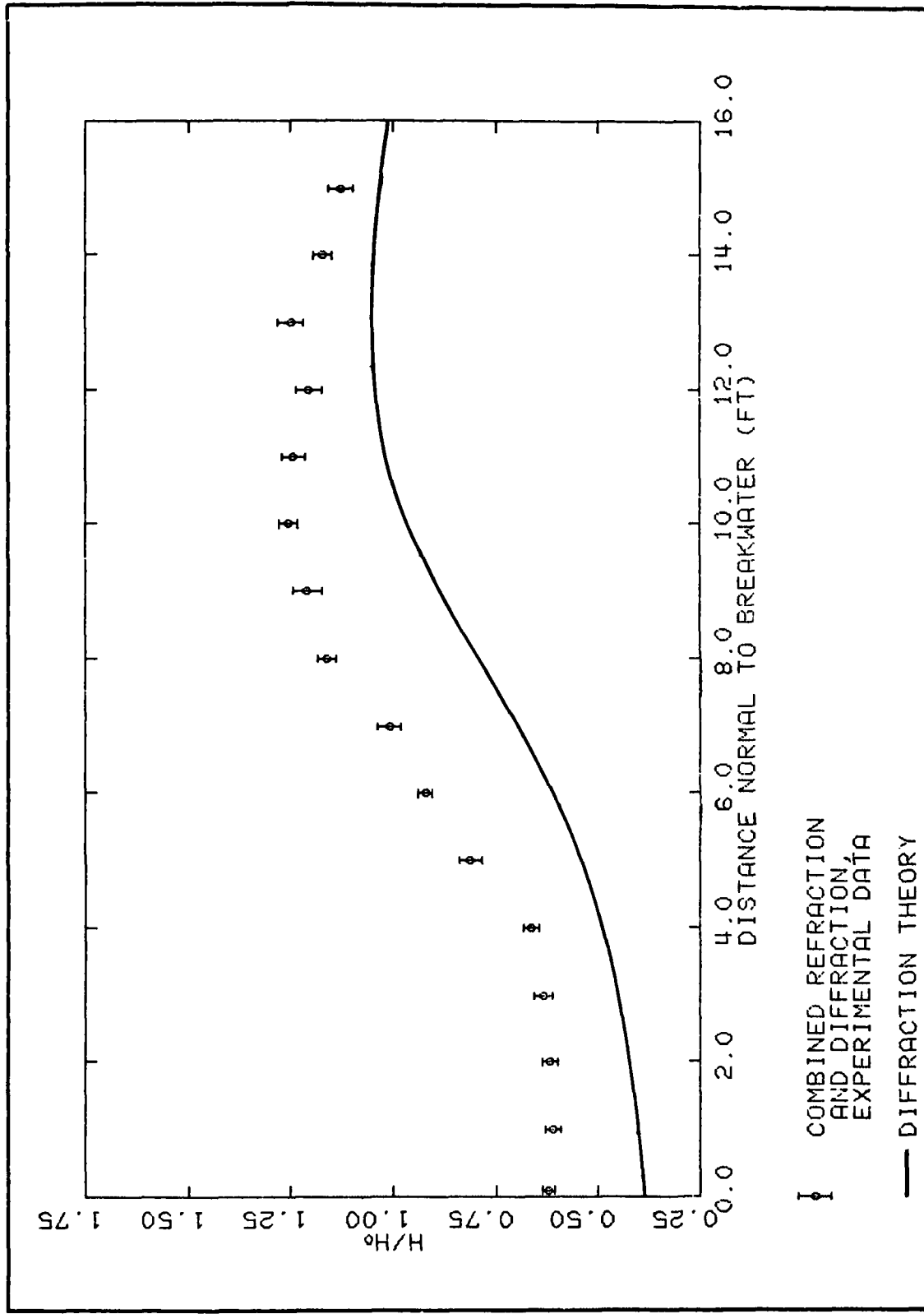


Figure 25. Typical representative wave-height amplification; angle of incidence 30 deg, period 1.00 sec, H_0 0.139 ft, distance along breakwater 6.00 ft

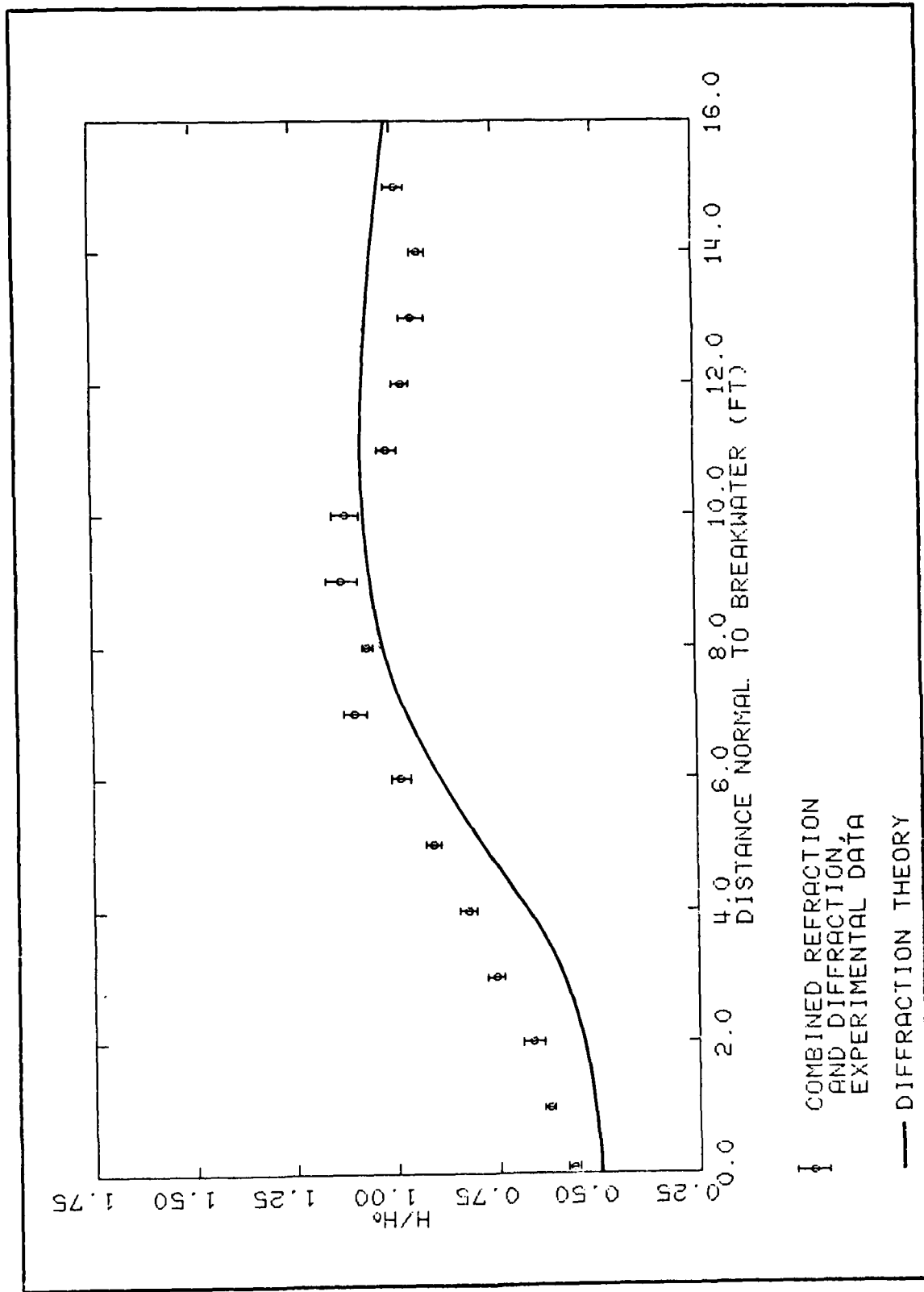


Figure 26. Typical representative wave-height amplification; angle of incidence 30 deg, period 1.00 sec, H_0 0.139 ft, distance along breakwater 10.00 ft

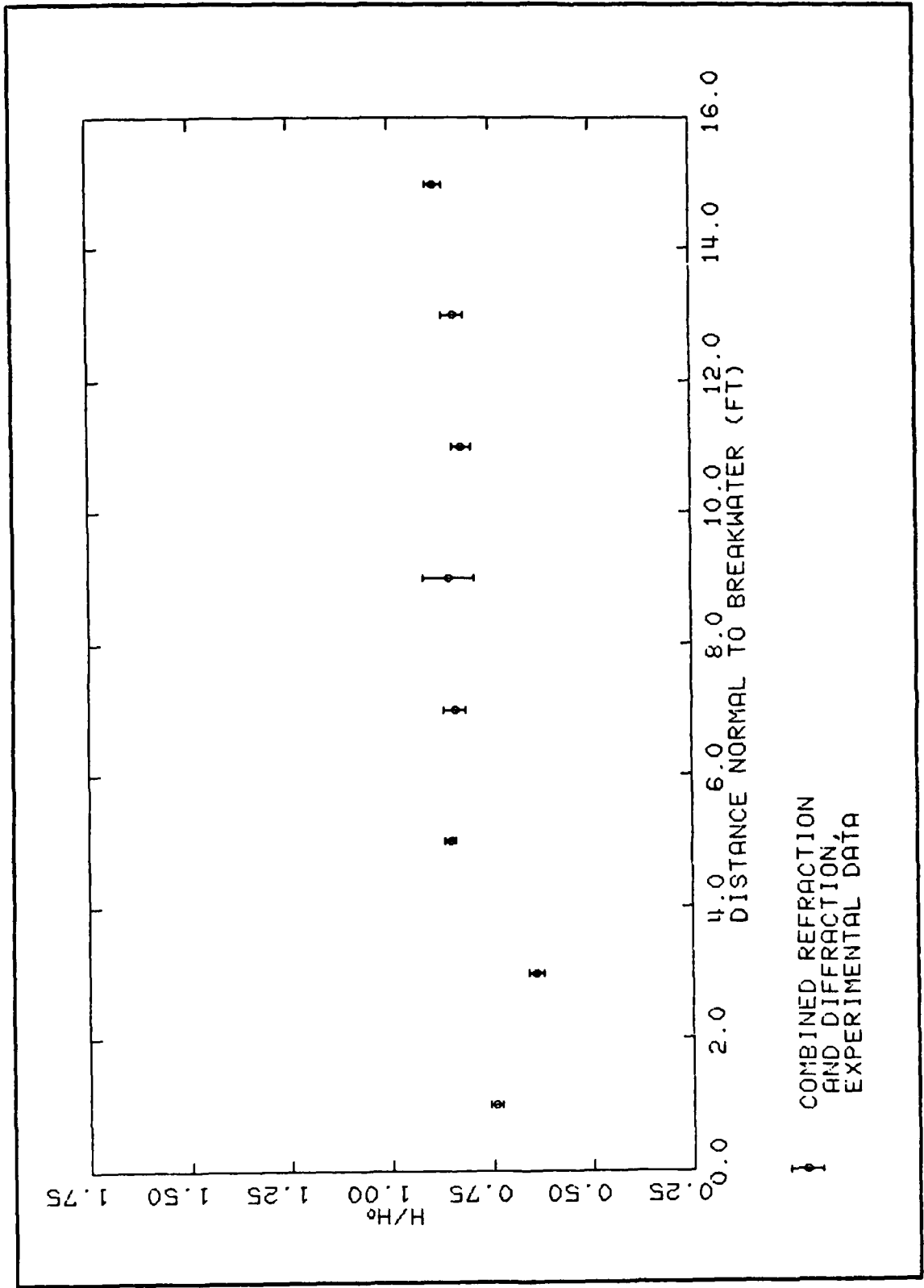


Figure 27. Typical representative wave-height amplification; angle of incidence 20 deg, period 0.75 sec, H₀ 0.245 ft, distance along breakwater 6.00 ft

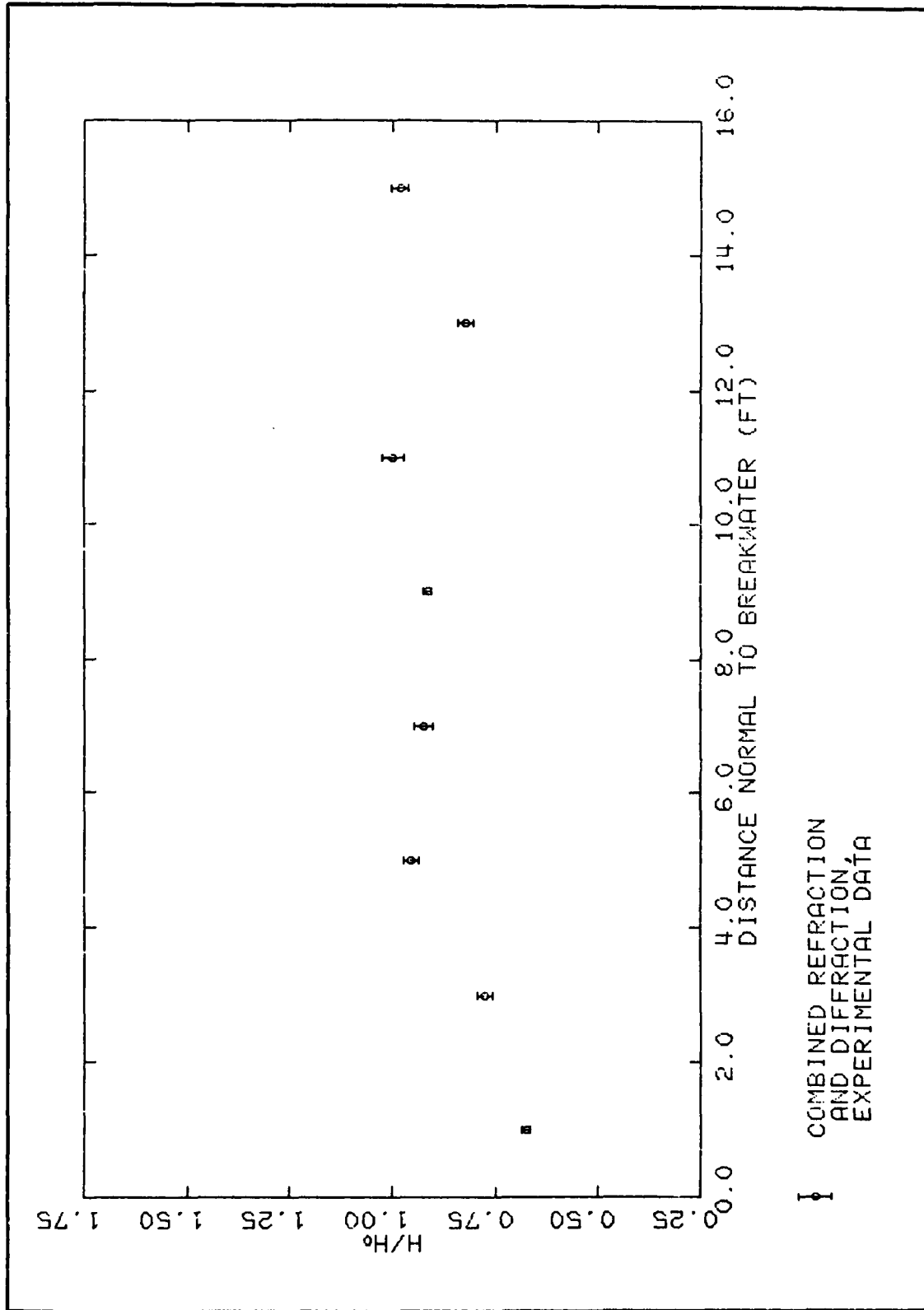


Figure 28. Typical representative wave-height amplification; angle of incidence 20 deg, period 0.75 sec, H_0 0.245 ft, distance along breakwater 10.00 ft

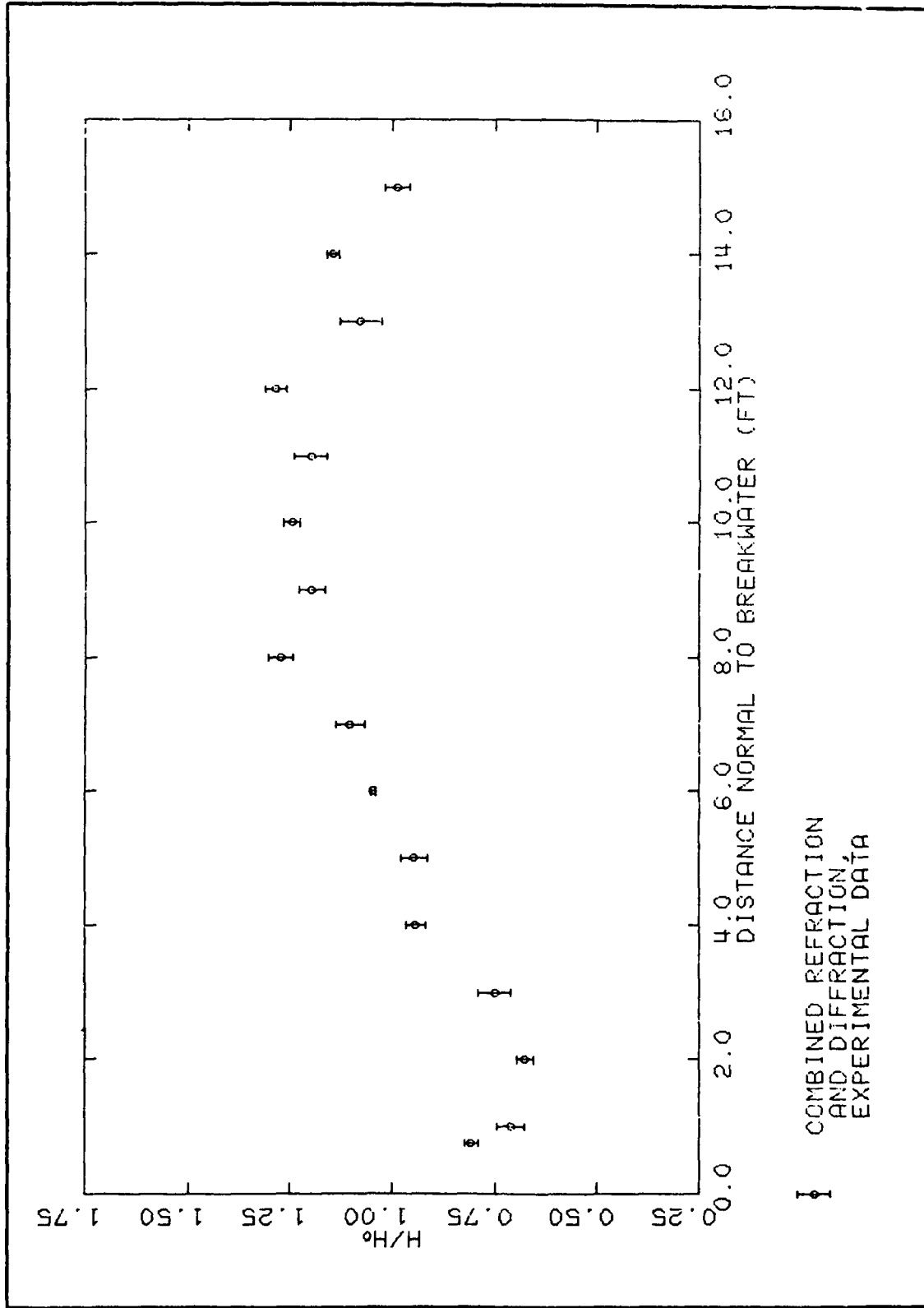


Figure 29. Typical representative wave-height amplification; angle of incidence 20 deg, period 1.00 sec, H₀ 1.154 ft, distance along breakwater 6.00 ft

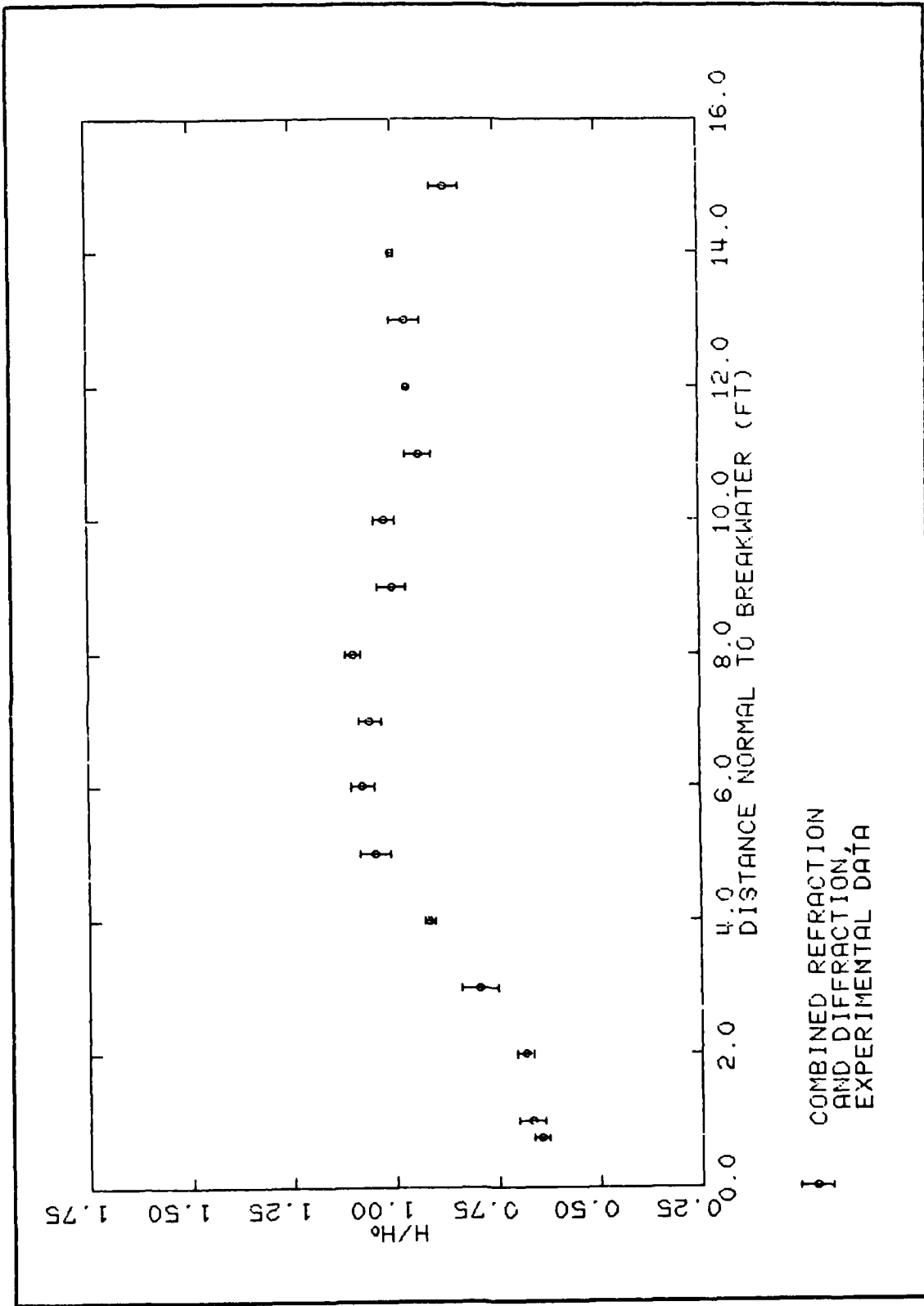


Figure 30. Typical representative wave-height amplification; angle of incidence 20 deg, period 1.00 sec, H₀ 0.154 ft, distance along breakwater 10.00 ft

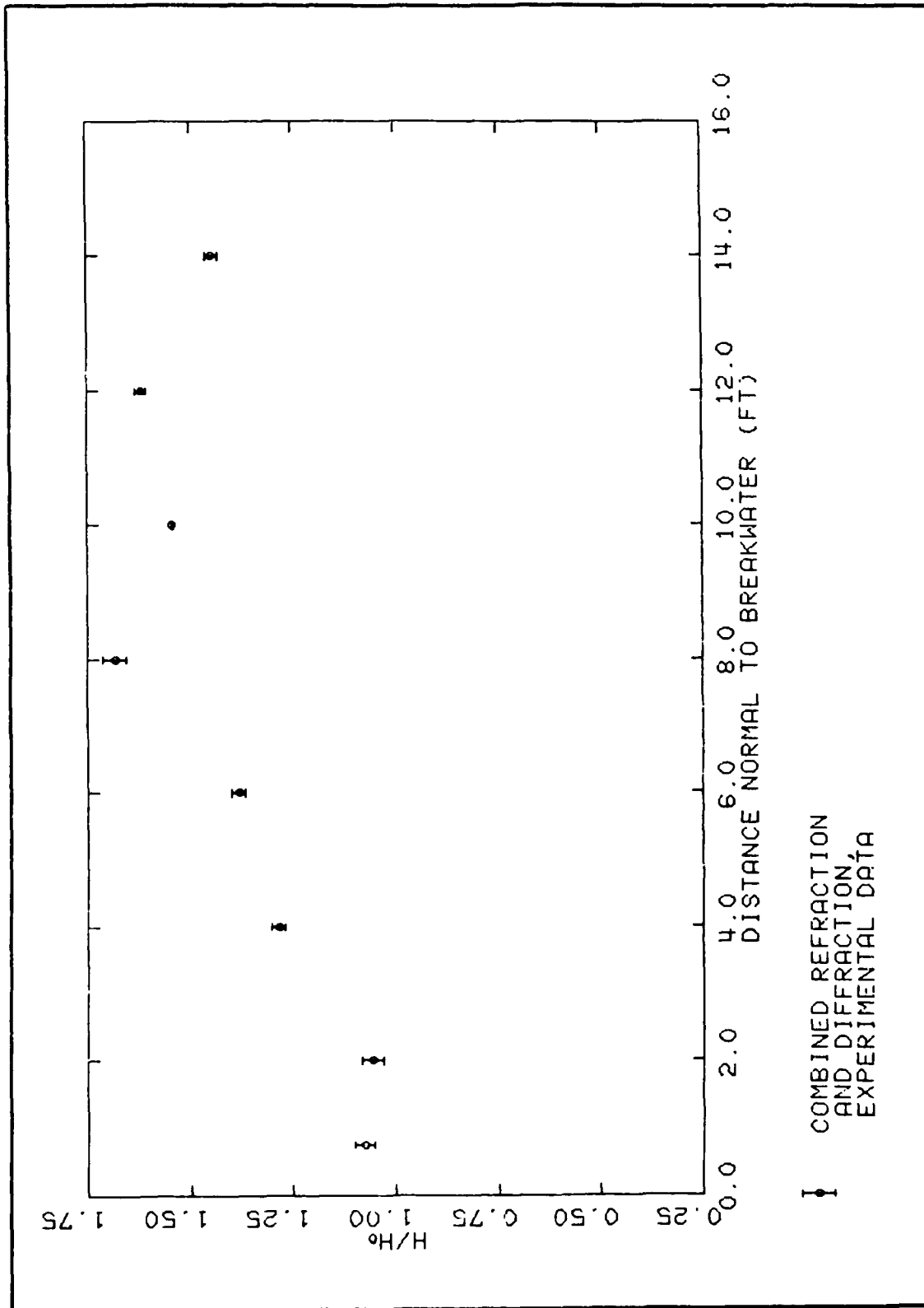


Figure 31. Typical representative wave-height amplification; angle of incidence 20 deg, period 1.50 sec, H_0 0.111 ft, distance along breakwater 6.00 ft

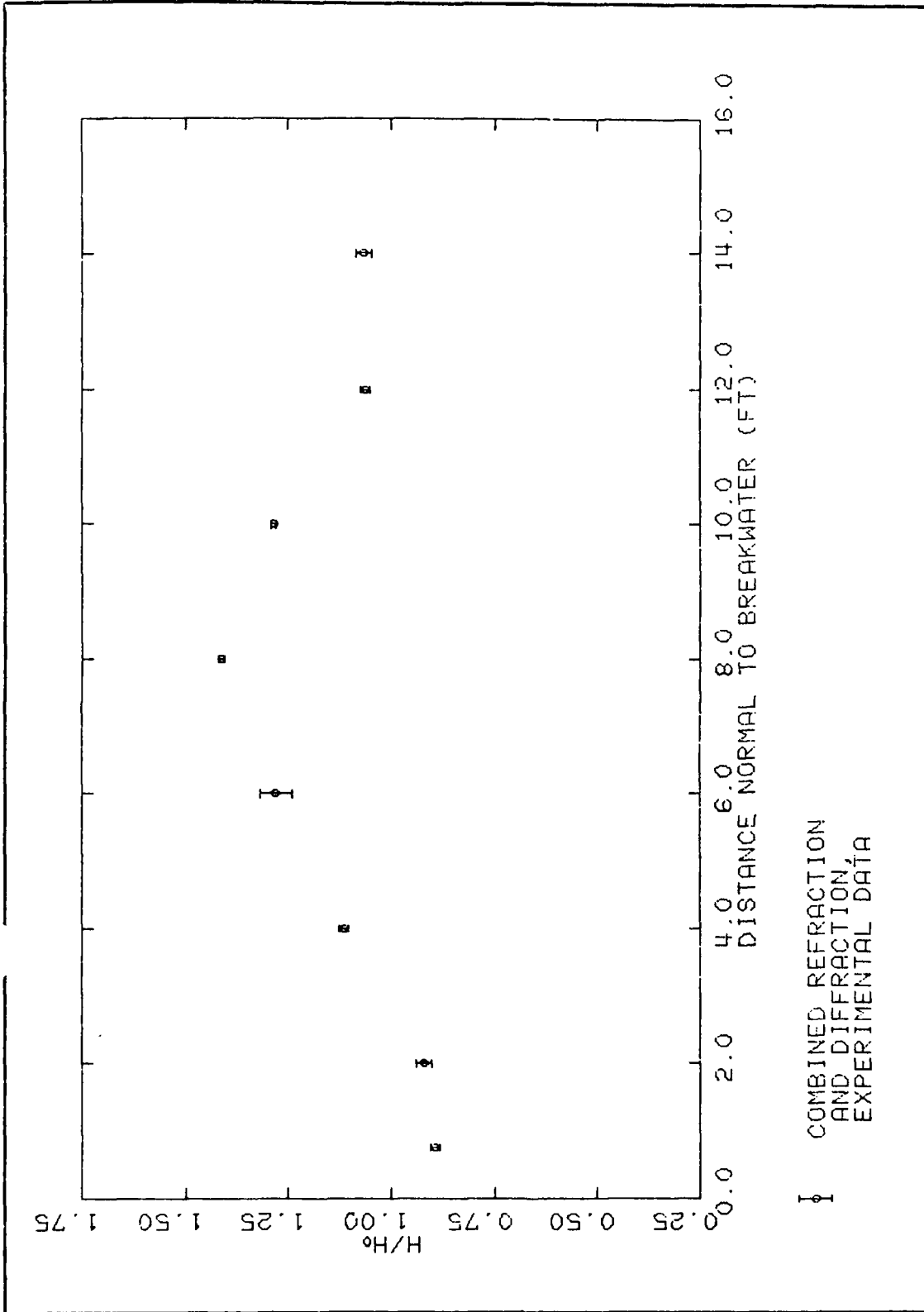


Figure 32. Typical representative wave-height amplification; angle of incidence 20 deg, period 1.50 sec, H_0 0.111 ft, distance along breakerwater 10.00 ft

$$\eta(x, y, t) = \gamma A(x) \left[G(\theta) e^{iS} + G(\theta) e^{iS} \right] e^{-i\omega t} \quad (27)$$

and the velocity potential can be expressed as:

$$\phi(x, y, z, t) = - \frac{ig\eta(x, y, t)}{\omega} \frac{\cosh k(z + h)}{\cosh kh} \quad (28)$$

where

$$\gamma = \pi^{-1/2} \exp \frac{-i\pi}{4} \quad (29)$$

and

$$G(\rho_1) = \int_{-\infty}^{\rho_1} e^{i\sigma^2} d\sigma \quad (30)$$

A(x) represents the combined refraction and shoaling factor:

$$A(x) = a_o \left[\left(\frac{\cos \theta_o}{\cos \theta} \right) \left(\frac{2k_o h_o + \sinh 2k_o h_o}{2kh + \sinh 2kh} \right) \right]^{1/2} \frac{\cosh kh}{\cosh k_o h_o} \quad (31)$$

The subscript o in Equation 31 denotes the quantities associated with incident waves in the far field. The function $G(\rho_1)$ defined in Equation 30 can be given in terms of the Fresnel integrals, whence:

$$G(\rho_1) = \frac{\pi^{1/2}}{8^{1/2}} (1 + i) + \frac{\pi^{1/2}}{2^{1/2}} \left[C_2(\rho_1^2) + iS_2(\rho_1^2) \right] \quad (32)$$

where

$$C_2 \rho_1^2 = \frac{1}{2\pi} \int_0^{\rho_1^2} \frac{\cos \tau}{\tau^{1/2}} d\tau \quad (33)$$

and

$$S_2 \rho_1^2 = \frac{1}{2\pi} \int_0^{\rho_1^2} \frac{\sin \tau}{\tau^{1/2}} d\tau \quad (34)$$

are the Fresnel cosine and sine integrals, respectively. The arguments of the function $G(\rho_1)$ in Equation 27 were defined by Liu (1982) as:

breakwater because of the inherent nature of the parabolic approximation. To remove this weakness, Liu, Lozano, and Pantazaras (1979) and Liu (1982) constructed a uniformly valid asymptotic solution for the same problem. The beach topography, which is required to be uniform in the alongshore direction, can be arbitrary in the onshore-offshore direction.

175. Following the development of Liu, Lozano, and Pantazaras (1979), and in the notation of Liu (1982), the geometry of the breakwater is generalized to be one of radiated wave rays emitted from the tip of the breakwater (Figure 41). The relation between the incident wave angle and the reflected wave angle along the breakwater is shown in Figure 42. Small-amplitude

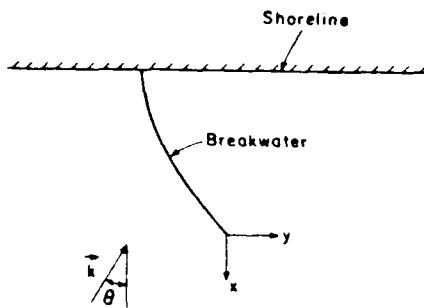


Figure 41. Definitive sketch, uniformly valid asymptotic theory (Liu, Lozano, and Pantazaras 1979)

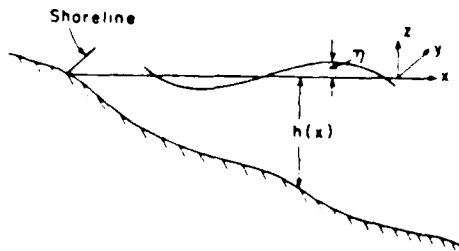
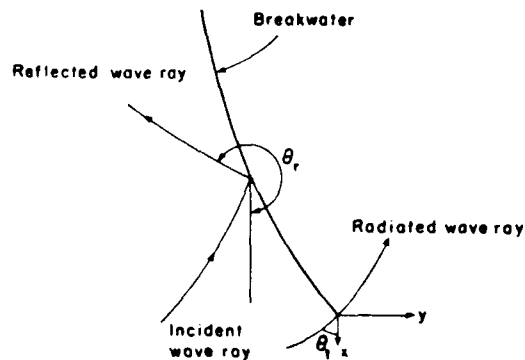


Figure 42. Definitive sketch, uniformly valid asymptotic theory, relation between incident wave angle and reflected wave angle along the breakwater (Liu, Lozano, and Pantazaras 1979)



incident waves with the incident wave amplitude, a_0 , and radian frequency, ω , are assumed in the development. The angle of incidence is defined as θ_0 . Liu, Lozano, and Pantazaras (1979) have shown that the leading order asymptotic solution for the free surface displacement, η , is:

downcoast of the structure and can be used for comparison with numerical or analytical studies of the same concept.

Analytical developments:
uniformly valid asymptotic theory

171. Analytical models of the physical arrangement of Hales (1980b) have been developed based on asymptotic theory and the parabolic approximation (for example, Liu and Mei 1975, 1976; Liu, Lozano, and Pantazaras 1979; and Lozano and Liu 1980). These models extrapolate the small amplitude wave theory to calculate the radiation stress distribution. These analytical models have been compared with the experimental data of Hales (1980b) by Liu (1982) and Tsay and Liu (1982), and the overall agreement between theory and experiment was considered to be good. Knowledge of these important phenomena can be used as the basis for advanced studies of sediment movement around major structures under combined effects of refraction and diffraction.

172. In recent years, the parabolic approximation has been developed extensively for studying wave scattering problems in different branches of the physical sciences. Radder (1979) and Lozano and Liu (1980) derived independently the parabolic approximation for water wave problems. Analytical solutions were obtained for the combined refraction and diffraction wave field near a thin breakwater perpendicular to the shoreline on a plane beach. The background wave field was assumed to have straight line wave rays.

173. Also based on the parabolic approximation, a numerical study of water-wave refraction and diffraction problems has been conducted by Tsay and Liu (1982) where the refraction index is not constant. Two problems were considered: (a) the wave field near a submerged shoal on a sloping bottom, and (b) the wave field in the neighborhood of a breakwater on a sloping beach. In the latter problem, the orientation of the breakwater is no longer limited to be perpendicular to the shoreline. For the perpendicular case, the accuracy of the parabolic approximation numerical results was verified by comparing with experimental data of Pantazaras (1979) and Hales (1980b). For this case, the uniformly valid asymptotic theory of Liu, Lozano, and Pantazaras (1979) was also used to verify the parabolic approximation.

174. For the case of a shore-connected breakwater on a linear plane beach, Liu and Mei (1976) and Lozano and Liu (1980) showed that an approximate closed form solution can be obtained by the parabolic approximation. However, Liu (1982) has shown that this solution becomes invalid near the tip of the

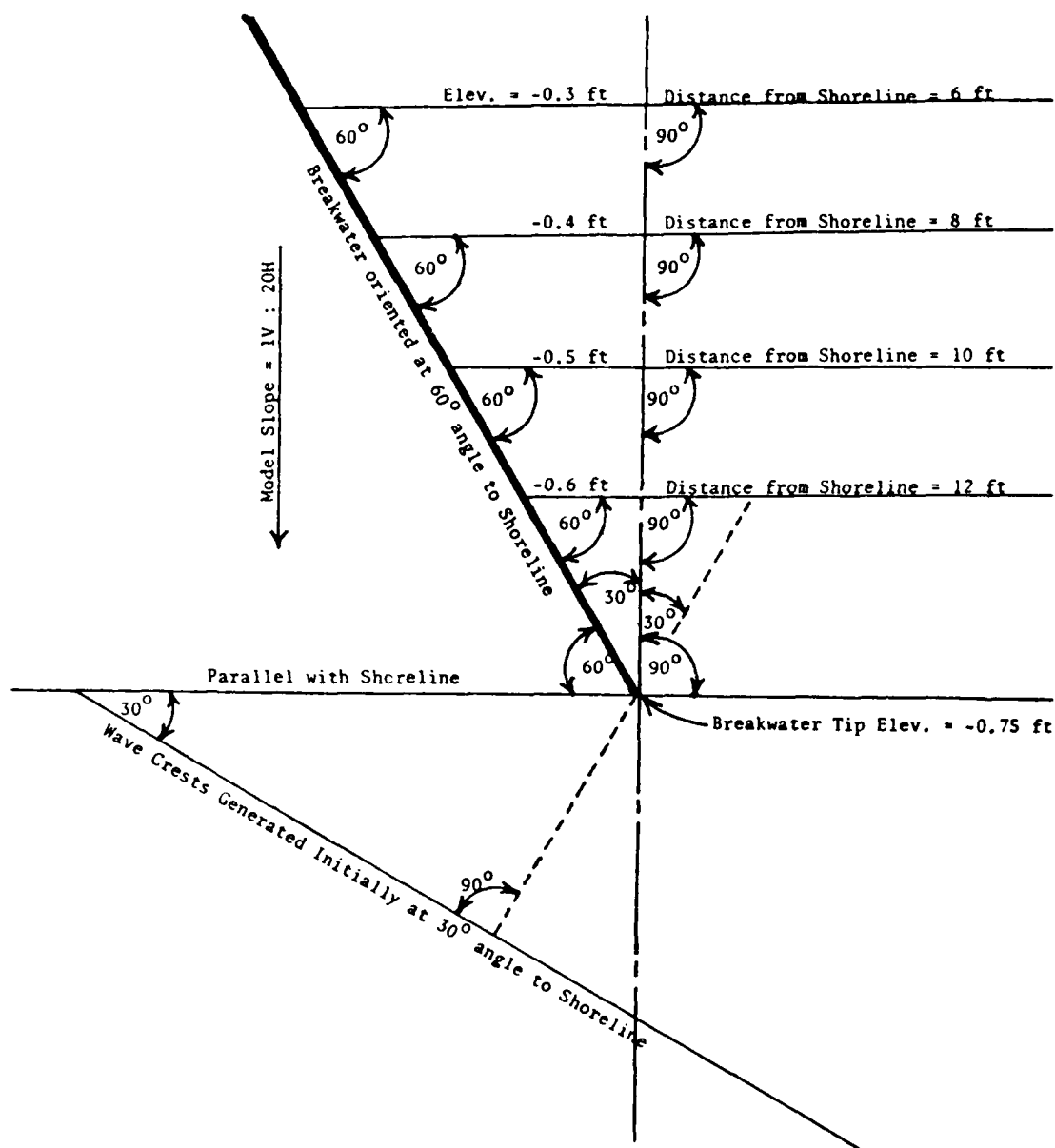


Figure 40. Experimental layout showing location of four sections parallel with shoreline along which wave-height sensors were positioned

data (period and height) was repeated. All data from these two gage arrangements resulted in a data set that presented the wave heights at 1-ft increments along the four sections which run parallel with the shoreline, with the data extending from very near the breakwater deep in the shadow zone and extending across the region where the waves experience both refraction and diffraction. These precise experiments provide data that define the wave height

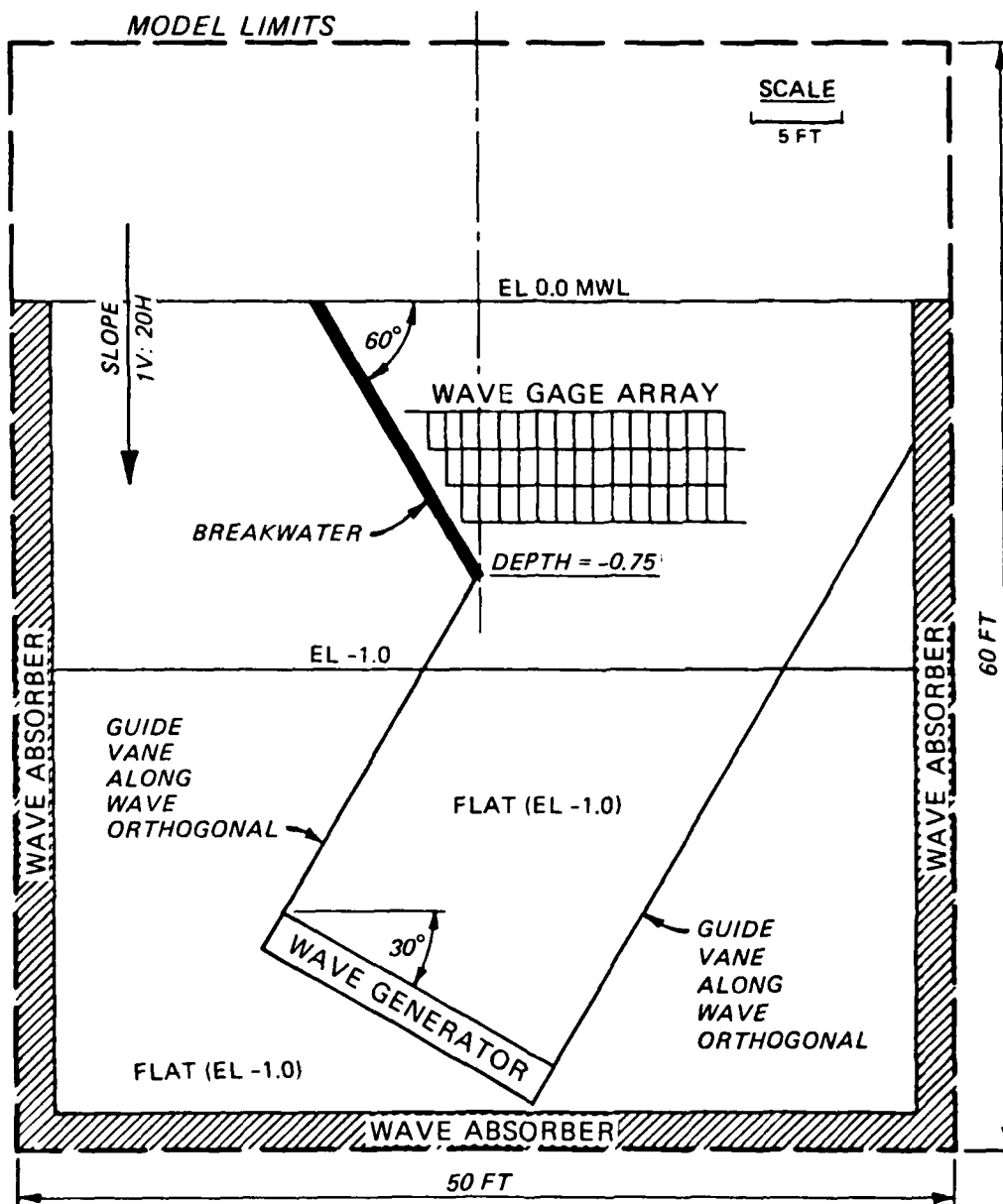


Figure 39. Experimental facility

170. In order to compare experimental results with numerical or analytical investigations, it is necessary to have good definition of the experimental data. The 34 wave-height sensors were initially placed at 2-ft intervals along the four sections parallel with the shoreline, and the complete set of experimental data was obtained. To provide a more dense data display, the entire physical arrangement of the wave sensors was displaced laterally along the four section lines for a distance of 1 ft, and the same set of wave

Shore-Connected Breakwater at a 60-deg Angle to Shoreline

167. The purpose of conducting physical experiments with the breakwater oriented at a 60-deg angle to the shoreline was to extend the previous work where the breakwater was positioned normal to the shoreline in order to simulate a larger range of prototype jetties and breakwaters in existence at the present time. Experimental measurements of refraction and diffraction down-coast of this oblique structure were made to obtain quantitative knowledge of these phenomena in the lee of the structure. These data were then compared with the uniformly valid asymptotic theory of Liu, Lozano, and Pantazaras (1979) for the same arrangement.

Experimental facility

168. The physical facility that had been utilized to investigate the wave field and wave-induced currents downwave of a shore-connected breakwater normal to the shoreline was modified to provide for a breakwater oriented at a 60-deg angle with the shoreline (Figure 39). The wave generator was positioned at a 30-deg angle with the shoreline in water that was 1 ft deep. Four sections parallel with the shoreline downwave of the breakwater were instrumented with wave-height sensors for determination of the wave field. These sections were located 6, 8, 10, and 12 ft from the mean waterline (shoreline end of the breakwater) and are labeled "distance from the shoreline" (Figure 40). Other features of this experimental study, and the data acquisition and analysis, are essentially as applicable to the experiments performed with the breakwater normal to the shoreline.

Wave gage locations

169. The wave-height data downcoast of the experimental breakwater which was positioned at a 60-deg angle with the shoreline were obtained by operating 36 wave-height sensors simultaneously for each test condition. Two of these wave-height sensors were located in the deeper water (1 ft deep) near the wave generator to ascertain the initial generated wave height. The remaining 34 sensors were positioned along four lines parallel with the shoreline at distances of 6, 8, 10, and 12 ft from the shoreline (Figure 40). The still-water depths at these four sections were 0.3, 0.4, 0.5, and 0.6 ft, respectively. The wave gages were placed on a supporting platform in such a manner that only the wave sensor probe penetrated the water surface, thereby eliminating any local disturbance caused by instrument stands touching the water surface.

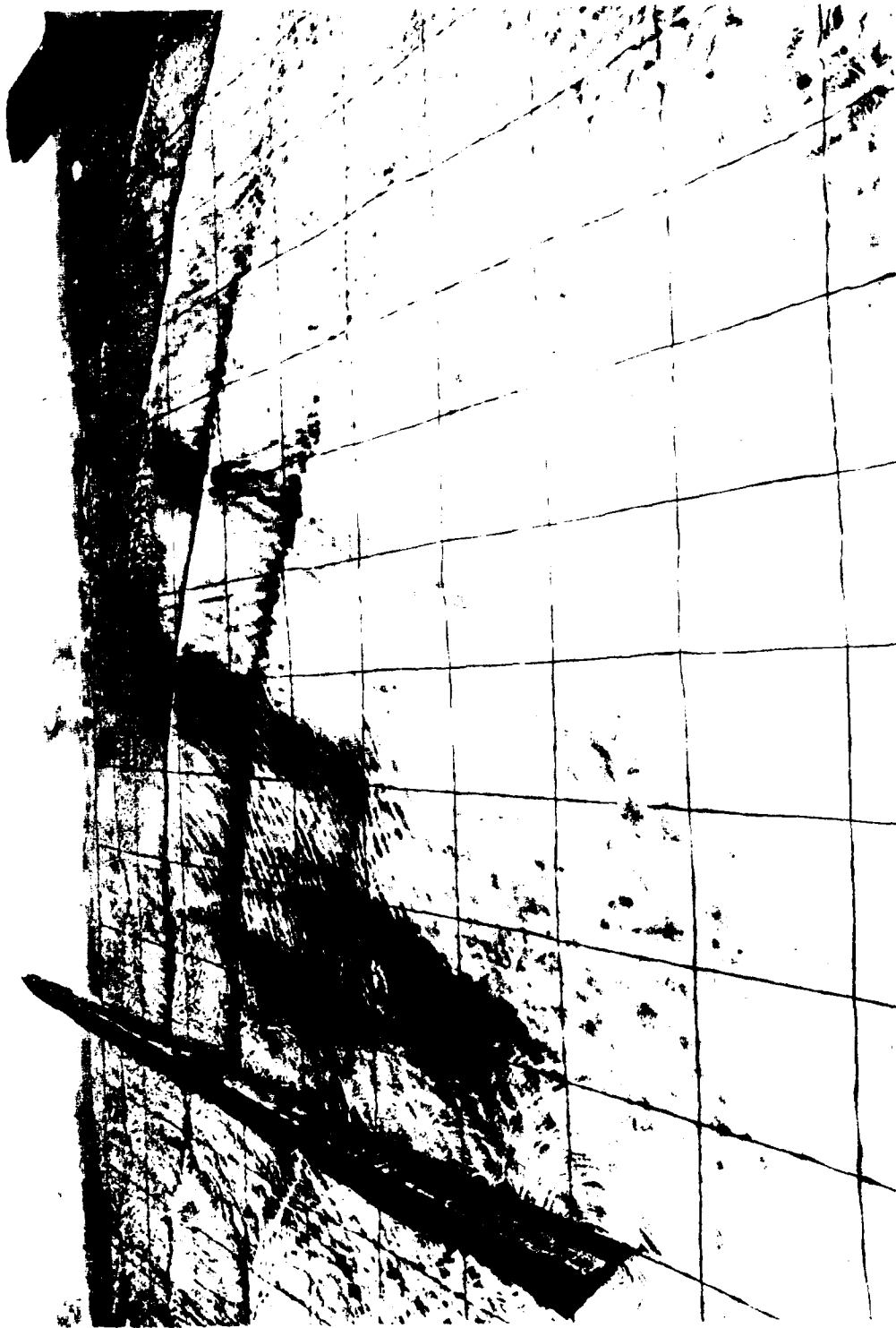


Figure 38. Net dye movement, time after starting generator 6.0 min, wave period 1.0 sec, wave height near generator 0.139 ft, angle of incidence 30 deg

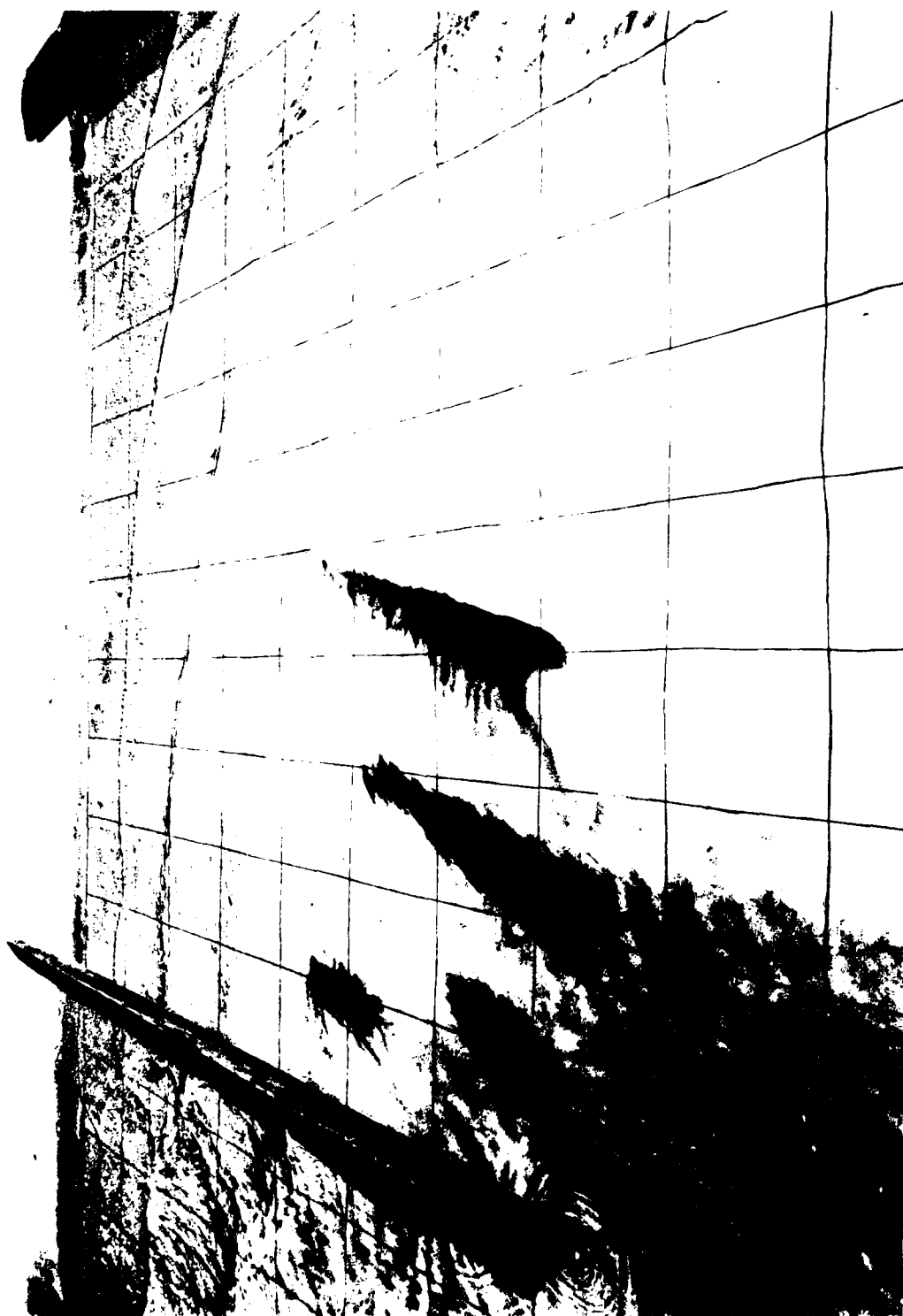


Figure 37. Net dye movement, time after starting generator 2.0 min, wave period 1.0 sec, wave height near generator 0.139 ft, angle of incidence 30 deg

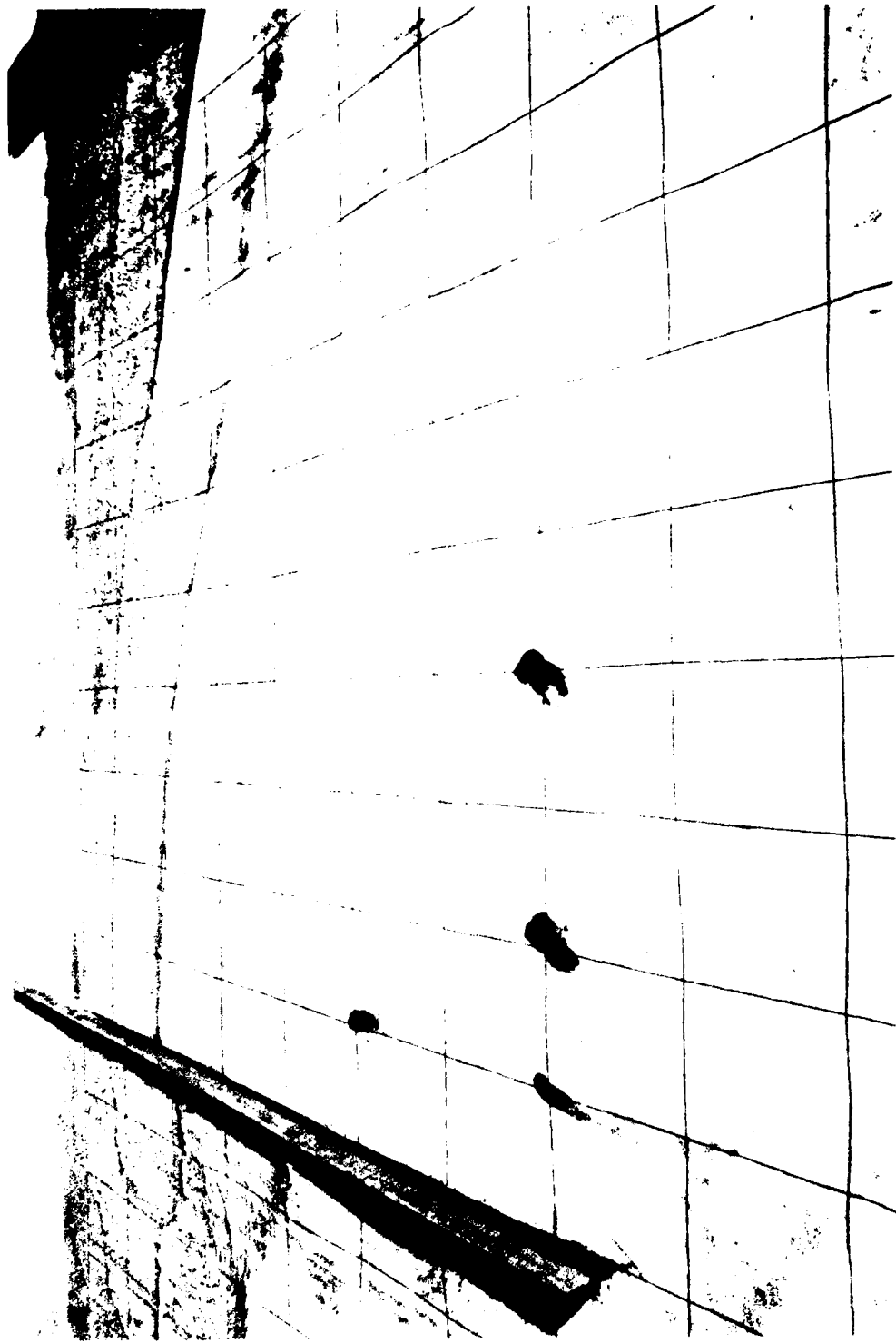


Figure 36. Net dye movement, time after starting generator 10 sec, wave period 1.0 sec, wave height near generator 0.139 ft, angle of incidence 30 deg

clockwise circulation cell that develops as a result of mass transport down-coast by the longshore current. The numerical model of Liu and Mei (1975) considered an infinitely long coastline and thus precluded the clockwise circulation pattern which developed in the physical model. However, the counterclockwise circulation expected, and indeed which occurred adjacent to the experimental breakwater, did not appear in the numerical computational procedures. A counterclockwise cell developed in the numerical model of Liu and Mei (1975) approximately a breakwater length downwave from the breakwater. At such a distance in the physical facility, however, the sidewall effects begin to be encountered. Therefore the experimental results for a finite section of beach should not be expected to be identical with numerical model results for an infinite section of beach. Numerical models can, however, be formulated that will represent the physical facility boundary conditions, including the sidewall effects. The development of numerical techniques for determining wave characteristics and current magnitudes near structures is presently under way. These techniques incorporate combined refraction and diffraction, and the results of these experiments will be used to verify such numerical models.

166. Net fluid particle movement was visualized by a series of photographs of successive locations of bottom dye streaks originating from four locations on the bottom of the facility. The dye placed at a distance of 4 ft laterally from the tip of the breakwater is seen in Figures 36-38 to move shoreward and become part of the development of the clockwise circulation cell associated with the downwave boundary. (A grid spacing of 2 ft is shown in these photographs.) Dye placed 2 ft laterally from the tip of the breakwater becomes part of the counterclockwise circulation cell near the breakwater. After the circulation cells had developed, dispersion of the dye upward from the bottom had had time to occur and the streaklines are less defined, although the upward dispersion is not necessarily associated with the cell formation. The dye movement patterns are in good agreement with the bottom velocity measurements shown in Figure 35. A circular wave pattern of reflected waves radiates outward from the tip of the breakwater and is clearly evident in this series of photographs.

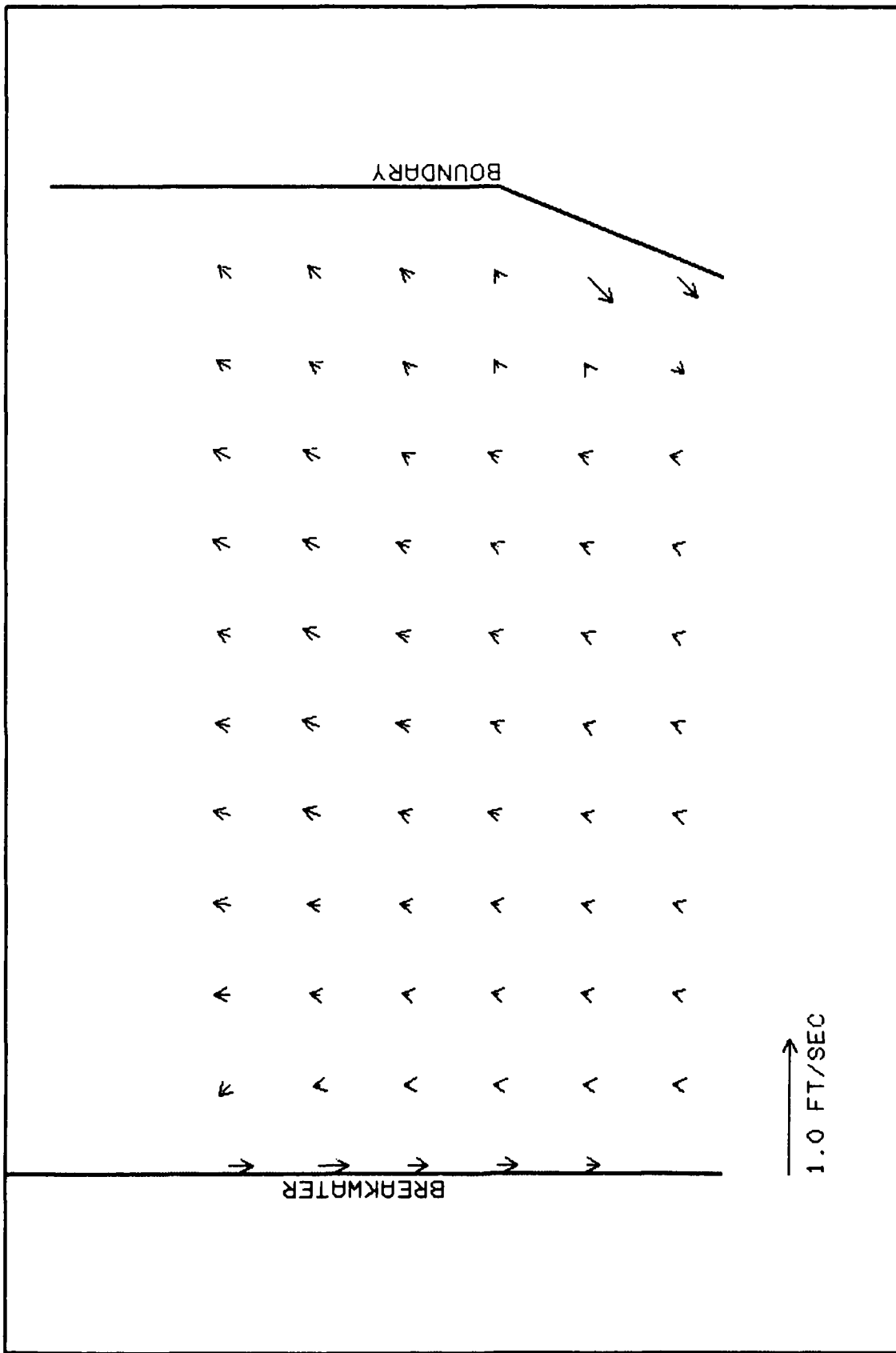


Figure 35. Average bottom velocities; angle of incidence 30 deg, wave period 1.0 sec, wave height near generator 0.139 ft

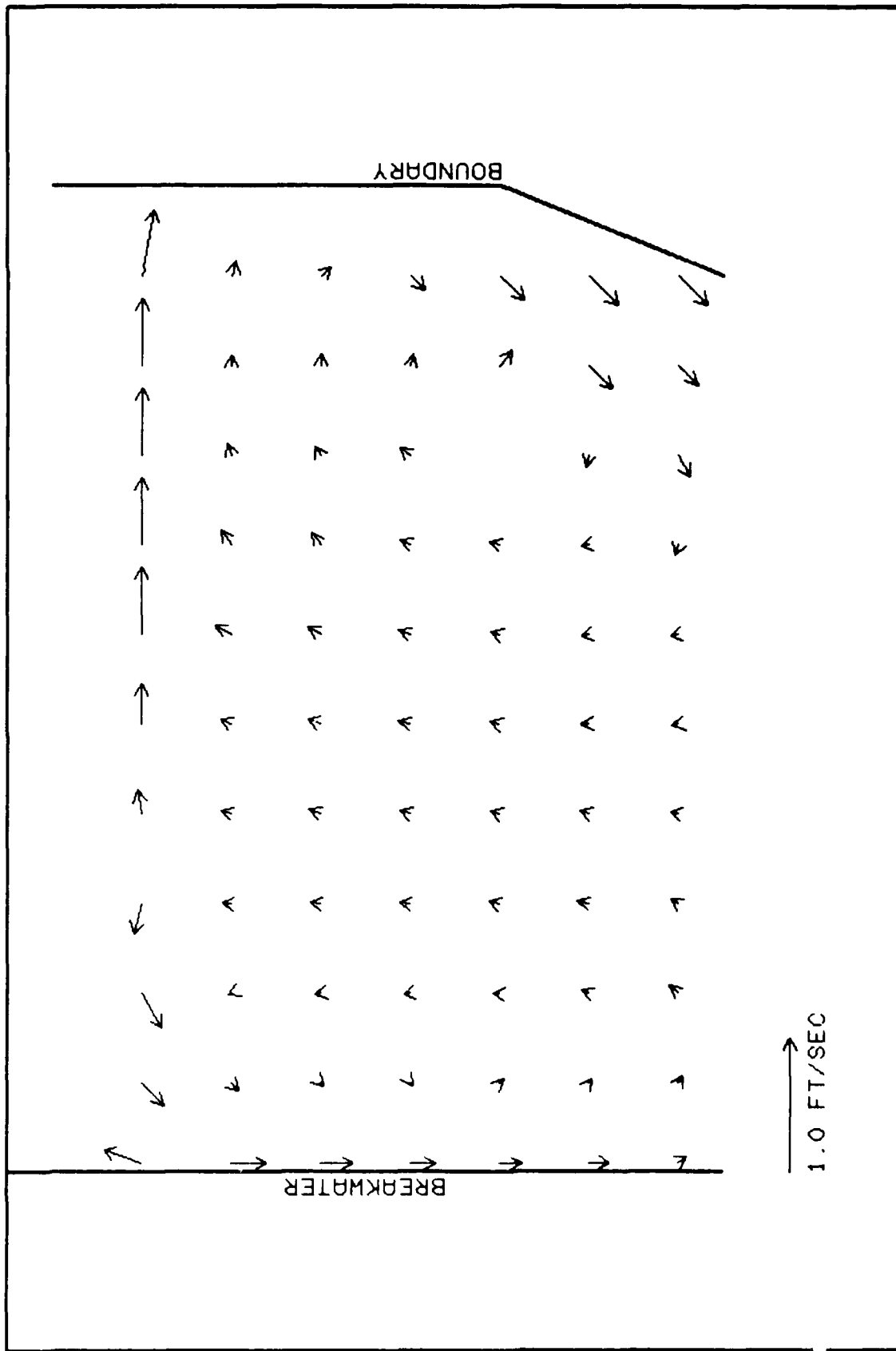


Figure 34. Average middepth velocities; angle of incidence 30 deg,
 wave period 1.0 sec, wave height near generator 0.139 ft

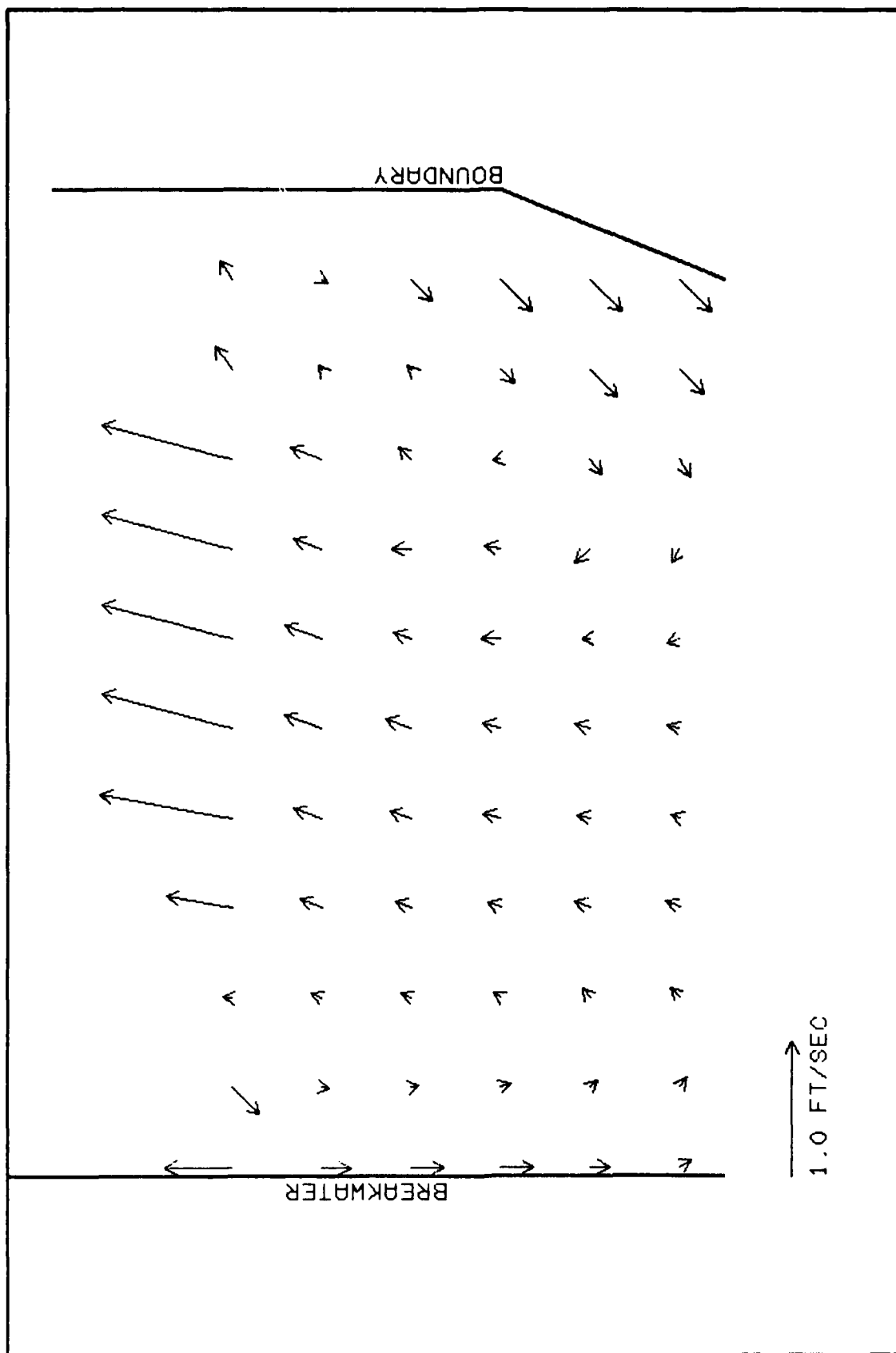


Figure 33. Average surface velocities; angle of incidence 30 deg,
 wave period 1.0 sec, wave height near generator 0.139 ft

wave field, the gages were repositioned at 2-ft intervals starting 1 ft from the breakwater and extending to a location 15 ft from the structure.

163. Also shown in Figures 23-26 are the wave heights determined by diffraction theory alone, based on the semigraphical constant depth procedure of USAEWES (1984). The fit is seen to be best at most locations for short-period waves. Agreement also is best at the seaward end of the breakwater, since refraction becomes more significant the farther the waves propagate toward the shoreline.

Current field downcoast of breakwater

164. In the neighborhood of the breakwater, currents existed that affected the wave heights. Opposing currents are known to produce significant increases in wave heights for relatively small values of current-to-wave velocity ratios. Since the magnitude of the currents is a function of the incident wave height, the ratio of measured wave height to incident wave height, H/H_0 , is expected to be a function of the incident wave height wherever the current is strong. The effect of varying the incident wave height on H/H_0 (defined as the amplification factor) was investigated, and it was determined that the greatest variation in H/H_0 occurred in the deep shadow zone near the breakwater and shore region where currents were strongest. From the experimental data for incident wave approach directions of 20 and 30 deg, the effect of initial wave height was found to be greatest near the breakwater and at the sensor location 6 ft from the shoreline. The effect of incident angle was also apparent, with the more acute angle producing the greatest degree of nonlinearity. The nonlinear effect diminishes rapidly away from the structure and at a distance of 5 ft downwave appears to be relatively insignificant except for the extreme shadow region at acute angles of incidence.

165. The establishment of a counterclockwise circulation cell approximately 4 ft wide adjacent to the downwave side of the breakwater results in a seaward flowing current all along the breakwater. The bottom current is especially intense approximately 40 percent of the breakwater length from the shoreline and decreases seaward along the structure as the water depth increases (since mass transport remains constant). Middepth velocities decrease seaward along the breakwater also but remain approximately 35 percent of the maximum value even at the seaward end of the structure. The middepth, surface, and bottom velocity measurements are displayed in Figures 33-35, respectively. The facility sidewall boundary is responsible for the creation of the

$$\theta^2 = R - S \quad (35)$$

and

$$\bar{\theta}^2 = R - \bar{S} \quad (36)$$

where

S = phase function of the incident wave, deg

\bar{S} = phase function of the reflected wave from the breakwater, deg

R = phase function of the radiated waves generated by an oscillatory point source at the tip of the breakwater, deg

These phase functions can be calculated according to the ray theory; i.e., S , \bar{S} , and R can be evaluated by the integral:

$$I = \int_0^{\bar{r}} \bar{k} \cdot d\bar{r} \quad (37)$$

where \bar{k} is the wave number vector representing each wave field, respectively.

176. The zero phase lines for S , \bar{S} , and R intercept at the tip of the breakwater ($x = 0$, $y = 0$). From Equation 37, the value of the phase function (S , \bar{S} , or R) at any arbitrary point can be considered as the sum of the wave number component in the radial direction between the arbitrary point and the tip of the breakwater. The value of the phase function for radiated waves at any arbitrary point is always greater than or equal to S and \bar{S} . The branches of the multivalued functions θ and $\bar{\theta}$ are defined by Liu (1982) as follows: The value of θ is negative inside the shadow region defined according to the geometrical optics theory and is positive elsewhere. $\bar{\theta}$ is positive in the reflection region and is negative elsewhere. In the case where the breakwater has a curved shape and coincides with one of the radiated wave rays from the tip, the phase function for the reflected wave is:

$$\bar{S} = - \int_0^x k \cos \theta dx + \bar{K}_r y \quad (38)$$

where

$$\bar{K}_r = k_r \sin \theta_r \quad (39)$$

k_r and θ_r represent the wave number and reflected wave angle along the breakwater, respectively.

177. The analytical development of the free surface displacement down-coast of a shore-connected breakwater, based on the uniformly valid asymptotic theory (Equation 27), was based on the fundamental assumption that the breakwater geometry in planform followed a radiated wave ray emitted from the tip of the breakwater. The detailed derivation of this and other expressions required in the development are presented in Liu, Lozano, and Pantazaras (1979). However, in actuality, the planform layout of most shore-connected breakwaters at an angle to the shoreline is that of a straight line. Hence, while the assumption of a planform layout following a wave ray radiated from the tip of the structure expedited the analytical development, the numerical model based on this development does not precisely conform with most prototype conditions. It was therefore desirable to adapt the numerical scheme to fit the case of a straight breakwater at an angle to the shoreline. For the case of a straight breakwater, the phase function S_s for the incident wave, the phase function \bar{S}_s for the reflected waves from the breakwater, and the phase function R_s for the radiated waves generated by the oscillatory point source at the tip of the breakwater can be expressed respectively as:

$$S_s = - \int_0^x k \cos \theta \, dx + \bar{K}_o y \quad (40)$$

$$\bar{S}_s = - \int_0^x k \cos \theta \, dx - \bar{K}_o y \quad (41)$$

$$R_s = - \int_0^x k \cos \theta \, dx + \bar{K}_t y \quad (42)$$

where

$$K_o = k \sin \theta = k_o \sin \theta_o \quad (43)$$

$$K_t = k \sin \theta = k_t \sin \theta_t \quad (44)$$

k_t and θ_t represent the wave number and the initial angle of incidence of a radiated wave ray, respectively. The numerical model developed by Liu based on the uniformly valid asymptotic theory of Liu, Lozano, and Pantazaras (1979) was modified to conform to a straight breakwater at an angle to the shoreline. This numerical simulation model served as the basis for comparison with the physical laboratory experimental results of this study of wave heights down-coast of a shore-connected breakwater at a 60-deg angle with the shoreline.

Wave field downcoast of breakwater

178. Preliminary tests indicated that for the area of major interest and for the range of wave periods considered pertinent, the specific test conditions shown in Table 6 could be experimentally investigated with height

Table 6
Experimental Conditions Tested Initial Wave
Heights, H_o , ft, near Wave Generator

<u>0.75</u>	<u>1.00</u>	<u>1.50</u>
0.106	0.102	0.070
0.168	0.130	0.106
0.218	0.211	0.147

Note: All test conditions were replicated
10 times.

changes remaining essentially linear, thus permitting comparisons with theoretical developments. Typical representative wave patterns covering the range of conditions tested in this study are shown in Figures 43-45. Wave-height amplification coefficient, H/H_o , for typical representative experiments are shown in Figures 46-57. Each of these figures constitutes a section parallel

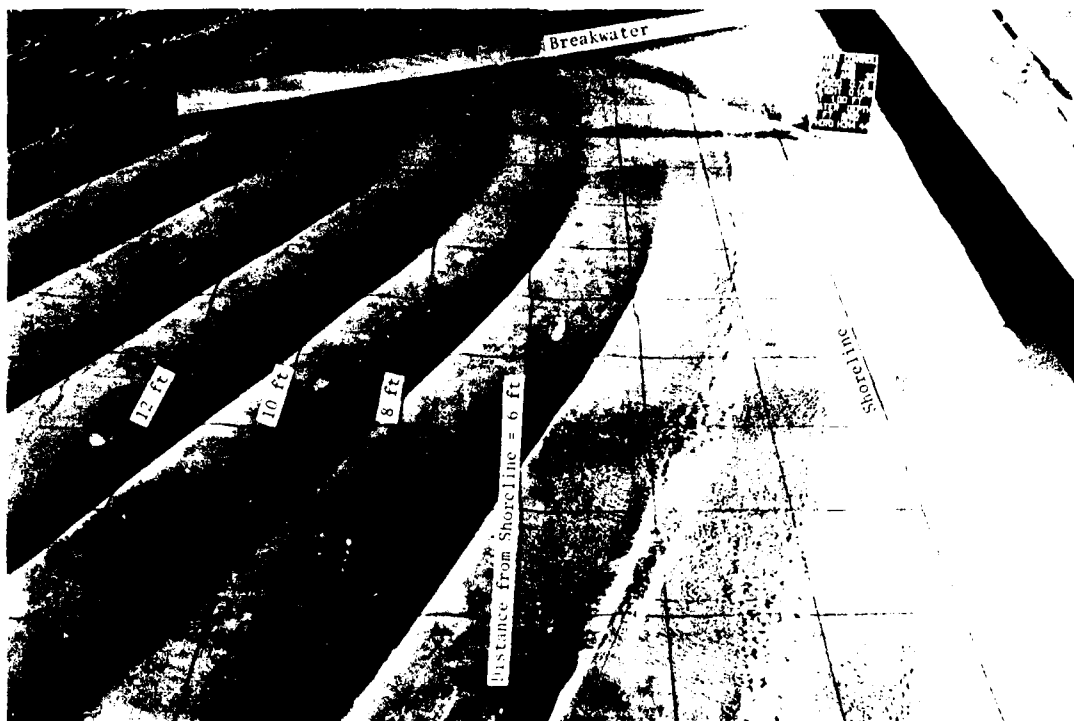


Figure 43. Typical wave pattern downwave of breakwater at 60 deg to shoreline for 0.75-sec wave of height 0.106 ft near the wave generator approaching from an incident direction of 30 deg

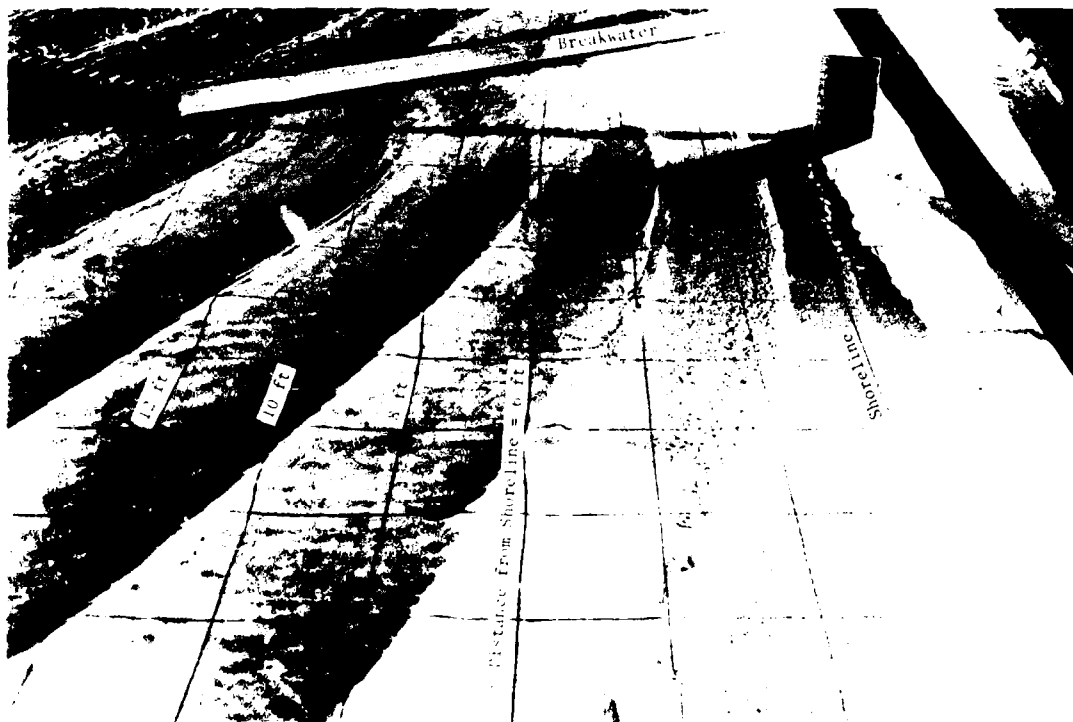


Figure 44. Typical wave pattern downwave of breakwater at 60 deg to shoreline for 1.0-sec wave of height 0.130 ft near the wave generator approaching from an incident direction of 30 deg



Figure 45. Typical wave pattern downwave of breakwater at 60 deg to shoreline for 1.5-sec wave of height 0.147 ft near the wave generator approaching from an incident direction of 30 deg

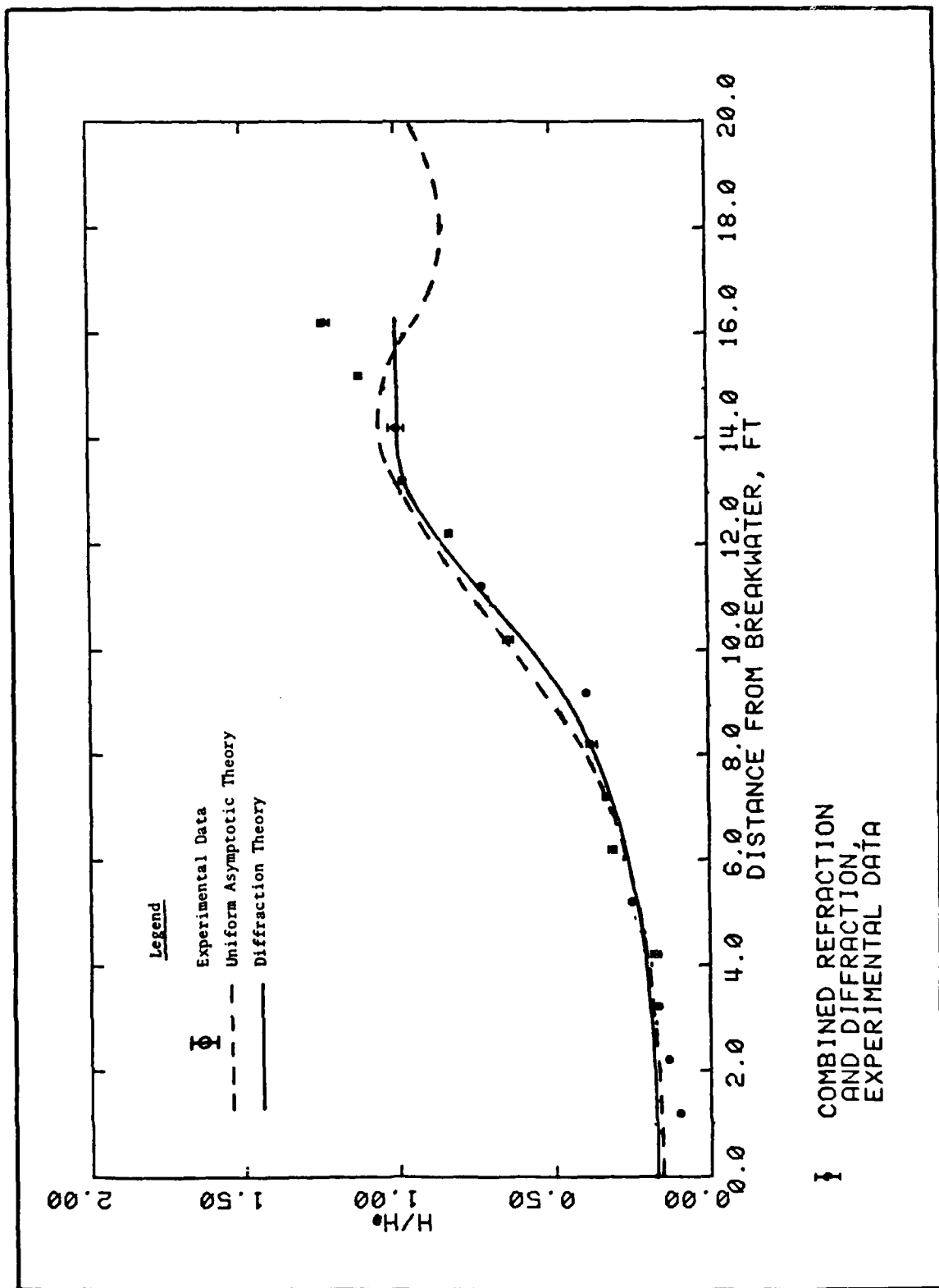


Figure 46. Typical representative wave-height amplification; angle of incidence 30 deg, period 0.75 sec, breakwater angle with shoreline 60.0 deg, H_0 0.106 ft, distance from shoreline 6.00 ft

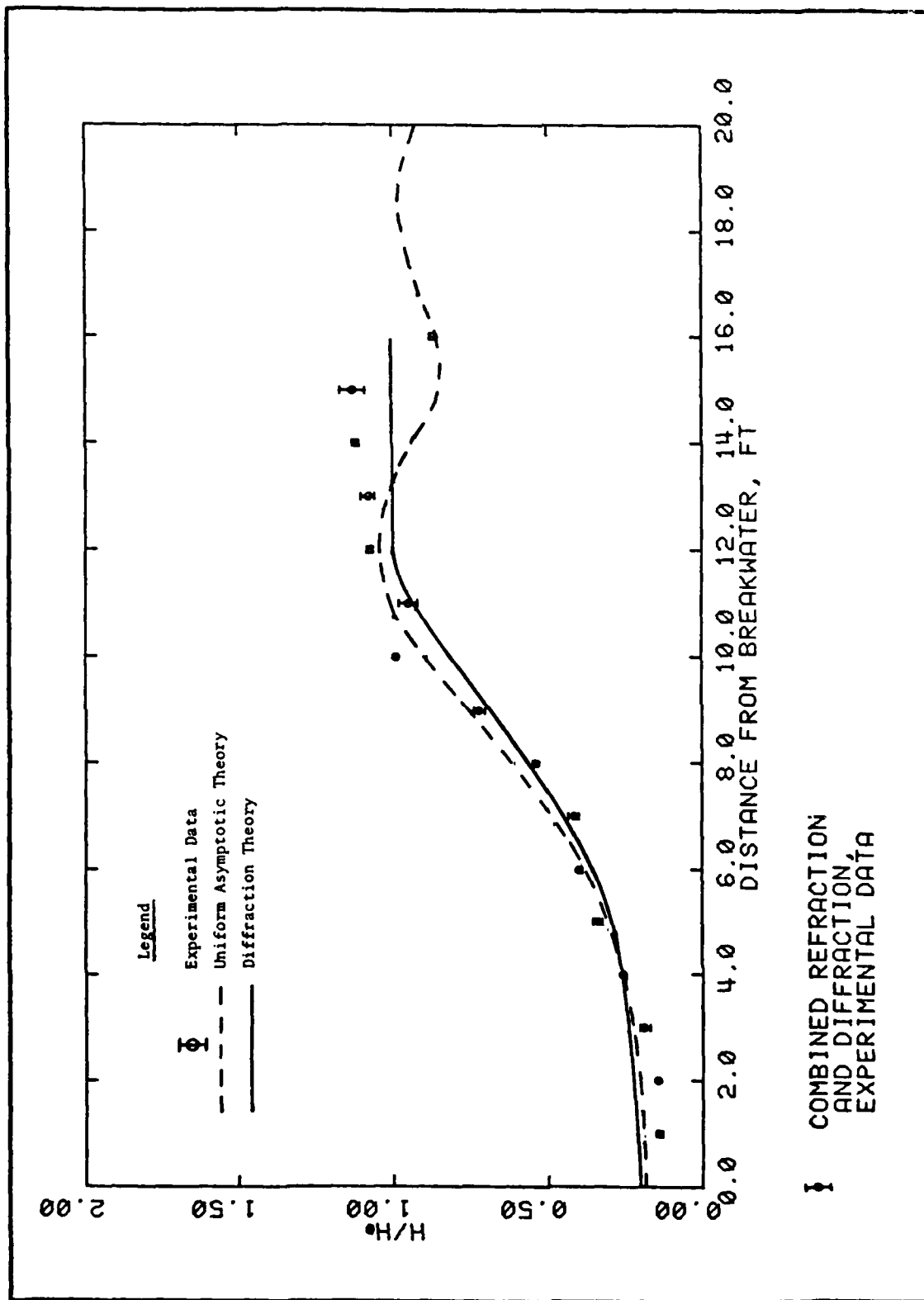


Figure 47. Typical representative wave-height amplification; angle of incidence 30 deg, period 0.75 sec, breakwater angle with shoreline 60.0 deg, H_0 0.106 ft, distance from shoreline 8.00 ft

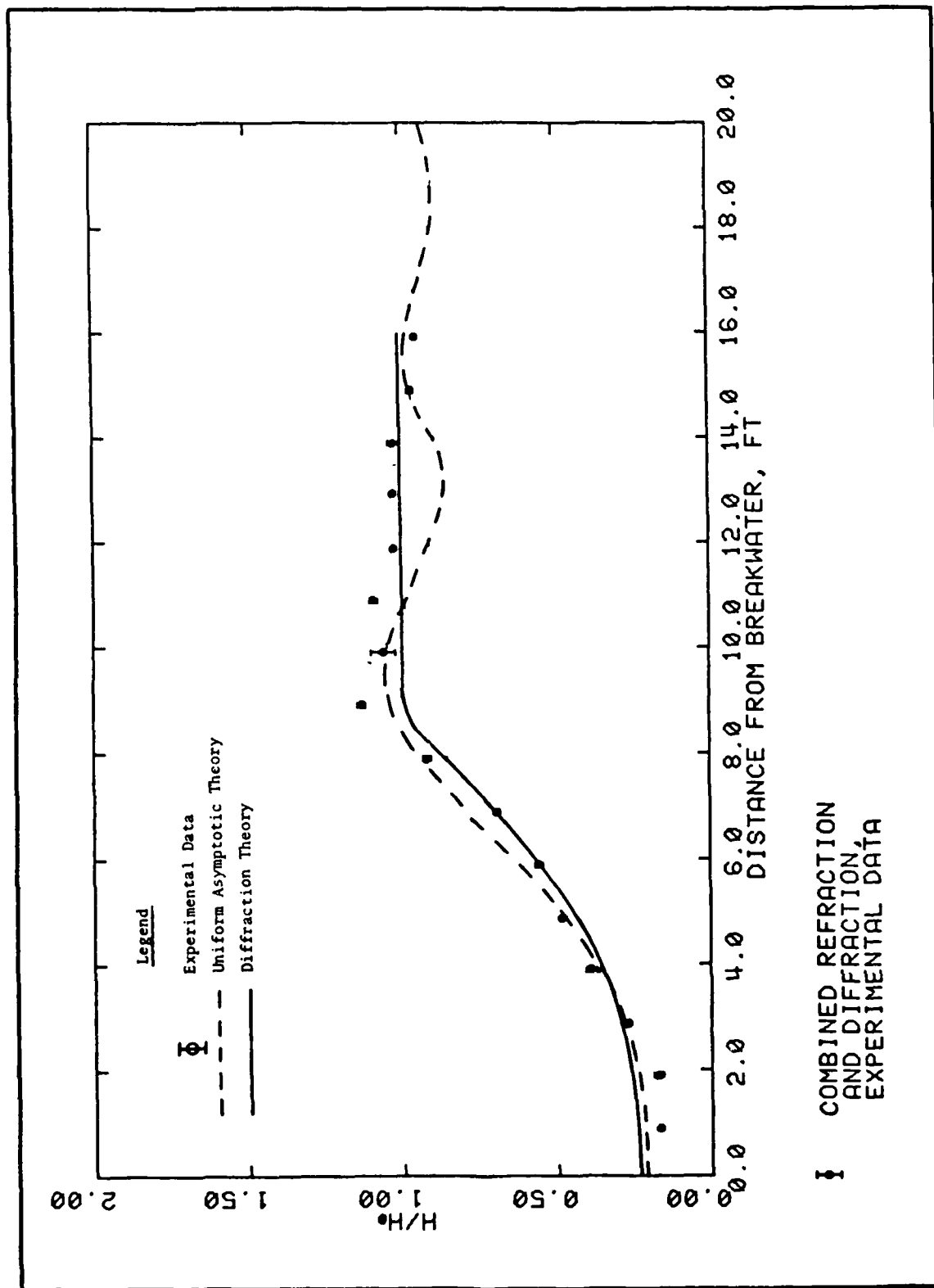


Figure 48. Typical representative wave-height amplification; angle of incidence 30 deg, period 0.75 sec, breakwater angle with shoreline 60.0 deg, H_0 0.106 ft, distance from shoreline 10.00 ft

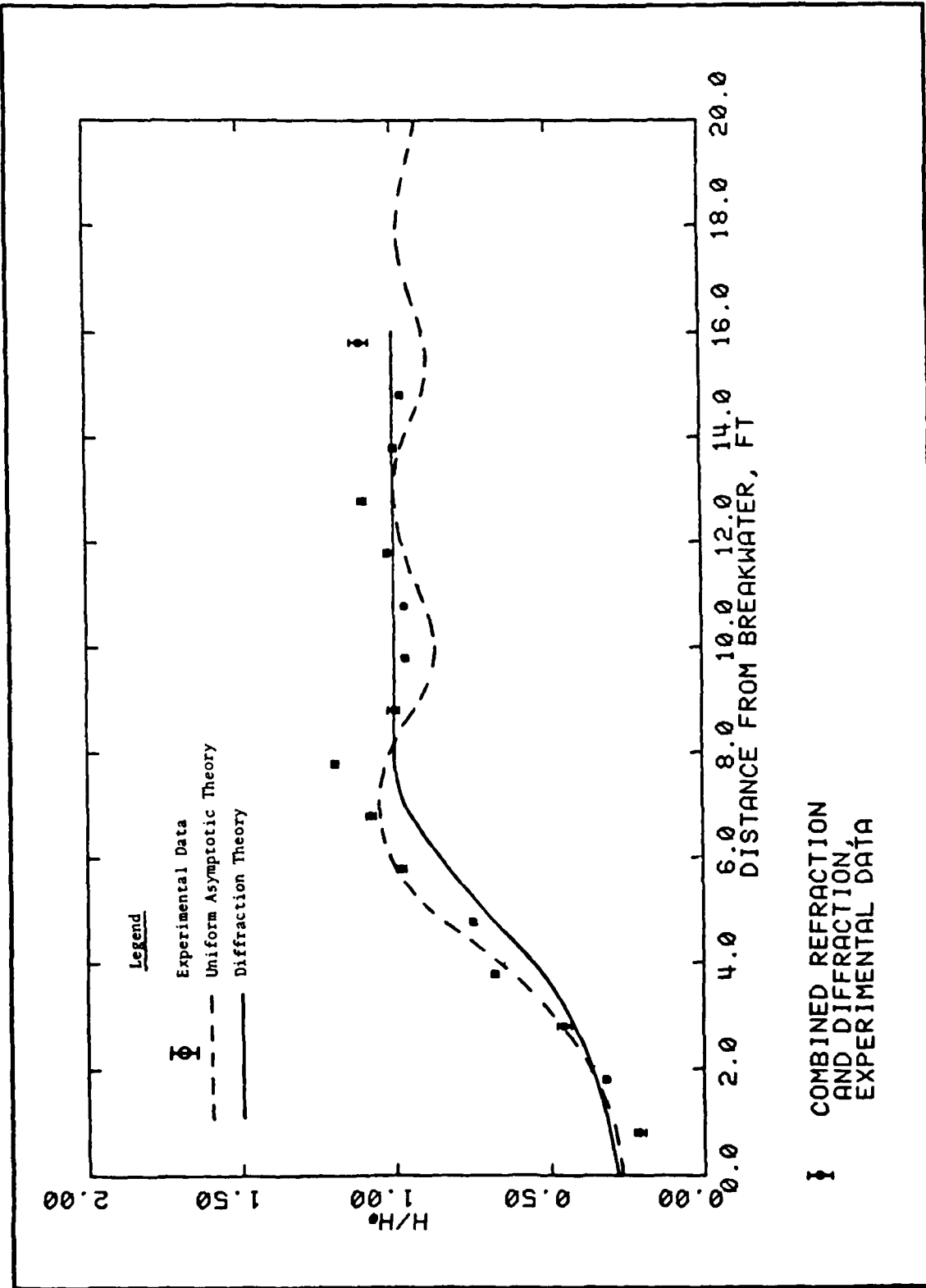


Figure 49. Typical representative wave-height amplification; angle of incidence 30 deg, period 0.75 sec, breakwater angle with shoreline 60.0 deg, H_0 0.106 ft, distance from shoreline 12.00 ft

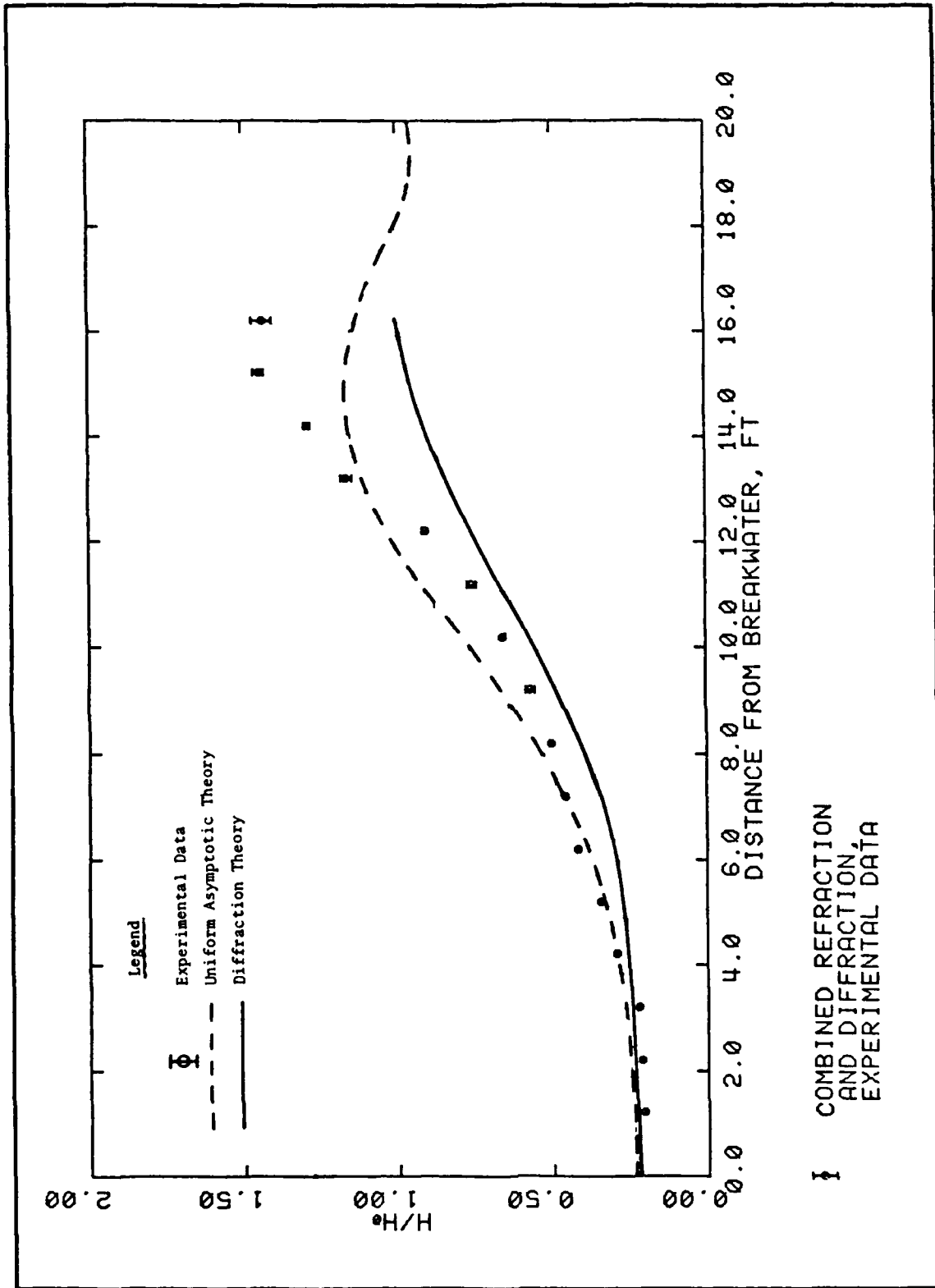


Figure 50. Typical representative wave-height amplification; angle of incidence 30 deg, period 1.00 sec, breakwater angle with shoreline 60.0 deg, H_0 0.102 ft, distance from shoreline 6.00 ft

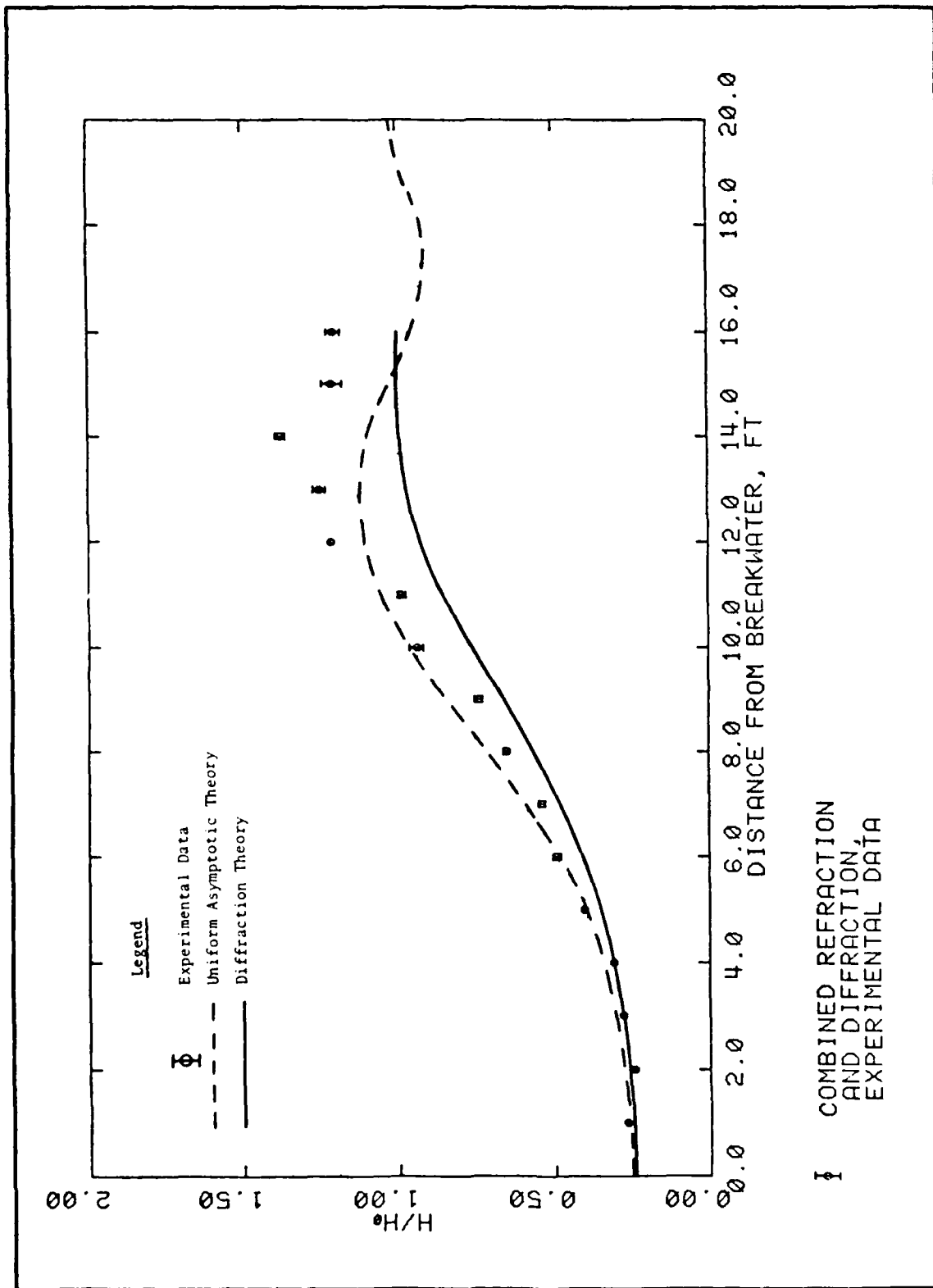


Figure 51. Typical representative wave-height amplification; angle of incidence 30 deg, period 1.00 sec, breakwater angle with shoreline 60.0 deg, H_0 0.102 ft, distance from shoreline 8.00 ft

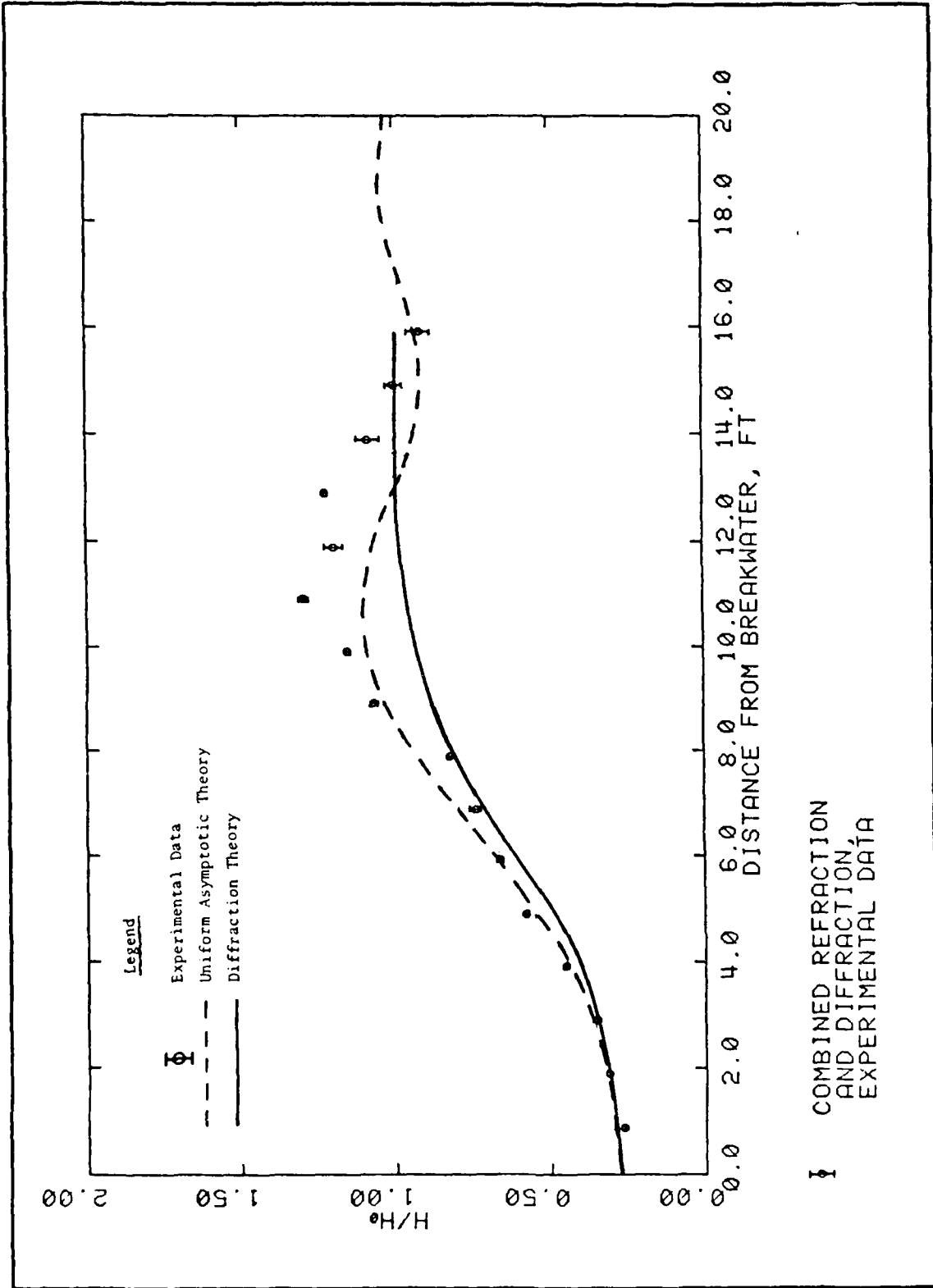


Figure 52. Typical representative wave-height amplification; angle of incidence 30 deg, period 1.00 sec, breakwater angle with shoreline 60.0 deg, H_0 0.102 ft, distance from shoreline 10.00 ft

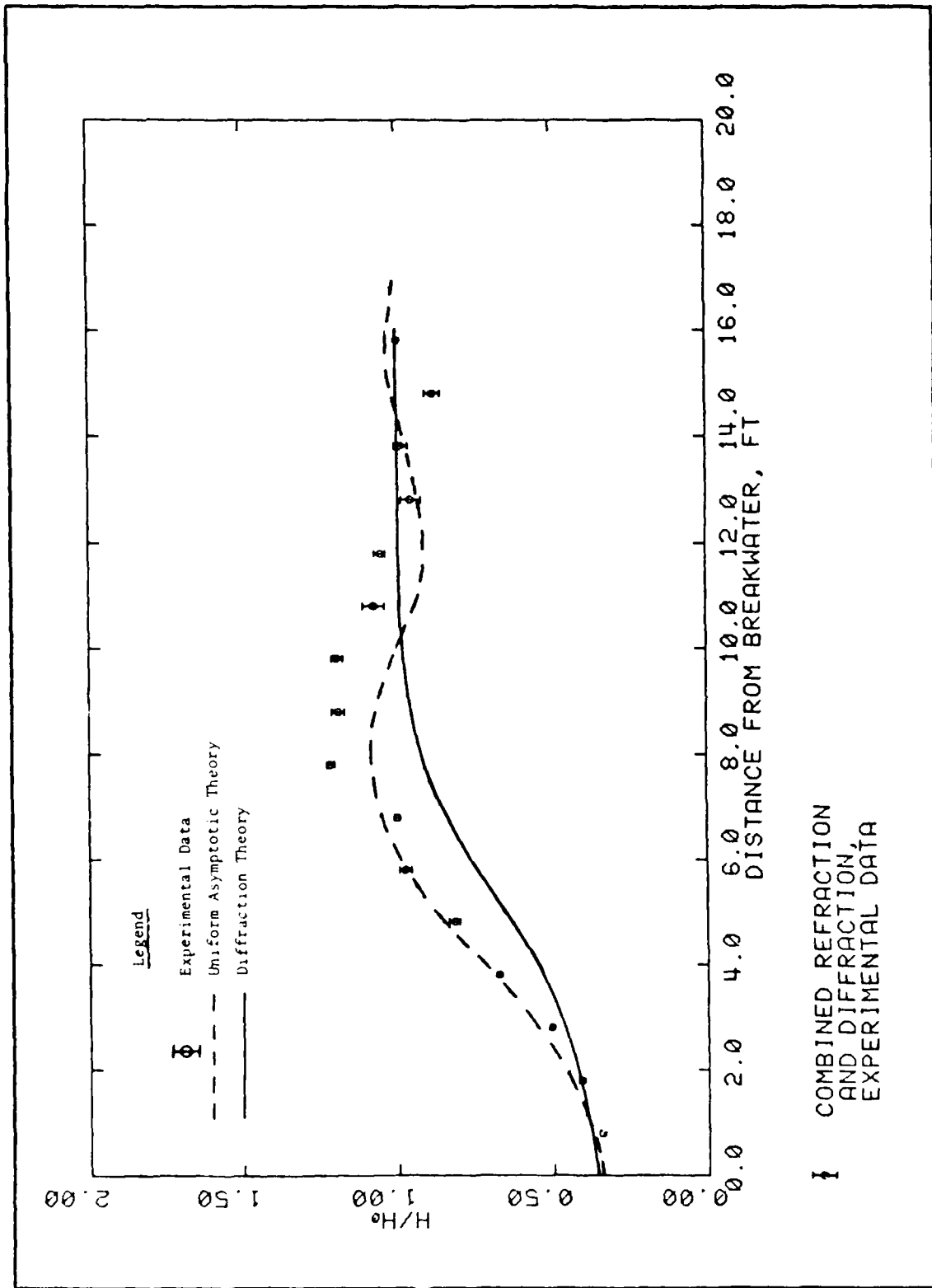


Figure 53. Typical representative wave-height amplification; angle of incidence 30 deg, period 1.00 sec, breakwater angle with shoreline 60.0 deg, H_0 0.102 ft, distance from shoreline 12.00 ft

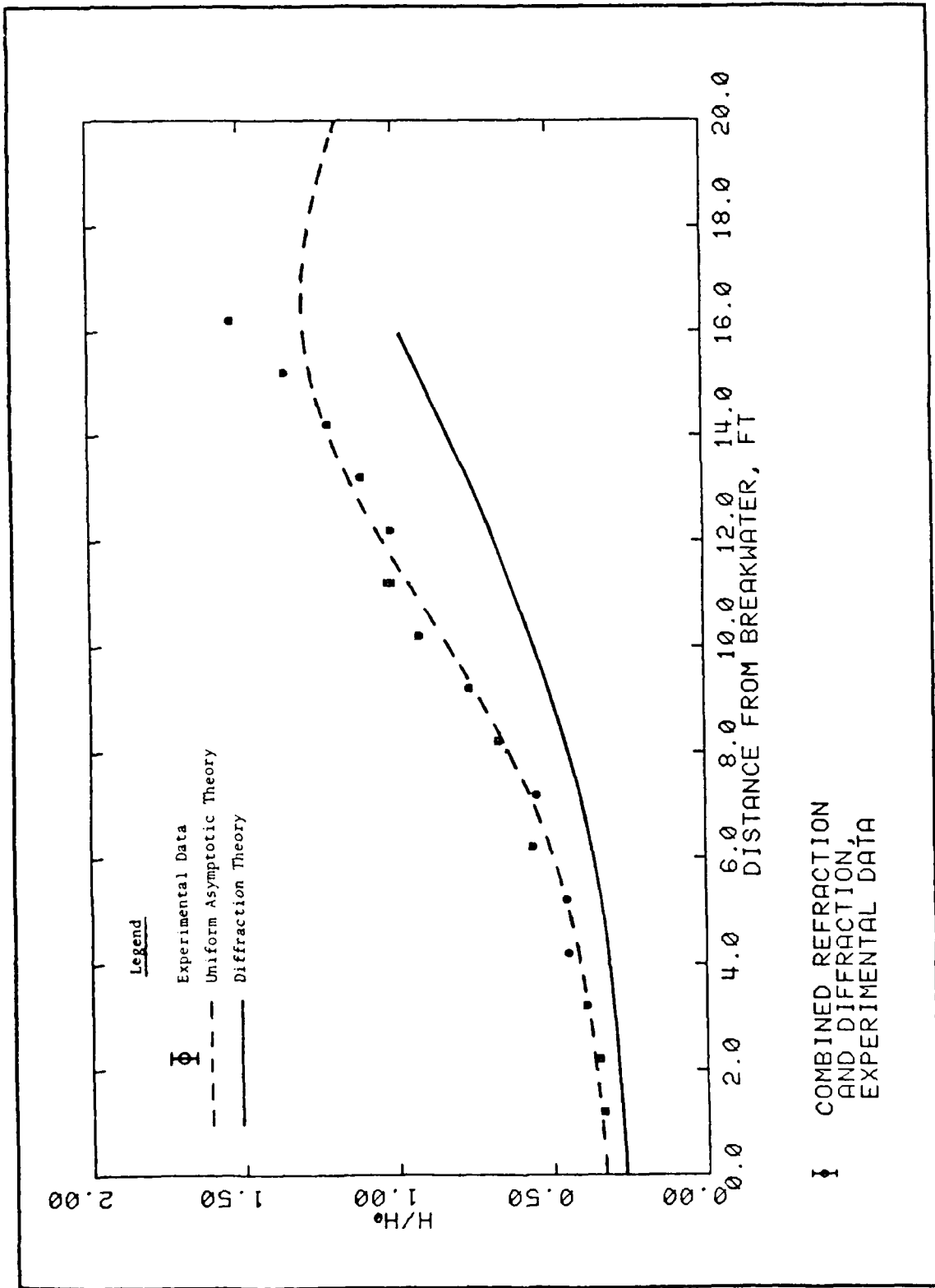


Figure 54. Typical representative wave-height amplification; angle of incidence 30 deg, period 1.50 sec, breakwater angle with shoreline 60.0 deg, H_0 0.070 ft, distance from shoreline 6.00 ft

difference numerical model with a third-order accurate implicit solution scheme. However, a time-marching scheme requires significant computational time. In addition, the finite difference method does not realistically model a complex land-water interface as a result of the stairstep representation and has difficulties in allowing scattered waves to propagate out of a finite extent grid, since these scattered waves are not known a priori.

185. Berkhoff (1972) and Schonfeld (1972) have derived a two-dimensional wave equation that governs short-wave propagation over moderately varying depths. Smith and Sprinks (1975) gave a formal derivation of this equation. In the analysis by Houston and Chou (1984), a hybrid finite element method is used to solve this wave equation. The method combines a finite element solution over a finite extent region of variable depth with an analytical solution for a surrounding infinite region of constant depth.

Wave Equation

186. The propagation of periodic, small amplitude surface gravity waves over a variable depth seabed of mild slope is governed by the following equation:

$$\nabla \cdot \left(c c_g \nabla \phi \right) + \frac{c}{c_g} \omega^2 \phi = 0 \quad (26 \text{ bis})$$

where

- ∇ = horizontal gradient operator, dimensionless
- c = phase velocity, ft/sec = $(g/k \tanh kh)^{1/2}$
- g = gravitational constant, 32.174 ft/sec²
- k = wave number, $2\pi/L$, 1/ft
- h = still-water depth, ft
- c_g = group velocity, ft/sec = $1/2 c (1 + G)$
- $G = 2 k h / \sinh 2 k h$, ft/sec
- ω = angular frequency, $2\pi/T$, 1/sec
- ϕ = velocity potential defined by $\bar{u} = \nabla \phi$, ft²/sec
- \bar{u} = two-dimensional velocity vector, ft/sec

187. Equation 26 was derived by Berkhoff (1972) and Schonfeld (1972) and is discussed in detail by Jonsson and Brink-Kjaer (1973). This equation governs both refraction and diffraction. It reduces to the well-known

PART V: NUMERICAL MODEL OF COMBINED REFRACTION AND DIFFRACTION

182. A two-dimensional finite element numerical model (FINITE) was developed by Houston and Chou (1984) that calculates combined refraction and diffraction of both long and short waves approaching structures from any arbitrary direction. The wave equation solved governs the propagation of periodic, small amplitude surface gravity waves over a variable depth seabed of mild slope. An efficient computational scheme is employed that allows the solution of practical problems that typically require large computational grids. Comparisons are presented between the finite element model calculations and an analytical solution, a two-dimensional numerical solution, a three-dimensional numerical solution, and measurements from hydraulic experimental studies of Hales (1980b).

Numerical Model Background

183. Short waves have wavelengths that are sufficiently short (wavelength to depth ratio less than approximately 20) that propagation speeds are a function of wave frequency. In the nearshore region, short waves with periods from a few seconds to approximately 15 sec play an important role in the movement of sediment and the stability of coastal structures.

184. Equations that govern long-wave propagation over variable depths have been known for some time (Lamb 1932). However, for shorter period waves where frequency dispersion is important, the theory has included only constant depths. Attempts have been made (Pierson 1951; Eckart 1952) to develop a two-dimensional equation for combined refraction and diffraction that would govern short-wave propagation in a region of variable depth; however, the equations developed do not reduce to the appropriate simple refraction equation after neglecting the curvature of the amplitude function and they also do not reduce to the linear long-wave equation in the case of small water depth. In recent years, Boussinesq-type equations also have been used to study the propagation of short-period waves. These equations include terms that govern both frequency dispersion and nonlinearity. Two-dimensional modeling of these equations is difficult since the frequency dispersion term is third order, therefore requiring a third-order accurate numerical scheme. Abbott, Petersen, and Skovgaard (1978) have presented a time-marching two-dimensional finite

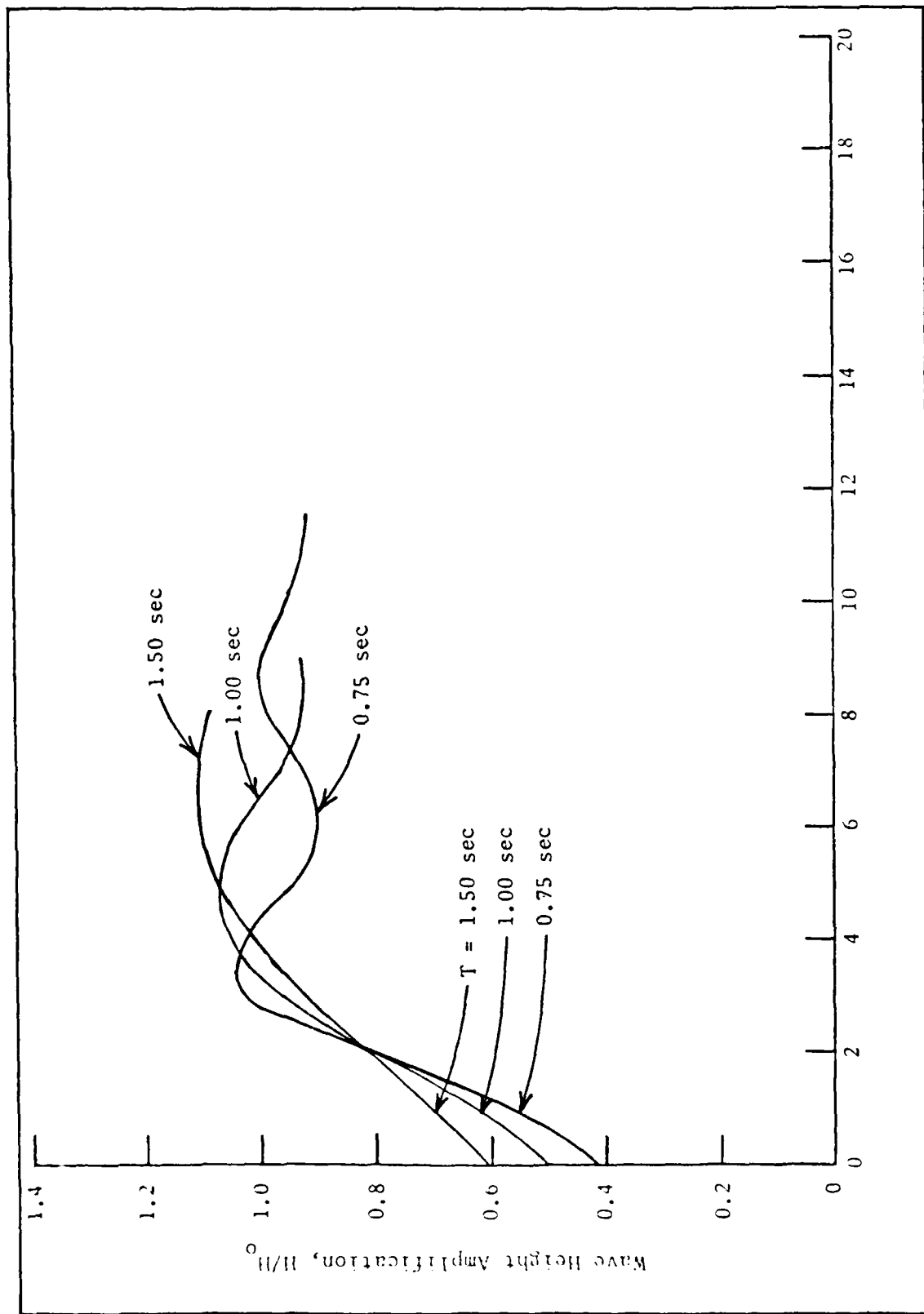


Figure 64. Uniformly valid asymptotic indication of period effect on wave-height amplification; incident wave angle 30 deg, breaker angle with shoreline 60 deg, distance from shoreline 14 ft

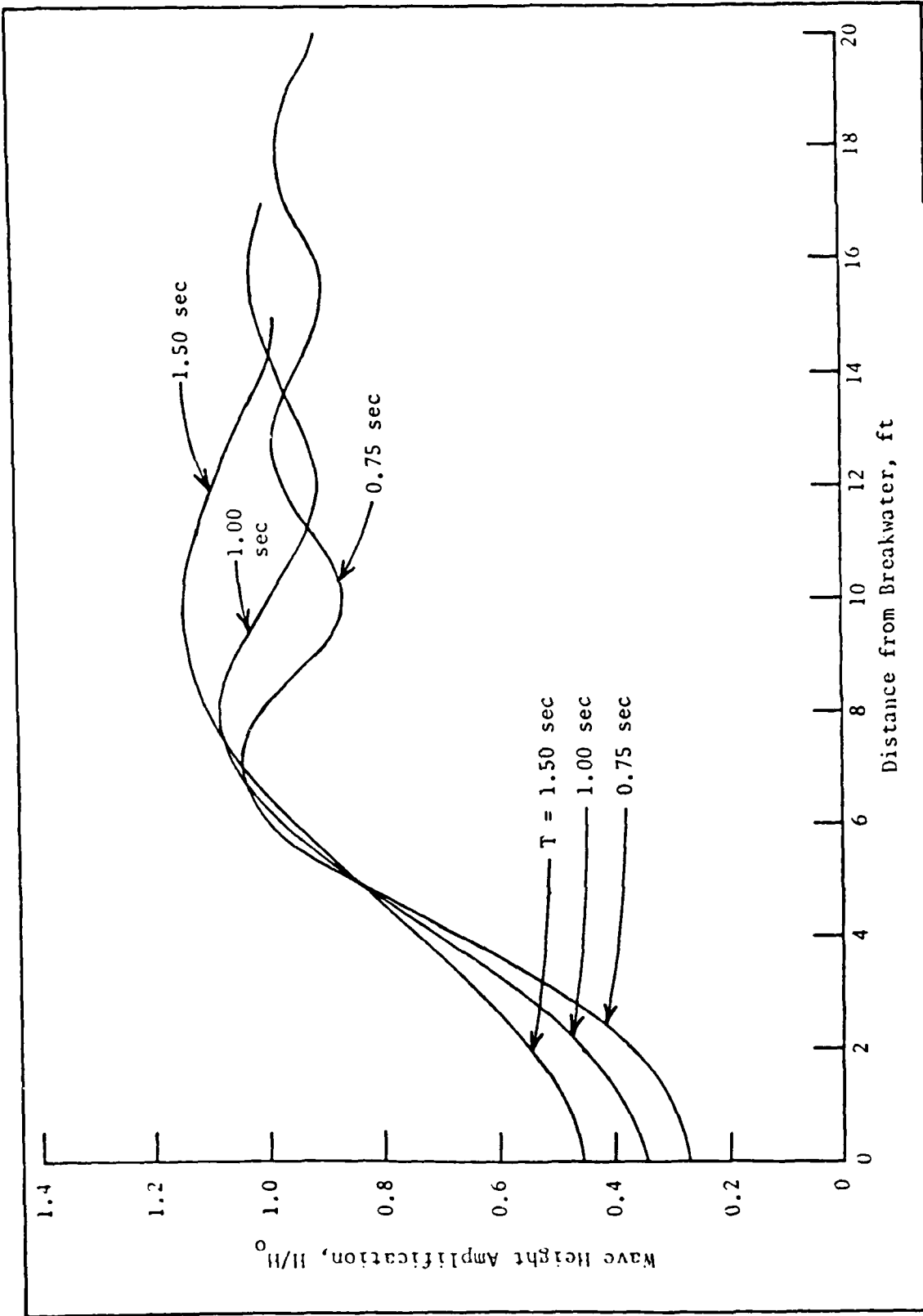


Figure 63. Uniformly valid asymptotic indication of period effect on wave-height amplification; incident wave angle 30 deg, breakwater angle with shoreline 60 deg, distance from shoreline 12 ft

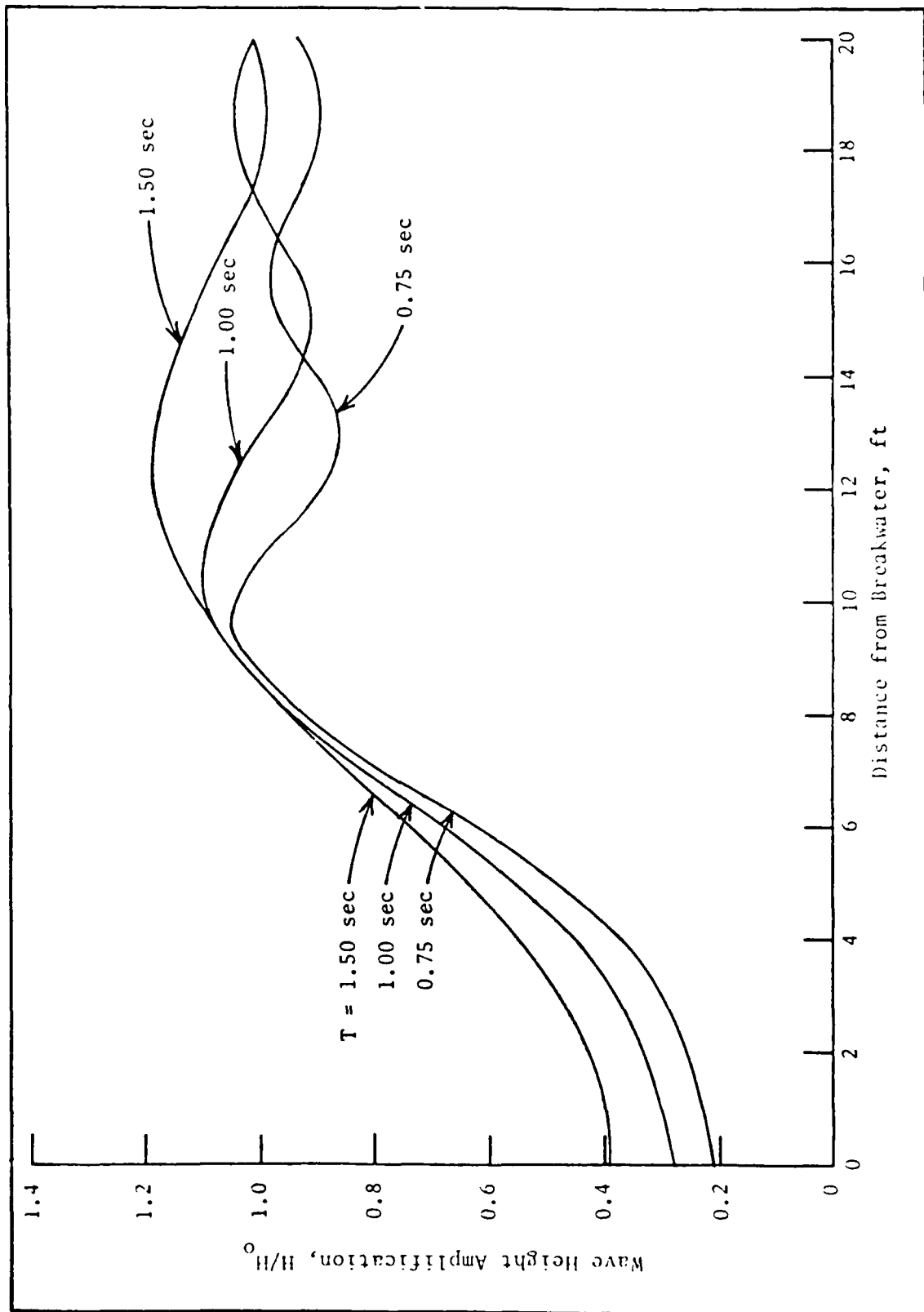


Figure 62. Uniformly valid asymptotic indication of period effect on wave-height amplification; incident wave angle 30 deg, breakwater angle with shoreline 60 deg, distance from shoreline 10 ft

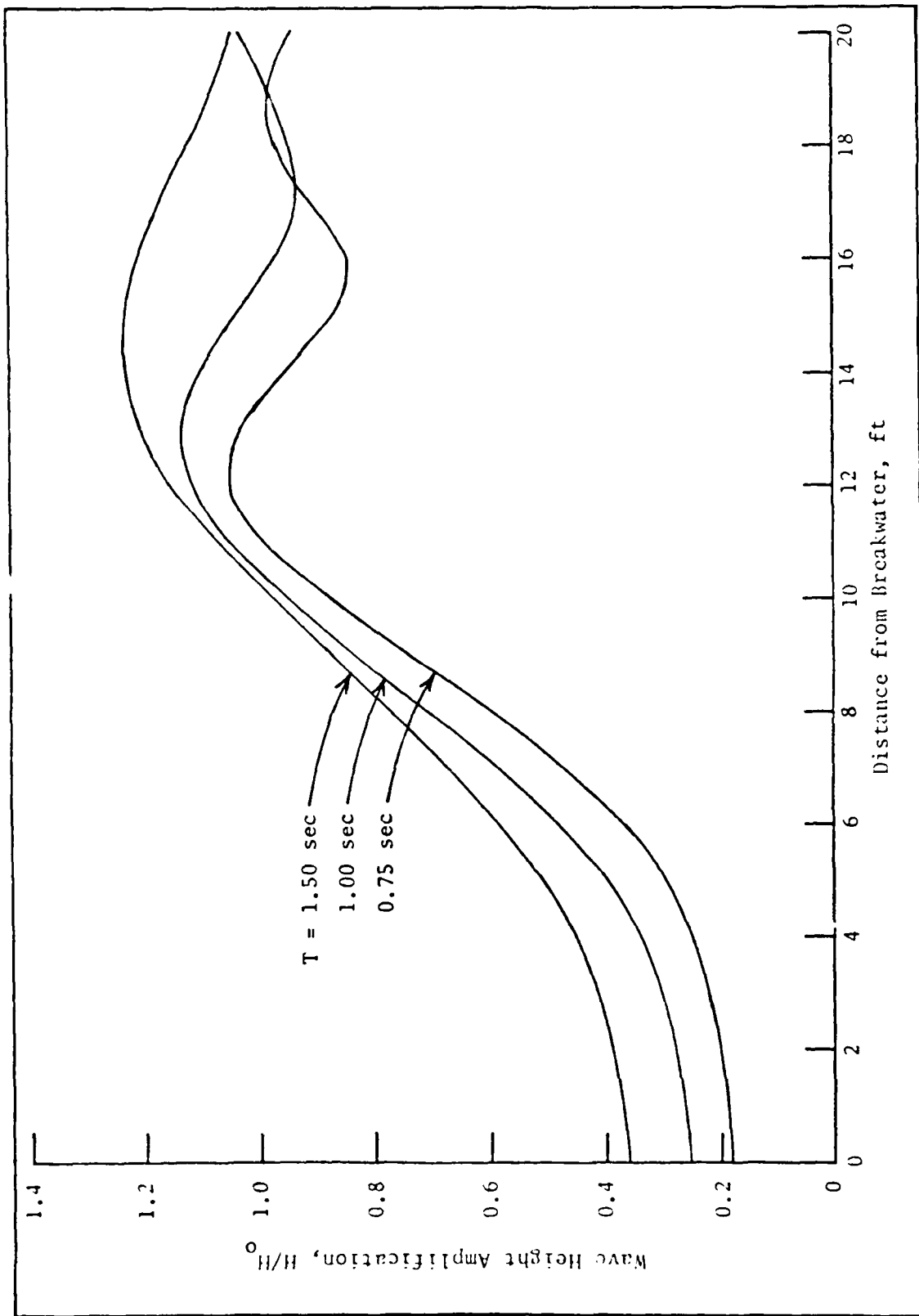


Figure 61. Uniformly valid asymptotic indication of period effect on wave-height amplification; incident wave angle 30 deg, breakwater angle with shoreline 60 deg, distance from shoreline 8 ft

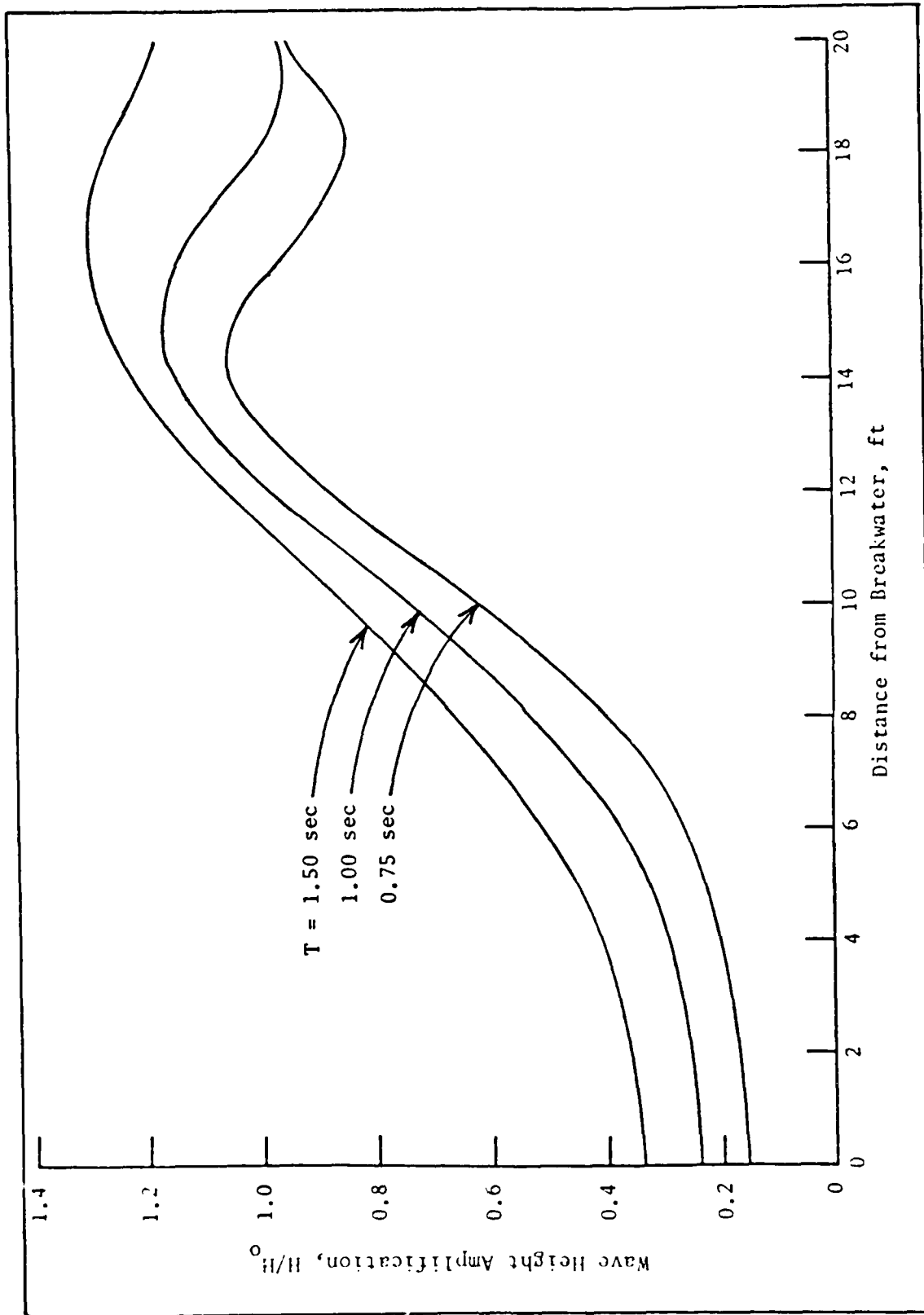


Figure 60. Uniformly valid asymptotic indication of period effect on wave-height amplification; incident wave angle 30 deg, breakwater angle with shoreline 60 deg, distance from shoreline 6 ft

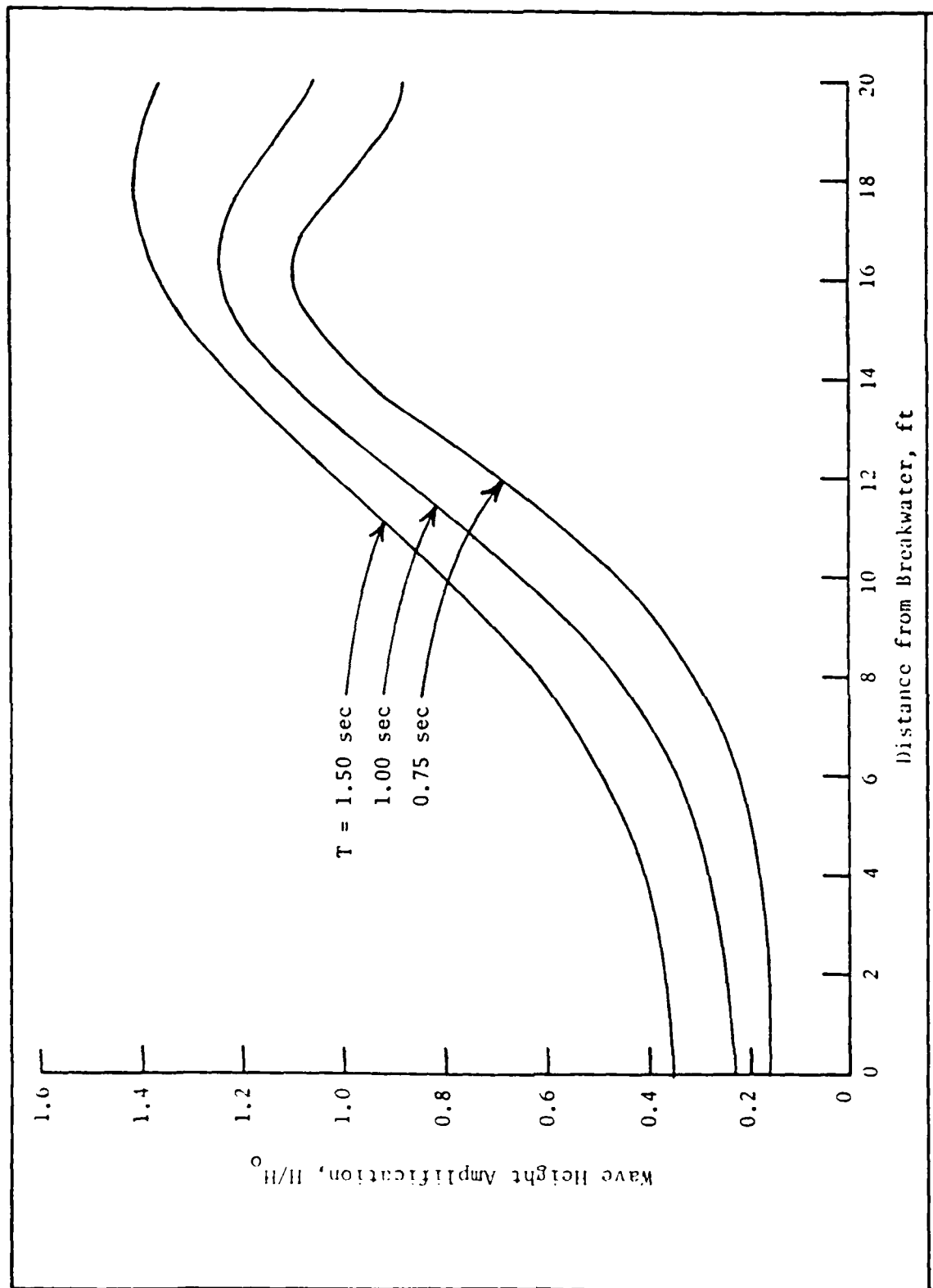


Figure 59. Uniformly valid asymptotic indication of period effect on wave-height amplification; incident wave angle 30 deg, breakwater angle with shoreline 60 deg, distance from shoreline 4 ft

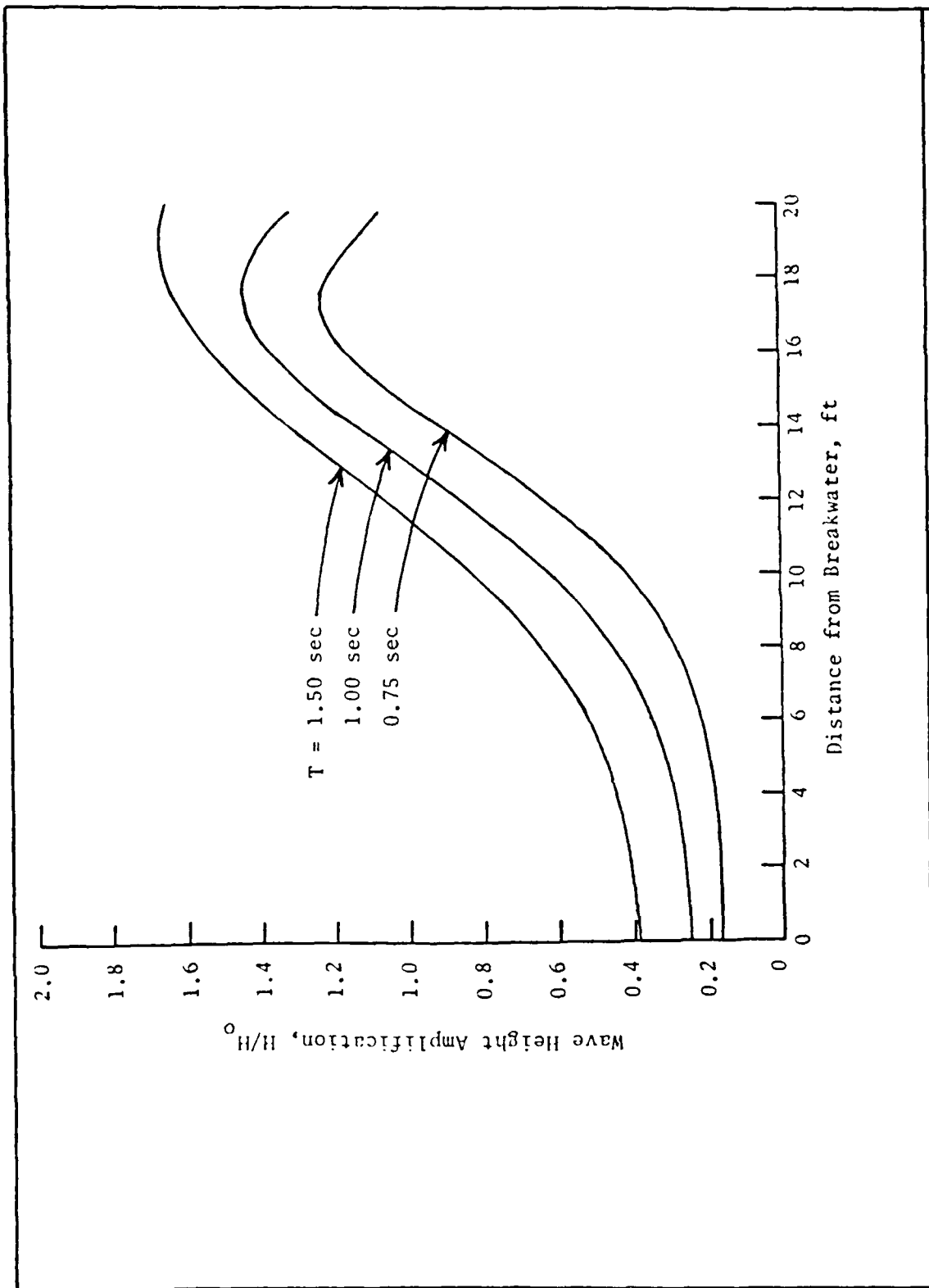


Figure 58. Uniformly valid asymptotic indication of period effect on wave-height amplification; incident wave angle 30 deg, breakwater angle with shoreline 60 deg, distance from shoreline 2 ft

numerical program developed from this theory and modified to fit the straight breakwater geometry was applied to the entire shadow zone region of the structure. These results are presented in Figures 58-64 for distances parallel to the shoreline of 2 to 14 ft, respectively, in increments of 2-ft displacement seaward toward the tip of the breakwater (which was located 15 ft from the shoreline). The three wave periods utilized in the experimental phase of this study (0.75, 1.00, and 1.50 sec) are shown in these plates as the independent parameters. It is apparent near the shoreline that the longer period waves allow for the greater wave-height amplification at all locations (particularly within the shadow zone). With increase in distance from the shoreline, the longer period waves continue to exhibit a greater wave-height amplification in the shadow zone; however, outside the shadow zone, the period effect becomes less apparent and eventually becomes entirely obscured as the undulations of the different periods engulf (overlap) each other.

with the shoreline at distances from the shoreline of 6, 8, 10, or 12 ft. The corresponding scatter of the experimental data is indicated by the error bars of plus-or-minus one standard deviation. Also shown in these figures is the wave-height amplification due to diffraction alone (as if the basin were horizontal beyond the structure), and the wave-height amplification as indicated by the uniformly valid asymptotic theory.

179. For small wave periods, small initial wave heights, and deep within the shadow zone (sections near the shoreline), both the diffraction theory and the uniformly valid asymptotic theory predict wave-height amplifications that compare consistently well with the experimental data. Nearer the tip of the breakwater, the diffraction theory tends to diverge rapidly from the experimental results, and the uniformly valid asymptotic theory more nearly approximates the experiments. As wave period increases, the deviation of the diffraction theory becomes more pronounced at all locations except very near the breakwater; and even in this region the uniformly valid asymptotic theory closely approximates the data from the experiments. The greatest deviation of the uniformly valid asymptotic theory from the experiments occurs outside the breakwater shadow zone in the area of the asymptotic undulations of the wave-height amplification factor. This can be attributed to reflection of longer period wave energy from the beach breaker zone not accounted for in the analytical development, since the uniformly valid asymptotic theory consistently underpredicts the wave-height amplification in this area.

180. In general, it can be concluded that the uniformly valid asymptotic theory is superior to diffraction theory alone for estimating wave heights downcoast of nearshore structures subjected to combined refraction and diffraction. Particularly for longer period waves and for the region near the structures where scour and erosion are known to frequently occur, this theory provides an estimation that consistently approximates the results of this experimental study and which is significantly better than diffraction theory. At the same time, it appears desirable to incorporate into this theory a degree of nonlinearity that is not presently available to account for variations in incipient wave height and to allow for higher orders of dynamics in the analytics.

181. Because the uniformly valid asymptotic theory compares favorably with the results of this experimental study (four sections parallel with the shoreline for three wave periods with three incident wave heights each), the

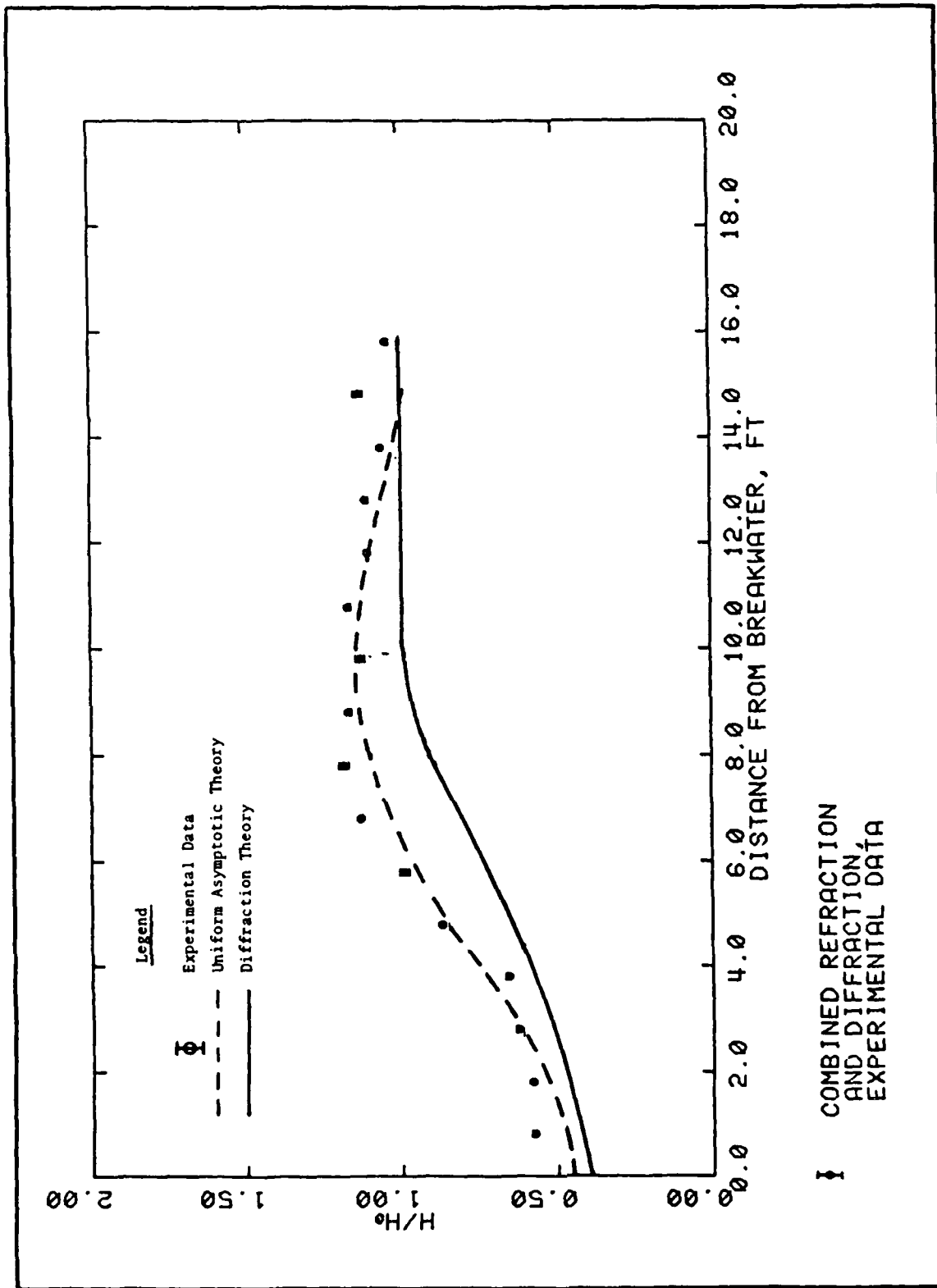


Figure 57. Typical representative wave-height amplification; angle of incidence 30 deg, period 1.50 sec, breakwater angle with shoreline 60.0 deg, H_0 0.070 ft, distance from shoreline 12.00 ft

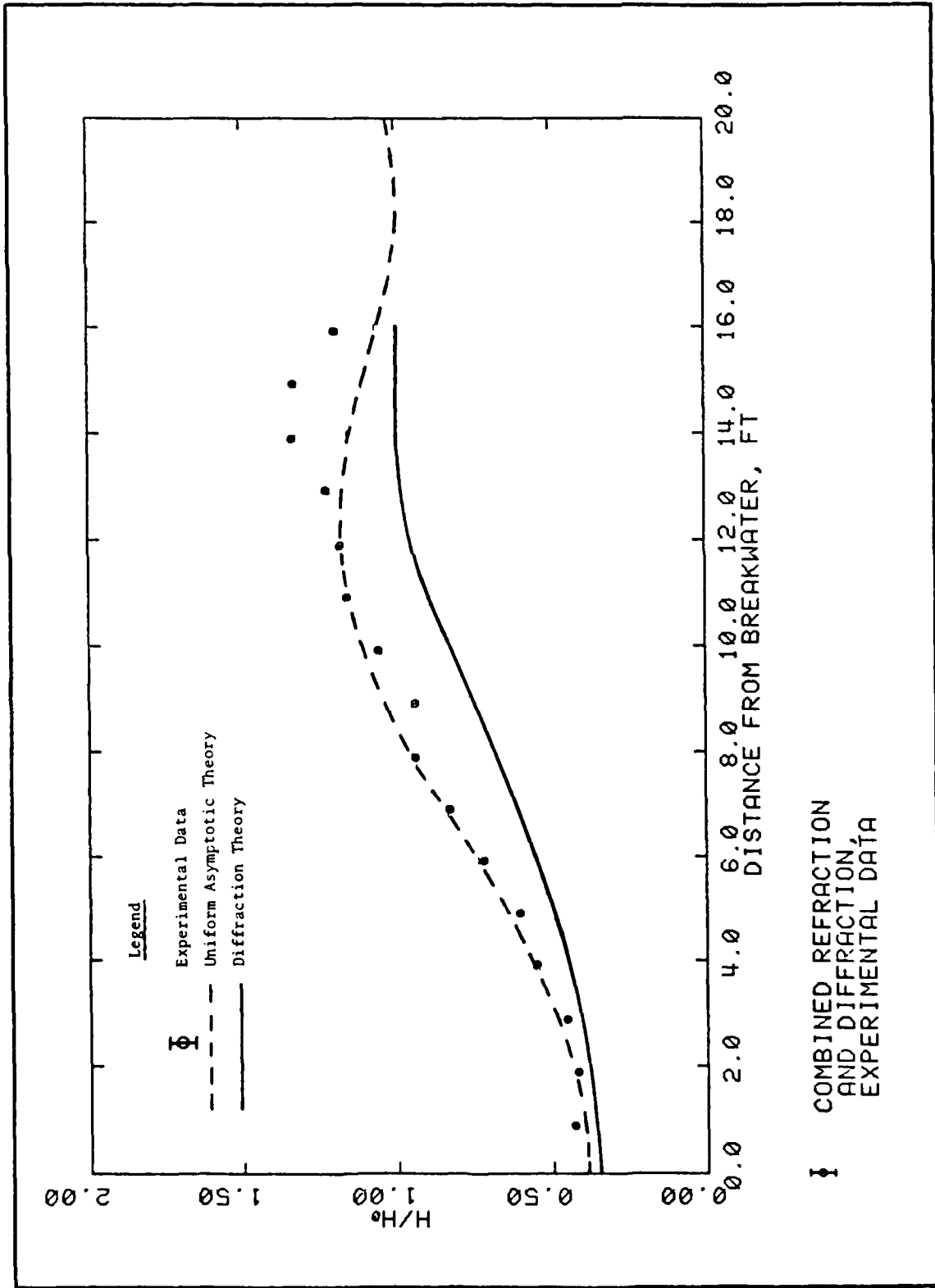


Figure 56. Typical representative wave-height amplification; angle of incidence 30 deg, period 1.50 sec, breakwater angle with shoreline 60.0 deg, H_0 0.070 ft, distance from shoreline 10.00 ft

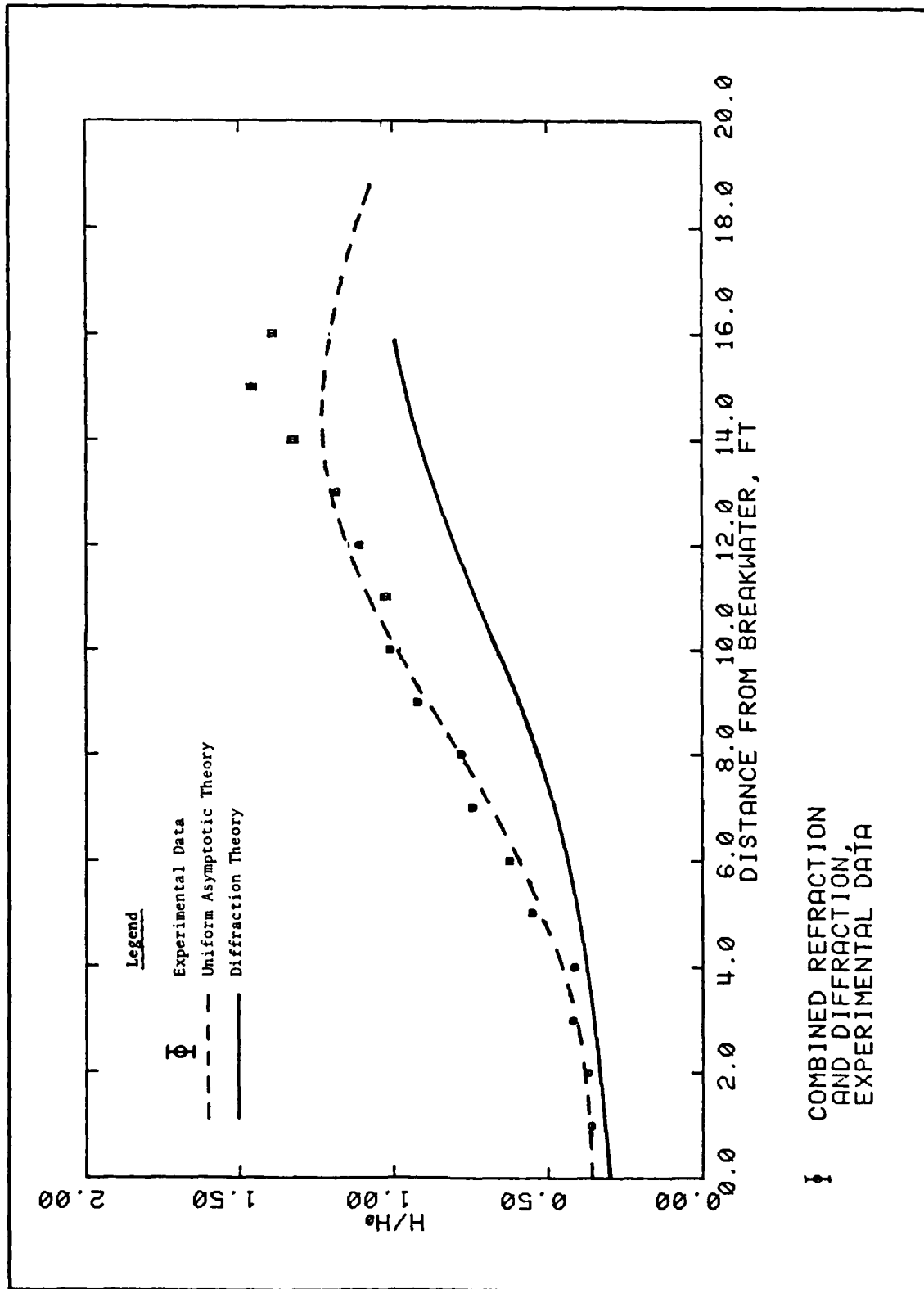


Figure 55. Typical representative wave-height amplification; angle of incidence 30 deg, period 1.50 sec, breakwater angle with shoreline 60.0 deg, H_0 0.070 ft, distance from shoreline 8.00 ft

"eikonal" equation governing refraction by neglect of the variation of the amplitude function in the horizontal plane. The equation reduces to the diffraction Helmholtz equation in deep or constant-depth water and to the linear long-wave equation in shallow water.

188. Finite element numerical models have been used to solve Equation 26. Berkhoff (1972, 1976) linked a finite element solution of Equation 26 over a variable depth region to a source distribution for a constant-depth outer region. However, as noted by Chen and Mei (1974), Berkhoff (1972) did not use a proper functional with the consequence that his global stiffness matrix was nonsymmetric and thus inconvenient numerically for all but the simplest problems. Bettess and Zienkiewicz (1977) also developed a finite element solution of Equation 26. However, they used infinite elements to cover the constant-depth outer region. The shape function used in the infinite elements had an exponentially decreasing term in the direction away from the inner region. The choice of a decay length was somewhat arbitrary; but the solutions were not, in general, too sensitive to the exact value. A disadvantage of this technique is that the infinite elements increase the number of equations to be solved. If a problem requires a large number of elements because the region of interest is large and the incident wavelengths are short, this solution can require substantial computational time.

189. Equation 26 also has been solved by a parabolic approximation (Radder 1979). The approximation is derived from splitting the wave field into transmitted and reflected components and then neglecting the reflected components. This approach is applicable to some propagation problems but is not appropriate for problems involving wave interaction with coastal structures such as breakwaters.

Finite Element Solution

190. Equation 26 is solved by program FINITE using a hybrid finite element method originally developed by Chen and Mei (1974) to solve the diffraction Helmholtz equation in a constant-depth region. Space is divided into two regions as shown in Figure 65 (finite inner region A and infinite outer region B). Conventional finite elements are used in the variable depth region A. A single superelement is used to cover the constant-depth infinite region B. Variational principles are used that incorporate the matching conditions

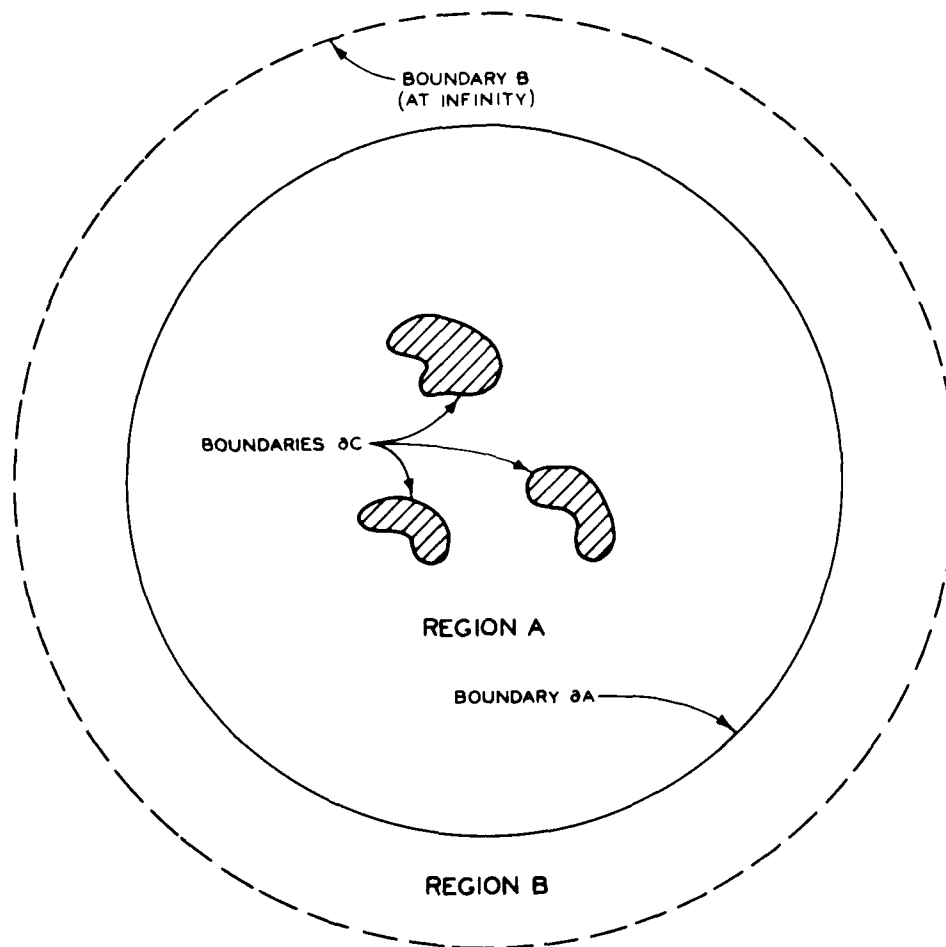


Figure 65. Regions of computation

between the regular elements and the superelement as natural conditions. Thus a symmetric global stiffness matrix is obtained that is very advantageous for highly complex problems.

191. The variational principle for the boundary value problem requires that the following functional be stationary with respect to arbitrary first variation of the velocity potential ϕ :

$$\begin{aligned}
 F(\phi) = & \iint_A \frac{1}{2} \left[\frac{cc}{g} (\nabla\phi)^2 - \frac{\omega^2 c}{gc} \phi^2 \right] dA \\
 & + \int_{\partial B_\infty} \frac{ikcc}{2g} \phi - \phi_I^2 dL - \int_{\partial B_\infty} \frac{cc}{g} \frac{\partial\phi_I}{\partial n} \phi dL
 \end{aligned}
 \tag{45}$$

where ϕ_I and ϕ_R are the incident and reflected wave velocity potentials, respectively; n is a unit normal; and the last two integrals are line integrals at infinity. Analogous to the derivation of Chen and Mei (1974), this functional can be rewritten as follows:

$$\begin{aligned}
 F(\phi) = & \iint_A \frac{1}{2} \left[\frac{cc}{g} (\nabla \phi_A)^2 - \frac{\omega^2 c}{gc} \phi_A^2 \right] dA \\
 & + \int_{\partial A} \frac{1}{2} \frac{cc}{g} (\phi_B - \phi_I) \frac{\partial(\phi_B - \phi_I)}{\partial n_A} - \int_{\partial A} \frac{cc}{g} \phi_A \frac{\partial(\phi_R - \phi_I)}{\partial n_A} \\
 & - \int_{\partial A} \frac{cc}{g} \phi_A \left| \frac{\partial \phi_I}{\partial n_A} \right| + \int_{\partial A} \frac{cc}{g} \phi_I \frac{\partial(\phi_B - \phi_I)}{\partial n_A} + \int_{\partial A} \frac{cc}{g} \phi_I \frac{\partial \phi_I}{\partial n_A}
 \end{aligned} \tag{46}$$

where ϕ_B and ϕ_A are the velocity potentials in regions B and A, respectively and n_A is a unit normal to the boundary separating regions B and A.

192. Note that all integrals are evaluated within region A or along ∂A . Thus the variational principle is a localized one. As discussed by Aranha, Mei, and Yue (1979), this variational principle can be replaced by an equivalent weak formulation.

193. The inner region A is assumed to have a variable depth and to be of finite extent. This region is subdivided into finite elements. Here the elements are triangular with simple linear shape functions. The infinite region B (or semi-infinite if a harbor located along an infinite coastline is of concern) is assumed to have a constant depth and is covered with a single superelement. Since region B has a constant depth, the governing equation is the diffraction Helmholtz equation. An analytical solution for the velocity potential in region B is well known and can be expressed as follows:

$$\phi_B = \sum_{n=0}^{\infty} H_n(kr) (\alpha_n \cos n\theta + \beta_n \sin n\theta) \tag{47}$$

where α_n 's and β_n 's are constant and unknown coefficients, $H_n(kr)$ are Hankel functions of the first kind, and r and θ are radial and angular

variables in polar coordinates. For a semi-infinite region B and a straight infinite coastline, ϕ_B can be expressed as follows:

$$\phi_B = \sum_{n=0}^{\infty} \alpha_n H_n(kr) \cos n\theta \quad (48)$$

The velocity potentials given in Equations 47 and 48 satisfy the Sommerfeld radiation condition that the scattered waves must behave as outgoing waves at infinity. Thus region B can be considered to be a single superelement with a shape function given by Equations 47 and 48.

194. If the shape functions are used to evaluate the integrals of Equation 46 and the functional is extremized with respect to the unknowns, a set of linear algebraic equations is obtained. Of course, the infinite series given by Equations 47 and 48 must be truncated at some finite extent. The number of terms that must be retained depends upon the incident wavelength and may be found by increasing the number of terms until the solution is insensitive to the addition of further terms. Solution of the boundary value problem thus reduces to the solution of N linear algebraic equations for N unknowns (where N is the number of node points in the finite element discretization plus the number of unknowns in the truncated series). That is,

$$\begin{matrix} [K] & \{\psi\} & = & \{Q\} \\ N \times N & N \times 1 & & N \times 1 \end{matrix} \quad (49)$$

The symmetric complex coefficient matrix $[K]$ is in general large, sparse, and banded. It can be stored and manipulated in the computer in a packed form (Chen and Mei 1974). The packed form is chosen to be a rectangular array (N variables in length and the semibandwidth in width). Only elements of $[K]$ on and above the diagonal and within the bandwidth need to be stored in the packed form.

195. Although the packed form of $[K]$ greatly reduces the required computer memory, the problems discussed later are so large that even memory requirements of the packed form of $[K]$ are excessive. However, since the symmetric coefficient matrix is positive definite, a solution is possible by elimination methods without pivoting. Without pivoting, elimination performed using one row affects only the triangle of elements within the band below that

row. Thus the packed form of $[K]$ can be partitioned into several smaller blocks. Using Gaussian elimination, only two blocks at a time are involved in the reduction and back substitution with the remainder of the blocks kept in peripheral storage. This technique allows the solution of extremely large matrices.

Verification

196. To verify this numerical model, comparisons were made between the finite element calculations and both an analytical and a numerical solution for the interaction of waves with a circular island on a paraboloidal shoal. Figure 66 is a sketch of the problem. Hom-ma (1950) presented the analytical solution to the long-wave equation for plane waves incident upon this island.

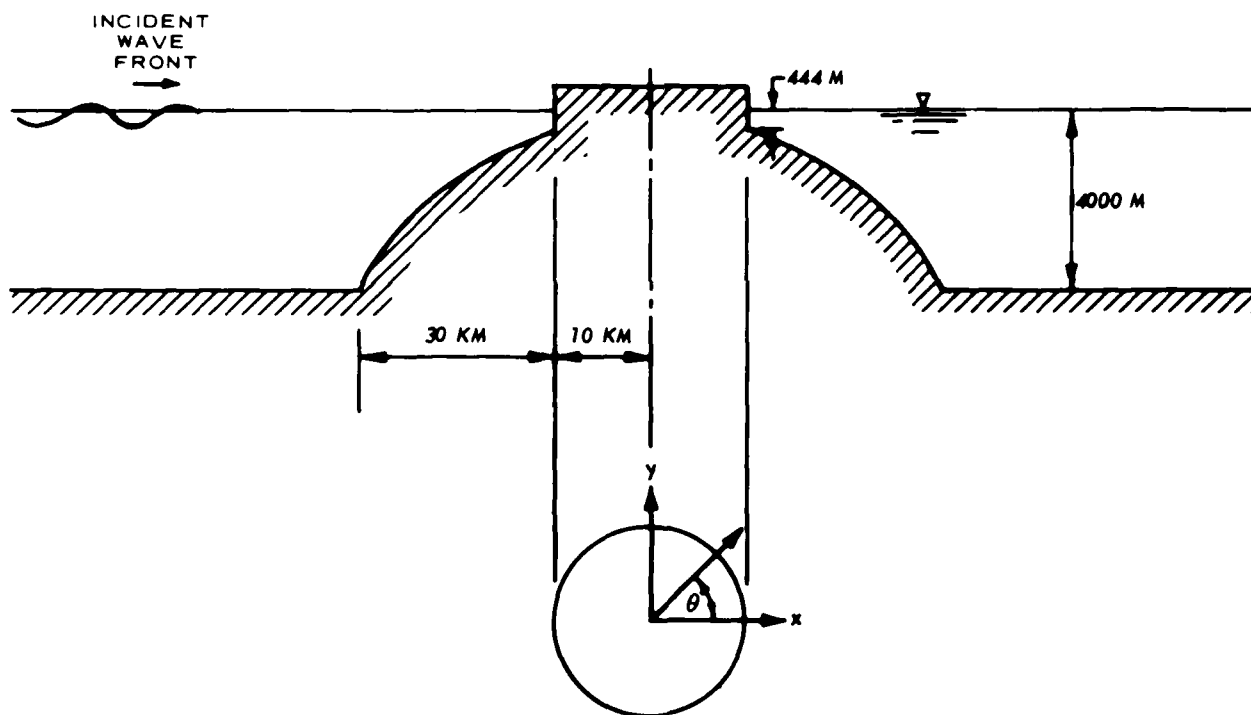


Figure 66. Circular island on a paraboloidal shoal

197. Many investigators, including Berkhoff (1972, 1976) and Bettess and Zienkiewicz (1977), have compared their finite element solutions of the long-wave equation with Hom-ma's solution. For example, Berkhoff (1972, 1976) used 156 elements to cover the paraboloidal shoal (actually one-half of the shoal since by symmetry the solution required calculations for just one-half

the shoal). This number of elements was not sufficient to adequately resolve features of the problem; consequently, Berkhoff's finite element solution differed from Hom-ma's analytical solution by as much as 70 percent at one location. Since Berkhoff did not attempt to use a finer grid, it is likely that his coarse grid required a moderate computational time. The model described in this paper would require less than 0.1 sec of computational time on a CRAY-1 computer to solve Equation 49 using Berkhoff's grid. Bettess and Zienkiewicz (1977) also used a fairly coarse grid similar to Berkhoff's grid.

198. Lautenbacher (1970) used an integral equation solution to solve the long-wave equation for waves interacting with a circular island on a shoal with linear side slopes. He used a coarse circular mesh grid with only 130 points. Because the resulting coefficient matrix was full, the computational time required for a solution was 60 min on an IBM 7094 computer.

199. Figure 67 shows a finite element grid with 2,640 elements used by the model described in this report to solve the problem of the interaction of long waves with a circular island on a paraboloidal shoal (by symmetry only half the shoal needs to be considered). Figure 68 shows comparisons between Hom-ma's analytical solution and the finite element model solution for incident waves with five different periods. The agreement is excellent with only slight differences for the 240-sec waves (resulting from lower resolution of the incident wave for shorter period waves). The computational time for solution is approximately 4 sec on a CRAY-1 computer.

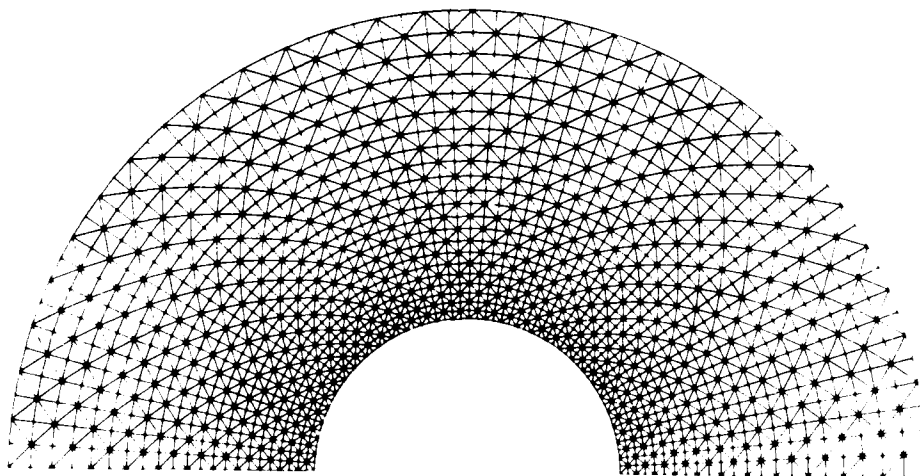


Figure 67. Finite element grid for paraboloidal island (2,640 elements)

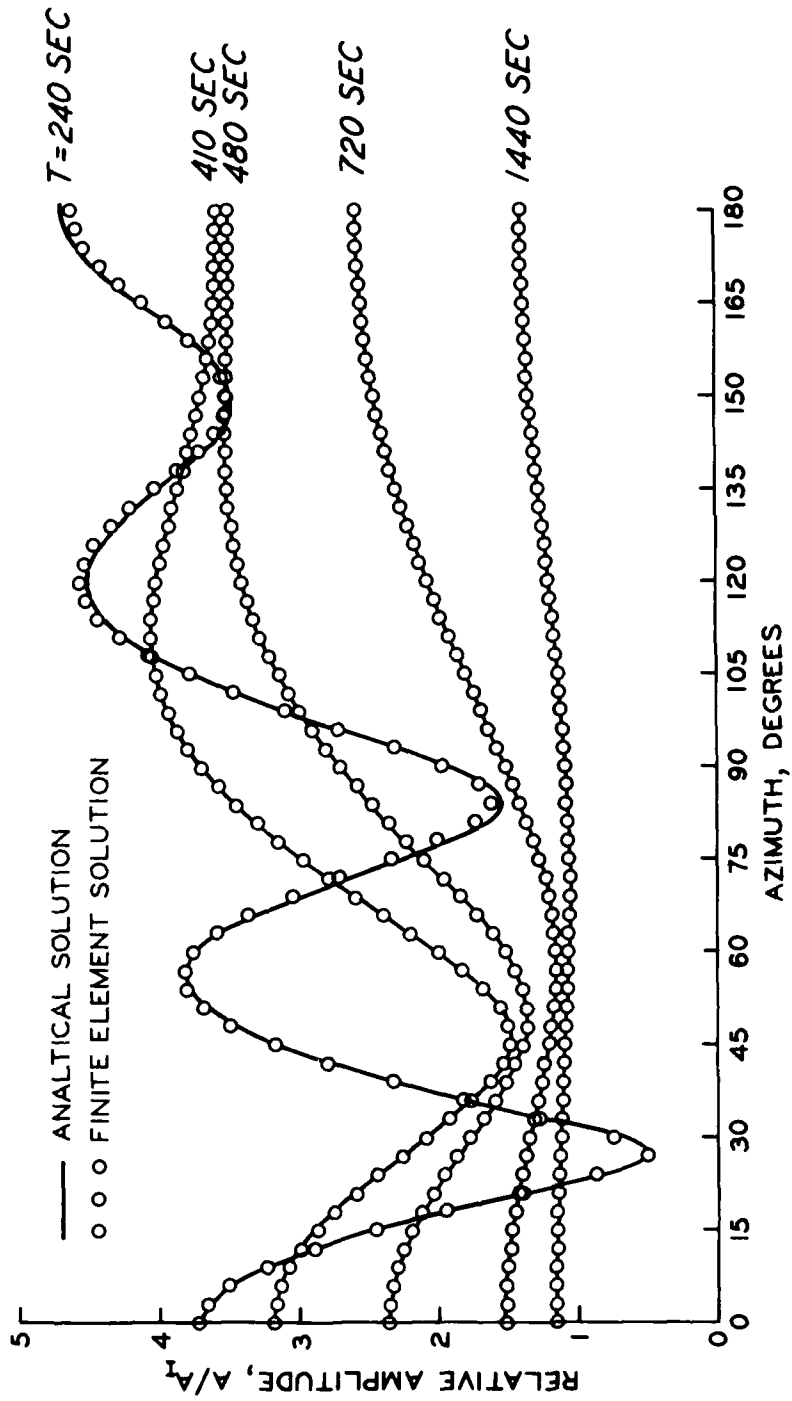


Figure 68. Solutions without dispersion (2,640 element grid)

200. Jonsson, Skovgaard, and Brink-Kjaer (1976) show that for a wave with a 240-sec period interacting with the circular island on a paraboloidal shoal the effect of frequency dispersion is not particularly significant. The ratio of wavelength to water depth for this case is approximately 11. However, for a 120-sec incident wave (wavelength to water depth ratio of less than 5), frequency dispersion is quite significant. In order to maintain a resolution of a 120-sec wave that is approximately equal to that obtained for the 240-sec wave using the 2,640-element grid, it is necessary to reduce element side lengths by a factor of approximately 2. This reduction results in a quadrupling of the number of elements. Figure 69 shows a finite element grid with 10,560 elements used to calculate the interaction of a 120-sec wave with the island.

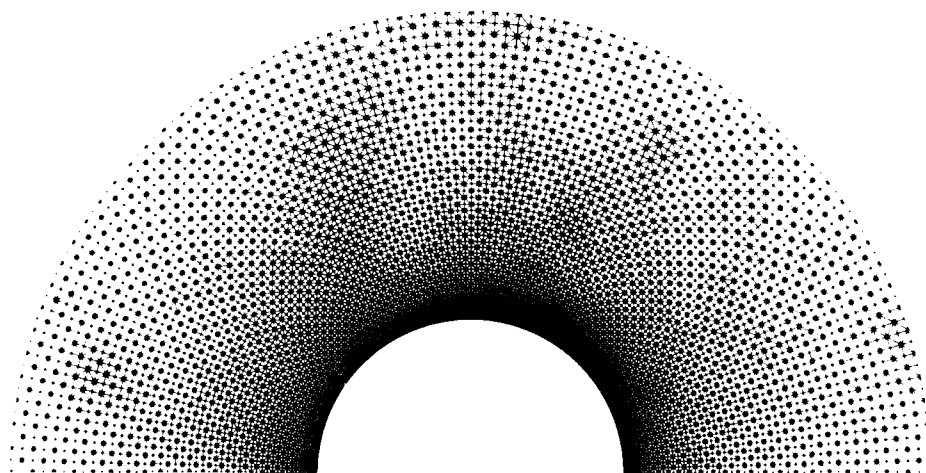


Figure 69. Finite element grid for paraboloidal island (10,560 elements)

201. Figure 70 shows a comparison between the analytical solution of the long-wave equation by Homma (1950) and the finite element solution (grid of Figure 69) for a 120-sec incident wave. Figure 71 also shows a comparison between a numerical solution of Equation 26 using an orthogonal collocation solution and the finite element model solution of this report. In both cases there is excellent agreement. The effect of frequency dispersion is quite significant as shown in Figure 72, where the solutions of the long-wave equation and Equation 26 are overlapped. In fact, the inclusion of frequency dispersion is much more significant a factor than is resolution of the wave form for this particular case. For example, Figure 73 shows a solution including

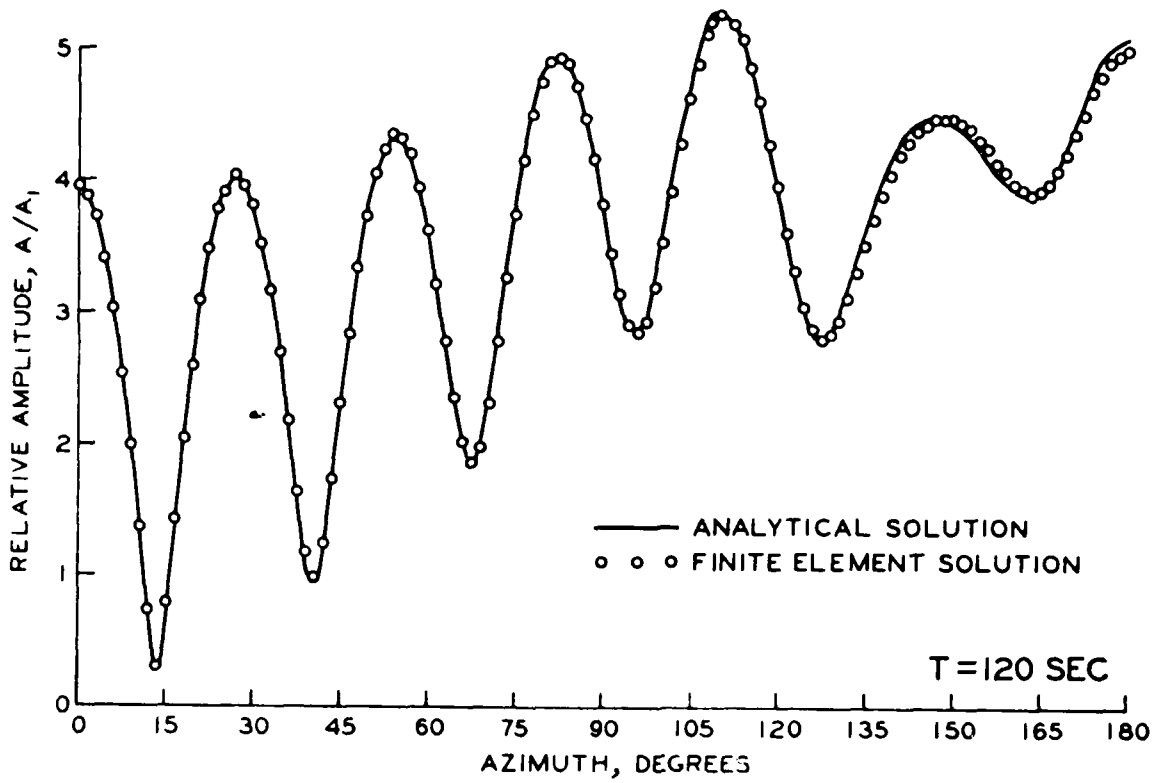


Figure 70. Solutions without dispersion (10,560 element grid)

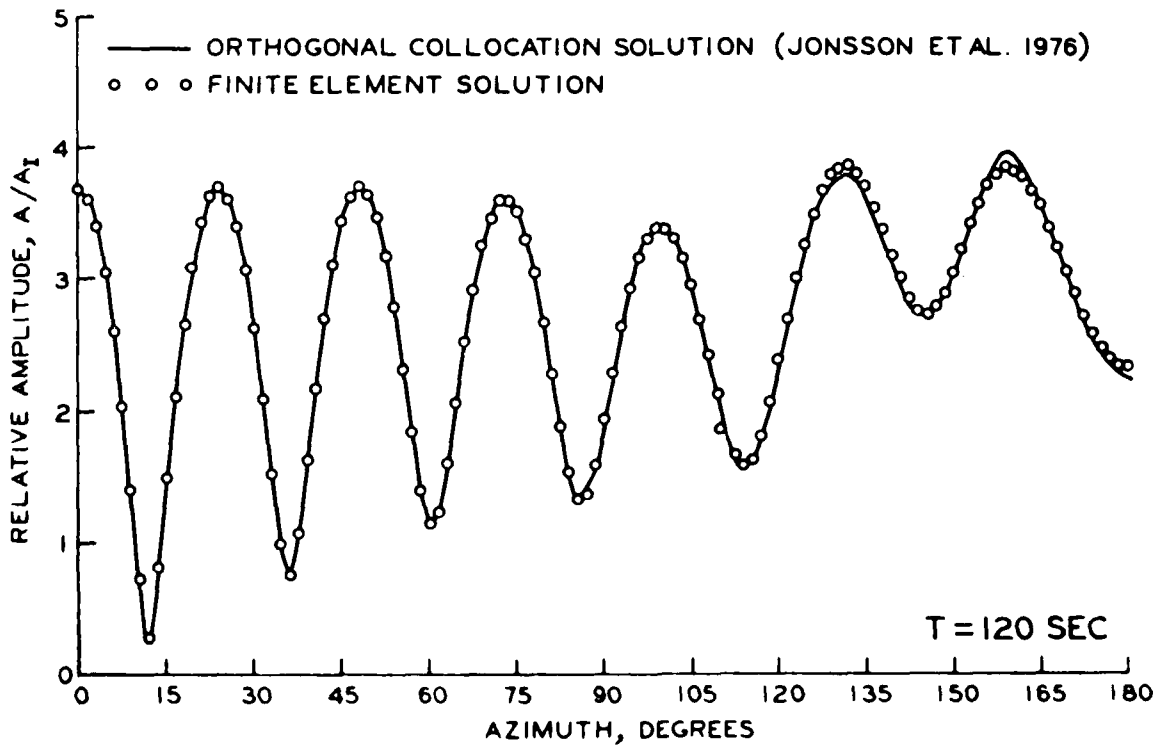


Figure 71. Solutions with dispersion (10,560 element grid)

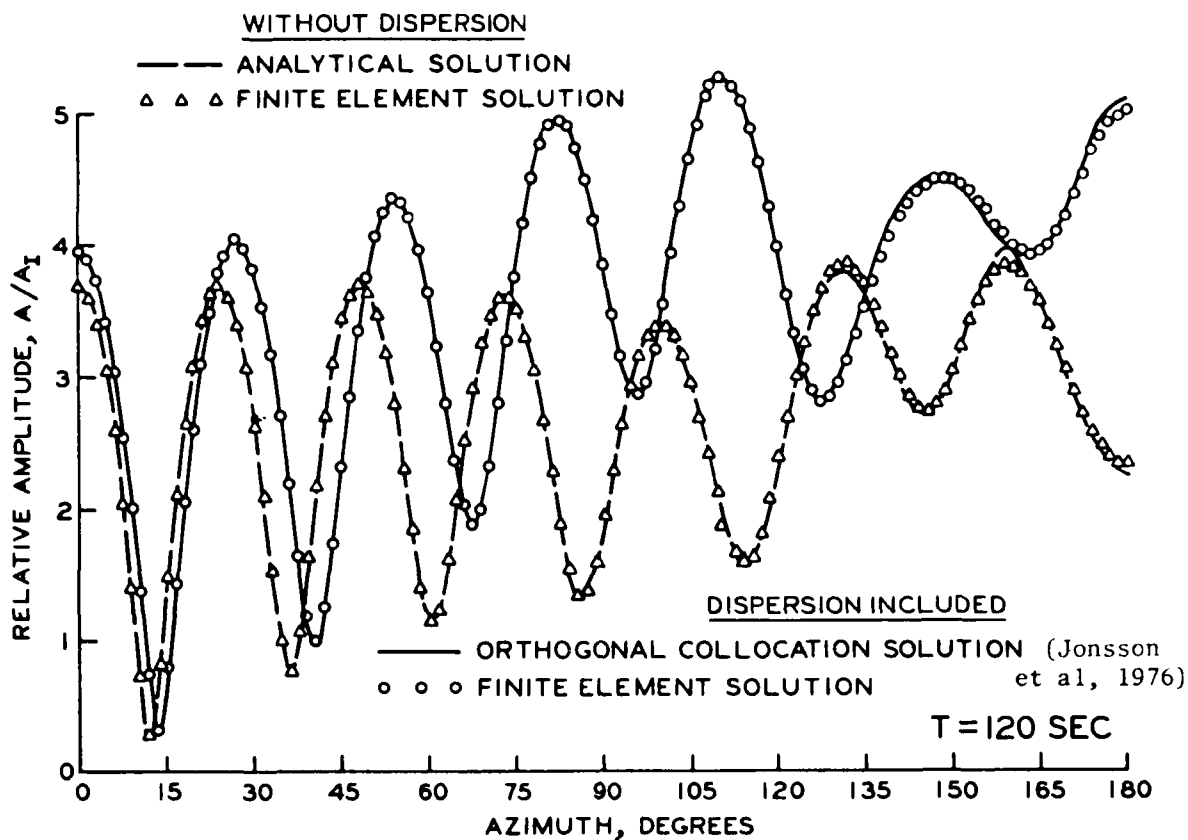


Figure 72. Effect of dispersion

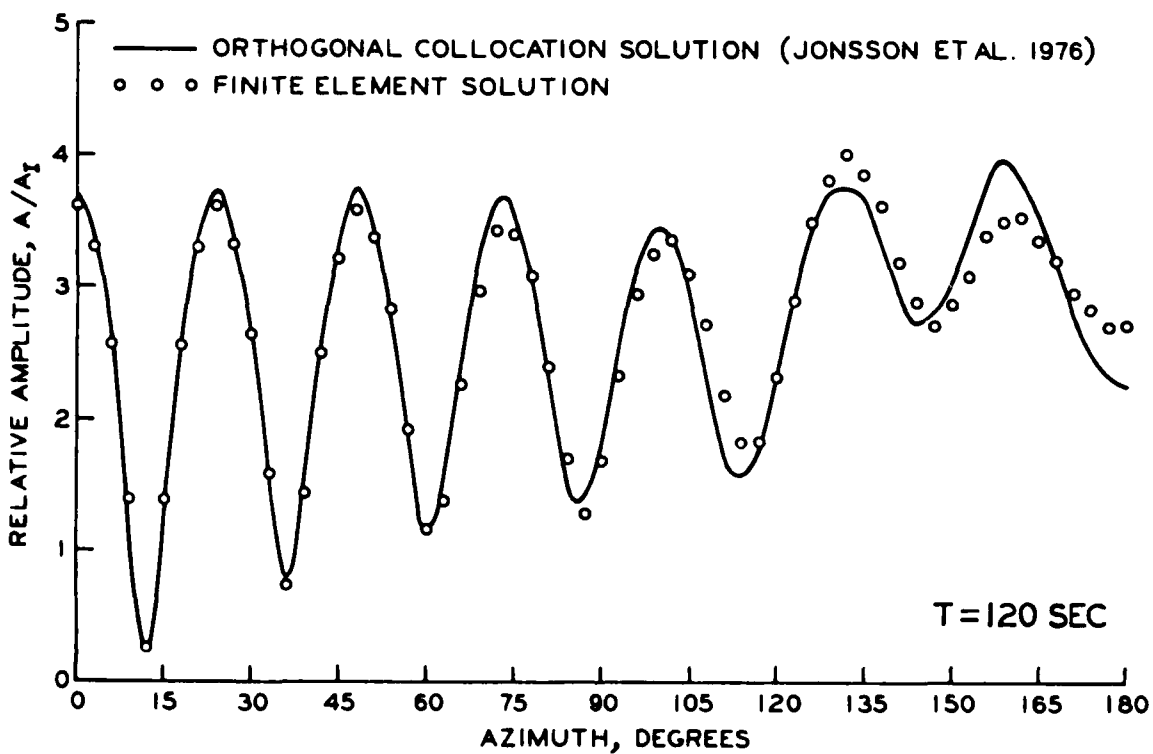


Figure 73. Solutions with dispersion (2,640 element grid)

dispersion using the 2,640-element grid. The agreement between the finite element and collocation solutions is much better using the 2,640-element grid and including dispersion than is obtained using the 10,560-element grid without dispersion.

202. The computational time requirement to solve a problem using the 10,560-element grid is less than 1 min on a CRAY-1. This is extremely modest considering the very large size of this finite element grid. The computational time of the model is proportional to the number of nodes times the bandwidth of the coefficient matrix squared. This grid has more than 50 times the number of nodes contained in the grid used by Berkhoff (1972, 1976) and a bandwidth approximately 3.3 times greater. Thus the computational time requirement is almost 600 times greater for this grid than for Berkhoff's grid. The computer memory requirements also are very modest as a result of the partitioning of the coefficient matrix. Although the packed form of the coefficient matrix had approximately 1.7 million terms for this problem, only 45,000 terms were in central memory at any given time with the remainder in peripheral storage.

Comparison with Three-Dimensional Numerical Model

203. Equation 26 was derived assuming that the bathymetry was slowly varying. This mild slope approximation is valid for the slow bathymetric variations of the paraboloidal shoal shown in Figure 66. However, the approximation is not appropriate for many practical problems involving the interaction of waves with manmade structures. For these problems, it is necessary to use a fully three-dimensional model such as the hybrid three-dimensional finite element developed by Yue, Chen, and Mei (1976). Of course, a three-dimensional model requires substantial computational time. Therefore it is of interest to consider how well a two-dimensional mild-slope model compares with a three-dimensional model for a problem where the mild-slope approximation is strongly violated.

204. Yue, Chen, and Mei (1976) used a three-dimensional model to consider the interaction of small amplitude plane waves with an elliptic island on a circular base. Figure 74 illustrates the problem and shows the finite element grid used by Yue, Chen, and Mei (1976). Bottom side slopes vary from 1 on 1H to 1 on 2H and violate the mild-slope assumption.

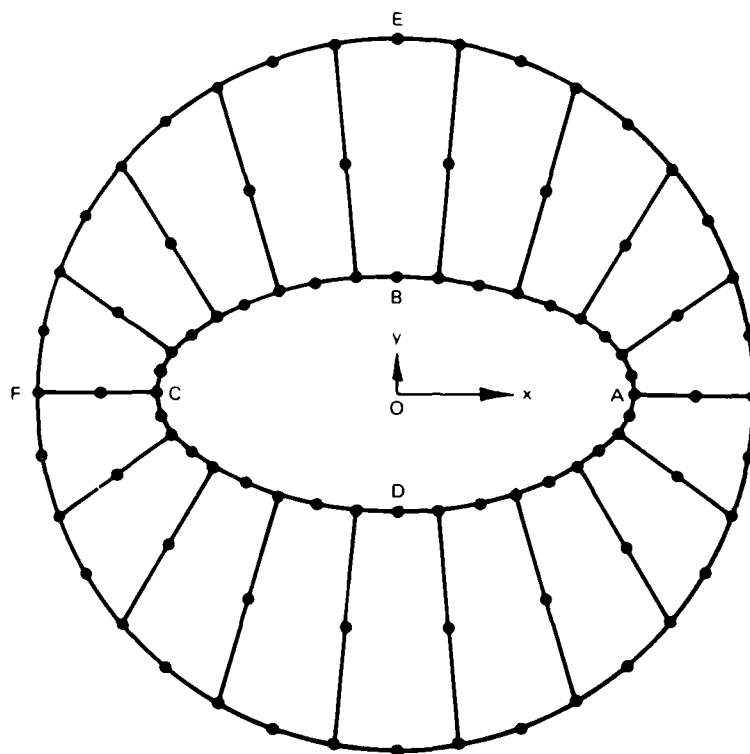
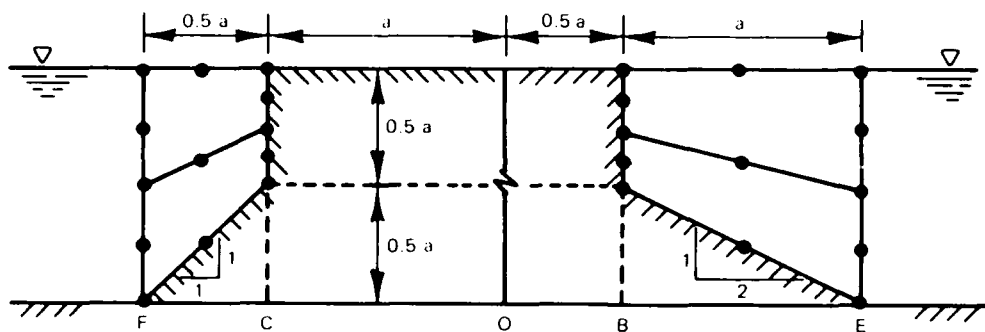


Figure 74. Elliptical island and three-dimensional grid

205. Figure 75 shows the two-dimensional finite element grid used by the model described in this report to simulate the interaction of small amplitude plane waves with the elliptical island. Figures 76 and 77 show the interaction of waves ($k_0 a = 1$ and two incident directions) with the elliptical island. The amplification factors and phases around the elliptical island calculated by the three-dimensional model of Yue, Chen, and Mei (1976) and the two-dimensional model described in this report are shown. The maximum difference in amplification factors is not much greater than 10 percent. Similar

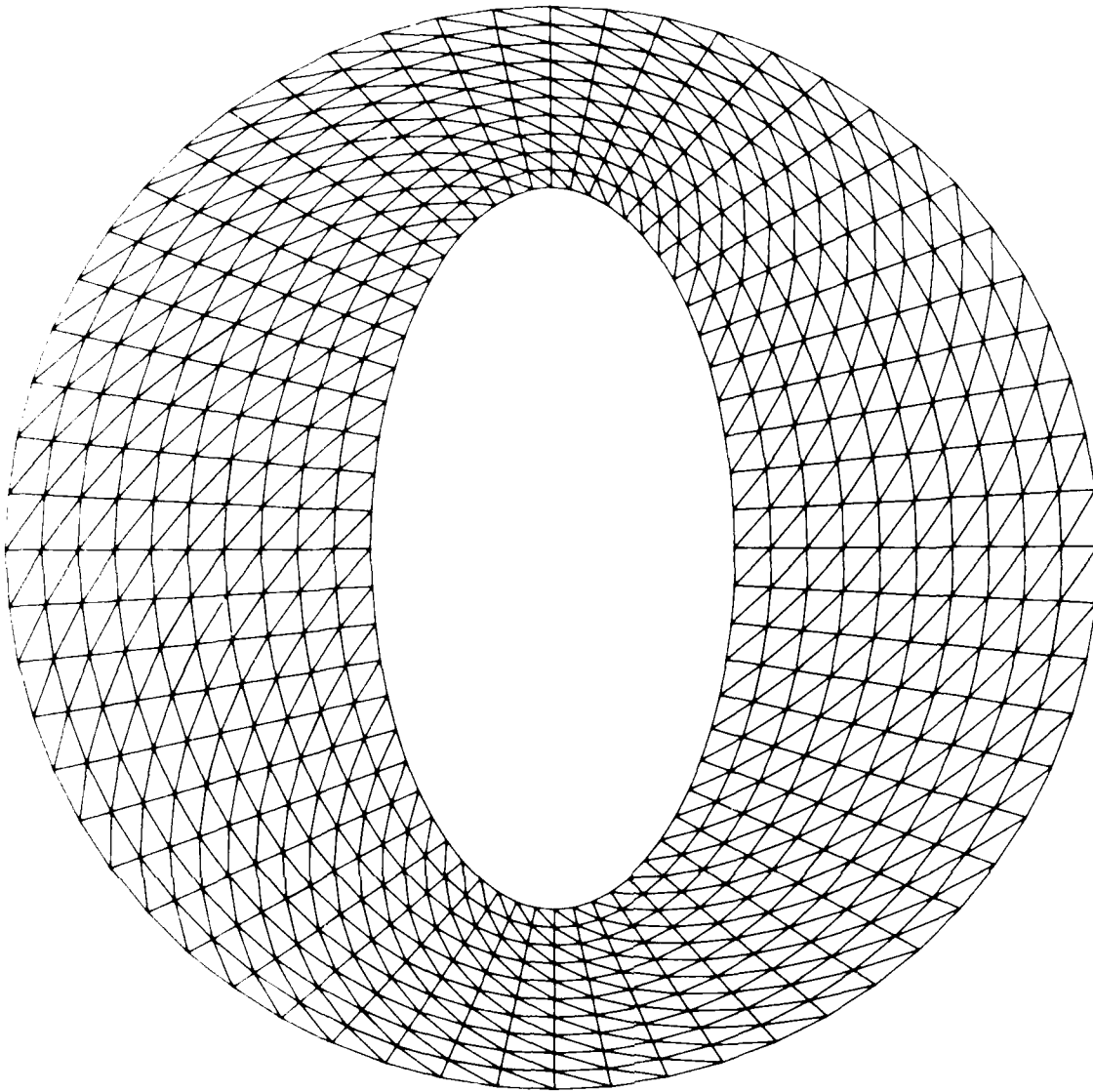


Figure 75. Finite element grid for elliptical island

agreement was found for greater values of $k_0 a$.

206. Although the two-dimensional model cannot perfectly reproduce the three-dimensional model results, the difference may be within the accuracy requirements of many engineering applications. Of course, the computational requirements of the two-dimensional model are very modest compared with the requirements of the three-dimensional model. For the problem of waves interacting with the elliptical island, the three-dimensional model required 2.6 min of computational time on an IBM 370/168 computer for each wave period. The two-dimensional model required less than 2 sec of computational time on a

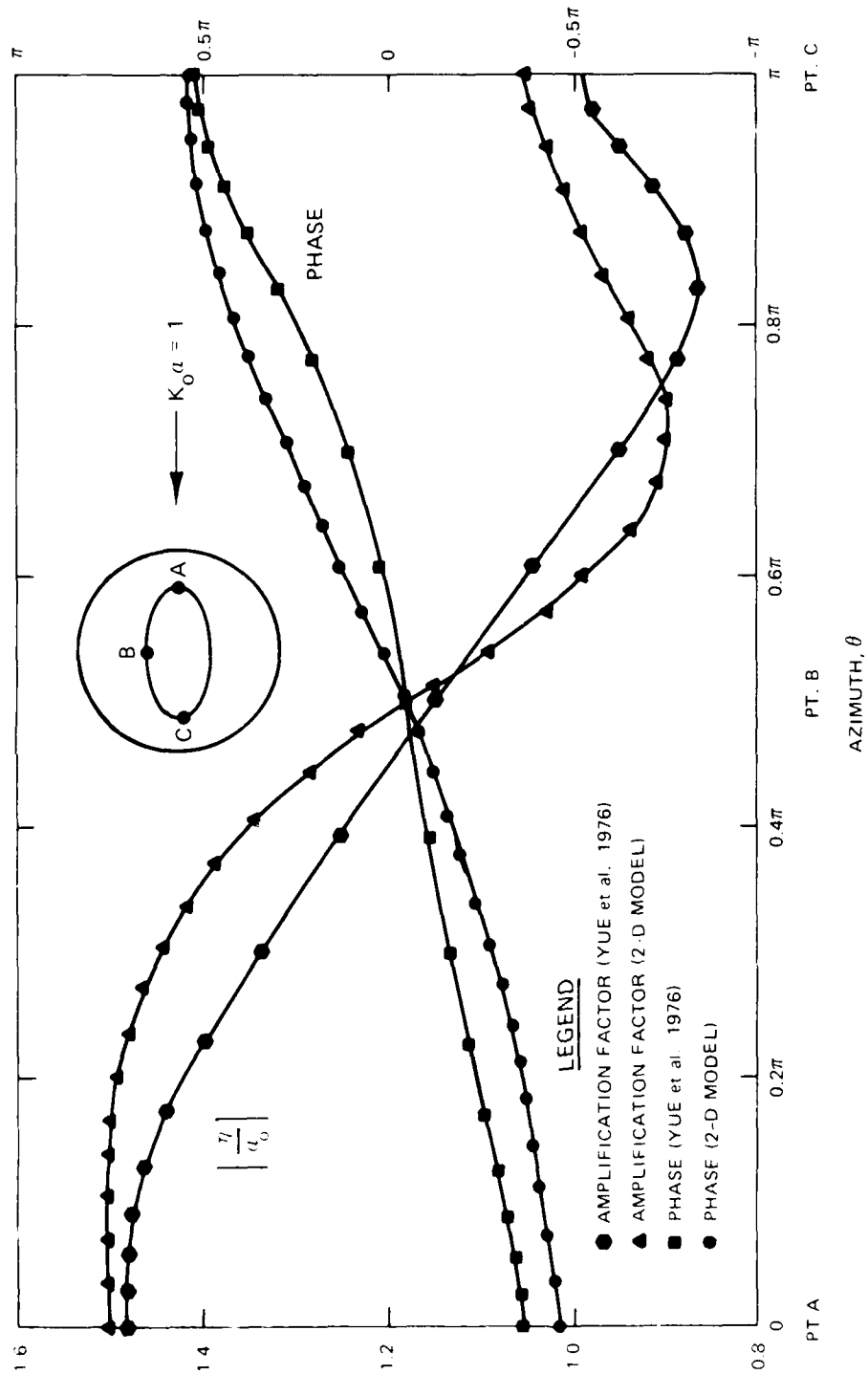


Figure 76. Comparison of model results (incident azimuth 0)

to use conditions of either "no flow" (wall) or constant elevation. However, both of these are highly reflective in nature; and as a result, the transients developed during the start-up of the numerical solution tend to bounce back and forth between the offshore and inshore boundaries and take a long time to damp out. Since this is highly undesirable, a radiation boundary condition of the type suggested by Orlanski (1976) was selected for the offshore boundary and implemented in the numerical scheme. This permitted the transients to propagate out of the grid and allowed the setdown at the boundary to assume an appropriate value.

Tests for Idealized Conditions

228. To develop confidence in the validity of the model and the accuracy of its results, several tests were run on the model and comparisons were made between model results and available laboratory data and analytic solutions.

Plane beach; normal incidence

229. The model was run for a case of normal incidence on a plane smooth laboratory beach (Bowen, Inman, and Simmons 1968). The conditions were as follows: $T = 1.14$ sec, deepwater wave height $H_0 = 6.45$ cm, and beach slope = $1V$ on $12H$. To run this case on the model, a 50×3 variable rectangular grid with overall dimensions of approximately $40 \text{ m} \times 30 \text{ cm}$ (the laboratory channel was 40 m long) was used with $\Delta\alpha_1 = \Delta\alpha_2 = 10 \text{ cm}$ and $\Delta t = 0.05$ sec. In this example, walls were used for the lateral boundaries as well as the offshore boundary to correspond to the laboratory situation. Since for normal incidence the velocities U and V would be zero everywhere corresponding to the steady state, advection, eddy viscosity, and friction terms were turned off in the model. The solution allowed for the effect of setup on the wave heights in the surf zone. As the solution proceeded, since $\bar{\eta}$ changed, the wave heights for cells in the surf zone were computed afresh for each time-step by using $H = \gamma(h + \bar{\eta})$, where γ is a breaking index and the radiation stresses were changed accordingly. As suggested by Bowen, Inman, and Simmons (1968), a γ of 1.15 was used. A buildup time of $10 \Delta t$ was used at the start. A comparison of the setup values from the model after $150 \Delta t$ with those observed by Bowen, Inman, and Simmons (1968) is shown in Figure 83. As shown, there is excellent agreement in the offshore region. In the surf zone, the numerical

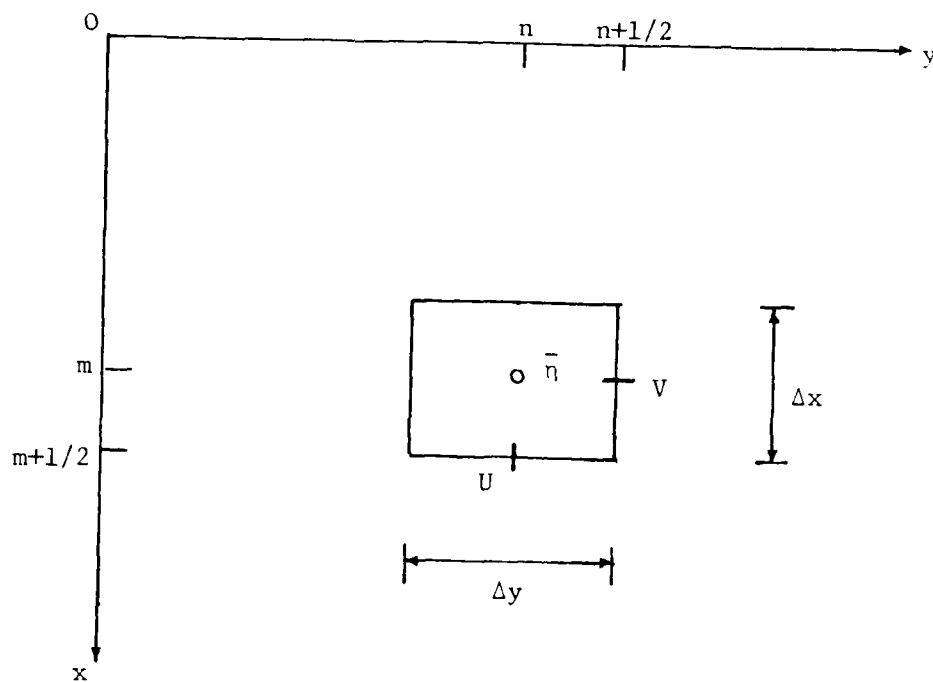


Figure 82. Notation for a cell

225. For each sweep, the governing equations for all the cells together with the boundary conditions can be arranged in the form of a matrix equation involving the unknown variables. Since the matrix is tridiagonal, the solution is obtained by recursion. Finally, it should be emphasized that even though we have discussed the solution procedure in terms of (x,y) coordinates for convenience, actually the governing equations are first transformed into the (α_1, α_2) coordinate scheme and solved in the computational space.

Initial and boundary conditions

226. In order to solve the problem under consideration, appropriate initial and boundary conditions must be applied. For the examples reported herein, an initial condition of rest was chosen so that η , U , and V are zero at the start of the calculations. To avoid shock, the radiation stress gradients were gradually built up to their full values over a number of time-steps. The solution was stopped when a steady state was reached.

227. As for the boundary conditions, along the shoreline a "no flow" (wall) condition was assumed at the still-water line. Thus no flooding was permitted on the beach. For the lateral boundaries, a flux type boundary condition was used; that is, the flux at a boundary cell was made equal to that at the next interior cell. For the offshore boundary, it is common practice

that the size of the grid cells in both horizontal directions may be varied so that the grid may be made finer in regions of greater interest such as the surf zone, inlets, around structures, etc. For this purpose, a mapping function defining the mapping from real (X) space to the computational space (α) is used. The function is:

$$X_i = a + b\alpha_i^c \quad i = 1,2 \quad (64)$$

where X_1 , X_2 correspond to x and y , respectively, and the coefficients a , b , and c are calculated for different regions of the grid by an interactive program. The mapping transforms the variable grid in real space to a uniform grid in computational space. Afterward, the relevant equations are solved in the computational space.

Solution technique

224. In order to apply the finite difference scheme, a rectangular grid is used to represent the region of interest. In real space, the cell dimensions in x and y directions are denoted by Δx and Δy . These dimensions may vary from cell to cell. This grid is mapped into a uniform grid with constant cell dimensions $\Delta\alpha_1$ and $\Delta\alpha_2$ in the computational space. Let m and n denote indices in the x and y directions corresponding to the center of an arbitrary cell (Figure 82). All the variables except the velocities U and V are defined at the cell centers. Velocities U and V are defined respectively at cell faces $m + 1/2$ and $n + 1/2$. The time level is indicated by a superscript k . The governing equations are written in a finite difference form. To advance the solution from a time level k to $k + 1$, an intermediate stage of the solution marked by a superscript $*$ is introduced. The solution procedure is carried out in a two-step operation. In the first step, the grid is swept in the x -direction. The x -momentum equation is centered about the cell face $m + 1/2$ and the continuity equation is centered about the center of the cell (m,n) and the two equations are solved, using in the process the result $U^* = U^{k+1}$. At the end of this sweep, the values η^* and U^{k+1} are known. Next the grid is swept in the y -direction. In this sweep, the y -momentum equation is centered about the cell face $n + 1/2$ and the continuity equation is centered about the cell center (m,n) . Upon solving the two equations, the values η^{k+1} and V^{k+1} for each cell are obtained. Thus the two sweeps together complete the solution.

This represents twice the value used by Thornton (1970). It was felt that Equation 58 represented the eddy viscosity values for the field situation more realistically than Equation 57.

Radiation stresses

222. The radiation stresses are of major importance since they furnish the "driving" forces for wave-induced longshore currents and nearshore circulation. Referring to Longuet-Higgins (1970), for monochromatic waves, these stresses are defined in terms of the local wave climate as:

$$S_{xx} = E \left[\left(2n - \frac{1}{2}\right) \cos^2 \theta + \left(n - \frac{1}{2}\right) \sin^2 \theta \right] \quad (59)$$

$$S_{xy} = E n \cos \theta \sin \theta \quad (60)$$

$$S_{yy} = E \left[\left(2n - \frac{1}{2}\right) \sin^2 \theta + \left(n - \frac{1}{2}\right) \cos^2 \theta \right] \quad (61)$$

where

$$E = \frac{1}{8} \rho g H^2 \quad (62)$$

and

$$n = \frac{1}{2} \left(1 + \frac{2kh}{\sinh 2kh} \right) \quad (63)$$

Note that n is the ratio of wave group celerity to phase celerity and θ is the local wave direction defined as shown in Figure 81. For the numerical model described here, the values of H , k , and θ are obtained by using a considerably modified form of the wave refraction program developed by Noda et al. (1974).

Numerical Model

Numerical scheme

223. The numerical current model, CURRENT, uses an alternating direction, implicit, finite difference scheme. The model is based on a long wave model known as WIFM (Butler 1980). In view of the similarity between the equations for long waves and currents, WIFM was converted into a model for currents by the addition of radiation stress terms and modification of friction and eddy viscosity terms, etc. Because of the advection terms, a stabilizing correction scheme was used. The numerical model has the capability

and c is a drag coefficient (of the order of 0.01) and $\langle |u_{orb}| \rangle$ is the time-average (over one wave period) of the absolute value of the wave orbital velocity. From linear wave theory,

$$\langle |u_{orb}| \rangle = \frac{2H}{T \sinh kh} \quad (55)$$

where T is the wave period, and all other symbols have been previously defined. Equations 53 and 54 amount to a "weak current" assumption. The numerical model described here, CURRENT, has the flexibility that other formulations such as a nonlinear friction can be easily incorporated in the future.

Lateral shear

219. In the numerical model, the coordinate scheme was chosen such that x was positive offshore and y was in the alongshore direction. An eddy viscosity formulation was chosen for the lateral shear, τ_{xy} . The eddy viscosity was assumed to be nonisotropic. Denoting ϵ_x and ϵ_y as the eddy viscosities in the x and y directions, respectively, in general, ϵ_y was assumed to be a constant and ϵ_x a function of x and y . Accordingly,

$$\tau_{xy} = \rho \left(\epsilon_y \frac{\partial U}{\partial y} + \epsilon_x \frac{\partial V}{\partial x} \right) \quad (56)$$

220. For the plane beach application with lateral mixing, the eddy viscosity ϵ_x was assumed to vary within the surf zone in the manner suggested by Longuet-Higgins (1970):

$$\epsilon_x = Nx \sqrt{gh} \quad (57)$$

where x is the distance from the shoreline and N is an empirical coefficient. The eddy viscosity was kept constant beyond the breaker line.

221. For the actual prototype field application, the eddy viscosity ϵ_x was chosen according to the relation given by Jonsson, Skovgaard, and Jacobsen (1974). Thus:

$$\epsilon_x = \frac{H^2 g T}{4\pi^2 h} \cos^2 \theta \quad (58)$$

Continuity

$$\frac{\partial \bar{\eta}}{\partial t} + \frac{\partial}{\partial x} (Ud) + \frac{\partial}{\partial y} (Vd) = 0 \quad (52)$$

where

g = gravitational constant, 32.174 ft/sec²

ρ = fluid mass density, 1.94 lb-sec²/ft⁴

d = total water depth, $h + \eta$, ft

η = free water surface, ft

h = still-water elevation, ft

τ_{bx} = bottom friction stress in the x-direction, lb/ft²

τ_{by} = bottom friction stress in the y-direction, lb/ft²

τ_{xy} = lateral shear stress due to turbulence, lb/ft²

S_{xx} = radiation stress in the x-direction (normal to the y-z plane),
lb/ft²

S_{xy} = radiation stress in the y-direction in the x-z plane, lb/ft²

S_{yy} = radiation stress in the y-direction (normal to the x-z plane),
lb/ft²

For monochromatic waves, the radiation stresses are defined in terms of the local values of the wave height H , wave number k , and wave direction θ (Longuet-Higgins and Stewart 1964). For the numerical model under consideration, the latter variables are obtained by using a considerably modified form of the refraction program developed by Noda et al. (1974). This particular program has the advantage that H , k , and θ can be computed at the centers of the cells of a rectangular numerical grid, and wave breaking can be accounted for by a breaking index model for wave heights in the surf zone. Wave-current interactions may also be taken into account; however, this last feature was not used in the results that follow.

Bottom friction

218. For the bottom friction, a linear formulation, similar to that of Longuet-Higgins (1970), was used for the applications that are described here. Thus:

$$\tau_{bx} = \rho c \langle |u_{orb}| \rangle U \quad (53)$$

$$\tau_{by} = \rho c \langle |u_{orb}| \rangle V \quad (54)$$

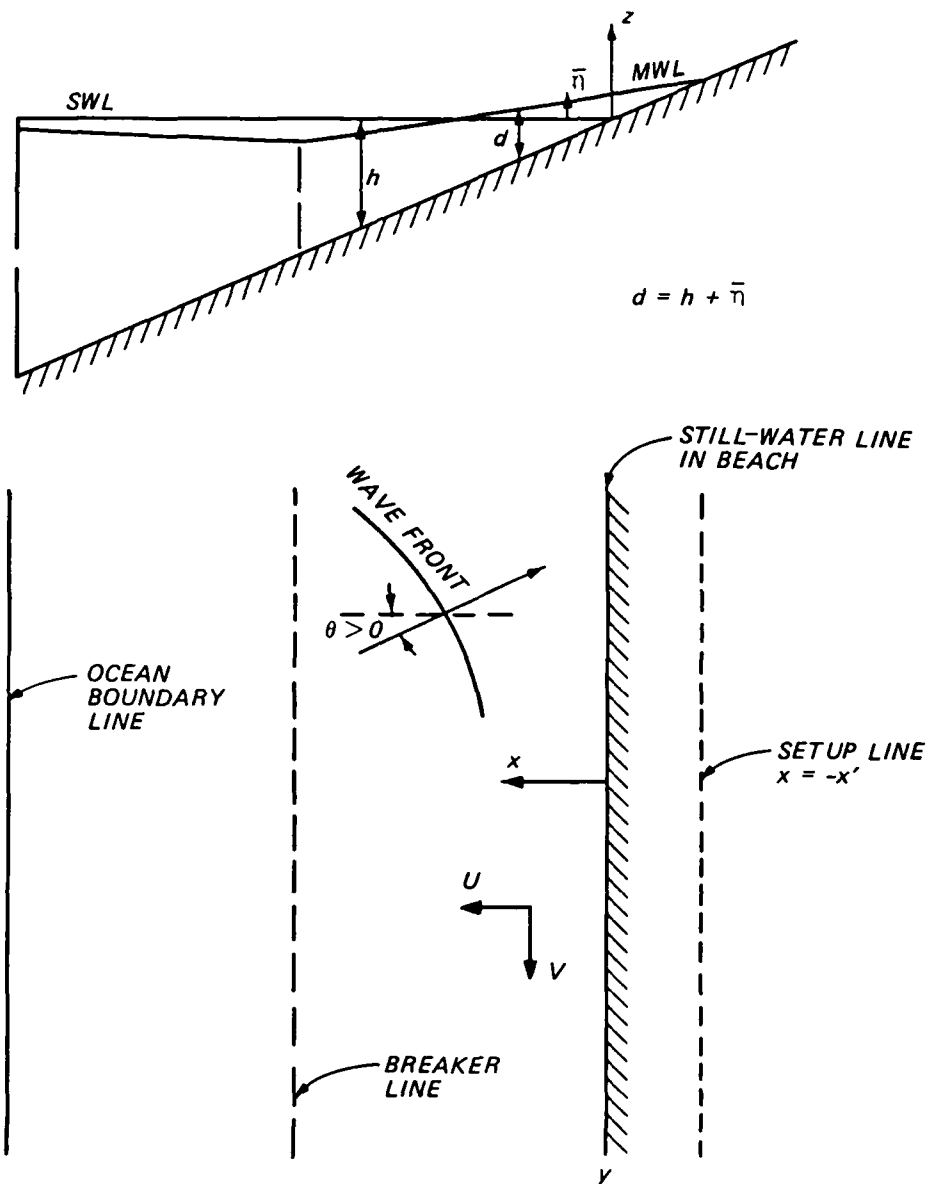


Figure 81. Definition sketch for a plane beach, cross section and plan

Momentum

$$\frac{\partial U}{\partial t} + U \frac{\partial U}{\partial x} + v \frac{\partial U}{\partial y} + g \frac{\partial \bar{\eta}}{\partial x} + \frac{1}{\rho d} \tau_{bx} + \frac{1}{\rho d} \left(\frac{\partial S_{xx}}{\partial x} + \frac{\partial S_{xy}}{\partial y} \right) - \frac{1}{\rho} \frac{\partial \tau_{xy}}{\partial y} = 0 \quad (50)$$

$$\frac{\partial v}{\partial t} + U \frac{\partial v}{\partial x} + v \frac{\partial v}{\partial y} + g \frac{\partial \bar{\eta}}{\partial y} + \frac{1}{\rho d} \tau_{by} + \frac{1}{\rho d} \left(\frac{\partial S_{xy}}{\partial x} + \frac{\partial S_{yy}}{\partial y} \right) - \frac{1}{\rho} \frac{\partial \tau_{xy}}{\partial x} = 0 \quad (51)$$

215. From the standpoint of practical engineering application, a generalized numerical model is needed that can handle realistic bathymetries which are often arbitrary and irregular. The model should be flexible in terms of alternate formulation of terms such as mixing and friction. It should be computationally efficient in view of the large numerical grids often required in engineering projects. This report describes one such numerical model for longshore currents and nearshore circulations developed at WES in response to the basic research needs and to the application to specific projects of US Army Engineer Districts. This model, CURRENT, has been applied successfully to the determination of longshore currents near open coasts, longshore currents and nearshore circulations near inlets, and can be applied to the near vicinity of major coastal structures.

216. In terms of its analytic formulation, the present model uses to a large extent, the approach of Ebersole (1980) and Ebersole and Dalrymple (1980). Whereas their numerical model used an explicit method of solution, the present model uses an alternating direction, implicit, finite difference scheme. In view of the similarity between the equations for longshore currents and long waves, the present model was created by modifying an existing, well-tested WES shallow-water wave numerical model known as WIFM (WES Implicit Flooding Model) (Butler 1980). The velocity version of WIFM used here has non-linear advective terms. The friction and mixing terms used in WIFM were modified to conform to the formulations normally used for longshore currents. Radiation stress terms were added to the model since these are usually the "driving" terms for longshore currents. Additional modifications were made as necessary. WIFM has wind stress terms; so far, these have not been used in the present model. Similarly, the flooding/drying capabilities of WIFM have not been utilized in the model for currents.

Equations of Motion

217. The governing equations for the problem under consideration are obtained from the general equations of conservation of momentum and mass, after averaging over time (one wave period) and depth. They are expressed in terms of the mean horizontal velocities U , V , and the mean free surface displacement, η (Figure 81) as follows:

PART VI: NUMERICAL MODEL OF WAVE-INDUCED CURRENTS

213. In recent years, there has been a growing interest in the numerical modeling of longshore currents and nearshore circulations caused by the action of breaking waves. This has resulted in a need for generalized numerical simulation models that solve the complete equations of motions, are flexible in the formulations chosen for various terms, and can be applied to actual prototype field situations at a reasonable cost. The development and application of one such model (CURRENT) have been described by Vemulakonda (1984). The model was first tested by comparing its results with known analytic solutions and experimental data, for which there was good agreement. It was next applied to a field situation near Oregon Inlet, North Carolina. The results appeared to be reasonable and the computational costs were modest.

Background of Model Development

214. The design and construction of large-scale engineering structures such as jetties or breakwaters require the determination of longshore currents and nearshore circulations not only near the open coast but also near inlets, and of the effect these phenomena have on the stability of such structures. Several publications on longshore currents and nearshore circulations have appeared in the literature during the past two decades. Some of these relate to experimental or field studies, and others relate to analytic solutions and numerical models. However, most of this literature (Bowen 1969, Longuet-Higgins 1970, Thornton 1970, Noda 1974) has been devoted to idealized situations such as plane beaches and periodic bathymetries. Often the analytical and numerical models used have been limited in scope. The limitations include assuming a steady state, using a linear friction, neglecting advection and/or eddy viscosity terms, etc. The development of generalized numerical models that can handle more complex situations is relatively new (Ebersole 1980, Ebersole and Dalrymple 1980, Vreugdenhil 1980). At the present time, very little work has been reported on the application of numerical current models to field situations at a reasonable cost. In view of the increasing tendency of the coastal engineering profession to employ numerical models for sediment transport in the nearshore region, there is a pressing need for generalized longshore current models.

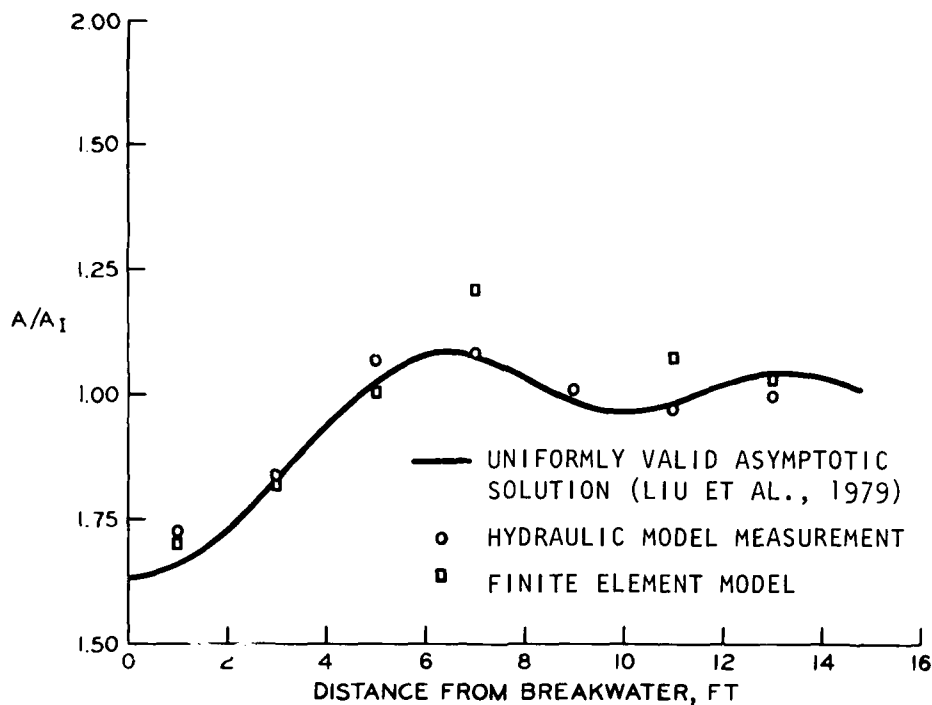


Figure 80. Comparison with laboratory experiments

rapid depth variations (at much lower cost than required by three-dimensional models that are appropriate for problems involving rapid depth variations). The model does not provide a mechanism for energy dissipation and thus energy loss through wave breaking is simulated by permitting waves to propagate out of the computational region. The program documentation, user guide, and sample problem output are provided by Houston and Chou (1984).

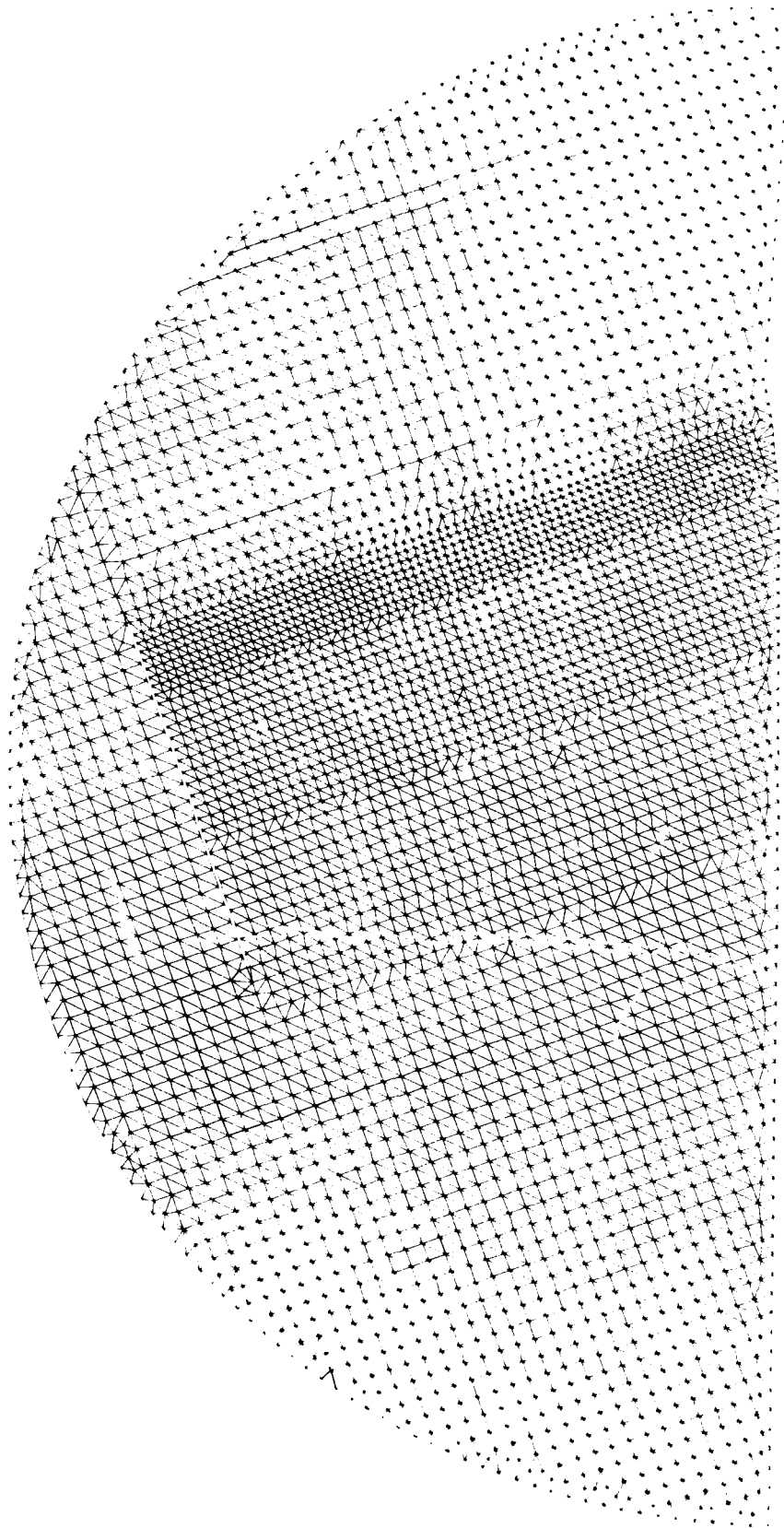


Figure 79. Finite element grid for wave interaction with breakwater

allowing waves to continue to propagate out of the problem area. Figure 78 illustrates schematically how this is done. The breakwater and the linear slope are numerically modeled only to the point where breaking occurs. The depth is then increased to the depth of the semi-infinite region surrounding the inner region and the waves are allowed to radiate away from the inner region. Figure 79 shows the finite element grid used for this simulation.

211. Figure 80 shows a typical comparison between the laboratory measurements and the finite element calculations. Also shown is a uniformly valid asymptotic solution derived recently by Liu and Lozano (1979), which solution is in excellent agreement with the laboratory tests. The finite element calculations agree quite well in the shadow zone with the laboratory tests. The agreement is not as good outside the shadow zone. The difference probably is attributable to the artificial increase in depth to allow the waves to radiate from the inner region. This depth transition would cause some energy to reflect back into the inner region.

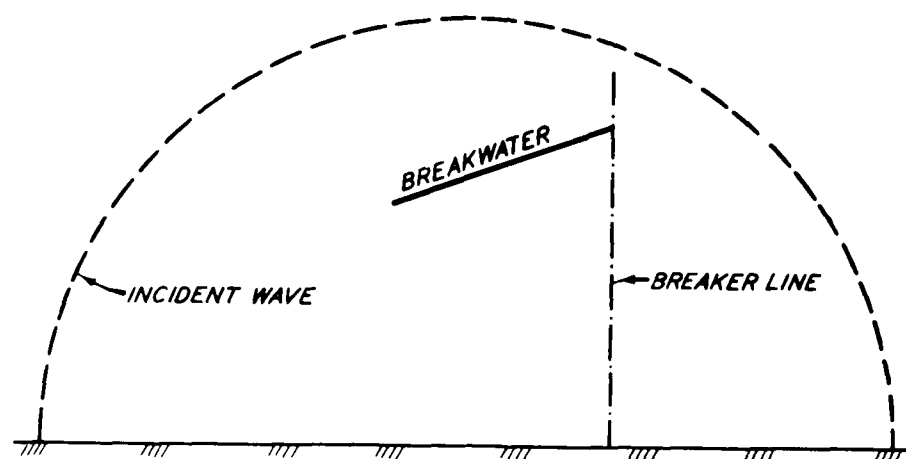


Figure 78. Wave interaction with impermeable breakwater

Finite Element Wave Model Summary

212. A hybrid element numerical model (FINITE) was developed that solves a linear mild-slope equation for short-wave propagation. The efficient formulation of the model permits the solution of large problems with relatively small time and memory storage requirements. Although the model solves an equation that is strictly valid only for mild bathymetric variations, the model can provide reasonable qualitative answers for problems where there are

CRAY-1 computer. Part of the difference in computational time is a consequence of the unknown relative speeds of the two computers.

207. The difference in computational time of the two- and three-dimensional models becomes more significant for larger problems. For example, Yue, Chen, and Mei (1976) estimate that approximately 6 hours of computational time on an IBM 370/168 computer would be necessary to calculate the interaction of a wave with a period of 8.5 sec or greater with a particular offshore harbor. If a resolution of 10 grid points per wavelength is maintained, the two-dimensional model would require an estimated computational time of only 0.5 to 1 min to perform the same calculation on a CRAY-1 computer.

Comparison with Laboratory Experiments

208. Putnam and Arthur (1948) performed the pioneering laboratory experiments that considered diffracted waves in the lee of an impermeable breakwater located in constant depth water. Mobarek (1962) performed similar experiments except that a linear bottom slope was used in the lee of the breakwater and a very small model (72 ft^2) was used. In order to study the phenomenon of combined refraction and diffraction near structures, laboratory experiments were performed by Hales (1980b). In these experiments an impermeable breakwater was located perpendicular to a straight coastline. A linear bottom slope extended from some distance in front of the breakwater to the shoreline.

209. The laboratory facility used in these tests covered an area of approximately $2,500 \text{ ft}^2$. The breakwater was 15 ft long and 1 in. thick. The water depth in the model decreased from 1.0 ft to 0.0 ft over a distance of 20 ft. The sidewalls that laterally bounded the facility were curved to follow wave orthogonals. A plunger-type wave maker was used to generate small amplitude sinusoidal waves that approached the breakwater at an angle. An array of 32 parallel-wire, resistance-type sensors was used to measure the waves. The gages were supported by a large stand so that only the measuring wires of the gages were in the water (i.e., the gages did not require individual feet for support). Information was recorded and analyzed by a minicomputer.

210. One problem in simulating these laboratory tests numerically is that the waves break in the hydraulic model near the shoreline and thus dissipate their energy. There is no mechanism to dissipate energy in the numerical model described in this paper. However, dissipation can be simulated by

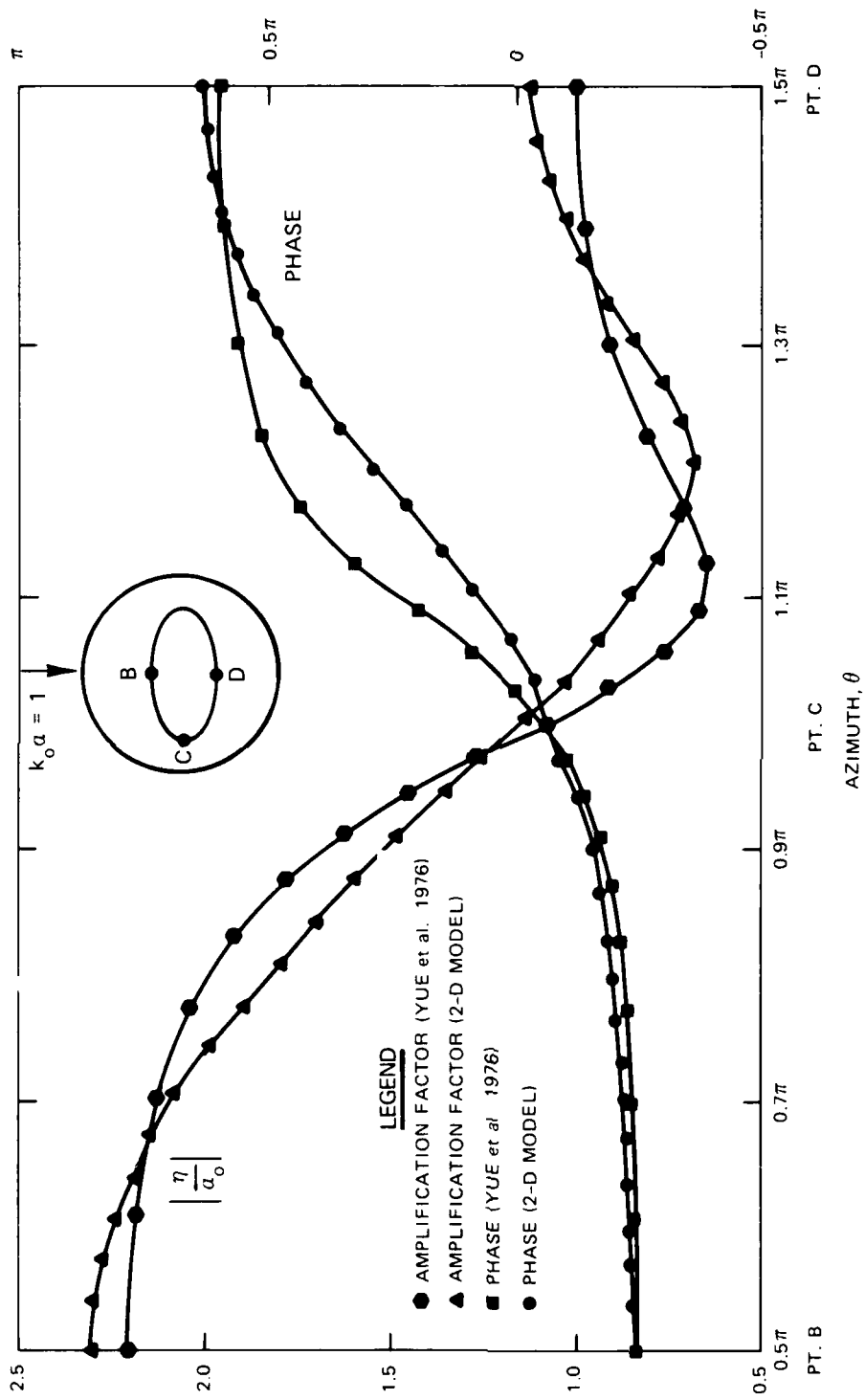


Figure 77. Comparison of model results (incident azimuth 90)

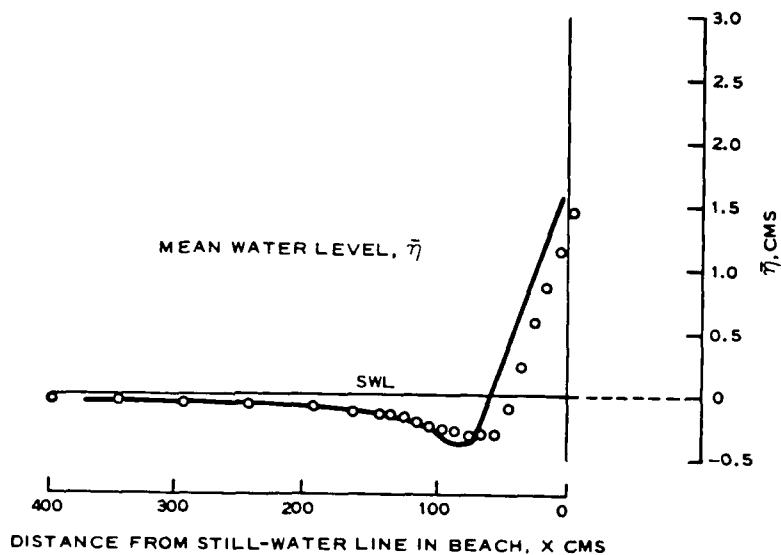


Figure 83. Comparison of the numerical solution for setup with experimental data (solid line is the WES numerical solution, data points are experimental data) (Bowen, Inman, and Simmons 1968)

model predicts higher setups than observed. This is not surprising since the model does not allow flooding and runoff. It is to be noted that the slope of the mean water line in the surf zone is approximately the same in both cases.

Plane beach; oblique incidence

230. For this case, a plane beach of constant bottom slope $s = 1:30$ was selected. A monochromatic wave with the following deepwater characteristics was chosen: $T = 12$ sec, $H_0 = 10$ ft, and angle of incidence in deep water, $\theta_\infty = 20$ deg. A drag coefficient $c = 0.01$ and a breaking index $\gamma = 0.82$ were used in the model. A 100×6 uniform grid with $\Delta x = \Delta y = 60$ ft was used for most of the runs. Uniform flux and radiation boundary conditions were used for the lateral and offshore boundaries, respectively. The buildup time varied from $15 \Delta t$ to $50 \Delta t$, depending on the Δt used.

231. First the model was run without allowing for the effect of setup on wave heights and radiation stresses. Mixing and advection were ignored. A time-step $\Delta t = 0.5$ sec was used. The steady-state velocity distribution obtained (after approximately $800 \Delta t$) is compared with the triangular distribution of Longuet-Higgins (1970) in Figure 84, for which there is good agreement. Note that for positive θ , V will be negative for this coordinate scheme. Next, a finer grid ($\Delta x = \Delta y = 30$ ft) with a $\Delta t = 0.25$ sec was used.

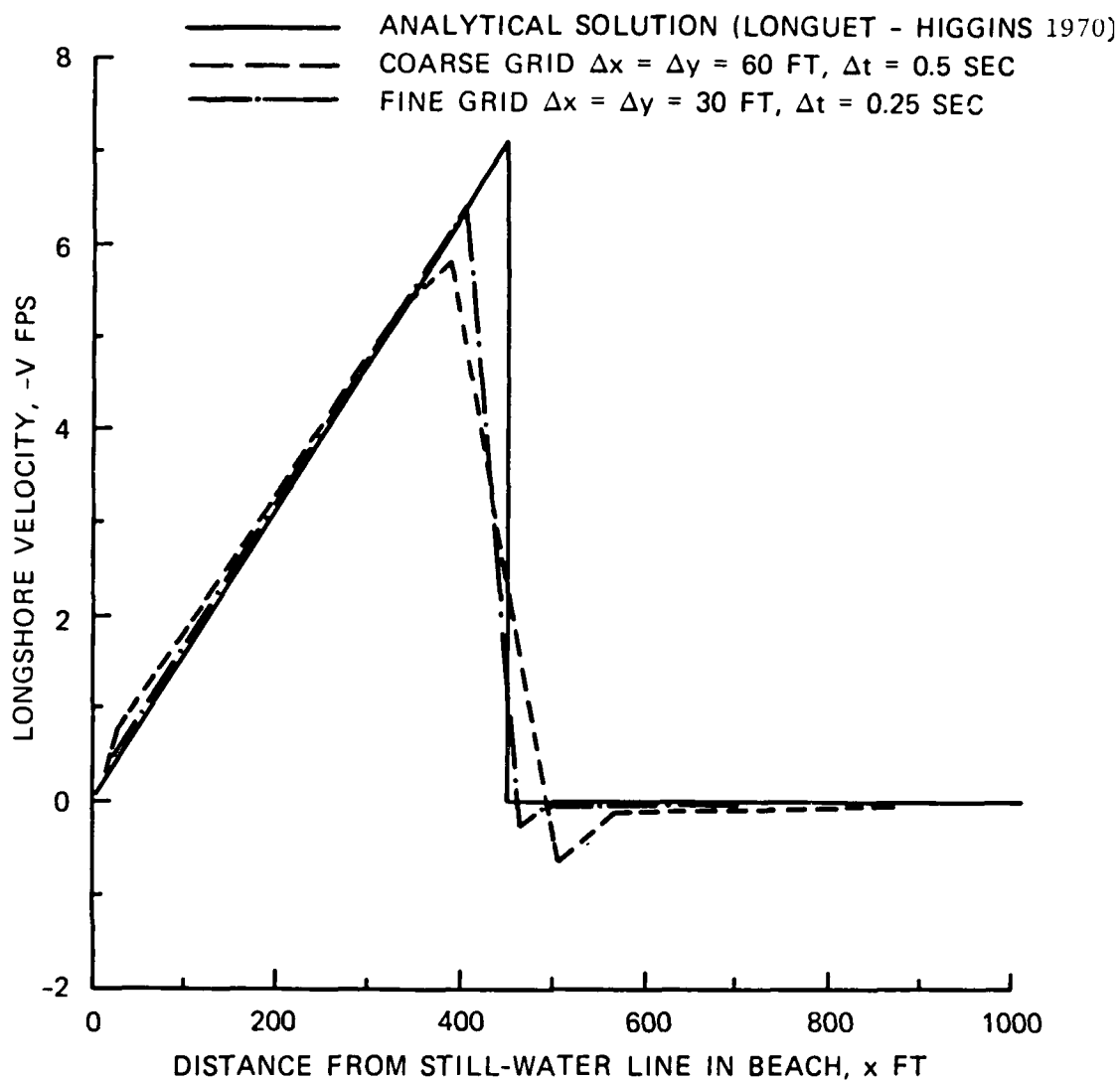


Figure 84. Plane beach, solution for longshore current without setup

Figure 84 shows that as the grid is made finer, the numerical solution tends to approach the analytical solution.

232. The effect of setup was taken into account next. The velocity distribution from the model is compared with the corresponding analytic solution in Figure 85, for which the agreement was good. Note that the numerical solution goes to zero at the still-water line because a wall was assumed there. On the other hand, Longuet-Higgins' (1970) solution goes to zero at the setup line. To plot his solution, the distance from the still-water line to the setup line was estimated by using a relation provided by Dalrymple, Eubanks, and Birkemeier (1977).

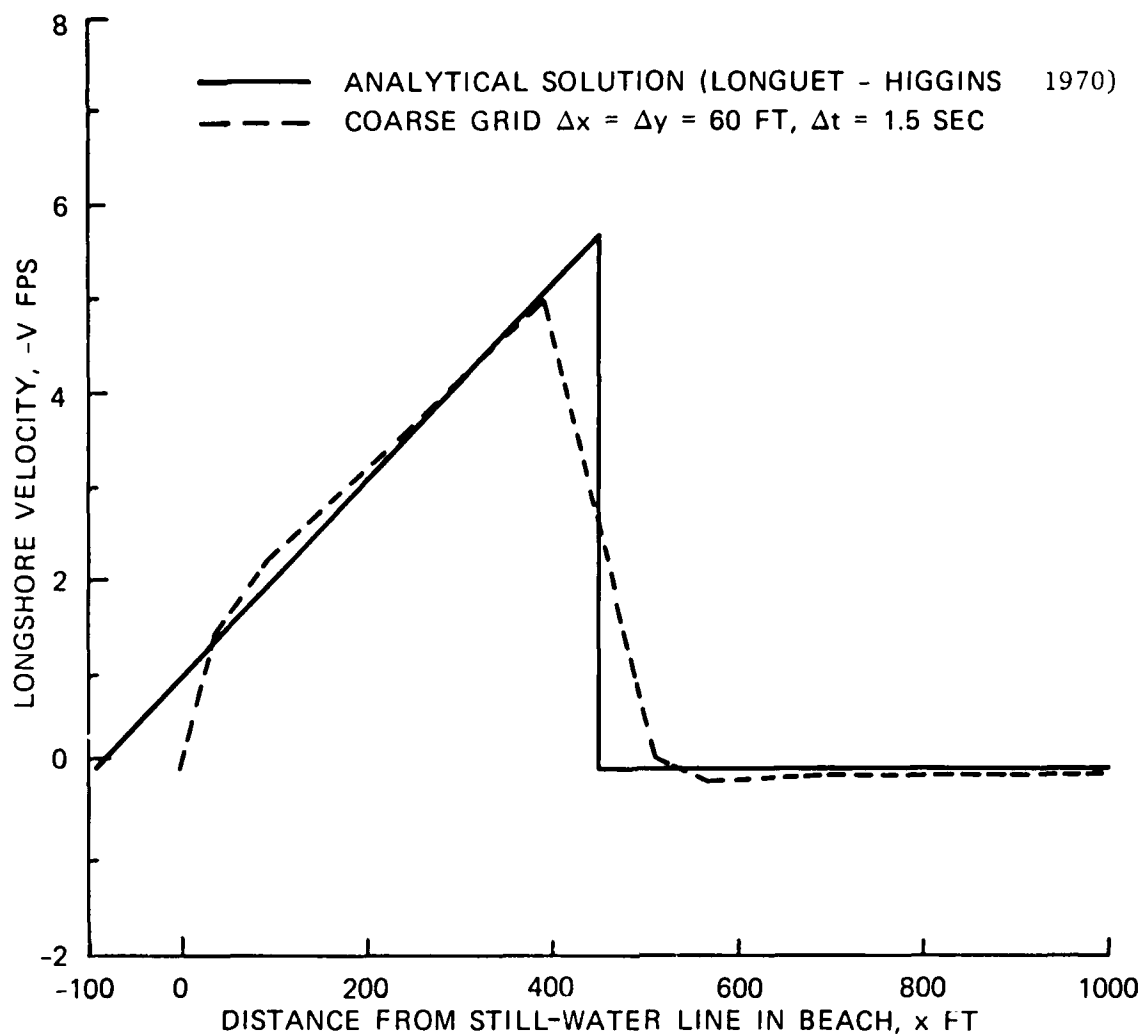


Figure 85. Plane beach, solution for longshore current with setup

233. The effect of lateral mixing was studied next, without taking the effect of setup into account. A time-step $\Delta t = 5.0$ sec was used for these computer runs. The mixing parameter P of Longuet-Higgins (1970) was varied between 0.01 and 0.40. Note that P is defined as:

$$P = \frac{\pi}{\gamma} \frac{sN}{c} \quad (65)$$

Figure 86 shows the effect of P on the numerical solution. As expected, the magnitude of the peak decreases, the peak moves closer to the shoreline, and the velocities offshore of the breaker line increase as P increases.

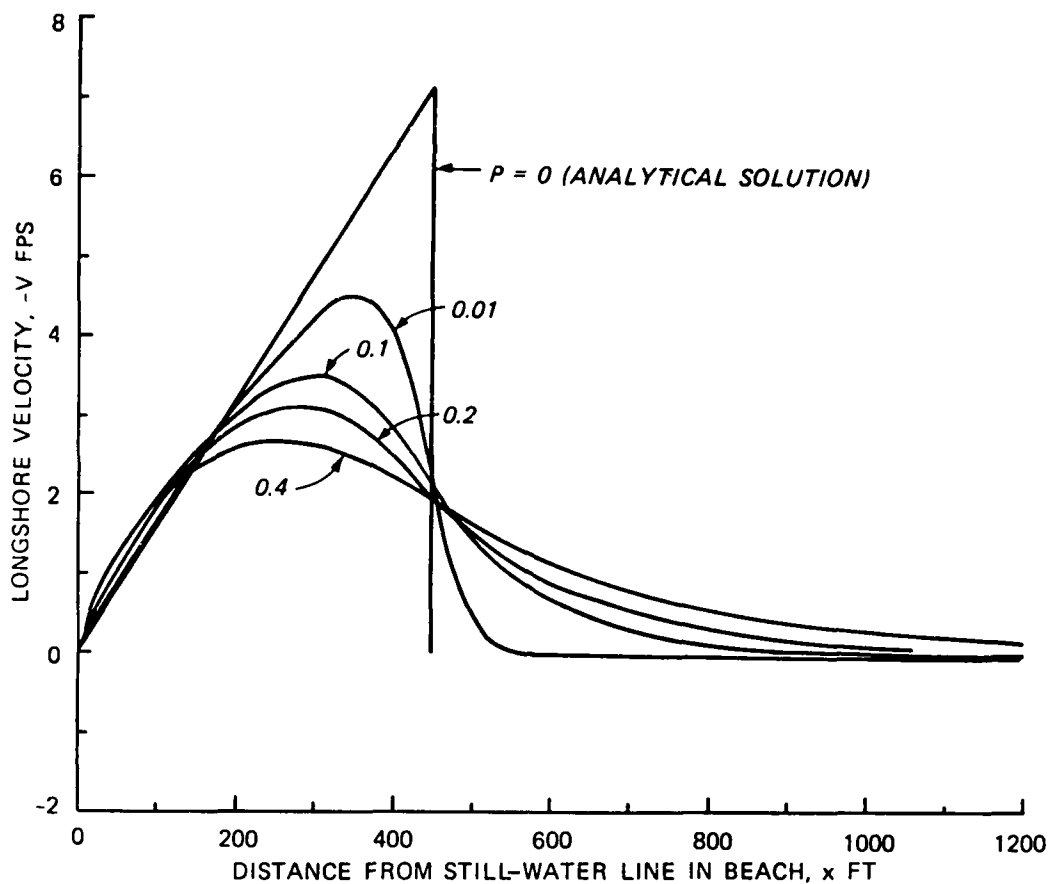


Figure 86. Plane beach, effect of mixing parameter P on the numerical solution for longshore current without setup

Difficulties in Applications to Field Situations

234. While it is relatively easy to apply a numerical current model to idealized cases, one must face several difficulties in applying the model to actual prototype field situations. Among these is the highly irregular nature of the bathymetry, especially near inlets where channels and shoals exist. The topography must be smoothed to a certain extent in order for the wave climate and longshore current models to work properly; yet one must be careful not to completely change the basic features of the topography. The shoreline as well as the breaker line may be irregular and may be oblique to the grid system axes. There may be more than one breaker line. There are problems connected with discretization of the shoreline and breaker line(s). Selection of appropriate values for empirical coefficients such as friction and eddy

viscosity is not easy. There are problems in connection with the wave climate model also, especially if wave-current interactions are to be taken into account.

Prototype Field Application

235. In order to demonstrate the applicability of the numerical model to actual prototype field situations, the case of Oregon Inlet, North Carolina, was selected. Oregon Inlet is a tidal inlet in a barrier island system; behind the inlet toward the mainland is Pamlico Sound. Most of the problems mentioned previously had to be addressed and solved satisfactorily in this application. For purposes of the present simulation, a rectangular region approximately 62,400 ft long in the alongshore direction and 29,400 ft wide in the offshore direction was considered. It included a portion of Pamlico Sound. The variable grid used for the simulation is shown in Figure 87. The grid was 77 cells wide in the alongshore direction and 54 cells wide in the offshore direction; the minimum cell widths in the alongshore and offshore directions were 400 and 100 ft, respectively. These widths were used near the inlet and surf zone, respectively. Note that $\Delta\alpha_1 = \Delta\alpha_2 = 100$ ft. The topography corresponding to this grid, used in the simulation, is shown in Figure 88. The elevations are shown in feet and the datum is mean low water (mlw). Several points must be mentioned about this three-dimensional perspective plot. First, the vertical dimensions are highly exaggerated compared with the horizontal. Secondly, the depths are plotted in the computational space and not the physical space, and the horizontal dimensions are distorted. The topography was somewhat modified compared with the actual topography, with respect to the depths near the offshore boundary and the land elevations of the islands. In spite of these factors, Figure 88 helps one to visualize the irregular nature of the bathymetry. Also, the locations of the channels and shoals in the region of the inlet are shown clearly in the figure.

236. A monochromatic wave with a height of 11.39 ft, period of 8.0 sec, and $\theta = 51.1$ deg in 60-ft depth of water was selected for the simulation (the depth of water at the offshore boundary of the numerical grid was 60 ft). This wave corresponded to the significant wave during a part of the Ash Wednesday storm of March 1962 at the inlet. In this case, besides using "no flow" conditions at the shoreline, a radiation boundary condition offshore and flux

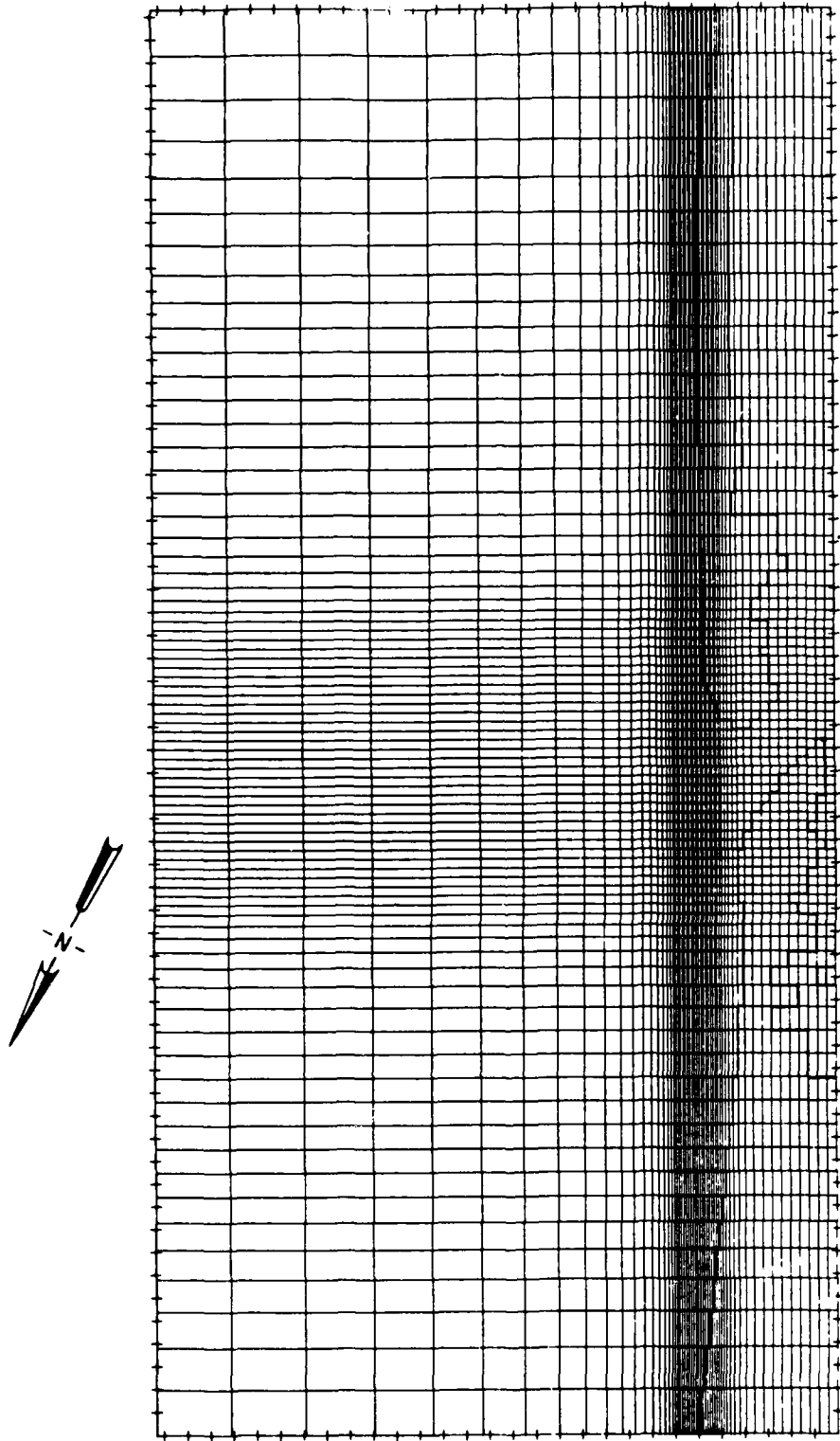


Figure 87. Computational grid for Oregon Inlet, North Carolina

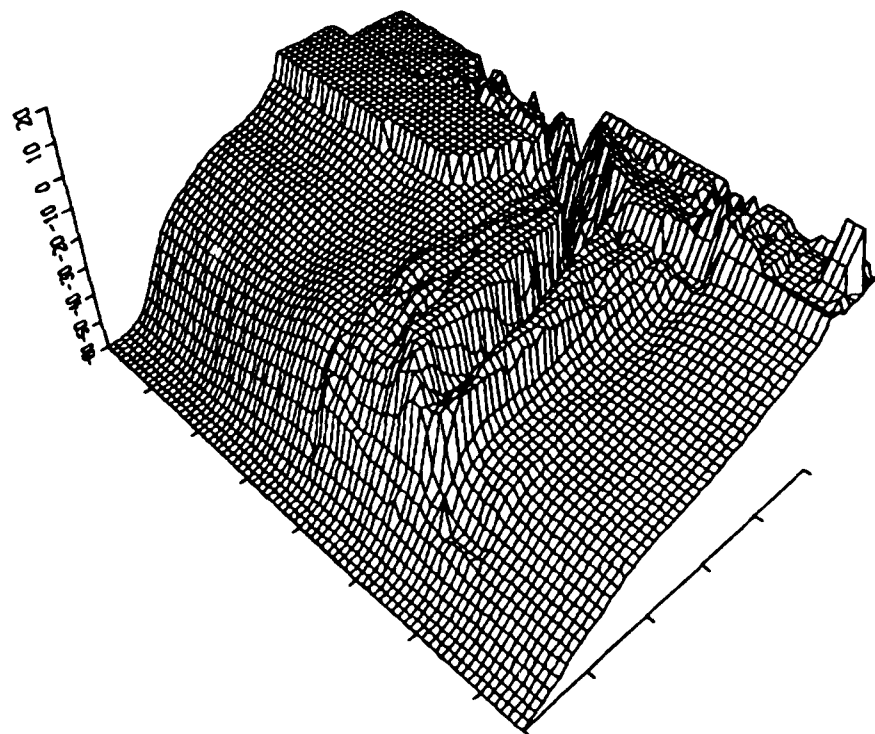


Figure 88. Topography for Oregon Inlet, North Carolina, numerical model

boundary conditions at the lateral boundaries, a flux boundary condition was used over a part of the inland side of the sound, while the rest of the sound was closed off. A time-step of $\Delta t = 18.0$ sec was used in the numerical model. A drag coefficient of $c = 0.01$ was used. The breaking index γ was chosen according to the breaking criterion employed by Noda (1974):

$$\frac{H_b}{L_b} = 0.12 \tanh \left(\frac{2\pi d_b}{L_b} \right) \quad (66)$$

where L corresponds to the wavelength and the subscript b indicates values at breaking. A buildup time of $15 \Delta t$ was used at the start. The eddy viscosity ε_x was chosen according to Equation 58 and the eddy viscosity ε_y was set equal to the value of ε_x at the offshore boundary. For the case under consideration, the complete equations (Equations 50-52) were solved. An approximate steady-state was reached after $67 \Delta t$. Figures 89 and 90 represent the corresponding mean water levels and velocity vectors, plotted on the grid in the computational space. The velocity vectors are plotted for each

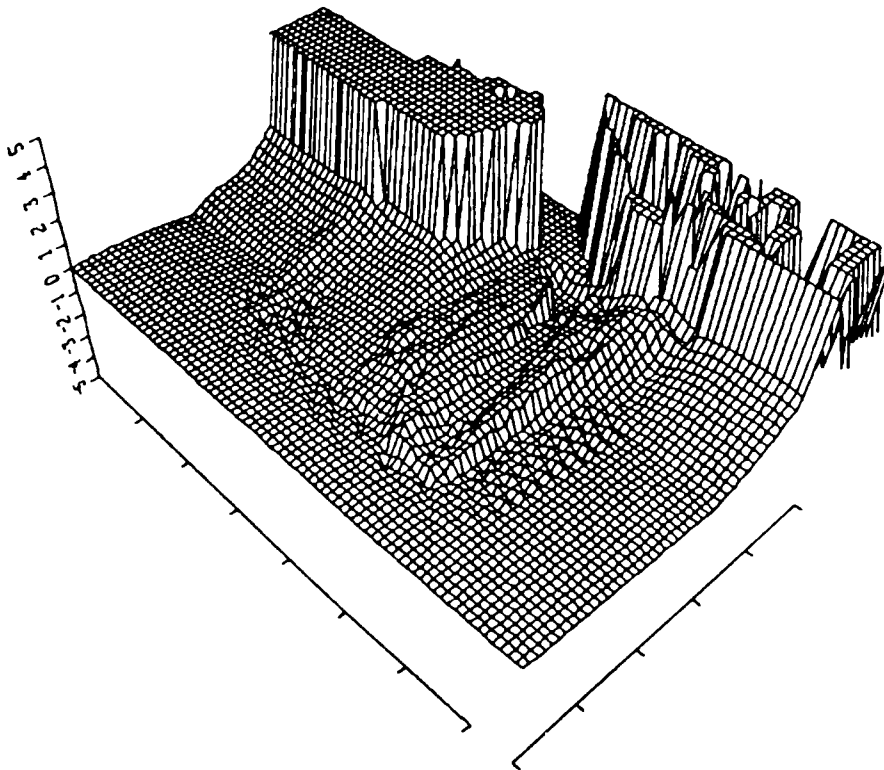


Figure 89. Surface elevation plot of Ash Wednesday storm, March 1962, at Oregon Inlet, North Carolina

cell in each coordinate direction. To avoid confusion, the plotting of velocities with magnitudes less than 0.10 ft/sec is suppressed.

237. Referring to Figures 88-90, first consider the two portions of the beach away from the inlet. The shorelines in these regions are approximately straight and the contours are approximately straight and parallel. As the shoreline is approached from the offshore, there is a small setdown followed by a setup. The velocities are mainly alongshore and the velocity distribution is similar to that for a plane beach except that it exhibits two peaks at some locations.

238. The situation is more complicated in the region of the inlet (the central part of the grid). Here the breaker line is farther offshore. The depth in the main channel decreases first and increases later as the inlet is approached. Because of these factors, the water sets up around the inlet and tends to create a flow into the inlet through the various channels as expected. A part of the main alongshore flow goes around the channels and shoals to the other side.

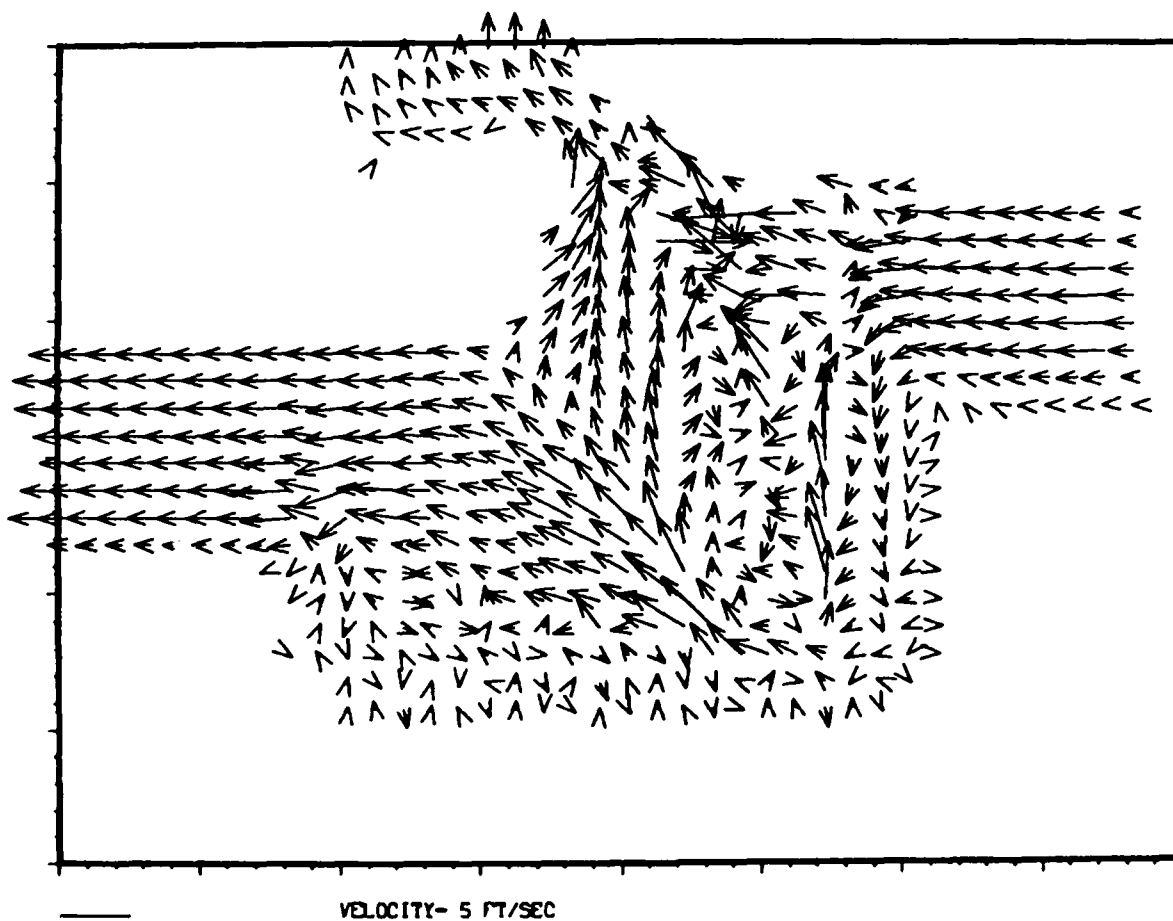


Figure 90. Velocity vector plot of Ash Wednesday storm, March 1962, at Oregon Inlet, North Carolina

239. Near the shoals, the patterns of mean water level and velocity are irregular. This is because the waves refract around the shoals and break, creating locally setups and currents that do not necessarily conform to the general patterns. As the waves go toward the islands, they re-form because the depth increases.

240. Figures 89 and 90 do not reflect the influence of tides and fresh-water flows through the inlet. In nature, these phenomena tend to modify the patterns shown in these figures.

241. All computations described in this report by Vemulakonda (1984) were performed on a Cray-1 computer, which has vectorizing capabilities. For the field application involving a 54×77 grid with 4,158 grid points, the Central Processor Unit (CPU) time for 67 time-steps of simulation was approximately 15.5 sec. The total cost for the job including program compilation,

CPU time, and data file manipulation, was approximately \$10.00. Hence, the computational cost for the operation of numerical simulation model CURRENT for the investigation of longshore currents and nearshore circulations may be considered reasonable.

Wave-Induced Current Model Summary

242. A generalized longshore current model CURRENT was developed to aid in the understanding of wave-induced currents that may contribute to scour and erosion near major structures in the surf zone. It retains the unsteady terms as well as advection and lateral mixing terms in the equations of motion and can be easily modified for different formulations of friction, eddy viscosity, etc. A radiation boundary condition was successfully applied to the offshore boundary. It permitted the transients due to start-up of the numerical scheme to be propagated out of the numerical grid. Comparisons were made with known analytic solutions and experimental results, and there was good agreement. The model was successfully applied to a complex actual prototype field situation and reasonable results were obtained. The computational costs were modest. Nonlinear friction can be introduced into the model, and coordinate transformations can be used to transform the shoreline and breaker line(s) into lines parallel to the coordinate axes. The effect of structures such as jetties and breakwaters on longshore currents and nearshore circulations can be simulated in CURRENTS. The program documentation and user manual are provided in Vemulakonda (1984).

PART VII: PREDICTED SCOUR MAGNITUDE

243. Scour and erosion that occur around most open-ocean structures are results of a combination of current and wave action, to a greater or lesser degree. On a straight section of coastline protected by groins or breakwaters, scour generally results from particles being tossed into suspension by wave action and then being transported from the region by wave-induced currents; hence these phenomena are all-inclusively considered to be the result of scour by wave action. On the other hand, in regions where strong currents (other than wave-induced) exist and where large expanses of open water allow the generation of surface gravity waves, scour effects that result are considered to be caused by a combination of current and wave interaction. Dominant examples of this situation are jetties stabilizing a river mouth on the coast, or jetties protecting a navigation channel through a tidal inlet into an estuary. In either case, strong unidirectional currents (riverflow or tidal) exist that act as a scouring mechanism in themselves, in addition to being a transporting vehicle for removing material placed into suspension by wave effects.

244. The forcing functions causing scour and erosion in all cases are the stresses induced by the currents and the incident wave climate. The determination of these forcing functions (unidirectional current magnitudes, wave characteristics of height and period, and wave-induced currents) must be ascertained in the regions where scour can be anticipated before estimates of the ultimate scour magnitude can be made. Unidirectional current magnitudes (river or tidal) may be determined by appropriate current gaging methods. A detailed determination of the wave field near structures may be obtained by the finite element numerical simulation model (FINITE) developed by Houston and Chou (1984) that calculates wave heights under combined refraction and diffraction of both long and short waves approaching structures from any arbitrary direction. Wave-induced currents caused by the incident wave climate may be determined by the numerical simulation model (CURRENT) developed by Vemulakonda (1984) that solves the complete equations of motion, and can be applied to actual prototype field situations at a reasonable cost. When the incident wave field and the current magnitudes (unidirectional and wave-induced) have been determined, these quantities may be utilized in conjunction with results of critical laboratory experiments and precise prototype

observations for predicting the ultimate extent of scour and erosion to be expected near coastal structures.

Scour by Unidirectional Currents

245. Local scour by unidirectional currents (river or tidal) results from localized changes to the streamline flow patterns caused by obstructions (structures) placed in the flow field. Local scour occurs when the capacity of the flow to remove or transport bed material is greater than the rate at which material is being supplied to the region. In flows without continuous sediment supply, the shear stresses on the bed surface generally decrease as scour hole size increases, until a state is reached wherein the stresses are unable to transport additional material from the scour hole. For given hydraulic or coastal conditions, the size of the ultimate scour will be directly related to the characteristics of the bed material and will require a finite time interval to reach full development.

246. Local scour is the erosion phenomenon that occurs in the immediate vicinity of hydraulic or coastal structures when the capacity of the flow to transport bed material exceeds the rate of material input to the area. This implies an inherent distinction between two types of local scour: (a) clear-water scour; and (b) sediment-transport scour. During the active process, the difference between the case of scour in the presence of sediment transport and the case of clear-water scour is primarily a difference in rate of scour, or the time evolution of erosion.

Clear-water scour

247. As finer materials are picked up and moved, a coarsening or armor-ing of the bed develops. The limit of clear-water scour is reached when the capacity to transport material out of the scour hole becomes zero, or when the boundary shear becomes equal to the critical tractive force on the bed material. This critical force is entirely a function of the bed material, while the boundary shear is related to the velocity of flow, the geometry of the locality, and the roughness of the surface. Hence depth of clear-water scour is some functional relation of the geometry, velocity, and sediment characteristics.

248. The temporal variation of local scour across a clear-water stream has been investigated experimentally by Cunha (1976), who developed an

expression for the time evolution of the scour. It was found that both the friction velocity u_* and the fall velocity of the particles v_f are pertinent parameters in describing the process. Maximum scour depth is approached asymptotically as:

$$\frac{S_{\max}}{y} = 325 \left(\frac{u_*}{v_f} \right)^{3.25} t^{0.16} \quad (67)$$

where

S_{\max} = maximum ultimate scour depth that will occur, ft

t = time increment, sec

y = initial unscoured water depth, ft

The maximum depth at any instant of time was determined by Meulen and Vinje (1977) for a similar experimental arrangement, and it was determined that:

$$\frac{S_{\max}}{y} = \left(\frac{t}{t_1} \right)^{0.38} \quad (68)$$

where t_1 is defined as the time at which $S_{\max} = y$. Scour growth appeared to have been caused primarily by vortices, since the deepest point of scour moved both longitudinally and laterally. The dependence of characteristic scouring time t_1 on flow conditions (i.e. velocity, material, and geometry) was further investigated, and it was concluded that the influences of these various factors on the rate of the scouring process can be described by the same general relation for both two- and three-dimensional local scour:

$$t_1 = 250 \left[\frac{(\rho_s - \rho)}{\rho} \right]^{1.7} y^2 (\alpha u - u_{cr})^{-4.3} \quad (69)$$

where u_{cr} is the flow velocity necessary for initiation of particle movement, and the coefficient α varies from 3 to 8, depending upon the particular geometry under consideration.

249. In investigations of the similarity of prototype scour to sediment motion during model tests, Yalin (1959) showed that the Froude time scale (the time scale based on gravity being the dominant force balancing inertia) is valid only when the sand used in the model has a characteristic diameter of at

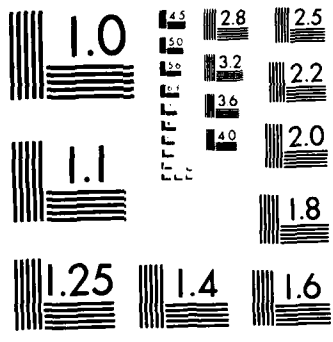
least 1.8 mm and, furthermore, that the relative densities of bed material should be the same between model and prototype. Dietz (1976) further determined that scale effects produce a nonlinearity of a nature such that small model scour should be scaled up with a smaller ratio than large model scour. Scale factors for the scour depths are not identical with the geometric scale factor; and scour depths measured in the model must be scaled up with a substantially smaller factor than the geometric scale.

250. Model tests conducted by Murphy (1971) at WES have demonstrated advantages of preforming a scour hole below dams and reservoirs so that flow can expand and dissipate its excess energy in turbulence rather than in a direct attack on the channel bottom. This makes it possible to stabilize the channel with rock of an economical size since the construction can be accomplished in a dry situation, and the necessary equipment will already be at the construction site. Also, the preformed scour hole need not be as large as that which would naturally occur under existing prototype hydrodynamic conditions.

Sediment-transport scour

251. Sediment-transport scour is generally considered to be scour that occurs around structures erected in sediment-laden rivers or tidal streams. The scour limit is reached when the capacity for transport of sediment out of the scour hole becomes equal to the supply of sediment into the hole. A significant type of scour problem of this nature which is of great economic importance is that scour around vertical cylindrical piling supporting bridge, wharves, or piers. These situations are strongly influenced by flow patterns, including vortices and separation generated by the obstructions. The process is heavily dependent on the flow field in the immediate vicinity of the obstruction, and thus knowledge of the redistribution of energy over the region is necessary for understanding the character of the scour.

252. When a vertical cylindrical piling is placed in a steady unidirectional flow field, velocities and accelerations are altered near the vicinity of the piling; and the resulting forces are sufficient to initiate sediment motion around the base of the structure. In real fluids, potential flow theory is not applicable in the immediate neighborhood of boundaries; hence a velocity gradient is generated and all streamlines have different velocities of approach. Thus the stagnation pressure along the vertical face of the piling will vary with a higher pressure near the surface and decreased pressure



MICROCOPY RESOLUTION TEST CHART
NATIONAL BUREAU OF STANDARDS 1963-A

downward. The resulting pressure gradients give rise to a vertical flow of fluid along the upstream face of the piling in a downward direction which interacts with flow around the piling to produce vortices and spiral flow. The streamlines are no longer in any horizontal plane but converge downward toward the bed, which leads to an increase in fluid velocities in the lower layers and to an increase in mean boundary shear. This appears to be an important mechanism of local scour around vertical cylindrical piling.

253. Due to large friction forces in the boundary layer, a fluid particle consumes so much of its kinetic energy moving around the cylinder that it cannot penetrate very far into the wake behind the cylinder; consequently, flow separation takes place as vortex motion is formed and moves downstream. This circumstance completely changes the flow field in the wake; and the pressure distribution suffers a radical change as the eddy region behind the cylinder causes a large pressure drag on the body. A regular shedding pattern of vortices which move alternately clockwise and counterclockwise, known as the Karman vortex street, can be discerned. The separation which rolls up ahead of the base of the pile is known as the horseshoe vortex system and plays the most important role in the local scour process around the pile.

254. In order to predict scour processes expected to occur at a prototype bridge crossing Akashi Channel, Japan, Nakagawa and Suzuki (1976) conducted similarity investigations by introducing a reference time defined as the time when the maximum scour depth becomes equal to the width of the bridge piers. The characteristics of this reference time were studied by systematic experiments for various scales of sand diameter, flow velocity, and pier width. Scour depth scale for the case in which the scale of sand diameter is distorted from the length scale of the pier also was investigated. Field tests were conducted by erecting a 9-m-diam vertical cylinder and comparing the results of these tests with a 1:150-scale model.

255. The problem situation investigated by Nakagawa and Suzuki (1976) was determined by strong tidal currents (about 4 m/sec). Two main piers of 40-m by 70-m rectangular cross section were to be constructed on a sand and gravel foundation. Because the periodicity of reversal of the flow process was of such long duration, it was determined that the experimental studies could be conducted with steady unidirectional flow conditions. One series of tests was conducted with steady flow in one direction, a second series consisted of the flow reversing periodically, and a third series of tests was

conducted with the piers rotated at specific angles to the steady and reversing flows.

256. In the case of the one-directional flow, scour began at the upstream corners of the pier with an inverse cone shape which developed from the corners. The deposition area of the sediment shifted downstream with time. In the case of the reversing flow, the scour became deepest at the corners of the pier, and the scour and deposition were repeated according to normal and reverse flows, respectively. The maximum scour depth for the periodic flow became slightly smaller than that of the one-directional flow because of the sediment supply of the reverse flow. When the pier was rotated 30 deg with the direction of flow, the diagonal corners became extremely scoured and their scour depths did not become smaller even by the reverse flow. The maximum scour depth became larger with the increase of the angle of attack. This is due to the increase of the apparent width of the pier with increase in angle of rotation.

257. The maximum scour depth S_{\max} was found to change linearly with time t according to:

$$\frac{S_{\max}}{D} = \left(\frac{t}{t_r} \right)^{0.22} \quad (70)$$

The reference time t_r , which is the time when $S_{\max} = D$, is dependent on a grain diameter d , a width of pier D , and a mean flow velocity U . When t_r has been determined, the time variation of the maximum scour depth can be expressed by Equation 70 for unidirectional flow around a piling. The similarity condition $u_* d / \nu > 70$ should be adhered to (Yalin 1971).

Scour by Wave Action

258. Seawalls and breakwaters are usually built to protect a portion of a beach from scour and erosion caused by the continual breaking of waves directly on or in front of the beach face. In order to properly locate the protective structure, an estimation of the beach profile that will exist after construction of the structure is necessary and can be determined to a first approximation by experience and general guidelines. The scour that is expected to occur at the toe of such structures will develop a trough with

dimensions based on the type of structure, the nature of the wave attack, and properties of the foundation. Where rubble-mound structures are concerned, the scour may be allowed for by overbuilding the structure to account for settlement into the scour hole, a stone blanket may be placed for some distance seaward of the structure toe to prevent formation of the scour hole, or excess stone may be placed on the toe to fill the anticipated scour trough. The Coastal Engineering Research Center (USAEWES 1984) estimates that as a general guideline in a wave climate only, the maximum depth of scour S_{max} in front of a structure below the unscoured natural bed is about equal to the height of the maximum unbroken wave H_{max} that can be sustained by the original water depth at the toe of the structure.

$$S_{max} = H_{max} \quad (71)$$

This maximum wave height, H_{max} , can be determined by numerical simulation model (FINITE) developed by Houston and Chou (1984).

259. Chesnutt and Schiller (1971) simulated the scour due to wave action in front of seawalls in laboratory experiments, and in their literature review found that Russell and Inglis (1953) had studied scour in front of a vertical wall by generating a constant wave height. This required the wave period and, therefore, the wavelength to be varied as the depth varied. The ultimate scour depth was found to be about one wave height below mean low water; but because of the peculiar experimental situation involved, the results are difficult to extrapolate to more general situations. Chesnutt and Schiller (1971) discovered that the relative position of a seawall (its location between natural shoreline and the breaker line), which changes with each change in wavelength, is as critical as the wave height in determining the amount of scour that occurs.

260. Observations of wave-induced toe scour reveal a strong correlation between its severity and the wave reflection coefficient, C_r , for the wave-structure interaction (Eckert 1983). Sawaragi (1966), in his investigations of scour at the toe of permeable structures, had previously found a relation between the void ratio of the structure, the coefficient of reflection, and the depth of scour. Herbich and Ko (1968) extended the work of Sawaragi (1966) and developed a mathematical model for determining the ultimate depth of scour S_{max} :

$$S_{\max} = \left(d - \frac{a}{2}\right) \left\{ (1 - C_r) u_{\max} \left[\frac{3}{4} C_D \rho \frac{\cot \phi}{d_{50} (\gamma_s - \gamma)} \right]^{1/2} - 1 \right\} \quad (72)$$

where

$$a = H_i + H_r \quad (73)$$

and

$$C_r = \frac{H_r}{H_i} \quad (74)$$

with

C_D = drag coefficient of a spherical particle, dimensionless

ϕ = bed material angle of repose, dimensionless

H_i = incident wave height, ft

H_r = reflected wave height from the structure, ft

All experiments performed indicated there is an asymptotic limit to scour depth. Scour depth increases very rapidly during the first few hours; subsequently, the erosive process slows and finally reaches a state of "ultimate" erosion.

261. Scour in front of 30-, 60-, and 90-deg seawalls was studied by Sato, Tanaka, and Irie (1968), for both normal and storm beach profiles, using several grain sizes. After an equilibrium beach profile had been established, a seawall was introduced into a mode; and five types of scour were observed and the mechanism producing each type was defined. They found that maximum scour depth would probably be no greater than the deepwater wave height which produced the scour. Also, the reflected wave was found to be a significant parameter in addition to the still-water depth. Along the breakwaters or jetties, the toe of the structures was scoured severely where the structure crossed the longshore bar, and at the tip of the structure. In a field situation, agitation due to waves breaking on the structure and the wave-induced currents around the structure play an important role in the scouring process.

262. Caisson-type structures exposed to wave action were experimentally investigated by Donnelly and Boivin (1968), and they determined that the most vulnerable part, from the standpoint of foundation erosion, is at joints

between abutting caissons. For direct wave attacks, the velocity through the open joint can be estimated approximately as:

$$v = 1.25 \left(2\pi \frac{H}{T} \right) \left[\frac{1}{\sinh\left(\frac{2\pi d}{L}\right)} \right] \quad (75)$$

Unless the material in the joint is coarse enough to resist this scouring velocity, erosion problems will likely occur. In practice, joints between abutting caissons should be effectively sealed if erosion problems are to be avoided. To seal the joints, two key placements are necessary: (a) one on the seaward side of the structure and (b) one on the harbor side. The height of the granular fill required to prevent erosion is:

$$h = 2 \frac{H}{\cosh\left(\frac{2\pi d}{L}\right)} \quad (76)$$

For coarser types of gravel fill with suitable filters, the height given by Equation 76 can be reduced by up to 30 percent.

263. Recently, the construction of permeable detached breakwater systems of concrete blocks has become widely practiced as a countermeasure against beach erosion in Japan. Most of these breakwaters function effectively; however, there are occasional reports of erosion caused by local scour and wave-induced currents around the breakwaters. Experiments were conducted by Hotta and Marui (1976) to investigate characteristics of the local scour; and it was found that local scour and beach change exist simultaneously. That is, the local scour is superposed upon larger scale changes in bathymetry and there is a complicated interaction. A lightweight concrete aggregate with specific gravity of 1.65 was used in their movable-bed studies, and it was found that the maximum scour depth varied from 0.6 to 1.0 times the incident wave height for different wave characteristics. The scouring depths were found to be greatest at $X/X_b = 38$ percent, where X_b is the distance from the shoreline to the point where the wave breaks.

264. On the basis of laboratory experimental studies, Song and Schiller (1973) developed a semilogarithmic regression model that predicts relative scour depth S/H as a function of relative seawall distance X/X_b and standing wave steepness H/L and is given as:

$$\frac{S}{H} = 1.94 + 0.57 \ln\left(\frac{X}{X_b}\right) + 0.72 \ln\left(\frac{H}{L}\right) \quad (77)$$

This expression is displayed in Figure 91, where it can be observed that for larger values of standing wave steepness, the relative scour depth is dependent upon the seawall position; but for small values of standing wave steepness, the relative scour depth is nearly independent of seawall location.

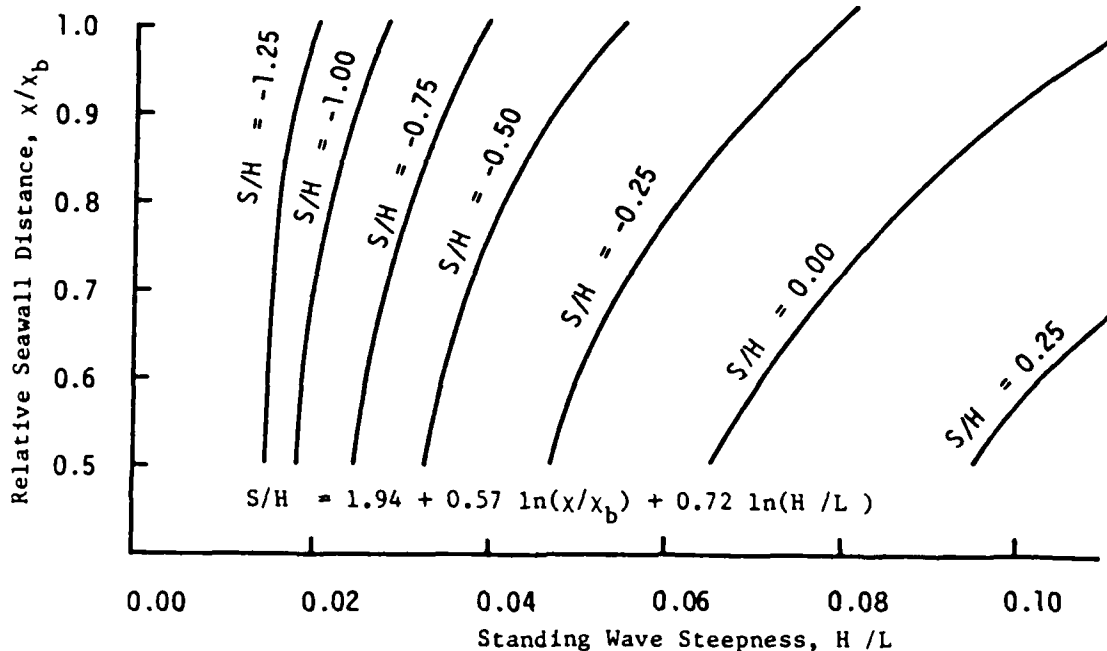


Figure 91. Variation of relative scour depth, S/H , with relative seawall distance, X/X_b , and standing wave steepness, H/L (after Song and Schiller 1973)

Scour by Combined Current and Wave Action

265. Objectives considered in the design of a jetty system (for example) at a tidal inlet include, among others, the minimization of (a) undesirable wave action on navigation; (b) artificial channel maintenance dredging; and (c) adverse effects on shoreline modifications caused by the interception of littoral sediment movement. Jetties assist in channel maintenance by directing ebb tidal currents such that their natural scouring potential is enhanced. Jetties also aid channel maintenance by intercepting longshore sediment transport due to wave action; hence many jetties are impermeable, extending from the beach to an offshore depth where sediment movement is minimal.

266. During the construction of a new jetty system, it is frequently necessary to build (or extend an existing system) across ebb tidal flow channels onto flood shoal regions. Bay tidal prism water masses develop tremendous momentum while discharging as an ebb jet, and have inherent characteristics that offer resistance to a change in direction of travel; i.e., the ebb flow emanating from a river or tidal channel tries to maintain movement in a straight line. As jetty construction proceeds across the ebb channel, partial closure of the ebb channel results. The new structure must deflect the ebb jet and thereby becomes subjected to the full intensity of the ebb flow scouring potential. Detrimental results of such effects consisting of unanticipated cost overruns in the United States are documented by Hales (1980a), and for severe scouring in front of structures in Japan by Irie and Nadaoka (1984). Not only does the potential exist for undermining the new structure, but the ebb channel actually migrates ahead of the new structure such that construction never actually crosses the ebb channel. Construction is continually being performed where the relocated ebb channel has scoured its new (most recent) location directly ahead of the new structure construction. A typical representative example of this phenomenon is shown in Figure 92, Murrells Inlet, South Carolina, during south jetty construction, 7 May 1979. Waves break across the flood shoal region during most of the tidal cycle, and this continual agitation contributes to the ebb current's ability to relocate its channel position in a highly expedient manner.

267. All movable boundaries will respond to the environmental forces to which they are subjected. Any natural or man-made channel in alluvial material will develop (evolve) one unique geometry (depth and width) determined by the dominant discharge (maximum ebb tidal flow) that it is required to transport and the particle size that comprises the movable boundaries. In an open channel with rigid boundaries, uniform flow can be described by a single formula, such as the Manning equation. That is, for a given dominant discharge, Q , and channel dimensions, one and only one depth can be established uniformly.

268. If the channel has a movable boundary, however, then the width, W , and slope can change, along with the establishment of the scoured depth, S . The adjusted slope will largely depend upon the ability of the flow to transport its bed load. If the bed load is too small, scour will result, thus decreasing the slope, and vice versa. Similarly, the sides may also erode and



Figure 92. Murrells Inlet, South Carolina, showing ebb channel relocation and scouring of shoal region in front of south jetty construction, 7 May 1979

the width thus increases. The depth of flow (ultimate scoured depth) then depends not only on discharge, but also on the adjusted width and slope, each of which also depends on discharge. Consequently, three independent equations are necessary to describe uniform (regime) flow in an erodible channel. The tidal channel sedimentation (transport) phenomena in coastal processes, though more complex than in streams or canals, are basically similar, except insofar as influenced by wave action (Morris 1963). The wave action essentially agitates the movable boundaries and allows the tidal current to transport the bed load and develop the ultimate scour depth more rapidly than would otherwise occur in the absence of wave action.

269. The ebb tidal channel scour depth in front of new jetty construction across an existing ebb channel onto a flood shoal region stems from observation that the Froude number for the flow, V^2/gS , is empirically related to the bed load as:

$$\frac{V^2}{gS} = \left(\frac{1.9}{g}\right) d_m^{1/2} \quad (78)$$

where d_m is the median diameter of the bed particles in millimetres. In terms of discharge, Q :

$$S = \left[\frac{Q^2}{(1.9 d_m^{1/2} w^2)} \right]^{1/3} - d \quad (79)$$

where d is the average water depth laterally outside the ebb flow channel. The width equation does not have a very obvious dynamic basis but has been empirically correlated with numerous field observations as:

$$W = 2.67 Q^{1/2} \quad (80)$$

It follows that:

$$S = \left[\frac{Q}{(13.5 d_m^{1/2})} \right]^{1/3} - d \quad (81)$$

which shows the direct dependence of ultimate ebb channel scour depth on the dominant ebb tidal flow and particle size comprising the flood shoal region.

270. All proposed coastal construction projects should be planned with detailed understanding of their site-specific nature in mind. Underwater topographic features, orientation for wave climate exposure, river or bay tidal currents, and availability of coastal sediments for longshore transport all play unique roles at each specific site. Those phenomena that may be dominant in one locality may exhibit only minimal consequences at other regions. Hence extrapolation of conclusions from one locality to another is probably not feasible. The determination of pertinent parameters such as river or tidal currents may be acceptably performed by current gaging techniques. However, the determination of the detailed wave climate in the vicinity of coastal structures is not nearly as direct due to the variable nature of the wave characteristics and approach directions. Such detailed wave features as might be required may expediently be determined by the finite element numerical simulation model (FINITE) developed by Houston and Chou (1984). Also, those wave-induced currents that may be pertinent to a specific locality may be obtained from the numerical model (CURRENT) developed by Vemulakonda (1984). Superposition of the two current fields may be necessary in some situations to approximate the ultimate current contributing to the scour and erosion potential.

PART VIII: RESEARCH PROGRAM SUMMARY

The Problem of Scour and Erosion During Construction

271. It is frequently necessary to construct large engineering works of improvement in the surf and nearshore zone to protect harbor entrances, recreational beaches, and navigation channels. These structures, usually built from quarried rock or precast concrete, are placed in position by crane or barge. When these major structures are erected in the coastal zone they alter the existing currents that normally occur at a particular location due to the unique topography and the wave climate peculiar to that specific region. Shallow-water surface gravity waves breaking on the new structure will cause bottom material to be suspended and transported from the region by longshore or other currents that may exist. This removal of material is often not compensated by an influx of additional material; and the result is a scour hole, or erosion, that usually develops along the toe of the structure.

272. In order to ensure structural stability and functional adequacy of the works of improvement, any scour area must be filled with nonerrodible material (sufficiently stable to withstand the environmental forces to which it will be subjected). This may result in additional quantities of material being required during construction that can potentially lead to substantial cost overruns. To minimize potential cost increases due to scour during construction, it is necessary to quantify the probability and ultimate extent of potential scour during the scheduled construction period. This is an extremely complex problem and quantification of the probability of potential scour will always be site-specific.

Present Design and Construction Practice

273. Scour and erosion of foundation material around major structures constructed in the coastal zone have been well-known and continuing problems since surf-zone work commenced. Over the years, those responsible for the integrity of such structures have developed construction techniques to minimize quantity and cost overruns, although in most cases these procedures are regional in nature. Because of varying wave and current conditions from one locality to another, those techniques that are optimum for one location may

not be strictly applicable to another region. The procedures presently being used to combat the problem of scour in the coastal zone during construction and to eliminate "secondary construction effects" which develop some time after completion of the initial construction work, and the underlying philosophy on which these procedures are based, are enumerated as follows:

- a. It is universally accepted that most major stone structures require a foundation blanket for bearing surfaces to support the mass of the structure above and to serve as scour protection during the actual construction. The thickness and design features of the blanket vary with location but, in general, are on the order of 2 to 3 ft thick and extend on either side of the structure from 5 to 25 ft beyond the toe. In parts of the Great Lakes, a layer of sand has been placed initially on soft unconsolidated muds, and then covered with quarry-run stone. Off the coast of Louisiana, where shell is plentiful, a layer of this material is frequently used.
- b. In recent years, a wide variety of plastic filter fabrics have come into vogue, and these are gaining acceptance as the initial item to be placed on unconsolidated materials to prevent migration of the fine materials up into the voids of the larger stones and a resulting hole into which the larger stone may settle. A layer of crushed stone or shell should be applied next in order to prevent puncture or tearing of the cloth by heavier stone. The cloth may be layered in sheets for the usual application or fabricated into bags or tubes for specialized features.
- c. Foundation bedding materials should be placed ahead of the core construction at least 50 ft to prevent temporal scouring from undermining the working section. Some have found it expedient to place one-half the thickness of the bedding initially and then to make a second application with the second half of the material. At the end of the construction day, a 30- to 50-ft section of bedding material should be applied to minimize overnight scouring. In the heavy wave climate of the Oregon coast, the foundation bedding layer is designed 5 ft thick and intended to extend beyond the toe of the structure for 25 ft.
- d. "Accelerated core placement" has been utilized successfully in crossing scour holes susceptible to continuing scour. On major structures where the work will continue over more than a single construction season, no more core stone should be placed than can be armored that season. Core stone of quarry-run rock instead of sorted stone has been determined to provide better keying action and a more stable, overdesigned structure at a lower unit cost as the contractor does not have to separate up to 80 percent of the materials.
- e. Gabion units have been fabricated and placed in a continuous layer as foundation bedding material, instead of a loose layer of crushed stone, to ensure that the bedding material will be evenly distributed after structure settlement.

REFERENCES

- Abbott, M. B., Petersen, H. M., and Skovgaard, O. 1978. "On the Numerical Modeling of Short Waves in Shallow Water," Journal, Hydraulic Research, Vol 16, p 173.
- Aranha, J. A., Mei, C. C., and Yue, D. K. P. 1979. "Some Properties of Hybrid Element Methods for Water Waves," International Journal of Numerical Methods Engineers, Vol 14, p 1627.
- Battjes, J. A. 1968 (Nov). "Refraction of Water Waves," Journal, Waterways and Harbors Division, American Society of Civil Engineers, Vol 94, No. WW4, pp 437-451.
- Bekaert Steel Wire Corporation. 1977. "Bekaert Gabions," Technical Memorandum, Reno, Nev.
- Berkhoff, J. C. W. 1972 (Jul). "Computation of Combined Refraction-Diffraction," Proceedings, Thirteenth Conference on Coastal Engineering, Vol 1, pp 471-490, Vancouver, British Columbia, Canada.
- _____. 1976. "Mathematical Models for Simple Harmonic Linear Water Waves," No. 163, Delft Hydraulics Laboratory, Delft, Holland.
- Bettess, P., and Zienkiewicz, O. C. 1977. "Diffraction and Refraction of Surface Waves Using Finite and Infinite Elements," International Journal of Numerical Methods Engineers, Vol 2, p 1271.
- Bowen, A. J. 1969. "The Generation of Longshore Currents on a Plane Beach," Journal of Marine Research, Vol 27, pp 206-215.
- Bowen, A. J., Inman, D. L., and Simmons, V. P. 1968. "Wave 'Set-Down' and Set-Up," Journal of Geophysical Research, Vol 73, No. 8, pp 2569-2577.
- Bretschneider, C. L. 1966. "Wave Refraction, Diffraction, and Reflection," Chapter 6, Estuary and Coastline Hydrodynamics, A. T. Ippen, ed., McGraw-Hill, New York, N. Y.
- Braun, P. 1979 (Sep). "Breakwater Design, Design of Mound Breakwaters, Proceedings, Civil Engineering in the Oceans IV, San Francisco, Calif., Vol 1, pp 344-366.
- Braun, P., and Gunbak, A. R. 1976 (Jul). "New Design Principles for Rubble Mound Structures," Proceedings, Fifteenth Coastal Engineering Conference, Honolulu, Hawaii, Vol III, pp 2429-2473.
- Butler, H. L. 1980. "Evolution of a Numerical Model for Simulating Long Period Wave Behavior in Ocean-Estuarine Systems," Estuarine and Wetlands Processes with Emphasis on Modeling, Marine Science Series, Vol 11, Plenum Press, N. Y.
- Carrier, G. F. 1966 (Apr). "Gravity Waves on Water of Variable Depth," Journal of Fluid Mechanics, Vol 24, Part 4, pp 641-659.
- Carver, R. D. 1976 (Apr). "Stability of Rubble-Mound Breakwater, Lahaina Harbor, Hawaii; Hydraulic Model Investigation," Miscellaneous Paper H-76-8, US Army Engineer Waterways Experiment Station, Vicksburg, Miss.

expected in the near-vicinity of such structures. The time evolution of scour by unidirectional currents can be approximated as:

$$\frac{S_{\max}}{y} = 325 \left(\frac{u_*}{v_f} \right)^{3.25} t^{0.16} \quad (67 \text{ bis})$$

where S_{\max} is the maximum scour depth. For wave action only, USAEWES (1984) suggests that as a general guideline, the maximum depth of scour is approximately the same as the height of the maximum unbroken wave, H_{\max} , that can be sustained by the original water depth at the toe of a structure:

$$S_{\max} = H_{\max} \quad (71 \text{ bis})$$

When the reflective properties of the structures are incorporated, the scour depth, S , may be approximated as:

$$S = \left(d - \frac{a}{2} \right) \left\{ (1 - C_r) u_{\max} \left[\frac{3}{4} C_D \rho \frac{\cot \phi}{d_{50} (\gamma_s - \gamma)} \right]^{1/2} - 1 \right\} \quad (72 \text{ bis})$$

where $a = H_i + H_r$ and $C_r = H_r/H_i$. When constructing a jetty or breakwater across an ebb or flood tidal channel, it has been observed that the channel migrates with the rate of new construction. The ebb channel depth can be approximated from the physics of regime theory, with the resulting scour depth being estimated as:

$$S = \left[\frac{Q}{(13.5 d_m^{1/2})} \right]^{1/3} - d \quad (81 \text{ bis})$$

where d is the average water depth laterally outside the ebb flow channel which is being traversed by the new coastal structure.

$$w_{UL} = \frac{w_r H_b^3}{5,360 (S_r - 1)^3 \left(\frac{L}{\lambda}\right)^2} \quad (15 \text{ bis})$$

Since these data were obtained from the most severe wave conditions (waves that break and plunge directly at the toe of the structure), the application of these results to less-severe wave climates will indicate a stone size requirement larger than necessary.

297. The uniformly valid asymptotic theory is superior to diffraction theory alone for estimating wave heights downcoast of nearshore structures subjected to combined refraction and diffraction. It is desirable to incorporate into this theory a degree of nonlinearity which is not presently available.

298. A two-dimensional finite element numerical simulation model (FINITE) was developed by Houston and Chou (1984) that calculates wave heights under combined refraction and diffraction of both long and short waves approaching structures from any arbitrary direction. Although the model solves an equation that is strictly valid only for mild bathymetric variations, the model can provide reasonable qualitative answers for problems where there are rapid depth variations (at much lower cost than required by three-dimensional models that are appropriate for problems involving rapid depth variations).

299. A generalized numerical simulation model (CURRENT) that solves the complete equations of motion to estimate longshore currents (wave induced) and nearshore circulations caused by the action of breaking waves has been developed by Vemulakonda (1984). This model is flexible in the formulations chosen for various terms and can be applied to actual prototype field situations at a reasonable cost. It retains the unsteady terms as well as advection and lateral mixing and can be modified for different formulations of friction, eddy viscosity, etc. The effect of structures such as jetties or breakwaters on longshore currents and nearshore circulations can be simulated in this model.

300. Unidirectional currents (river or tidal) may be determined by current gaging methods. Wave climate in the vicinity of coastal structures may be ascertained by numerical model (FINITE). Wave-induced currents generated by the wave climate may be determined by numerical model (CURRENT). These values can then be utilized in predicting the magnitude of scour to be

PART IX: CONCLUSIONS

295. The procedures presently used to combat the problem of scour in the coastal zone during construction include:

- a. A foundation blanket placed beneath most major stone structures as a bearing surface and to serve as scour protection; in general, 2 to 3 ft thick and extending on either side of the structure from 5 to 25 ft beyond the toe.
- b. A wide variety of plastic filter fabrics placed on unconsolidated material to prevent migration of fines, covered by a layer of crushed stone or shell to prevent tearing of the cloth by heavier stone.
- c. Foundation bedding material placed at least 50 ft ahead of the core construction to prevent temporal scouring.
- d. "Accelerated core placement" to cross scour holes susceptible to continuing scour.
- e. Use of gabion units in place of foundation bedding material to ensure even distribution of the bearing surface; to a lesser extent, Gobimat material can be utilized in special nearshore cases.
- f. On high wave energy coasts, the extent of ultimate scour is estimated, and the foundation is excavated to that depth or down to a firm solid foundation.
- g. In emergency situations, scour has been minimized by filling ebb or flood channels with dredged material to allow construction to continue.
- h. The proper selection of the construction season, since many problems arise because of contractor procedures such as trying to work in adverse weather or wave conditions of excessive height.

296. The stability of an underlayer section of crushed stone can be expressed in a manner similar to that of Hudson (1957) for the armor slope stability of rubble-mound structures. Based on experimental model studies of seven uniform material sizes for three different lengths of underlayer sections, the expression for the conservative stability number, N_s , is:

$$N_s = \frac{w_r^{1/3} H_b}{(S_r - 1) w_{UL}^{1/3}} = 17.5 \left(\frac{L}{\lambda} \right)^{2/3} \quad (14 \text{ bis})$$

with the corresponding conservative expression for the weight, w_{UL} , of the representative stone comprising such an underlayer material section:

Scour by combined
current and wave action

293. During the construction of a new jetty system, it is frequently necessary to build across ebb or flood tidal flow channels onto flood shoal regions. Partial closure of these channels results as construction advances oceanward. The new structure must deflect the high momentum ebb flow, and thereby becomes subjected to the full intensity of the ebb current scouring potential. In addition to possibly undermining the new structure, the ebb channel has been observed to migrate ahead of the new structure construction such that construction never actually crosses the ebb channel. The construction is being performed where the relocated ebb channel has scoured its new (most recent) location directly ahead of the new structure construction. Waves breaking across the flood shoal region provide continual agitation that contributes to the ebb current's ability to relocate its channel position far more easily than would be possible in the absence of any wave action.

294. The analysis of this phenomenon can be approached from the standpoint of regime theory of canals with movable boundaries. For a dominant flow (ebb discharge) only one unique channel geometry will evolve, and this geometry is determined solely by the dominant flow in the channel, Q , and the material comprising the movable boundaries, d_m . The ebb channel scour can be approximated as:

$$S = \left[\frac{Q}{(13.5 d_m^{1/2})} \right]^{1/3} - d \quad (81 \text{ bis})$$

where d is the average water depth laterally outside the ebb flow channel.

$$S_{\max} = H_{\max} \quad (71 \text{ bis})$$

This maximum wave height, H_{\max} , can be determined by numerical model (FINITE).

291. Sawaragi (1966), in experimental investigations of scour at the toe of permeable structures, noted a relation between the coefficient of reflection, C_r , and the depth of scour. Herbich and Ko (1968) extended this work and developed a mathematical model for determining the ultimate depth of scour, S , as:

$$S = \left(d - \frac{a}{2} \right) \left\{ (1 - C_r) u_{\max} \left[\frac{3}{4} C_D \rho \frac{\cot \phi}{d_{50} (\gamma_s - \gamma)} \right]^{1/2} - 1 \right\} \quad (72 \text{ bis})$$

where

$$a = H_i + H_r \quad (73 \text{ bis})$$

and

$$C_r = \frac{H_r}{H_i} \quad (74 \text{ bis})$$

The scour process is temporal in nature, with the scour depth increasing very rapidly during the first few hours, then slowing until a state of ultimate scour is attained.

292. On the basis of laboratory experimental studies of impermeable seawalls, Song and Schiller (1973) developed a semilogarithmic regression model that predicts relative scour depth S/H as a function of relative seawall distance X/X_b and standing wave steepness H/L , as:

$$\frac{S}{H} = 1.94 + 0.57 \ln\left(\frac{X}{X_b}\right) + 0.72 \ln\left(\frac{H}{L}\right) \quad (77 \text{ bis})$$

For larger values of standing wave steepness, the relative scour depth is dependent upon seawall position; however, for small values of standing wave steepness, the relative scour depth is nearly independent of seawall location.

the stresses induced by the currents and the incident wave climate. When the magnitude of these forcing functions (unidirectional current magnitudes, wave characteristics of height and period, and wave-induced current values) have been ascertained, predictions can be made about the ultimate scour to be expected at a particular site. Unidirectional currents (river or tidal) may be determined by appropriate current gaging methods. The wave climate in the vicinity of structures may be ascertained by the finite element numerical simulation model (FINITE) that calculates wave heights under combined refraction and diffraction. Wave-induced currents caused by the incident wave climate may be determined by the numerical simulation model (CURRENT).

Scour by unidirectional currents

289. Local scour is the erosion phenomenon that occurs in the immediate vicinity of coastal structures when the capacity of the flow to transport bed material exceeds the rate of material input to the area. As finer materials are picked up and moved, a coarsening or armoring of the bed develops. Cunha (1976) developed an expression for the time evolution of scour by unidirectional currents as:

$$\frac{S_{\max}}{y} = 325 \left(\frac{u_*}{v_f} \right)^{3.25} t^{0.16} \quad (67 \text{ bis})$$

where S_{\max} is the maximum scour depth, u_* is the friction velocity, and v_f is the fall velocity of the particles. The maximum depth at any instant of time was determined by Meulen and Vinje (1977) as:

$$\frac{S_{\max}}{y} = \left(\frac{t}{t_1} \right)^{0.38} \quad (68 \text{ bis})$$

where t_1 is defined as the time at which $S_{\max} = y$.

Scour by wave action

290. The Coastal Engineering Research Center (USAEWES 1984) estimates that as a general guideline in a wave climate only, the maximum depth of scour S_{\max} in front of a coastal structure below the unscoured natural bed is about equal to the height of the maximum unbroken wave H_{\max} that can be sustained by the original water depth at the toe of the structure.

energy dissipation and thus energy loss through wave breaking is simulated by permitting waves to propagate out of the computational region. The program documentation, user guide, and sample problem output are provided by Houston and Chou (1984).

Numerical Model of Wave-Induced Currents

286. There has been a growing interest in recent years in the numerical modeling of longshore currents (wave induced) and nearshore circulations caused by the action of breaking waves. This has resulted in a need for generalized numerical simulation models that solve the complete equations of motion, are flexible in the formulations chosen for various terms, and can be applied to actual prototype field situations at a reasonable cost. The development and application of one such model (CURRENT) have been performed by Vemulakonda (1984).

287. This generalized longshore current model (CURRENT) was developed to aid in the understanding of wave-induced currents that may contribute to scour and erosion near major structures in the surf zone. It retains the unsteady terms as well as advection and lateral mixing terms in the equations of motion and can be easily modified for different formulations of friction, eddy viscosity, etc. A radiation boundary condition was successfully applied to the offshore boundary. This permitted the transients due to start-up of the numerical scheme to be propagated out of the numerical grid. Comparisons were made with known analytic solutions and experimental results, and there was good agreement. The model was successfully applied to a complex actual prototype field situation and reasonable results were obtained. The computational costs are modest. Nonlinear friction can be introduced into the model, and coordinate transformations can be used to transform the shoreline and breaker line(s) into lines parallel to the coordinate axes. The effect of structures such as jetties or breakwaters on longshore currents and nearshore circulations can be simulated in CURRENT. The program documentation and user manual are provided in Vemulakonda (1984).

Predicted Scour Magnitude

288. The forcing functions causing scour and erosion in all cases are

breakwater, and even in this region the uniformly valid asymptotic theory closely approximates the data from the experiments. The greatest deviation of the uniformly valid asymptotic theory from the experiments occurs outside the breakwater shadow zone in the area of the asymptotic undulations of the wave-height amplification factor. This can be attributed to reflection of longer period wave energy from the beach breaker zone not accounted for in the analytical development, since the uniformly valid asymptotic theory consistently underpredicts the wave-height amplification in this area.

284. In general, it can be concluded that the uniformly valid asymptotic theory is superior to diffraction theory alone for estimating wave heights downcoast of nearshore structures subjected to combined refraction and diffraction. Particularly for longer period waves and for the region near the structures where scour and erosion are known to frequently occur, this theory provides an estimation that consistently approximates the results of this experimental study and which is significantly better than diffraction theory. At the same time, it appears desirable to incorporate into this theory a degree of nonlinearity that is not presently available to account for variations in incipient incident wave height and to allow for higher orders of dynamics in the analytics.

Numerical Model of Combined Refraction and Diffraction

285. A two-dimensional finite element numerical simulation model (FINITE) was developed by Houston and Chou (1984) that calculates wave heights under combined refraction and diffraction of both long and short waves approaching structures from any arbitrary direction. The wave equation solved governs the propagation of periodic, small amplitude surface gravity waves over a variable depth seabed of mild slope. The efficient formulation of the model permits the solution of large problems with relatively small time and memory storage requirements. A computational scheme is employed that allows the solution of practical problems that typically require large computational grids. Although the model solves an equation that is strictly valid only for mild bathymetric variations, the model can provide reasonable qualitative answers for problems where there are rapid depth variations (at much lower cost than required by three-dimensional models that are appropriate for problems involving rapid depth variations). The model does not provide a mechanism for

alone for a shore-connected breakwater on a horizontal bottom. As expected, the comparison was found to be best for short-period waves and for waves at the seaward end of the breakwater, since short-period waves experience less shoaling and refraction and these effects become more significant the farther the waves propagate toward the shoreline. The incident waves generated in the model were sufficiently small that the waves were usually linear within the measurement region.

282. In the neighborhood of the breakwater, currents existed that affected the wave heights. The magnitude of these wave-induced return currents is a function of incident wave characteristics. The effect of varying the incident wave height on the wave-height amplification factor, H/H_0 , was investigated and it was determined that the greatest variation in H/H_0 occurred in the deep shadow zone near the breakwater and shore region where the currents are the strongest. This nonlinear effect diminishes rapidly away from the structure and at a distance of 5 ft downwave appears to be relatively insignificant except for the extreme shadow region at acute angles of the incidence. The establishment of a counterclockwise circulation cell approximately 4 ft wide adjacent to the downwave side of the breakwater results in a seaward flowing current all along the breakwater. The bottom current is especially intense approximately 40 percent of the breakwater length from the shoreline and decreases seaward along the structure. The physical facility sidewall boundary was responsible for a clockwise circulation cell that developed as a result of mass transport downcoast by the longshore current. Based on these experiments, any numerical techniques for describing scour and erosion near structures should account for wave-induced currents and nearshore circulation cells near the structure as well as tidal, wave-induced, or other currents that may exist in the near region.

Breakwater at 60-deg angle to shoreline

283. For small wave periods, small initial wave heights, and deep within the shadow zone (sections near the shoreline), both the diffraction theory and the uniformly valid asymptotic theory predict wave-height amplifications that compare consistently well with the experimental data. Near the tip of the breakwater the diffraction theory tends to diverge rapidly from the experimental results, and the uniformly valid asymptotic theory more nearly approximates the experiments. As wave period increases, the deviation of the diffraction theory becomes more pronounced at all locations except very near the

with the corresponding conservative expression for the weight, W_{UL} , of the representative stone comprising such an underlayer material section:

$$W_{UL} = \frac{\omega_r H_b^3}{5,360 (S_r - 1)^3 \left(\frac{L}{\lambda}\right)^2} \quad (15 \text{ bis})$$

Equation 15 is the recommended equation for determining the weight, W_{UL} , of rock that will remain stable during construction for given wave conditions. Since these data were obtained from the most severe wave conditions (waves that break and plunge directly at the toe of the structure), the application of these results to less-severe wave climates will indicate a stone size requirement larger than necessary. Hence Equation 15 is additionally conservative.

Combined Refraction and Diffraction

280. The purpose of this effort was to obtain detailed and precise experimental data regarding wave-height variations and currents (patterns and magnitudes) downwave from a shore-connected breakwater or jetty under the simultaneous effects of refraction and diffraction. Two different breakwater geometries were investigated: (a) shore-connected breakwater normal to the shoreline and (b) shore-connected breakwater at a 60-deg angle to the shoreline. These data provide insight into the phenomenon of combined wave refraction and diffraction and can be used to verify numerical models that simulate this phenomenon. The investigation was conducted in a wave basin that was molded in cement mortar and consisted of an area 50 ft \times 60 ft with a water depth of 1 ft in the open-ocean region.

Breakwater normal to the shoreline

281. This experimental study used 34 wave-height sensors to ascertain the average maximum wave heights downwave of the shore-connected breakwater, with up to 10 replications of each individual experiment to quantify the experimental variability. The measurements were highly accurate with a standard deviation for repeated observations of usually 2 to 3 percent of the average value of the observations. A comparison of these experimental data of combined refraction and diffraction was made with analytical theories of diffraction

data of constant values of d/λ , then the stability number, N_s , of Equation 10 is simply a function of only one other dimensionless parameter, that being the relative underlayer section length, L/λ .

$$N_s = \frac{\omega_r^{1/3} H_b}{(S_r - 1) W_{UL}^{1/3}} = f\left(\frac{L}{\lambda}\right) \quad (11 \text{ bis})$$

This functional relation can be determined by separating the regions of stability from the unstable regions on a display that plots the stability number, N_s , versus the relative underlayer section length, L/λ (Figure 11).

278. The average best-fit line separating stable from unstable regions for all of the experimental data of this physical model investigation generated a stability number, N_s :

$$N_s = \frac{\omega_r^{1/3} H_b}{(S_r - 1) W_{UL}^{1/3}} = 28.5 \left(\frac{L}{\lambda}\right)^{2/3} \quad (12 \text{ bis})$$

From this expression can be deduced the weight, W_{UL} , of a representative stone comprising an underlayer material section for this average best-fit line:

$$W_{UL} = \frac{\omega_r H_b^3}{23,150 (S_r - 1)^3 \left(\frac{L}{\lambda}\right)^2} \quad (13 \text{ bis})$$

279. Because of experimental scatter in some of the data points, some tests were found to exceed the values of stone weight, W_{UL} , indicated by Equation 13. In order to ensure that all the experimental data fall within the stability region described by a stability number, a conservative stability number was developed which included all the experimental data used to generate the representative stone weight, W_{UL} , of the underlayer section. The expression for this conservative stability number, N_s , is:

$$N_s = \frac{\omega_r^{1/3} H_b}{(S_r - 1) W_{UL}^{1/3}} = 17.5 \left(\frac{L}{\lambda}\right)^{2/3} \quad (14 \text{ bis})$$

contours. A two-dimensional section of this stone structure was tested (16-to-1 linear scale ratio) oriented along the major axis of the structure. The waves that produced the most severe movement of the underlayer section (scour) were those with characteristics that caused breaking with plunging to occur directly at the toe of the rubble-mound structure. Seven uniform material sizes were used to construct three different lengths of underlayer material sections (3-, 5-, and 7-ft model dimensions; 48-, 80-, and 112-ft prototype dimensions, respectively). These 21 different underlayer sections were subjected to breaking waves with periods of 2-, 3-, 4-, and 5-sec model time (8-, 12-, 16-, and 20-sec prototype time, respectively). The characteristics of these 168 individual tests are presented in Table 4. All tests were performed with an underlayer material section thickness of 2.0 ft prototype, which is a typically representative value presently being utilized under prototype conditions.

276. The stability of an underlayer section may be expressed as some functional relation between nine basic parameters:

$$f(\omega_w, \omega_r, W_{UL}, H_b, T, g, d, L, \lambda) = 0 \quad (9 \text{ bis})$$

The effect of thickness of the underlayer material section was not investigated in these tests. Since it was desired to display these experimental data in a manner similar to that of Hudson (1957) for the armor slope stability of rubble-mound structures, the stability number, N_s , can be developed and is functionally related to two other fully independent dimensionless terms:

$$N_s = \frac{\omega_r^{1/3} H_b}{(S_r - 1) W_{UL}^{1/3}} = f\left[\frac{L}{d}, \left(\frac{d}{g}\right)^{1/2} \frac{1}{T}\right] = f\left(\frac{L}{d}, \frac{d}{\lambda}\right) \quad (10 \text{ bis})$$

277. It was determined that for constant values of the structure parameter, L/d , a straight line could be fit to a display of the stability number, N_s , versus relative water depth, d/λ . Furthermore, a straight line of the same slope could be fit to a display of the stability number, N_s , versus the structure parameter, L/d , for constant values of relative water depth, d/λ , when all data are displayed on log-log plots. This implies that if the same slope line can be fit to data of constant values of L/d as it can be fit to

- f. To a lesser extent, the use of Gobimat revetment material has been utilized in special cases of nearshore coastal structures such as seawalls, slope protection structures, and foreshore dike work.
- g. On high wave energy coasts where erosion may occur some time after the initial construction, the extent of the ultimate scour is estimated; and the foundation is excavated to that depth (usually 2 to 6 ft in sand). When conditions prohibit the foundation excavation, an excess quantity of rock is placed on the lower slope and toe to fill any scour hole that may develop later. On the Hawaiian coast, it is frequently possible to excavate down to a firm coral foundation.
- h. In emergency construction situations, scour has been minimized by filling ebb or flood channels with dredged material to allow construction operations to continue unabated.
- i. The expeditious selection of the construction season, as well as the specification of a select series of days when tide predictions indicate favorable working conditions, has been found to contribute significantly to the successful completion of coastal structure work.
- j. Many construction technique problems arise because of poor contractor procedures such as trying to work in adverse weather or wave condition of excessive height.

274. Most of the above procedures are seriously hampered by the inability to predict the extent of scour to be expected. The development of the predictive capabilities of the wave-height numerical simulation model and the wave-induced current numerical model will greatly enhance the effectiveness of present procedures and will provide a basis for the development of alternate procedures for controlling scour and erosion during construction. The stability design curves of the underlayer material developed experimentally in this research program provide guidance regarding the size of material and extent of underlayer section to be optimally effective under storm wave conditions.

Stability of Underlayer Material

275. The purpose of this effort was to determine the stability during construction of such an underlayer material section, which also serves as the foundation blanket for rubble-mound structures constructed on a movable bottom. A simple beach profile consisting of straight, uniform contours parallel with the shoreline was physically molded on a 1V-on-25H slope in a 6-ft-wide wave flume. A major stone structure was assumed to be under construction perpendicular to the shoreline and thus perpendicular to the uniform parallel

- Carver, R. D. 1980 (Jan). "Effects of First Underlayer Weight on the Stability of Stone-Armored Rubble-Mound Breakwater Trunks Subjected to Nonbreaking Waves with No Overtopping; Hydraulic Model Investigation," Technical Report HL-80-1, US Army Engineer Waterways Experiment Station, Vicksburg, Miss.
- Carver, R. D., and Davidson, D. D. 1977 (Nov). "Dolos Armor Units Used on Rubble-Mound Breakwater Trunks Subjected to Nonbreaking Waves with No Overtopping," Technical Report H-77-19, US Army Engineer Waterways Experiment Station, Vicksburg, Miss.
- _____. 1983 (Sep). "Jetty Stability Study, Oregon Inlet, North Carolina," Technical Report CERC-83-3, US Army Engineer Waterways Experiment Station, Vicksburg, Miss.
- Cavanilles, R. T. 1938 (Jul). "A Formula for the Calculation of Rock-Fill Dykes," TR-He-116-295, University of California, Berkeley, Calif.
- Chen, H. S., and Mei, C. C. 1974. "Oscillations and Wave Forces in an Off-shore Harbor," Report No. 190, Massachusetts Institute of Technology, Cambridge, Mass.
- Chesnutt, C. B., and Schiller, R. E., Jr. 1971. "Scour of Simulated Gulf Coast Sand Beaches due to Wave Action in Front of Sea Walls and Dune Barriers," Sea Grant Publication No. 71-207, Texas A&M University, College Station, Tex.
- Cunha, L. V. 1976. "Time Evolution of Local Scour," Technical Memorandum No. 477, Laboratorio Nacional De Engenharia Civil, Lisbon, Portugal.
- Curren, C. R., and Chatham, C. E., Jr. 1979 (Feb). "Newburyport Harbor, Massachusetts, Design for Wave Protection and Erosion Control," Technical Report HL-79-1, Report 1, US Army Engineer Waterways Experiment Station, Vicksburg, Miss.
- Dalrymple, R. A., Eubanks, R. A., and Birkemeier, W. A. 1977 (Feb). "Wave-Induced Circulation in Shallow Basins," Proceedings, Journal of the Waterway, Port, Coastal and Ocean Division, American Society of Civil Engineers, Vol 103, No. WW1, pp 117-135.
- Davidson, D. D. 1971 (Nov). "Proposed Jetty-Head Repair Sections, Humboldt Bay, California; Hydraulic Model Investigation," Technical Report H-71-8, US Army Engineer Waterways Experiment Station, Vicksburg, Miss.
- _____. 1978 (Jan). "Stability Tests of Nawiliwili Breakwater Repair," Miscellaneous Paper H-78-4, US Army Engineer Waterways Experiment Station, Vicksburg, Miss.
- Dietz, J. W. 1976. "The Reproduction of Scour Processes in Model Tests," Bundesanstalt Fuer Wasserbau, Communication No. 40, pp 71-85.
- Donnelly, P., and Boivin, R. 1968. "Pattern of Wave-Induced Erosion Under Caisson-Type Breakwater," Proceedings, Eleventh Conference on Coastal Engineering, London, England, Vol I, pp 599-605.
- Dunham, J. W. 1951 (Oct). "Refraction and Diffraction Diagrams," Proceedings, First Conference on Coastal Engineering, Long Beach, Calif., pp 33-49.
- Ebersole, B. A. 1980 (Jun). A Numerical Model for Nearshore Circulation Including Convective Accelerations and Lateral Mixing, M.S. Thesis, University of Delaware, Newark, Del.

- Ebersole, B. A., and Dalrymple, R. A. 1980. "Numerical Modeling of Nearshore Circulation," Proceedings, 17th Conference on Coastal Engineering, Vol III., Chapter 163, pp 2710-2725.
- Eckart, C. 1952. "The Propagation of Gravity Waves from Deep to Shallow Water," Circular 521, National Bureau of Standards, Washington, D. C.
- Eckert, J. W. 1983 (Mar). "Design of Toe Protection for Coastal Structures," Proceedings of Coastal Structures '83, pp 331-341, Arlington, Va.
- Gravesen, H., Jensen, O. J., and Sorensen, T. "Stability of Rubble Mound Breakwaters II" (unpublished), Danish Hydraulic Institute and Technical University of Denmark.
- Hales, L. Z. 1980a (Mar). "Erosion Control of Scour During Construction; Present Design and Construction Practice," Technical Report HL-80-3, Report 1, US Army Engineer Waterways Experiment Station, Vicksburg, Miss.
- Hales, L. Z. 1980b (Sep). "Erosion Control of Scour During Construction; Experimental Measurements of Refraction, Diffraction, and Current Patterns near Jetties," Technical Report HL-80-3, Report 3, US Army Engineer Waterways Experiment Station, Vicksburg, Miss.
- Hales, L. Z., and Houston, J. R. 1983 (Jun). "Erosion Control of Scour During Construction; Stability of Underlayer Material Placed in Advance of Construction to Prevent Scour," Technical Report HL-80-3, Report 4, US Army Engineer Waterways Experiment Station, Vicksburg, Miss.
- Hannoura, A. A., and McCorquodale, J. A. 1979 (Sep). "Environmental Wave Forces on Rubble-Mound Breakwaters," Proceedings, Civil Engineering in the Oceans IV, San Francisco, Calif., Vol 1, pp 367-379.
- Herbich, J. B., and Ko, S. C. 1968. "Scour of Sand Beaches in Front of Seawalls," Proceedings, Eleventh Conference on Coastal Engineering, London, England, pp 622-643.
- Hollyfield, N. W., McCoy, J. W., and Seabergh, W. C. 1983 (Jun). "Functional Design of Control Structures for Oregon Inlet, North Carolina," Technical Report HL-83-10, US Army Engineer Waterways Experiment Station, Vicksburg, Miss.
- Hom-ma, S. 1950. "On the Behavior of Seismic Sea Waves Around Circular Island," Geophys. Mag., Vol 21, p 199.
- Hotta, S., and Marui, N. 1976. "Local Scour and Current Around a Porous Breakwater," Proceedings, Fifteenth Conference on Coastal Engineering, Honolulu, Hawaii, Vol II, pp 1590-1604.
- Houston, J. R. 1980 (May). "Modeling of Short Waves Using the Finite Element Method," Proceedings, Third International Conference on Finite Elements in Water Resources, Vol 2, pp 5.181-5.195, University of Mississippi, Oxford, Miss.
- Houston, J. R., and Chou, L. W. 1984 (Sep). "Erosion Control of Scour During Construction; FINITE--A Numerical Model for Combined Refraction and Diffraction of Waves," Technical Report HL-80-3, Report 6, US Army Engineer Waterways Experiment Station, Vicksburg, Miss.
- Hudson, R. Y. 1957 (Jun). "Laboratory Investigation of Rubble-Mound Breakwaters," Proceedings, American Society of Civil Engineers.

- Hudson, R. Y. 1958 (Jul). "Design of Quarry-Stone Cover Layers for Rubble-Mound Breakwaters," Research Report No. 2-2, US Army Engineer Waterways Experiment Station, Vicksburg, Miss.
- _____. 1961 (Sep). "Wave Forces on Rubble-Mound Breakwaters and Jet-ties," Miscellaneous Paper No. 2-453, US Army Engineer Waterways Experiment Station, Vicksburg, Miss.
- _____. 1974 (Jan). "Concrete Armor Units for Protection Against Wave Attack; Report of Ad Hoc Committee on Artificial Armor Units for Coastal Structures," Miscellaneous Paper H-74-2, US Army Engineer Waterways Experiment Station, Vicksburg, Miss.
- _____. 1975 (Jun). "Reliability of Rubble-Mound Breakwater Stability Models," Miscellaneous Paper H-75-5, US Army Engineer Waterways Experiment Station, Vicksburg, Miss.
- Hudson, R. Y., and Jackson, R. A. 1953 (Jun). "Stability of Rubble-Mound Breakwaters; Hydraulic Model Investigation," Technical Memorandum No. 2-365, US Army Engineer Waterways Experiment Station, Vicksburg, Miss.
- Irie, I., and Nadaoka, K. 1984 (Sep). "Laboratory Reproduction of Seabed Scour in Front of Breakwaters," Coastal Engineering Abstracts 1984 (abstracts of the papers presented at the 19th International Conference on Coastal Engineering), pp 524-525, Houston, Tex.
- Jonsson, I. G., and Brink-Kjaer, O. 1973. "A Comparison Between Two Reduced Wave Equations for Gradually Varying Depth," Technical Report No. 31, Technical University of Denmark.
- Jonsson, I. G., Skovgaard, O., and Brink-Kjaer, O. 1976. "Diffraction and Refraction Calculations for Waves Incident on an Island," Journal Marine Research, Vol 34, p 469.
- Jonsson, I. G., Skovgaard, O., and Jacobsen, T. S. 1974. "Computation of Longshore Currents," Proceedings, 14th Conference on Coastal Engineering, Vol II, Chapter 40, pp 699-714.
- Keller, J. B. 1958. "Surface Waves on Water of Non-Uniform Depth," Journal of Fluid Mechanics, Vol 4, pp 607-614.
- Keulegan, G. H. 1950. "Wave Motion," Engineering Hydraulics, Wiley, New York, N. Y.
- Keulegan, G. H. 1973 (Feb). "Wave Transmission Through Rock Structures; Hydraulic Model Investigation," Research Report H-73-1, US Army Engineer Waterways Experiment Station, Vicksburg, Miss.
- Keulegan, G. H., and Patterson, G. W. 1940 (Jan). "Mathematical Theory of Irrotational Translation Waves," Journal of Research, National Bureau of Standards, Vol 24, No. 1, pp 47-101.
- Koh, R. C. Y., and LeMéhauté, B. 1966 (Apr). "Wave Shoaling," Journal of Geophysical Research, Vol 71, No. 8, pp 2055-2012.
- Lamb, H. 1932. Hydrodynamics, Cambridge University Press.
- Lautenbacher, C. C. 1970. "Gravity Wave Refraction by Islands," Journal Fluid Mech, Vol 41, p 655.

- LeMéhauté, B. 1965 (Jun). "Wave Absorbers in Harbors," Contract Report No. 2-122, US Army Engineer Waterways Experiment Station, Vicksburg, Miss.
- Lick, W. 1978 (May). "Diffraction of Waves by a Wedge," Journal, Waterway, Port Coastal and Ocean Division, American Society of Civil Engineers, Vol 104, No. WW2, pp 119-133.
- Liu, P. L., 1982 (Jul). "Combined Refraction and Diffraction: Comparison Between Theory and Experiments," Journal of Geophysical Research, Vol 87, No. C8, pp 5723-5730.
- Liu, P. L., and Lozano, C. J. 1979 (Mar). "Combined Wave Refraction and Diffraction," Proceedings, Coastal Structures 79, Alexandria, Va., Vol II, pp 978-997.
- Liu, P. L., and Mei, C. C. 1975 (Nov). "Effects of a Breakwater on Nearshore Currents due to Breaking Waves," Technical Memorandum No. 57, US Army Coastal Engineering Research Center, Washington, DC.
- _____. 1976 (Jun). "Wave Motion on a Beach in the Presence of a Breakwater; 1, Waves," Journal of Geophysical Research, Vol 81, No. 18, pp 3079-3084.
- Liu, P. L., Lozano, C. J., and Pantazaras, N. 1979. "An Asymptotic Theory of Combined Wave Refraction and Diffraction," Applied Ocean Research, Vol 1, No. 3, pp 137-146.
- Longuet-Higgins, M. S. 1970 (Nov). "Longshore Currents Generated by Obliquely Incident Sea Waves, 1 and 2," Journal of Geophysical Research, Vol 75, No. 33, pp 6778-6789 and pp 6790-6801.
- Longuet-Higgins, M. S., and Stewart, R. W. 1964. "Radiation Stresses in Water Waves; A Physical Discussion, with Applications," Deep-Sea Research, Vol 11, pp 529-562.
- Lozano, C. J. and Liu, P. L. 1980. "Refraction-Diffraction Model for Linear Surface Water Waves," Journal of Fluid Mechanics, Vol 101, Part 4, pp 705-720.
- Masch, F. D. 1964. "Cnoidal Waves in Shallow Water," Proceedings, Ninth Conference on Coastal Engineering, Lisbon, Portugal, pp 1-21.
- Meulen, T. V., and Vinje, J. J. 1977. "Three-Dimensional Local Scour in Non-Cohesive Sediments," Publication No. 180, Delft Hydraulics Laboratory, Delft, The Netherlands.
- Mobarek, I. 1962 (Nov). "Effect of Bottom Slope on Wave Diffraction," Technical Report No. HEL-1-1, University of California, Berkeley, Calif.
- Morris, H. M. 1963. Applied Hydraulics in Engineering, Ronald Press Co., New York.
- Murphy, T. E. 1971 (Mar). "Control of Scour at Hydraulic Structures," Miscellaneous Paper H-71-5, US Army Engineer Waterways Experiment Station, Vicksburg, Miss.
- Nakagawa, H., and Suzuki, K. 1976. "Local Scour Around Bridge Pier in Tidal Current," Coastal Engineering in Japan, Vol 19.
- Noda, E. K. 1974 (Sep). "Wave-Induced Nearshore Circulation," Journal of Geophysical Research, Vol 29, No. 27, pp 4097-4106.

- Noda, E. K., Sonu, C. J., Rupert, V. C., and Collins, J. I. 1974 (Feb). "Nearshore Circulations Under Sea Breeze Conditions and Wave-Current Interactions in the Surf Zone," Tetra Tech Report TC-149-4.
- Orlanski, I. 1976. "A Simple Boundary Condition for Unbounded Hyperbolic Flows," Journal of Computational Physics, Vol 21, pp 251-269.
- Pantazaras, N. 1979. "Combined Diffraction and Refraction of Water Waves," Thesis presented to Department of Environmental Engineering, Cornell University, in partial fulfillment of the degree of Master of Science, Ithaca, N. Y.
- Penny, W. G., and Price, A. T. 1944. "Diffraction of Sea Waves by Breakwaters," Technical History Report No. 26, Directorate of Miscellaneous Weapons Development, Washington, DC.
- Perry, F. C., Jr., Seabergh, W. C., and Lane, E. F. 1978 (Apr). "Improvements for Murrells Inlet, South Carolina; Hydraulic Model Investigation," Technical Report H-78-4, US Army Engineer Waterways Experiment Station, Vicksburg, Miss.
- Pierson, W. J., Jr. 1951 (Jan). "The Interpretation of Crossed Orthogonals in Wave Refraction Phenomena," Technical Memorandum 21, US Army Beach Erosion Board, Washington, DC.
- Putnam, J. A., and Arthur, R. S. 1948. "Diffraction of Water Waves by Breakwaters," Transactions, American Geophysical Union, Vol 29, No. 4, pp 481-490.
- Radder, A. C. 1979. "On the Parabolic Equation Method for Water-Wave Propagation," Journal of Fluid Mechanics, Vol 95, pp 159-176.
- Rayleigh, J. W. S. 1877. "On Progressive Waves," Proceedings, London Mathematical Society, Vol 9, pp 21-26.
- Russell, R. C. H., and Inglis, C. 1953. "The Influence of a Vertical Wall on a Beach in Front of It," Proceedings, Minnesota International Hydraulics Convention, Minneapolis, Minn., pp 221-226.
- Sato, S., Tanaka, N., and Irie, I. 1968. "Study on Scouring at the Foot of Coastal Structures," Proceedings, Eleventh Conference on Coastal Engineering, London, England, Vol I, pp 579-598.
- Sawaragi, T. 1966. "Scouring due to Wave Action at the Toe of Permeable Coastal Structure," Proceedings, Tenth Conference on Coastal Engineering, Tokyo, Japan, pp 1036-1047.
- Schonfeld, J. 1972. "Propagation of Two-Dimensional Short Waves," Delft University of Technology, Delft, The Netherlands.
- Seabergh, W. C. 1976 (Apr). "Improvements for Masonboro Inlet, North Carolina; Hydraulic Model Investigation," Technical Report H-76-4 (in 2 Vols), US Army Engineer Waterways Experiment Station, Vicksburg, Miss.
- Smith, R., and Sprinks, T. 1975. "Scattering of Surface Waves by a Conical Island," Journal of Fluid Mechanics, Vol 72, pp 373-384.
- Sollitt, C. K., and DeBok, D. H. 1976 (Jul). "Large Scale Model Tests of Placed Stone Breakwaters," Proceedings, Fifteenth Coastal Engineering Conference, Honolulu, Hawaii, Vol III, pp 2572-2588.
- Sommerfeld, A. 1896. "Mathematical Theory of Diffraction," Annals of Mathematics, Vol 47.

Song, W. O., and Schiller, R. E., Jr. 1973. "Experimental Studies of Beach Scour due to Wave Action," Sea Grant Publication No. 73-211, Texas A&M University, College Station, Tex.

Stambler, I. 1972. Shorelines of America, Grossett and Dunlap, Inc., New York.

Thornton, E. B. 1970. "Variation of Longshore Current Across the Surf Zone," Proceedings, 12th Conference on Coastal Engineering, Vol I, Chapter 18, pp 291-308.

Tsay, T. K., and Liu, P. L. 1982 (Sep). "Numerical Solution of Water-Wave Refraction and Diffraction Problems in the Parabolic Approximation," Journal of Geophysical Research, Vol 87, No. C10, pp 7932-7940.

US Army Engineer Division, South Pacific. 1977. "California Water Resources Development," San Francisco, Calif.

US Army Engineer Waterways Experiment Station. 1955 (Nov). "Plans for the Improvement of Grays Harbor and Point Chehalis, Washington; Hydraulic Model Investigation," Technical Memorandum No. 2-417, Vicksburg, Miss.

_____. 1984. Shore Protection Manual, Coastal Engineering Research Center, Vicksburg, Miss.

van Heemskerck, W. C. B. 1963. "Foundation and Scour Problems Associated with Various Methods of Closing an Estuary," Houille Blanche, Vol 18, No. 2, pp 143-158.

Vemulakonda, S. R., 1984 (Sep). "Erosion Control of Scour During Construction, CURRENT--A Wave-Induced Current Model, Theory and Program Documentation," Technical Report HL-80-3, Report 7, US Army Engineer Waterways Experiment Station, Vicksburg, Miss.

Vreugdenhil, C. B. 1980 (Aug). "A Method of Computation for Unsteady Wave-Driven Coastal Currents," Report R 1174, Part I, Waterloopkundig Laboratorium, Delft Hydraulics Laboratory.

Whalin, R. W. 1972 (Jul). "Wave Refraction Theory in a Convergence Zone," Proceedings, Thirteenth Conference on Coastal Engineering, Vancouver, British Columbia, Canada, pp 451-470.

Whillock, A. F., and Price, W. A. 1976 (Jul). "Armour Blocks as Slope Protection," Proceedings, Fifteenth Coastal Engineering Conference, Honolulu, Hawaii, Vol III, pp 2564-2571.

Wiegel, R. L. 1962 (Jan). "Diffraction of Waves by Semi-Infinite Breakwaters," Journal, Hydraulics Division, American Society of Civil Engineers, Vol 88, No. HY1, pp 27-44.

Yalin, M. S. 1959. "On the Full-Scale Similarity of Sediment Transport in Model Tests," Die Bautechnik, Vol 36, No. 3, pp 96-99.

_____. 1971. Theory of Hydraulic Models, Macmillan, New York.

Yue, D. K. P., Chen, H. S., and Mei, C. C. 1976. "A Hybrid Finite Element Method for Calculating Three-Dimensional Water Wave Scattering," Report No. 215, Massachusetts Institute of Technology.

APPENDIX A: NOTATION

a	Mapping function, dimensionless
a	Local wave amplitude, ft
a_o	Incident wave amplitude, ft
a_{xx}	Second derivative of wave amplitude in x-direction, 1/ft
a_{yy}	Second derivative of wave amplitude in y-direction, 1/ft
A	Numerical computational region, dimensionless
A	Surface area, ft^2
A(x)	Combined refraction and shoaling factor, ft
b	Mapping function, dimensionless
b_1	Wave ray spacing, ft
b_2	Wave ray spacing, ft
B	Numerical computational region, dimensionless
c	Drag coefficient (of the order of 0.01), dimensionless
c	Mapping function, dimensionless
c	Wave phase speed of propagation, ft/sec
c_g	Wave group velocity, ft/sec
C	Wave celerity, ft/sec
C_D	Drag coefficient, dimensionless
C_r	Wave reflection coefficient, dimensionless
$C_2(\rho_1^2)$	Fresnel cosine integral, dimensionless
d	Local still-water depth, ft
d	Sediment particle diameter, ft
d_b	Local still-water depth at wave breaking, ft
d_m	Median diameter of bed particles, mm
d_{50}	Fifty percent finer of a material by weight, dimensionless
D	Hudson damage parameter, dimensionless
D	Pier width, ft
e	Base of Napierian system of natural logarithms, 2.71828, dimensionless
E	Wave energy density, ft-lb/ft^2
F	Mathematical function for wave equation in cylindrical coordinates, dimensionless
F(r,θ)	Function satisfying wave equation in cylindrical coordinates, dimensionless
g	Gravitational acceleration constant, 32.174 ft/sec^2

G	Computational parameter, $(2kh/\sinh 2kh)$, ft/sec
$G(\rho_1)$	Arbitrary mathematical function, dimensionless
h	Arbitrary still-water depth, ft
h	Height of fill required to seal caisson joint, ft
h_o	Incident still-water depth, ft
$h(x)$	Water depth as a function of distance x , ft
H	Local wave height, ft
H_b	Wave height at breaking, ft
H_B	Iribarren breaking wave height, m
H_i	Incident wave height, ft
H_n	Hankel function of the first kind, dimensionless
H_o	Deepwater wave height, ft
H_r	Reflected wave height, ft
H_s	Significant wave height (average of highest one-third of waves), ft
H_{max}	Maximum wave height, ft
H_{10}	Average of highest 10 percent of waves, ft
i	$(-1)^{1/2}$, dimensionless
I	Integral for evaluating phase function, deg
k	Wave number, $2\pi/L$, 1/ft
k_o	Incident wave number, $2\pi/L_o$, 1/ft
k_r	Wave number of reflected wave along breakwater, $2\pi/L_r$, 1/ft
k_t	Wave number of radiated wave from breakwater tip, $2\pi/L_t$, 1/ft
k_Δ	Rubble-mound armor unit layer coefficient, dimensionless
kHz	kilo-Hertz, 1,000 cycles/sec
K	Symmetric complex coefficient matrix, dimensionless
K_B	Iribarren breakwater coefficient, kg/m^3
K_d	Diffraction coefficient, dimensionless
K_D	Rubble-mound structure armor unit stability coefficient, dimensionless
K_r	Refraction coefficient, dimensionless
K_r	Arbitrary reflected wave parameter for curved breakwater, 1/ft
K_t	Arbitrary radiated wave parameter for straight breakwater, 1/ft
\bar{K}_o	Arbitrary initial wave parameter for straight breakwater, 1/ft
K_{r-d}	Combined refraction and diffraction coefficient, dimensionless
L	Underlayer material extent, ft
L	Wavelength at arbitrary location, ft

L_b	Breaking wavelength, ft
L_o	Incident wavelength, ft
L_r	Reflected wavelength, ft
L_t	Radiated wavelength, ft
m	Cell number in x-direction, dimensionless
n	Cell number in y-direction, dimensionless
n	Number of quarrystone or concrete armor units in thickness comprising the cover layer, dimensionless
n	Ratio of group velocity to wave velocity, dimensionless
n_A	Unit normal to the boundary separating computational regions A and B, dimensionless
N	Longshore current parameter, dimensionless
N	Number of node points in the finite element discretization, dimensionless
N_s	Stability number, dimensionless
P	Mixing parameter which varies between 0.01 and 0.40, dimensionless
P	Rate of wave power transmission, lb/sec
Q	Ebb tidal flow discharge, ft ³ /sec
r	Average cover layer thickness, ft
r	Radius in cylindrical coordinates, ft
\bar{r}	Phase function parameter, ft
R	Phase function of waves radiated from curved breakwater tip, deg
R_s	Phase function of waves radiated from straight breakwater tip, deg
s	Beach slope, dimensionless
S	Scour depth, ft
S	Phase function of incident wave for curved breakwater, deg
S_r	Specific gravity of rock or concrete unit relative to water ($S_r = \omega_r/\omega_w$), dimensionless
S_s	Phase function of incident wave for straight breakwater, deg
S_{cr}	Iribarren specific weight of cap rock, metric tons/m ³
S_{xx}	Radiation stresses in the x-direction (normal to the y-z plane), lb/ft
S_{xy}	Radiation stresses in the y-direction in the x-z plane, lb/ft
S_{yy}	Radiation stresses in the y-direction (normal to the x-z plane), lb/ft
S_{max}	Maximum scour depth, ft
$S_2 \rho_1^2$	Fresnel sine integral, dimensionless

\bar{S}	Phase function of wave reflected from curved breakwater, deg
\bar{S}_s	Phase function of wave reflected from straight breakwater, deg
t	Time increment, sec
t_r	Time at which $S_{\max} = D$, sec
t_l	Time at which $S_{\max} = y$, sec
T	Wave period, sec
u	Fluid velocity, ft/sec
\bar{u}	Two-dimensional velocity vector, ft/sec
u_*	Friction velocity, ft/sec
u_{cr}	Fluid particle movement initiation velocity, ft/sec
u_{\max}	Maximum wave orbital velocity, ft/sec
u_{orb}	Time-averaged wave orbital bottom velocity, ft/sec
u_1	Diffraction integration limits, dimensionless
u_2	Diffraction integration limits, dimensionless
U	Depth-averaged horizontal velocity at time t in x-direction, ft/sec
v_f	Full velocity, ft/sec
V	Depth-averaged horizontal velocity at time t in y-direction, ft/sec
W	Weight of individual armor stone in rubble-mound structure, lb
W	Ebb tidal channel width, ft
W_R	Iribarren cover-stone weight, kg
W_{UL}	Weight of representative individual stone in underlayer material section, lb
x	Horizontal direction in Cartesian coordinate system, ft
X	Real space coordinate
X_b	Distance from shoreline to point where wave breaks, ft
y	Initial unscoured water depth, ft
y	Arbitrary vertical location, ft
y	Horizontal direction in Cartesian coordinate system, ft
z	Vertical direction in Cartesian coordinate system, ft
α	Local scour coefficient, dimensionless
α	Local wave angle with shoreline or breakwater, deg
α_n	Coefficients of the Hankel functions of the first kind, dimensionless
α_1	Computational space coordinate, dimensionless
α_2	Computational space coordinate, dimensionless
β	Angle between wave ray and breakwater, deg
β_n	Coefficients of the Hankel functions of the first kind, dimensionless

γ	Arbitrary parameter, dimensionless
γ	Unit weight of fluid, lb/ft ³
γ	Wave breaking index on the order of 1.15, dimensionless
γ_s	Unit weight of solids, lb/ft ³
δ	Defined parameter $(a_{xx} + a_{yy})/k^2 a$, dimensionless
Δb	Wave ray spacing, ft
Δt	Time increment, sec
Δx	Real space cell dimension in x-direction, ft
Δy	Real space cell dimension in y-direction, ft
$\Delta \alpha_1$	Computational space cell dimension in α_1 -direction, ft
$\Delta \alpha_2$	Computational space cell dimension in α_2 -direction, ft
ϵ_x	Eddy viscosity in the x-direction, ft ² /sec
ϵ_y	Eddy viscosity in the y-direction, ft ² /sec
η	Complex wave amplitude, ft
η	Local water-surface elevation, ft
η^*	Water-surface elevation at intermediate time level solution, ft
$\bar{\eta}$	Displacement of the mean free surface with respect to still-water level, ft
θ	Angle of rubble-mound structure slope with horizontal, deg
θ	Arbitrary wave angle, deg
θ	Direction in cylindrical coordinate system, deg
θ_o	Angle between breakwater and undiffracted wave crests beyond breakwater, deg
θ_o	Incident wave angle, deg
θ_r	Reflected wave angle along breakwater, deg
θ_t	Radiated wave angle from oscillatory point source at breakwater tip, deg
θ_∞	Incident deepwater wave angle, deg
λ	Wavelength at arbitrary location, ft
μsec	Microsecond, 0.000001 sec
ν	Fluid kinematic viscosity, ft ² /sec
π	3.141592654, dimensionless
ρ	Fluid density, lb-sec ² /ft ⁴
ρ_s	Sediment particle density, lb-sec ² /ft ⁴
ρ_1	Fresnel integral limit, dimensionless
σ	Fresnel integral parameter, dimensionless

τ	Fresnel integral parameter, dimensionless
τ_{bx}	Bottom friction stresses in the x-direction, lb/ft^2
τ_{by}	Bottom friction stresses in the y-direction, lb/ft^2
τ_{xy}	Lateral shear stresses due to turbulent mixing, lb/ft^2
ϕ	Velocity potential, ft^2/sec
ϕ	Velocity potential, ft^2/sec
ϕ_A	Velocity potential in region A, ft^2/sec
ϕ_B	Velocity potential in region B, ft^2/sec
ϕ_I	Incident wave velocity potential, ft^2/sec
ϕ_R	Reflected wave velocity potential, ft^2/sec
ϕ	Bed material angle of repose, deg
ω	Wave angular frequency, $2\pi/T$, $1/\text{sec}$
ω_r	Unit weight of rock, lb/ft^3
ω_w	Unit weight of water, lb/ft^3

Symbols

>	Greater than, dimensionless
<	Less than, dimensionless
∂	Partial derivative symbol, dimensionless
∇	Horizontal gradient operator, $1/\text{ft}$
\ominus	Argument of mathematical function $G(\rho_1)$, dimensionless
$\bar{\ominus}$	Argument of mathematical function $G(\rho_1)$, dimensionless
∞	Infinity, dimensionless

END

FILMED

6-85

DTIC